THE FRACTURE AND AUTOGENOUS COMMINUTION OF QUARTZITE

ACHILLES CONSTANTINE KANELLOPOULOS

A THESIS PRESENTED TO FULFIL THE REQUIREMENTS
FOR THE DEGREE OF DOCTOR OF PHILOSOPHY
OF THE
UNIVERSITY OF CAPE TOWN

1978

SYNOPSIS

Comminution is the process which aims at increasing the surface area and the resultant liberation of a particular constituent from the mass of a solid. The autogenous mill uses tumbling to effect comminution, but instead of special milling bodies being added, pebbles of the material to be comminuted are used. The autogenous comminution process utilises less than 0,1 per cent of the energy input.

The principal objective of the present work was to analyse autogenous milling behaviour in terms of the individual comminuting mechanisms and to establish the inter-relationships between the main process variables, namely rock petrography, size distribution of the feed, applied load, relative velocity and environment. In this manner the optimisation the process and an improvement of its efficiency was sought. In addition the establishment of testing procedures to predict the autogenous milling behaviour of a given type of rock was aimed. In the present work the gold bearing Witwatersrand quartzite was used, although the findings are applicable to other types of rocks.

Since fracture phenomena are involved in all comminuting mechanisms of impact-compression, chipping and abrasion, slow compression and Brazilian tests were performed. The grain size and the mineral composition of the rock has been found to have a large influence on the local stresses required for these processes. Indeed the results show that the fragility and therefore ease of comminution increases with increasing grain size of the quartzite. Brazilian tests on drill cores of varying diameters may allow the prediction of the critical size of rock of the mill feed which can survive in a mill of given characteristics.

The study of the frictional behaviour of the rock during sliding under controlled conditions of speed and normal load aimed at an understanding of the mechanisms of abrasion. The magnitude of the frictional force, which is associated with the sliding of two rock surfaces, and the scanning electron microscopy study of the friction tracks indicate the occurence of three different sliding mechanisms. No distinguishable damage on the sliding track and low values of the coefficient of sliding friction indicate that the rock surface asperities "climb" each other in a smooth manner when the values of the sliding speed and applied normal load are low; for higher values of the sliding speed and/or of the normal load the breakage of the tips of the interlocked asperities is indicated. When the sliding speed or the normal load are further increased a distinctive friction groove with a smooth extruded appearance, indicative of fracture and plastic flow, is formed.

The wear due to abrasion, as measured on rotating drill cores, was found to increase with the grain size and the applied normal load. The influence of the relative speed and of the total process time was found to be small upon the measured wear rates due to abrasion. The similarity in appearance of the abrasion detritus and the autogenously milled particles indicates the importance of abrasion in autogenous milling and that material loss by wear occurs by spalling under the influence of the stress field. The spalling involves brittle cleavage fracture and a limited amount of plastic deformation.

The nature and concentration of the environment was found to influence the frictional, abrasion and autogenous milling behaviour of the rock. These results can be explained satisfactorily in terms of changes of the zeta-potential between each mineral constituent of the rock and the environment. The resulting change in the mobility of near surface dislocations allows plastic deformation to affect the

sharpness of near surface cracks and their subsequent initiation and propagation behaviour. The mass removed by plastic flow due to difference in scratch hardness between two mineral constituents of the rock is also affected.

The application of prior surface heating was considered as a process to improve autogenous milling. Differences in thermal expansion characteristics between the mineral constituents of the rock, the quartz $\alpha \rightarrow \beta$ transition, the dehydration and oxidation of some mineral constituents were found to increase the fragility of the rock. Although comminution is improved by thermal treatments, the application of a such process is prohivitive due to its high energy requirements.

In view of the results of this thesis the following considerations should be made when the application and optimisation of the autogenous milling is contemplated:

(i) The rate of comminution by impact and abrasion is a function of the grain size and the mineralogy of the rock;

(ii) Certain additives can improve the efficiency of autogenous comminution;

(iii) The design of the mill should aim at increasing the proportion of wear by abrasion; and

(iv) A series of small scale tests using drill cores can give strong indications of the suitability of an ore for autogenous milling.

TABLE OF CONTENTS

APPENDICES

TABLE OF FIGURES

TABLE OF PLATES

TABLE OF TABLES

1. GENERAL INTRODUCTION

Comminution is the process which aims at increasing the surface area and the resultant liberation of a particular constituent from the mass of a solid. The origins of comminution are almost coeval with man. Homer, describes at least six comminution processes, much more complicated than the pestle and mortar, which were employed before 2000 B.C.

Rumpf (1959) estimates, that the comminution of solids in present times consumes five per cent of all the electrical energy produced in the world. The mineral processing of the excavated ores is the forerunner of the manufacture of most of the metals that man uses. Energetically comminution is an inefficient process and utilizes only of the order of one per cent of the power supplied. Therefore there is much opportunity for financial improvements and even a ten per cent increase in useful size reduction would warrent a major scientific and technological research effort. An efficient comminution process will be associated with increased recovery rates of any ore and make possible the utilization of low grade ores in order to satisfy the world demands in materials, especially the ones which will be in short supply in the near future.

Although the principle of the autogenous* mill was established as soon as primitive man aimed a large piece of stone to break another piece, the method is relatively new, which has only recently made inroads into industrial mineral processing. The autogenous mill uses tumbling to effect comminution, but instead of special milling bodies such as rods or balls being added, lumps of the material to be comminuted are used. The first report of a tumbling mill being worked autogenously is by Graham in 1907. This successful application of autogenous milling took place in the Witwatersrand goldfields mineral processing production line and resulted in an improved milling efficiency.

---

*Autogenous derives from the greek adjective αὐτογενής meaning self-born or self-sufficient.

Graham reported the effect of both composition of milling pulp and mill charge on this efficiency but he discontinued his effort because of shortage of necessary labour required for the preparation of the feed. During the first half of the twentieth century a number of wet and dry autogenous milling applications took place, particularly in the U.S.A. and Canada, with and without auxiliary wear media (Lawrison, 1974). In 1960, autogenous milling was successfully applied in Sweden for the comminution of silicious lead ore (Fahlström, 1962, 1974) and in 1965, autogenous milling was successfully applied in Turkey (Dogan, 1975) for the comminution of quartzite ore. Autogenous milling should be initially considered as one of the most applicable processes for any new reduction plant, since the advantages offered may include:

(i) ability for size reduction of a run-of-mine product, without any primary preparation such as jaw crushing.

(ii) a product with a reduced amount of contamination by auxiliary wear media.

(iii) reduced capital and operational costs in comparison with other comminution methods.*

Unfortunately all ores do not respond to autogenous milling. In some cases auxiliary media ore added in order to achieve an acceptable milling efficiency.

---

*The comminution cost may be analyzed into the capital charges, the energy cost, the parts renewal cost and the operating labour accounts. The view which is widely accepted (Rose and Sullivan, 1961), is that each of the first three charges account for about the third of the total comminution cost, while the labour represents a negligible expenditure.

The capital cost for the autogenous milling depends upon the magnitude of the throughput of the mill. For small units the capital charges are lower than the ones of similar in size units of the conventional size reduction plants i.e. ball milling. But, there is a tendency for the new comminution systems to be designed for higher throughputs aided by automatic control in order to optimize operation that involves a higher capital investment, which results to proportionally higher capital charges, corresponding with longer pay-back periods. The same time the renewal costs become higher due to the size and the complexity of the plant. The elimination of the comminution stages, of course, also reduces the total capital cost i.e. jaw, gyratory crushers (primary) and ball, rod mills (secondary).

Studies on the suitability of ores for the application of autogenous milling are usually carried out on a pilot plant scale basis prior to the full scale application of the methods. These empirical studies normally investigate the need of auxiliary wear media or the desirability of several processing stages. Plant scale tests are expensive and time consuming and in addition require appreciable quantities of the ore. These large quantities are not usually available at the early feasibility studies stage.

The complexity of the process and the absence of detailed knowledge about the physical mechanisms involved in autogenous milling, preclude further increases in comminution efficiency and predictive selection criteria of ores suitable for the technique. An examination of the nature of the physical processes that occur during autogenous milling and the separate consideration of each of these processes in relation to all the physical and chemical variables involved is the approach adopted in the present study. Ideally a full understanding of the comminution mechanisms in the mill and the associated variables should enable us to accurately predict the suitability of autogenous milling to a particular ore body.

The comminution process in general was considered by Schuhmann (1960) as a summation of many individual and independent events, each of which was assumed to have substantially constant characteristics during the progress of the comminution process. With a given feed material and a given comminution device, all of these comminution events could be classified into families which employ certain mechanisms with characteristic energy utilization and resulting size distributions of the product. An analysis of the three main comminuting mechanisms employed in a tumbling mill, namely impact, chipping and abrasion, has been proposed by Crabtree, Kinasevich, Mular, Meloy and Fuerstenau (1964). A fourth comminuting mechanism, attrition, was proposed by the same authors as comprising both abrasion and chipping mechanisms.

The impact or compression fracture mechanism, as proposed by Crabtree et al, has been examined by Arbiter, Harris and Stamboltzis (1969), for the understanding of the autogenous milling. Three

component processes were proposed by the authors, namely, free fall impact, double simultaneous impact and slow compression. The free fall impact is produced by falling rock pieces and the double impact may be characterized by diametrical point shock loading of a rock piece. In these impact mechanisms the distribution modulus n is unity in the Rosin-Rammler presentation (Appendix A) for the total mill product, viz: $y = 1-\exp(-(x/k)^n)$ where y is the mass fraction undersize x and k is a constant.

The chipping mechanism, (Crabtree et al, 1964), involves the breaking of edges or corners from a rock piece, when there is insufficient energy to produce fracture into nearly equal parts. The size distribution produced is unclassified in terms of the Rosin-Rammler presentation (i.e. n is inderminate) and thus different than that of the impact mechanism.

Abrasion, according to Crabtree et al (1964), is a form of surface wear produced when rocks rub against each other. Stanley (1974, 1975) defined abrasion in relation to autogenous milling as the mode of comminution by which the comminuting media are reduced by gradual breaking away of their surfaces leaving a slowly diminishing core and a gradually increasing quantity of much finer detritus. Digre (1970) suggests that abrasion is the wear of rock pieces which occurs during autogenous milling. When these pieces are sufficiently small, (about the one tenth of the dominant feed size) they are caught between larger pieces and the distribution modulus n, in the Rosin-Rammler presentation of the comminuted product by abrasion, is much smaller than unity. The hypothetical particle size distribution, resulting from eighty-nine per cent impact events, ten per cent chipping events and one per cent abrasion events has a value for n = 0,7 (Crabtree et al, 1964).

Attrition is the mechanism, by which the material particles which are small enough to be caught between larger pieces, are comminuted by the larger pieces. Attrition is thought to be a major comminuting mechanism for ball milling, while abrasion is the main comminuting mechanism for autogenous milling since a continuous size range of particles exists.

The above mentioned comminuting mechanisms are usually infered from an examination of the characteristics of the size distribution of their respective product. The whole process is thought to be controlled only by the mechanical conditions of the comminuting system i.e. geometry, mass of mill charge, mill speed and type of liners. Little attention has been paid to the physicochemical conditions of the system and how these affect the fracture of rocks. However, recent research studies have been made on the effects of the environment on the various forms of comminution. Rehbinder (1947) pioneered the idea that adsorption reduced the effective surface energy of solids , and therefore changed their mechanical properties. This may result in the enchancement of the efficiency of comminution or drilling processes. The essential feature of the Rehbinder hypothesis is that "embryo-microcracks" which are permanent points of weakness in a material are affected by the adsorption of certain environments. As an example the strength of materials has been found to be profoundly influenced by moisture (Orowan 1948, Rumpf 1959, 1972, Colback and Wiid, 1965). Orowan (1949) suggested that the concentrated stress at the tip of an elastic crack must be equal to the molecular strength of the solid, when the increments in separation of the atoms become comparable with the interatomic spacing. The stress required for fracture σ_f, can be shown to be given by $(\frac{E\gamma r}{\pi a C})^{\frac{1}{2}}$, which means that the ratio of the radius r of the crack tip to the crack length C, is of critical importance. If chemical events between surface atoms and environment aid the breaking of the bonds then the surface energy* in this equation is effectively reduced and the material will fail at much lower applied tensile load. The environment can reduce, in other words, the cohesive strength of the surface bonds and particularly the bonds at the crack tip. There have been many investigations, (Wiederhorn, 1967, Friedman, Handin & Alani, 1972 McCammond, Newmann and Natarajan, 1975) on the influence of the environment on the reduction of the effective surface energy in relation to the strength of glass, quartz and some rocks. The variation in the surface energy due to absorption is described by the Gibbs

---

*Units of γ are Jm^{-2} or Nm^{-1} and can be called as surface energy per unit area or surface tension.

adsorption equation:

$$d\gamma = RT\beta \ln p$$

where R is the gas constant
T the absolute temperature
β the number of adsorbed molecules per surface unit
and p the equilibrium pressure
can be replaced from the equation:

$$\beta = \frac{k'}{MSm}$$

where M is the molecular weight of the environment adsorbed
k' is the mass of the environment adsorbed per mass unit of the adsorbent and
Sm is the specific surface of the adsorbent
Thus: $\Delta\gamma = RT/MSm \int_0^p k' d\ln p$, and

$$\gamma_e^2 = \sigma_o^2 - (2E/MC')\Delta\gamma = \gamma_o^2 - (2E/MC')(RT/MS_m)\int_0^p k \ln p$$

where γ_o is the surface energy in vacuum and γ_e the effective surface energy in the environment and C' constant, which is function of the heats of adsorption.

The reduction of the surface energy, calculated by the above manner, has not in general been found to be in agreement with the one experimentally determined (for example Hardie and Petch, 1965). It appears, that adsorption according to the Gibbs theory, cannot adequately account for the effect of the environment on the strength of the solid.

Since chemical reactions are activated processes, fracture phenomena such as static fatigue should be activated processes, deriving the necessary activation energy from the applied stress. Accordingly the environment is expected to react most rapidly at the crack tip and change the geometrical characteristics (r/C) of the crack until the Orowan (1948) criterion for carnstrophic failure is satisfied. The hypothesis, which states that the reaction between siloxane bonds of glass and water, (Moulson and Roberts, 1960) may describe the chemical attack by the environment at the crack tip of a silicious material. In the presense of water and stress, the following reaction was suggested:

$$HO\text{-}H + (\text{-}Si\text{-}O\text{-}Si\text{-}) \longrightarrow (\text{-}Si\text{-}OH\text{-}OH\text{-}Si\text{-})$$

In the vicinity of the tip of a Griffith crack, (a region of the order of 10nm to 10μm) plastic deformation may also occur, during initial crack growth. The amount of plastic energy dissipated in this region, can be large in comparison to the surface free energy and in addition, heat may be evolved. The plastic flow will, in addition to chemical action, change the geometry of the crack tip.

Thus, two stages of crack growth can be visualized:

(i) Slow crack motion and geometry changes due to the chemical attack and/or plastic flow (Static fatigue).

(ii) A catastrophic stage of crack motion initiated when the crack geometry satisfies the Orowan (1948) criterion.

Wear and abrasion processes are considered to consist of microfracturing events. Then the processes described above will be expected to influence the rates of comminution. Hockey (1971), in his study of surface abrasion correlates the dislocations density with the fraction of work which goes into plastic deformation of alumina. Gregg (1968) suggested that the stress exerted on the particles of quartz would be expected to produce numerous near-surface dislocations. This lattice distortion may be so intense as to destroy any long range order. The existence of an amorphous surface layer, approximately 15 nm thick, was determined by Talbot and Kempis (1960) and Burton (1966) using a solubility technique.

The phenomena of near surface plastic deformation and formation of amorphous mass, cannot be expected to be independent of the environment present. Westwood and co-workers (1962, 1970, 1974, 1976) suggested that there must be a relationship between the near-surface electronic structure of the solid and the environment present, based upon chemisorption induced changes. These changes can be expected to influence the formation and motion of dislocations and hence possibly effect the plastic blunting of surface flaws and the consequently change the fracture behaviour of the material. Westwood (1974) correlated the hardness of crystalline

materials to values of zeta potential* of the material-environment interface. When the zeta potential is zero the electronic structure of the near surface region of the material approaches that of the bulk, and a maximum in hardness results.

Apart from the influence the environment may have on strength and hence on autogenous milling behaviour, other changes may result from the local temperature rise which occurs during the abrasion of two rocks or between a rock and a mill liner. (Jaeger, 1942 , Bowden and Thomas, 1954 , Rabinowicz, 1965). These temperature rises were found to be as much as 600°C during abrasion of aragonite on silicon carbide paper. Because these conditions may be similar to those in an antogenous mill, similar local thermal effects may take place and result in changes in the comminution behaviour of the material.

---

*When particles are placed in an aqueous medium they undergo an electrical rearrangement at the solid-liquid interface with the formation of an electrical double layer. A variable related to these phenomena is the zeta-potential, which can be defined as that at the shearing plane when the particle or the liquid surrounding it moves under the influence of an external potential gradient. All the phenomena, which have in common the feature that a relative motion is involved between a charged surface and a liquid environment, are called electrokinetic. The main electrokinetic phenomena used for zeta potential measurement are (a) Electrophoresis, consisting of setting up a potential gradient in a solution containing charged particles and determining their rate of motion; (b) Electroosmosis, consisting of a applied field on a fixed surface or particle in aqueous medium resulting in the movement of the mobile difuse layer and subsequently of the solution; (c) Streaming potential, a reversed electroosmosis phenomenon, consisting of a liquid environment caused to flow in a tube containing fixed charged solids resulting to an induced potential, which is measured; (d) Sedimentation potential, consisting of a potential which is induced by charged particles caused to move relative to the liquid environment, usually via a centrifugal field.

The principal objective of the present work was to assess the autogenous milling behaviour in terms of the comminuting mechanisms involved and to inquire into the inter-relationships existing between the following process variables: material structure, material strength, temperature, mill charge, mill speed and environment present. Investigations on the nature of the impact-compression comminuting mechanisms in relation to the Witwatersrand quartzite characteristics are presented in chapter two together with a classification of the petrography of the quartzite used for all the experiments described in the thesis. Chapter three presents investigations on the effects of the temperature on the rock properties in relation to comminution. The frictional behaviour of the material in relation to variables corresponding with the mill speed, mill diameter, milling environment and mill charge and its characteristics, is examined in chapter four. Studies on the comminuting mechanism of abrasion are presented in chapter five. Chapter six presents investigations on autogenous milling, with an emphasis on the milling environment. The general discussion is presented in chapter seven, while the conclusion and recommendations are included in chapter eight.

Appendix A is related to the Rosin-Rammler presentation of the distribution of the comminuted quartzite product. Appendix B presents evidence offered by Diodorus on the use of the thermal comminution. Some calculations related to the frictional testing procedures, namely the surface temperature developed during sliding and the pressure applied at the contact area of two rock specimens are presented in appendices C and D. The values of some physical properties of the used liquid environments are listed in appendix E. Appendix F describes aspects related to the design of the control system of the motors used for the rotation of the rock specimens in the abrasion testing apparatus, while design aspects of the clamping device, the power transmission joints and the idler rollers of the abrasion testing apparatus are presented in appendix G. Data of the scanning electron microscopy image analysis of comminuted quartzite particles from autogenous mills are listed in appendix H. Appendix I includes reprints of three papers published during the period the present thesis was carried out.

CHAPTER 2

THE PETROGRAPHY AND FRACTURE PROPERTIES OF THE WITWATERSRAND QUARTZITE

2.1. Introduction

An understanding of the fracture mechanisms involved in autogenous milling in relation to the nature of the material, the size distribution of the feed and resulting product, and the manner of load application is a prerequisite for developing and optimising an autogenous comminution system. Although little work has been devoted to this objective, rock failure in relation to a wide spectrum of engineering situations, is a subject extensively studied in the field of rock mechanics. The fracture mechanisms, excluding abrasion processes, involved in autogenous milling can be divided into those produced by slow compression and by free-fall impact. The study of these fracture processes, in terms of the examination of single test specimens has been the subject of a number of published works.

Uniaxial and triaxial compression tests on the Witwatersrand quartzite have shown that the behaviour of the rock under these conditions is dependent upon the microstructure of the material and the precise loading conditions. Hallbauer, Wagner and Cook (1973) correlated the compressive strength of quartzite with the petrographical type of specimen tested and found that the microcracking due to triaxial compression in a stiff testing machine was mainly transgranular and parallel to the maximum principal stress. Compression tests on various petrographical types of the Witwatersrand quartzite were also performed by Hoek (1965) and Bieniawski (1967), and their results exhibited a dependence on the rock petrography. John (1972), working on the time dependence of the fracture properties of the rocks, found that the uniaxial compression load required for the failure of the specimen is an increasing linear function of the loading rate applied for a given petrographical type of quartzite.

The tensile strength of the Witwatersrand quartzite has been examined by a number of investigators Bieniawski (1967), Hoek (1965), John (1972) employing both direct and indirect techniques.

In the direct tests performed, "dogbone" shape rock specimens were used, while in the indirect ones, as-received drill core specimens, were utilised for Brazilian tests. This type of indirect test was developed for concrete, Carneiro (1947), Wright (1958), and more recently been used by Hobbs (1966) and Jaeger and Hoskins (1966) as a sufficient method for the measurement of the tensile strength of rocks. Reproducible results, which agree with the ones found by the direct method, are obtained. In this test, cylindrical specimens are compressed parallel to a diametrical plane across which a uniform tensile stress is developed. The value of this stress at failure provides a measurement of the tensile strength of the rock. The values obtained for Witwatersrand quartzite employing both direct and indirect techniques, Hoek (1965), John (1972), were found to be dependent upon the petrography of the rock and the rate of the applied stress in a manner similar to that found for compression strength.

Free-fall impact testing techniques have been employed in order to predict the comminution behaviour of an ore for both ball and autogenous milling (Rose, 1975, Arbiter et al 1969.) Jackson (1968) developed thus free-fall impact technique for the prediction of the autogenous milling behaviour of the Witwatersrand quartzite ore. The irregularities of the shape of the run-of-mine rock specimens promote large deviations in the results and hence the performance of a large number of tests is necessary.

The described testing procedures may provide criteria which will enable one to predict the autogenous milling behaviour of a particular type of an ore. The variations of the mechanical properties found for the various petrographical types of the Witwatersrand quartzite indicate that a microscopic examination of a particular ore is also an essential prerequisite for the prediction of the applicability of autogenous milling.

A quartzite may be described as a polycryctalline aggregate which contains crystal defects and flaws and in addition precipitates of second phase particles, produced during sedimentation and metamorphism, both within the grains and at the grain boundaries.

The rock has, in general, an inhomogenous size and spatial distribution of these microstructural features, which are associated with the geological history of the material. It should be noted that the size distribution of the comminution product of the fracture mechanisms may be obtained on the basis of Griffith's theory (1921) which postulates crack propagation occurs when flaws such as the ones mentioned above are activated by stress. Gilvarry (1961), in his statistical analysis, discriminated between three different kinds of cracks, viz. those within the volume, those at the surface and those on the edges of the material. He suggested that three kinds of cracks occur according to a Poisson distribution and the probability M_p of formation of a particle of sieve size x, is $M_p = 1-\exp(^{-x}/k)$, where k is constant. Gilvary's theoretical concept will result in a slope of unity in the Rosin-Rammler presentation of the mass per cent undersize versus particle size.

There is a difficulty of establishing an uniform petrographical description of the Witwatersrand quartzite samples, since in general, this ore is a sedimentary metamorposed rock appearing in a wide range of grain sizes and mineral compositions. The natural deformations which have occured in the quartzite have resulted in a complex microstructure, including transgranular and intergranular microcracks, microcavities and dislocation structures. A large variation in the mechanical properties of the rock is therefore expected and any correlation between mechanical strength characteristics and the suitability of autogenous milling would be incomplete without a paraller examination of the rock microstructure. This chapter therefore attempts to classify the quartzite used in this study and correlate the petrography with fracture strength. The classification will be used in the following chapters in relation to thermal and abrasion properties.

2.2. Experimental Techniques and Results

2.2.1. Rock petrography

Witwatersrand quartzite is a metamorphosed sedimentary rock consisting mainly of seventy to ninety per cent by volume of quartz, two

to twenty per cent of the phyllosilicates group of minerals, 0,1 to 10 per cent of pyrite, 1 per cent or less of other sulphides, grains of primary minerals at 1 per cent or less, titanium 0,1 to 0,2 per cent, gold 25 to 45 parts per million, silver 3 to 5 parts per million and uranium in the form U_3O_8, 0,03 to 0,09 per cent. Quartz often appears in the form of "pebbles" of size up to 50 mm, while phyllosilicates appear in sheet-like structures. From the phyllosilicates group, the following minerals seem to appear more often in the Witwatersrand quartzite examined:

(i) Muscovite $KAl_2 (OH)_2 (Al Si_3 O_{10})$

(ii) Serpetine $Mg_6 (OH)_8 (Si_4 O_{10})$

(iii) Pyrophyllite $Al_2 (OH)_2 (Si_4 O_{10})$, and

(iv) Chloritoid $Mg_2 Al_2 (OH)_4 (Al_2 Si_2 O_{10})$

Both reflected and transmitted light microscopy techniques were employed, for the petrographic examination of quartzite used in this study and the quantitative mineral distribution in the quartzite sections examined, was obtained by a similar method, employing a from of 1 cm^2, with subdivisions of 1 mm^2, using the colour and pleochroism characteristics of each mineral constituent of the Witwatersrand quartzite. Characteristic petrographic data of the quartzites examined, are shown in the micrographs of the plates 1 to 4 and listed in table I.

The grain size of quartzite was determined via the Teusher counting method (Niggli, 1954) by laying a counter on the thin or polished section and then counting the number of grains enclosed by the frame, of 1 cm^2 area. The square root of the specific number of grains, as defined the number of grains per cm^2 obtains the mean grain size of the rock. This counting method, applied for ten random positions on a polished or a thin section, was used for the determination of the average grain size of the rocks examined.

The grain size of the Witwatersrand quartzite examined, was found to vary in the range from 100 μm to 2,3 mm, while the average grain

size, found to vary in the range of 300 μm to 2 mm. The determination of the average grain size in relation to strength (Table I) allowed us to classify the material into the following four types:

(a) Fine grained quartzite, designated as A (100 to 750 μm), (Plate 1).

(b) Fine to medium grained quartzite, designated as B (300 μm to 1,1 mm), (Plate 2).

(c) Medium grained quartzite, designated as C (200 μm to 1,5 mm), (Plate 3) and

(d) Coarse grained quartzite, designated as D (400 μm to 2,3 mm)

The frequency of the microstructural defects such as microcracks, cavities and inclusions was determined by counting the number of defects per cm, at 10 random directions.

The relative frequency of the intergranular and intragranular defects was found to be 38 per cent to 62 per cent respectively for a coarse grained quartzite while, for a fine grained, was 56 per cent to 44 per cent respectively.

In order to study the fracture morphology by scanning electron microscopy small fragments of the quartzite samples were mounted on metal stubs and coated under vacuum with a gold palladium alloy in order to attain a conducting surface layer of approximately 30 nm thickness. A Cambridge Stereoscan 180 scanning electron microscope was used to investigate the fractography and to obtain the photomicrographs. Fracture patterns are indicative of transgranular cleavage fracture in the case of the Brazilian tests specimens of type C, while separated phyllosilicates flakes are indicative of intergranular fracture (Plate 5). Similar features can be observed during the examination of the particles produced by a test of the compressive strength of the rock of type C (Plate 6, 7).

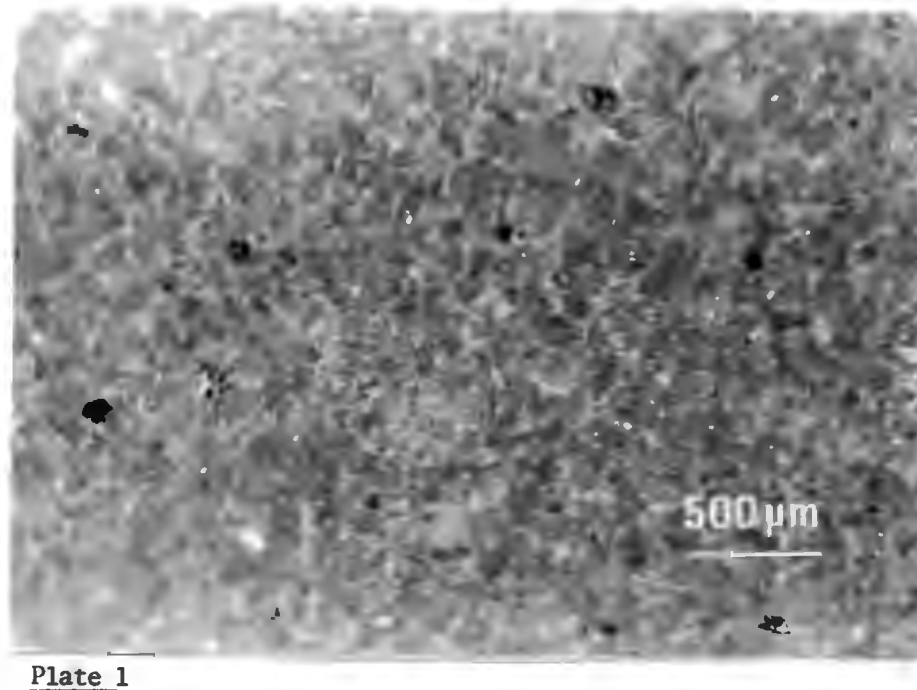

Plate 1

Light optical photomicrograph of quartzite A.

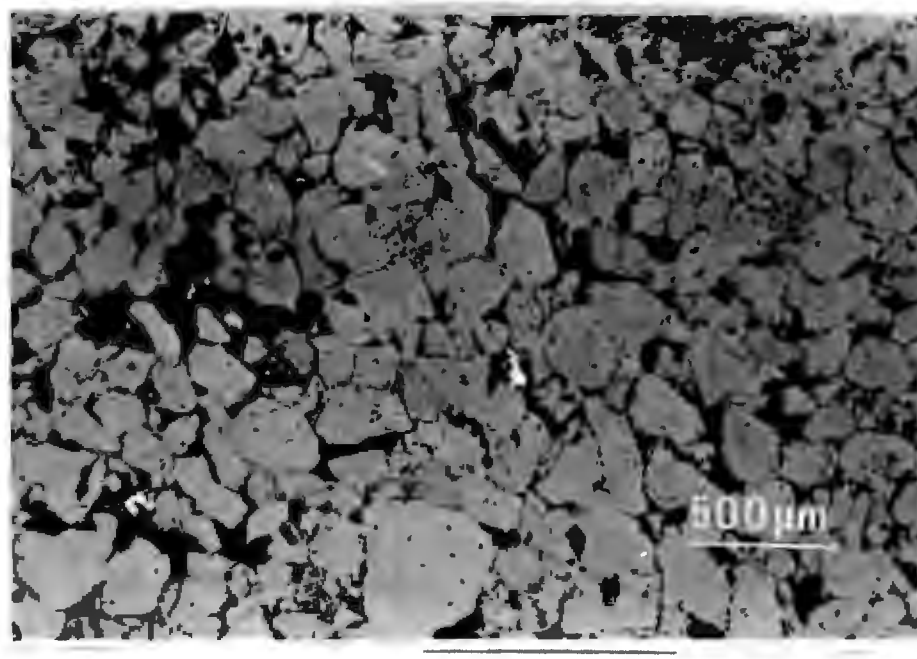

Plate 2

Light optical photomicrograph of quartzite B.

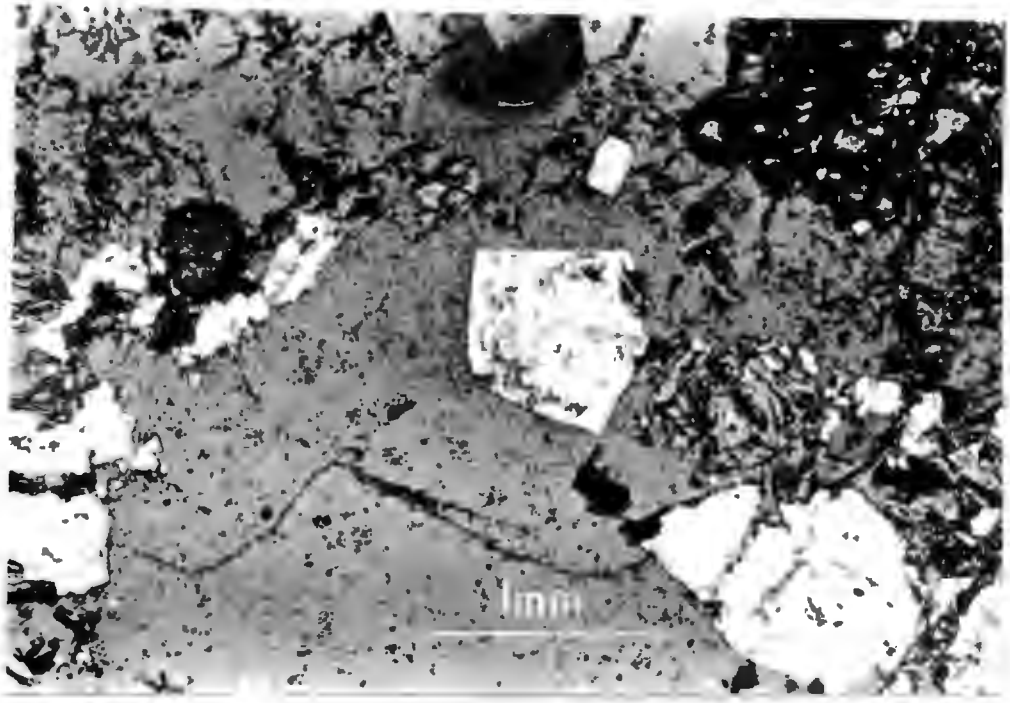

Plate 3

Light optical photomicrograph of quartzite C.

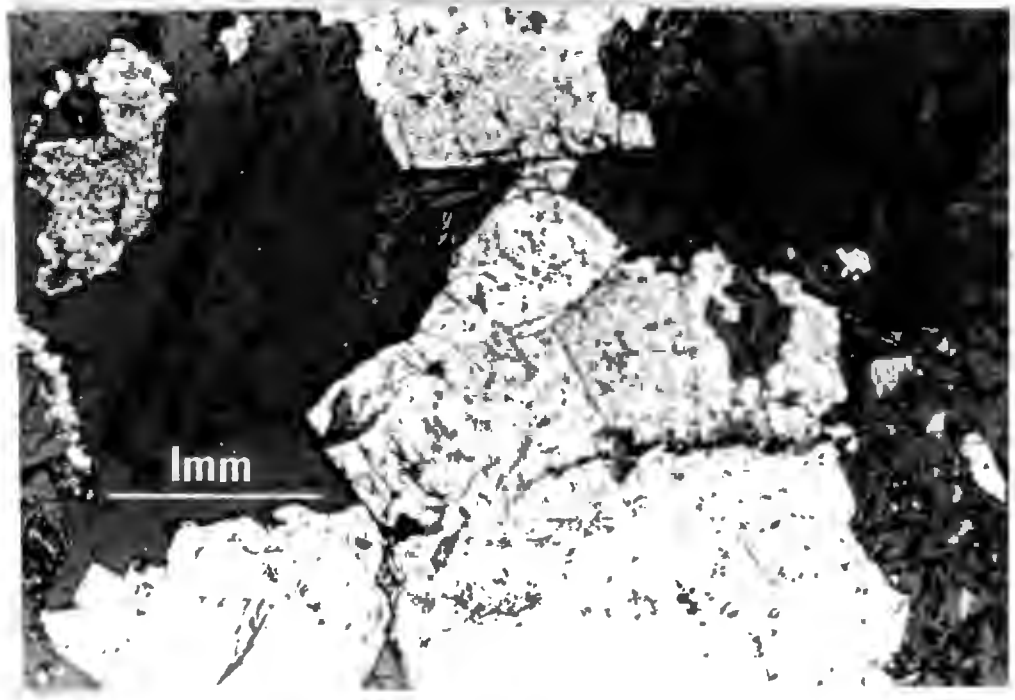

Plate 4

Light optical photomicrograph of quartzite D.

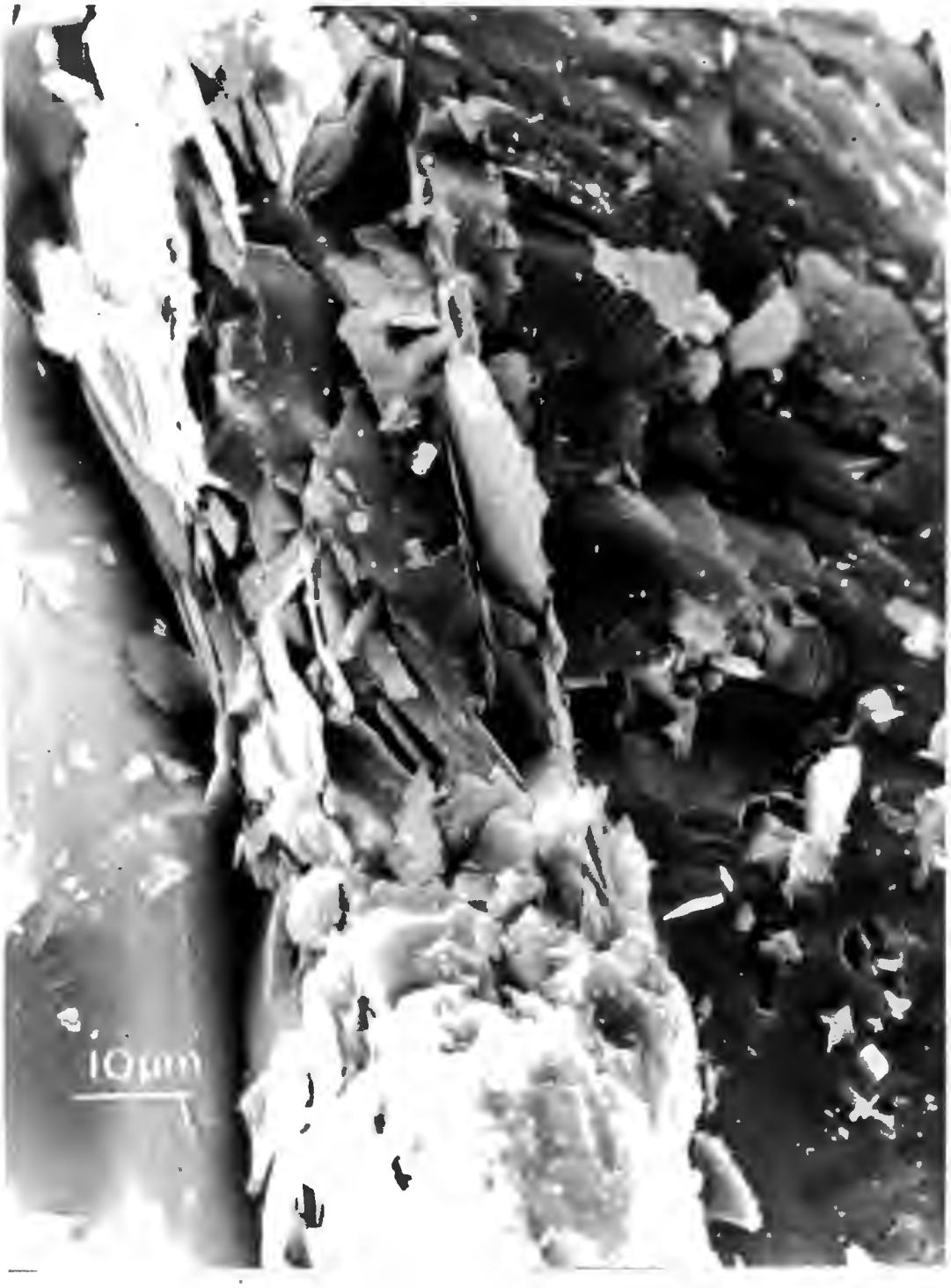

Plate 5

Fracture surface of a Brazilian test on a quartzite C specimen showing phyllosilicates flakes indicative of intergranalar fracture.

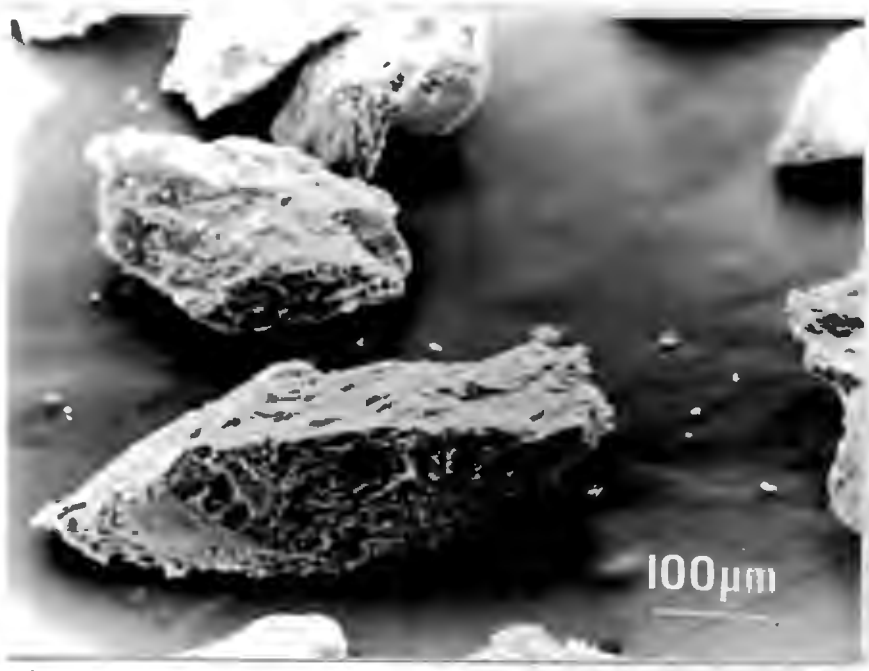

Plate 6

Quartzite particles, taken from the comminuted product of a compression test.

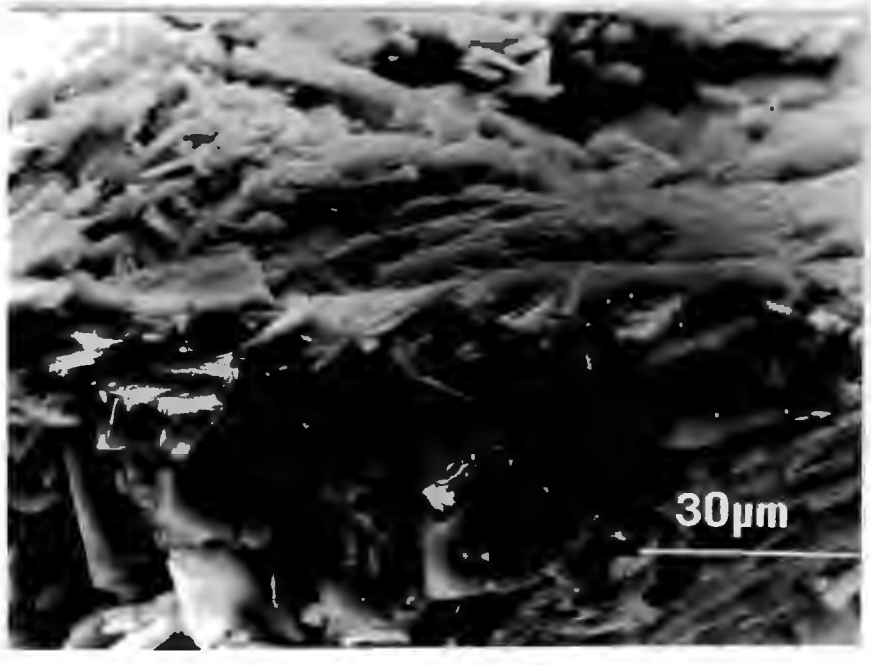

Plate 7

Surface morphology of the lower particle, shown in plate 6.

2.2.2. Brazilian and compressive strength tests

An Instron Universal testing machine of 89 kN capacity was used in the first series of Brazilian tests, on specimens of 25,4 and 32,2 mm diameter. The testing of specimens of 42,2, 50 and 60 mm diameter, was performed by an ESH servo-hydraulic universal testing machine of 250 kN capacity. A displacement rate of $4{,}23 \times 10^{-7}$ ms^{-1} was used in both cases. Quartzite drill cores of 25,4 ($\pm$ 0,2), 32,4 ($\pm$ 0,1), 44,2 ($\pm$ 1), 54,6 ($\pm$ 2) and 60,2 ($\pm$ 0,1) mm diameter and 50,0 mm ($\pm$ 0,2 mm) long were compressed diametrically between two parallel steel plattens. Plywood packing strips, 6 mm thick, were used between the plattens and samples in order to maintain a more uniform loading conditions. Three tests on the same drill core were performed, while the petrographic characteristics of each core used were examined.

The results of the petrographic examination together with values of tensile fracture stress σ_t, obtained from the equation $\sigma_t = 2P/\pi lD$, where P the fracture load, l the length and D the diameter of the specimen, are shown in tables I and II.

The values of the compressive load at which the test specimens were fractured, presented as the mean value of three separate tests for specimens taken from the same drill core, (types A, B, C, D) are presented in figure 1. The values of σ_t which are taken from these tests are shown in figure 2. The influence of the size upon the load required for fracture of quartzite specimens of type B is shown in figures 1, 2. Parallel ended quartzite drill core specimens of 25,4 ($\pm$ 0,2) mm diameter and 50,0 ($\pm$ 0,2) mm long, were compressed between two steel plattens in the ESH-testing machine using upper platten displacement control, in order to determine the uniaxial compressive strength of the rock. Table III shows the values of the compressive strength σ_c obtained which were obtained by the four petrographical types of the Witwatersrand quartzite.

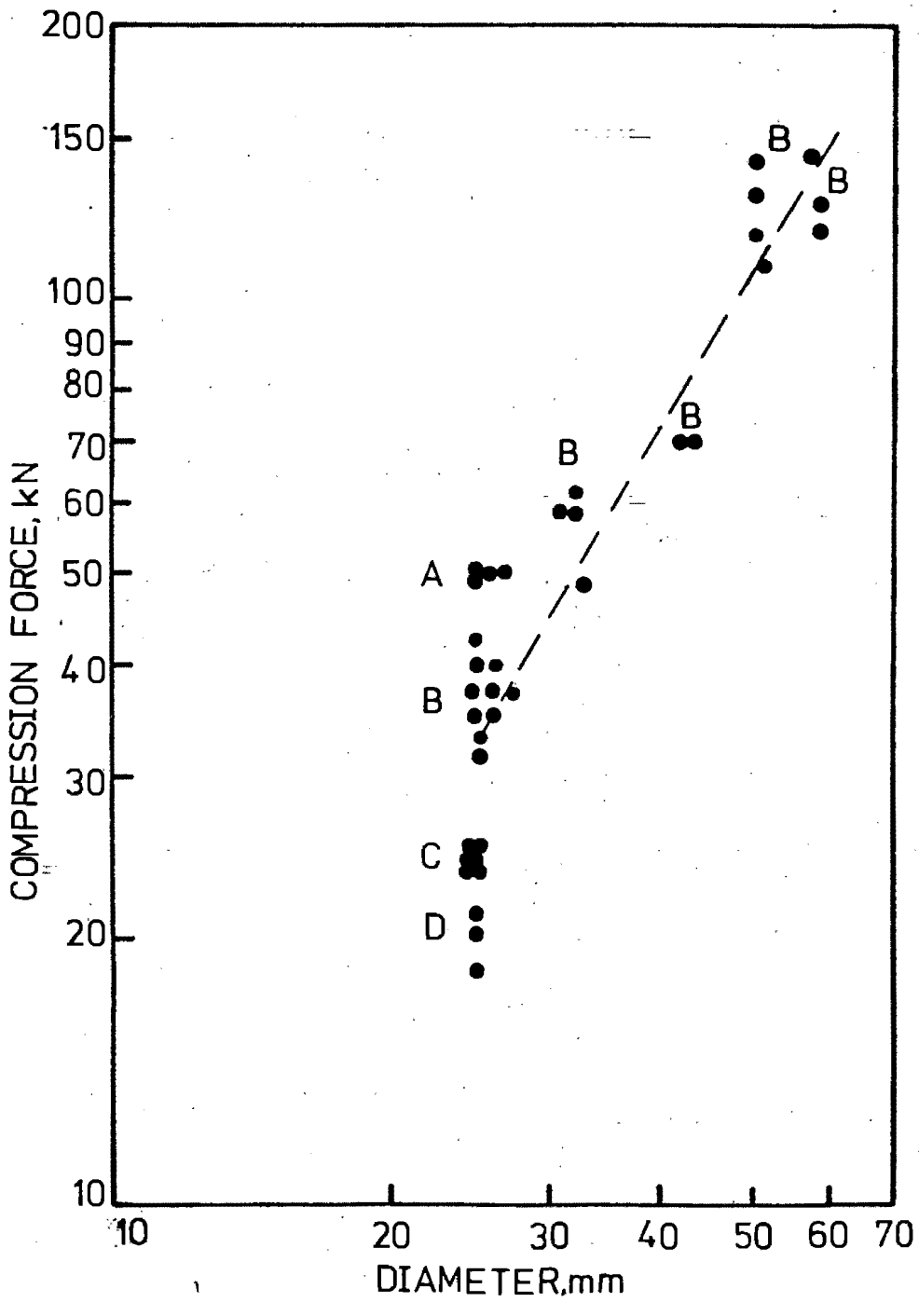

Figure 1

Relationship between compressive force required for fracture and diameter of cylindrical quartzite specimen, for various petrographic types of rock.

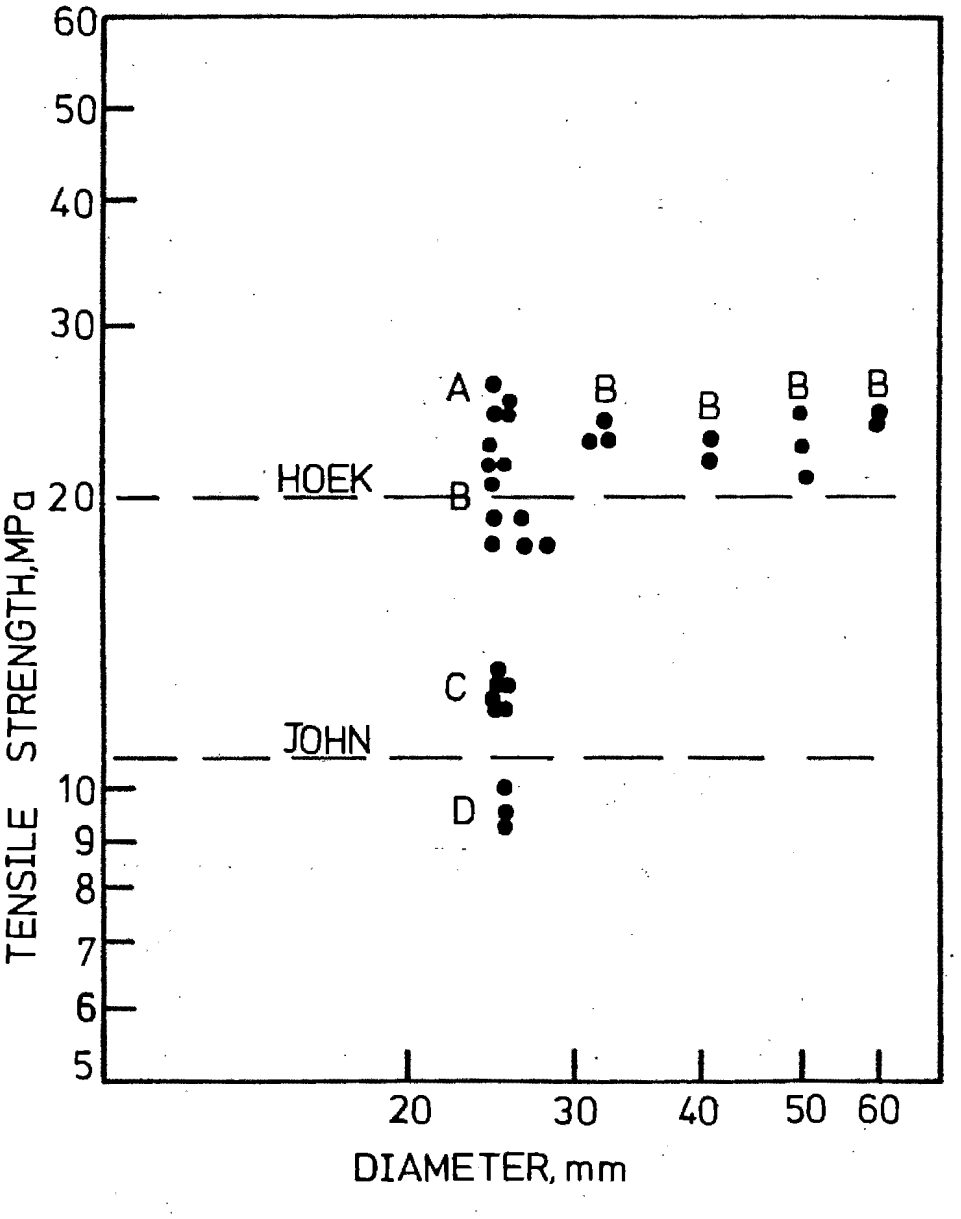

Figure 2

Tensile strength of various petrographical types of the Witwatersrand quartzite, determined by the Brazilian test. The values of the tensile strength of the Witwatersrand quartzite, determined by direct tests (Hoek, 1965, John, 1972) are also shown.

The strength of the quartzite specimens tested was indeed found to be dependent upon the petrographical data of each specimen. Large grain size was found to correspond with low compressive and tensile strength, while small grained correspond with high strength. The A and D quartzites were found to obtain the maximum and the minimum strength, respectively. The mineral composition characteristics, were also found to influence the strengh of the rock. Muscovite mainly and the other phyllosilicates were found to decrease the strength of the material, when they are found to represent a large fraction of the quartzite mineral constituents. The presence of pyrite in a high percentage was found to be associated with a large average grain size, and subsequently with low values of strength. Pyrite, present in small quantities was also found to reduce the strength of the rock.

2.2.3. The free-fall impact tests

Run-of-mine rocks, of approximately 5 kg mass, were tested for their free-fall impact behaviour. The rock specimens were dropped onto a massive steel plate of 0,8 x 0,8 x 0,05 m dimensions, from a release device which was set at heights of 3 and 4 m above the plate. The testing procedure used was similar to the one proposed by Jackson (1968) and consisted of fifty free-fall tests for each specimen, with a weight measurement of the largest remaining piece after every ten successive drops.

The results of tests performed for three different rocks, two of type B and one of type A, are shown in figure 3. For one specimen of type B, a number of 100 free-fall tests from the height of 4 m was performed.

The shape of the graphs indicates that the fracturing of sharp edges and corners takes place in a continuous manner after an initial number of drops has propagated flaws in the rock piece and produced fragments, which are approximately 50 per cent of the initial weight.

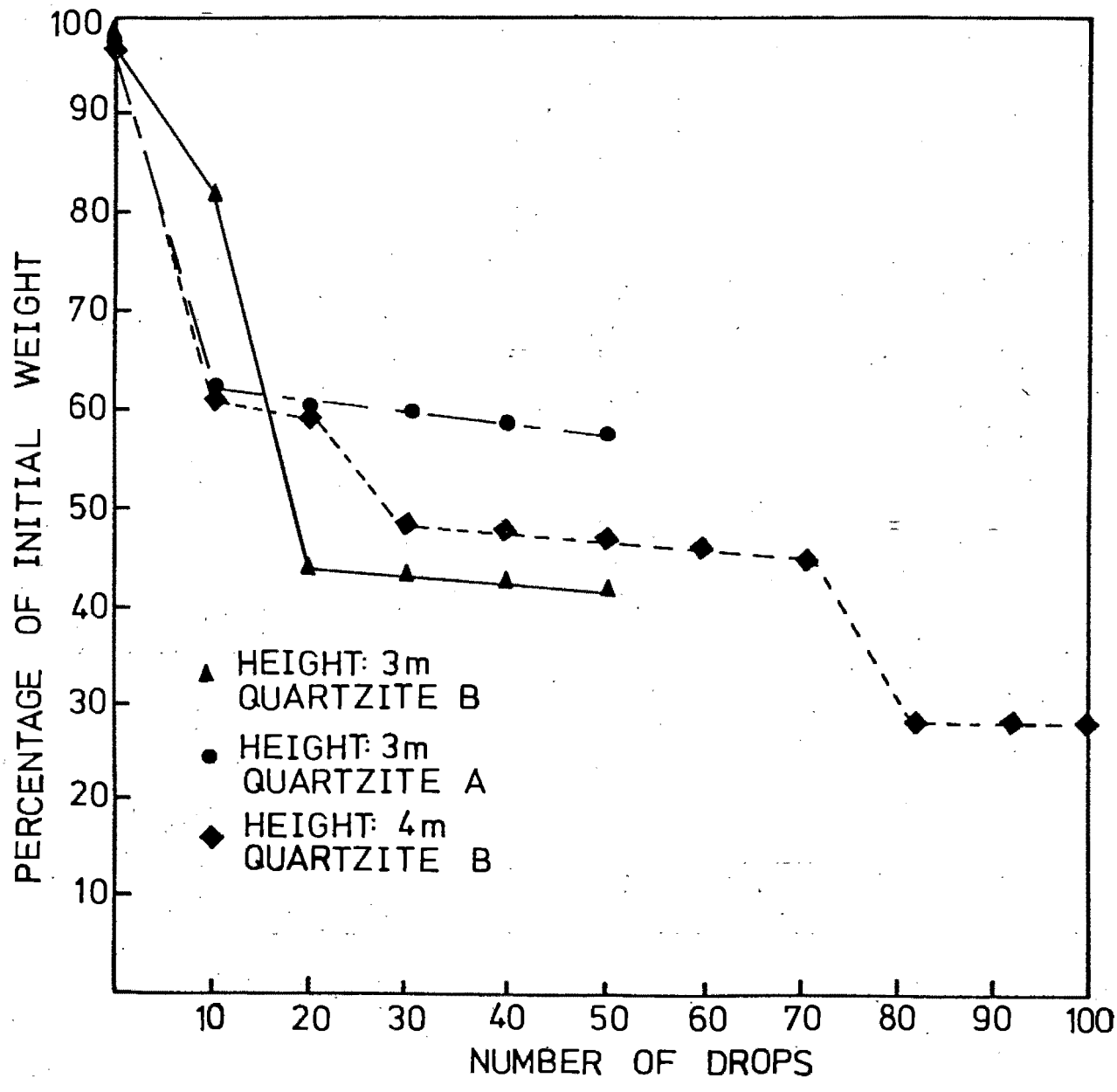

Figure 3

Relationship between weight of largest piece as a percentage of initial weight and total number of drops, taken from free fall impact tests on quartzites A and B.

TABLE I

Mineralogical composition, grain size and tensile stength characteristics of various types of the Witwatersrand quartzite, designated as A, B, C and D.

Mineral Composition, Per Cent by Volume			Grain Size, μm					
Quartz	Phyllosilicates	Primary Minerals	Min	Max	Average	Class	Type	σ_t MPa
90	9,9	0,1	100	500	300	Fine	A	23,2
92	7,9	0,1	100	750	500	Fine	A	24,9
88	11,7	0,3	300	900	700	Fine to Medium	B	22,8
86	13,8	0,2	300	1100	800	Fine to Medium	B	21,3
79	20,0	1,0	200	1400	1100	Medium	C	14,1
77	21,3	1,7	400	1500	1200	Medium	C	13,3
69	22,0	9,0	400	2300	2000	Coarse	D	10,2
71	19,0	10,0	600	2100	2000	Coarse	D	9,3

TABLE II

Classification of various petrographical types of the Witwatersrand quartzite via the tensile strength of the rock specimens

TYPE	σ_t, MPa	MEAN VALUE, MPa
A	24,2	
A	24,9	
A	24,2	
A	23,4	23,9
B	22,8	
B	21,3	
B	21,5	
B	19,2	
B	19,4	
B	18,7	
B	18,3	
B	18,2	19,9
C	14,1	
C	13,3	
C	13,2	
C	12,9	
C	12,4	
C	12,4	13,0
D	10,2	
D	9,3	
D	9,1	9,5

TABLE III

Uniaxial compressive strength of quartzite

TYPE	σ_c, MPa	MEAN STRENGTH σ_c, MPa
A	284,4	
A	257,3	
A	266,1	269,3
B	238,0	
B	219,7	
B	235,1	
B	241,1	233,5
C	193,0	
C	207,2	
C	200,9	
C	175,4	194,2
D	66,1	
D	59,4	
D	97,0	
D	45,9	67,1

CHAPTER 3

THE THERMAL WEAKENING IN COMMINUTION

3.1. Introduction

A large fraction of the mechanical energy input into a comminution system is dissipated as heat during the fracture of the rock particles (Kidybinski, 1973) or during friction phenomena between the rock particles and components of the mill charge (Jaeger, 1942). Although the mean temperature increase is very small, local temperature rises during friction of rock surfaces can be as high as 500°C (McPherson, 1973). This temperature rise may have an influence on the fracture behaviour of rocks. Schönert, Umhauer and Klemm (1969) reported that the slow crack propagation in glass was dependent on temperature from 20 to 100°C. Also the thermally induced internal stresses in rocks may add another type of comminuting mechanism, to those of impact, chipping and abrasion. A comminution method may be established by using heat as the only form of energy input or by a judicious combination of heat and other forms of energy in order to overcome the limitations of the conventional methods.

3.1.1. The use of thermal treatments

The application of heat for the comminution of rocks is one of the oldest methods of the mining and mineral technology as evidenced by the considerable quantity of charcoal and wood ash found in ancient workings. This technique, known as firesetting in archeology, was a standard practice used from prehestoric times to aid mechanical methods. Diodorus Siculus (1st century B.C.) gives the first description of a mining method which includes a thermal treatment of the ore as part of the comminution process. Rocks containing gold were heated by a fire for a long period and while the rocks were still hot, impact was applied by iron bars, resulting in the breakage of the rocks without an excessive manual effort (see appendix B). Pliny (1st century A.D.) describes a mining technique, called "igne et aceto", which consisted of the heating and quenching of limestone rocks. A careful study of Pliny's writings makes clear the following facts. Firstly the rocks were heated by the means of a fire; secondly, water was poured on the hot rocks; thirdly, vinegar was poured, which slowly attacks certain rocks of limestone type. The technique was applied by

Chakravarti and Jowett (1967) examined the beneficial effects of thermal treatment on the comminution of quartz, calcite, feldspar and other minerals. They used a laboratory stamp mill and a tumbling mill. Grinding was done dry, mostly for 100 seconds and substantial increases in grinding rate were apparent after heat treatment. Thirumulai and Demou (1970), examined the rock fracture caused by internal thermal stresses during heating and cooling in atmosphere and vacuum. They studied the microstructural damage between adjacent grains of granodiorite specimens after tests for thermal dilation. They found that the structural damage of the rock was caused by thermal stresses induced in rocks during thermal expansion cycling below 300^{o}C. Thirumalai and Cheung (1974) examined the principles and effectiveness of combination methods for the comminution of rocks using thermal energy to initiate subsurface fractures and rock weakening. A thermohydraulic method for primary breaking and a thermomechanical method for secondary breaking were examined. The potential of a thermomechanical method was also examined with the help of theoretical and laboratory tests on rock spheres. They found that this method reduces the comminution energy requirement in comparison to the thermal treatment used alone, and significantly improves the size reduction of hard rocks. Geller and Tervo (1975) investigated the combined thermal-mechanical comminution of quartz. The quartz $\alpha \rightarrow \beta$ phase-transformation did not appear to be of importance in the effects of the thermal treatments. The quenching of the heated material was found to be an important factor in determining the efficiency of the process. Moore and Sibson (1977) examined thermal fragmentation of rocks in relation to seismic faulting and suggested that surface damage was caused by heat, during slip on a seismically active fault.

3.1.2. A consideration of thermal fissuring

The importance of introducing high densities of sharp cracks or fissures into quartzite which would subsequently act as crack nuclei during the comminution process has been investigated by Rumpf (1973) and Kanellopoulos and Ball (1975). The later authors considered the

energy balance from which the Griffith fracture criterion is based and the stress criterion of Orowan. A high density of sharp cracks is necessary if a low mechanical energy comminution process is to be achieved. The required fissuring could be produced by thermal techniques on account of four types of stresses viz:

(i) The trigonal symmetry of α-quartz is manifested in the anisotropy of the coefficients of thermal expansion. The coefficient of expansion along the C axis is $7,5 \times 10^{-6}\ K^{-1}$ and normal to the C axis the expansion coefficients have the value of $13,7 \times 10^{-6}\ K^{-1}$. Thus on heating or cooling of a polycrystalline quartzite sample, stress will be generated due to the misfit of any one grain with respect to the surrounding matrix. An estimate of the misfit can be made in the following way. Consider the removal, at a given temperature, of a spherical anisotropic grain of unit diameter from the average matrix. Now, on change of temperature ΔT, the hole will have increased (or decreased in the case of cooling) its diameter by $10,6 \times 10^{-6} \times \Delta T$, and the grain will have changed its dimensions by $7,5 \times 10^{-6}\ \Delta T$ and $13,7 \times 10^{-6}\ \Delta T$ along and normal to the C axis respectively. The resulting stresses will be about 40 MNm^{-2} and 120 MNm^{-2} if the grain is imagined to be made to refit into the hole.

(ii) The maximum triaxial tension which can be developed at the centre of sphere of quartz with a radius b of 10 mm, an average thermal conductivity $k_{th} = 8,9\ W\ m^{-1}\ K^{-1}$, a specific heat $c = 1,18 \times 10^{3}\ Kg^{-1}\ C^{-1}$, density $\rho = 2,6 \times 10^{3}\ kg\ m^{-3}$, a mean coefficient of linear thermal expansion $\alpha = 10,6 \times 10^{-6}\ C^{-1}$ and Young's modulus $E = 100\ GNm^{-2}$, when it is subjected to a sudden increase in temperature ΔT is given approximately by $t_{\Delta T} = 0,38\ \alpha\ E\ \Delta T$. The maximum tensile stress is attained after the time $t = 0,057\ b^{2} c \rho k^{-1}$. Thus in the present case the stress will reach 200 MNm^{-2} in about two seconds when suddenly heated to 200°C and 360 MNm^{-2} in a similar time when suddenly heated to 600°C. Temperature gradients produced on rapid cooling will produce stresses of similar magnitudes.

(iii) The stresses generated during the decompostion of mineral constituents such as pyrite is difficult to estimate but the volume

changes and the release of gaseous products may well be sufficient to initiate flaws. The oxidation and decomposition of pyrite takes place between 590°C and 680°C (Kopp and Kerr 1957, Levy 1968, (Reference Deer, Howie and Zussman, 1962). In the presence of iron oxides the following reaction takes place:

$$FeS_2 + 3Fe_3O_4 \underset{\longleftarrow}{\overset{T = 675^oC}{\longrightarrow}} 2FeS + 4Fe_2O_3$$

pyrite magnetite **pyrrhotite** haematite

Fine grained muscovites show an expulsion of absorbed water below 400°C and at temperatures up to 900°C the expulsion of their structural water takes place (Deer et al, 1962). Pyrophyllite is dehydrated between 640°C and 850°C. In lower temperatures, this phyllosilicate remains stable. Thermal decomposition of serpetines (Chrysotite, Lizardite, Antigorite) takes place at about 600°C. A characteristic reaction describing the decomposition of serpetine is:

$$2\ Mg_3Si_2O_5(OH)_4 \underset{\longleftarrow}{\overset{T = 600^oC}{\longrightarrow}} 3\ Mg_2SiO_4 + SiO_2 + 4H_2O$$

Serpetine **Forsterite** Amorphous silica

(iv) During the $\alpha \rightarrow \beta$ transformation in quartz at 573°C, there is sudden change in density. The volume increases by 0,86 per cent at the phase change and the axial ratio of the structure shows a discontinuous change. On heating a sample of quartz or quartzite through the transformation temperature internal stress will be produced on account of the volume change at the interface between untransformed regions and transformed regions. Very uniform heating would be required to avoid this cause of stress. If the anisotropy of linear dimensions is ignored then the introduction of a small volume of α-quartz in place of an equal mass of a-quartz would result in an "unconstrained" strain of $^1/_3 \times 8{,}6 \times 10^{-3}$ and a constrained strain of $^2/_9 \times 8{,}6 \times 10^{-3}$ or about 2×10^{-3}.

It can be seen that the strains generated for the reasons considered above can attain values in the region of 2 to 3×10^{-3}.

The magnitude of the resulting tensile stress which may induce cracking is not easy to assess since the shape of the particles and grains will not be spherical as assumed in the above treatments. Stress concentration geometries may increase the stress to values above those calculated above viz. 40→300 MNm^{-2}. The criterion for fissuring will then be the relative magnitude of the stress created and the measured strength of unnotched crystals and transgranular strength of quartzite. The former is given as 83 to 110 MNm^{-2} while the latter will be considerably smaller. It can thus be concluded that considerable microfracturing will be produced and by supplying a rapid temperature increase to about 600°C. Further cracking could be produced by a subsequent quench from this temperature.

3.2. Experimental Techniques and Results

3.2.1. The heating and quenching of the tensile strength testing specimens

Brazilian tensile tests were made to compare directly the fracture energy requirements of heated and unheated specimens of the Witwatersrand quartzite of type B (Chapter 2). Cylindrical rock specimens of 25 mm diameter and 50 mm long, were used for the elevated temperature tests. A fluidised sand bath furnace was used to heat the specimen under uniform and constant temperatures in the range 100°C to 600°C. A feedback signal control maintained for this furnace the desired temperature for every test, (with a error smaller than $\pm$ 3°C). Another muffle furnace, was used for heating to temperatures, in the range 500°C to 1000°C. This furnace, in which the temperature distribution was less uniform than the one of the fluidized sand bath, was controlled by a thermostat with a maximum error of $\pm$ 15°C. After the heating of the rock specimens for standard times of 15 minutes, a quench into a room temperature water bath in less than 30 seconds was performed. After the thermal treatment, the specimens were dried and tested in the Instron Universal machine, according to the technique described in chapter 2.

The values of tensile strength obtained from rock specimens of type B after quenching from various temperatures are shown in figure 4. The strength falls continually with heating temperatures and a 50 per cent reduction is achieved by heating the rock at 600°C and quenching in water.

3.2.2. The examination of the thermal expansion

Dilatometry was carried out on the three petrographical types (B, C and D), of quartzite rock and synthetic quartz (parallel to Z axis) samples. Specimens relatively free of cracks and defects, were carefully chosen and cut to the dimensions: length; 49,20 to 49,70 mm; width: 3,00 to 3,50 mm; and height: 3,00 to 4,00 mm. Moderate rates 8°C/min. of heating or cooling of the tubular shaped furnace were controlled by a thermostat maintaining the desired temperature with a maximum error less than 0,8°C. A continuous measurement of the strain indicator output and the thermocouple output was obtained by a system operating via reflected light beams. Thermal dilation measurements were carried out for temperatures up to 900°C.

The results of the dilatometry on quartzite and quartz specimens are shown in figure 5. The curves for the thermal expansion of quartz crystals are very similar and approximate to those previously published (Kosu and Saiki, Reference Sosman, 1927).

It should be noticed that the quartzite specimens (type D), which contain pyrites in their matrix in a reasonable quantity, show large dilations at temperatures above 600°C. This may take place due to decomposition or oxidation of pyrites, which was previously discussed (3.1.2.) The permanent deformations measured after slow cooling from various temperatures, are shown in figure 6 for types B and D. The curves shows a smooth exponential increase with temperature and no discontinuity at the $\alpha \rightarrow \beta$ transition temperature. The permanent deformations are presumably due to microfractures which have resulted from the large strains generated during mineral transformations.

3.2.3. The size distribution of the product of comminution achieved by both thermal and mechanical methods

Run-of-mine quartzite rocks type D were selected and cut into the

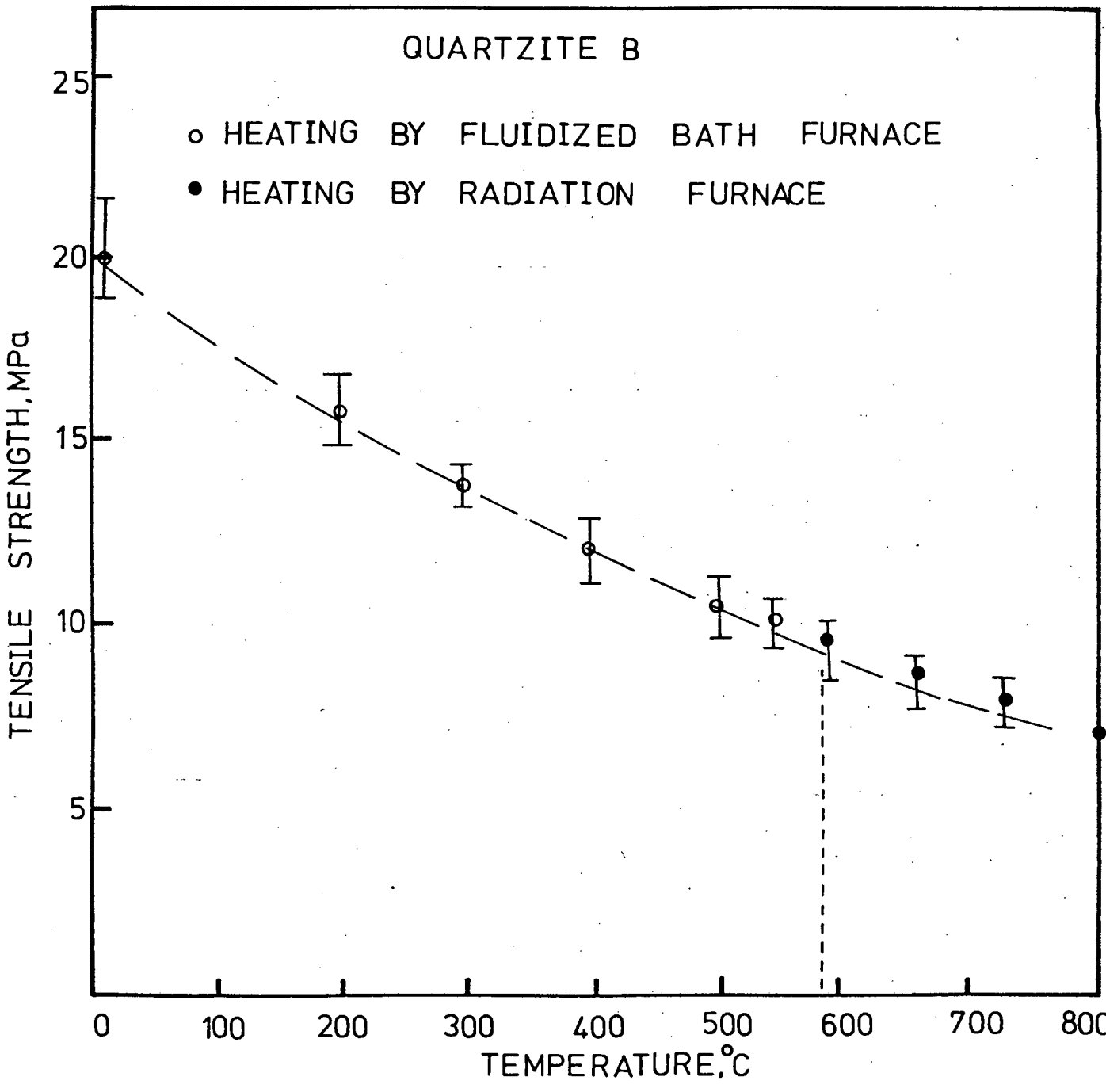

Figure 4

Influence of the temperature of heating on the tensile strength of quartzite.

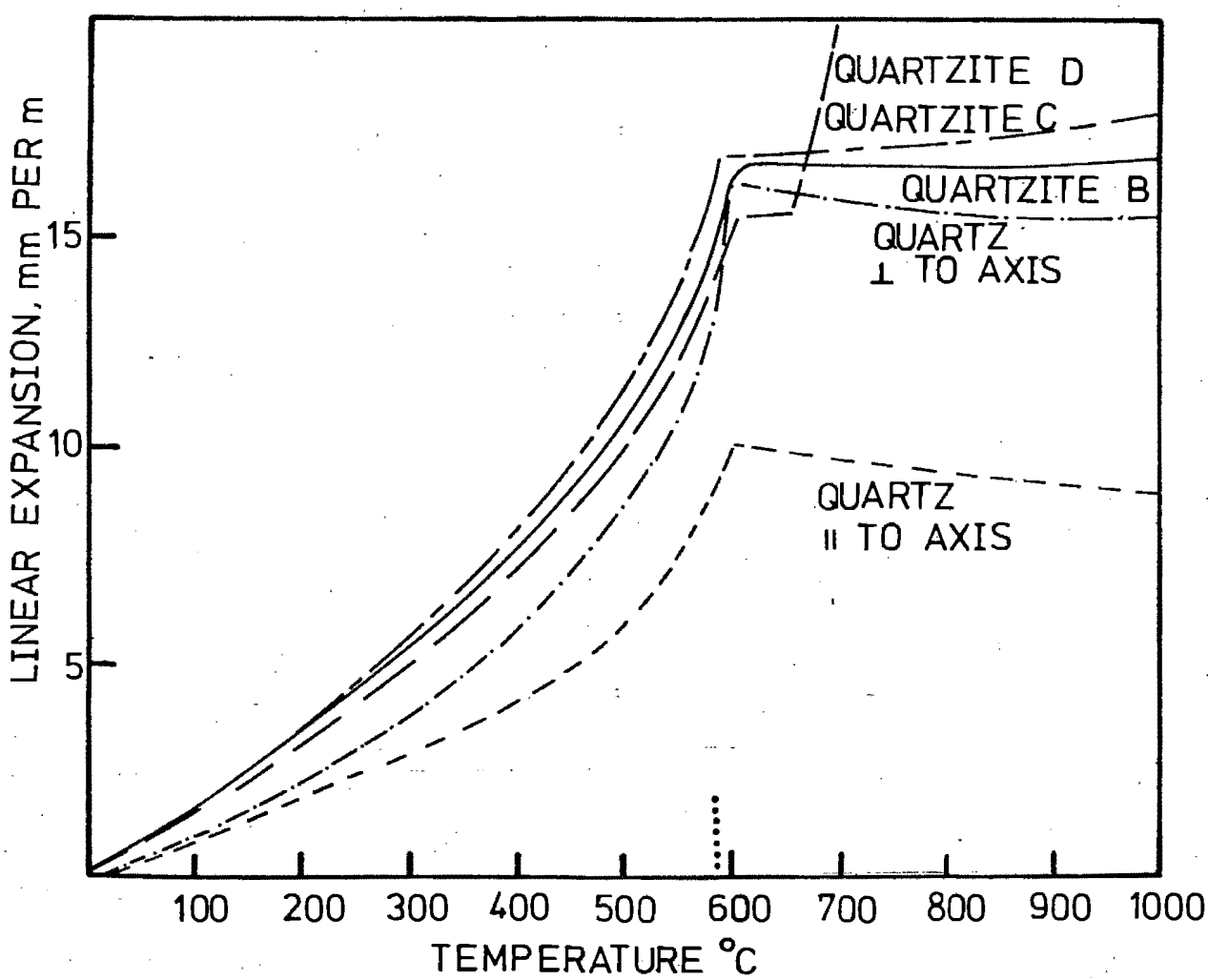

Figure 5

Relationship between linear thermal expansion and temperature of heating for quartzites B, C and D and for synthetic quartz.

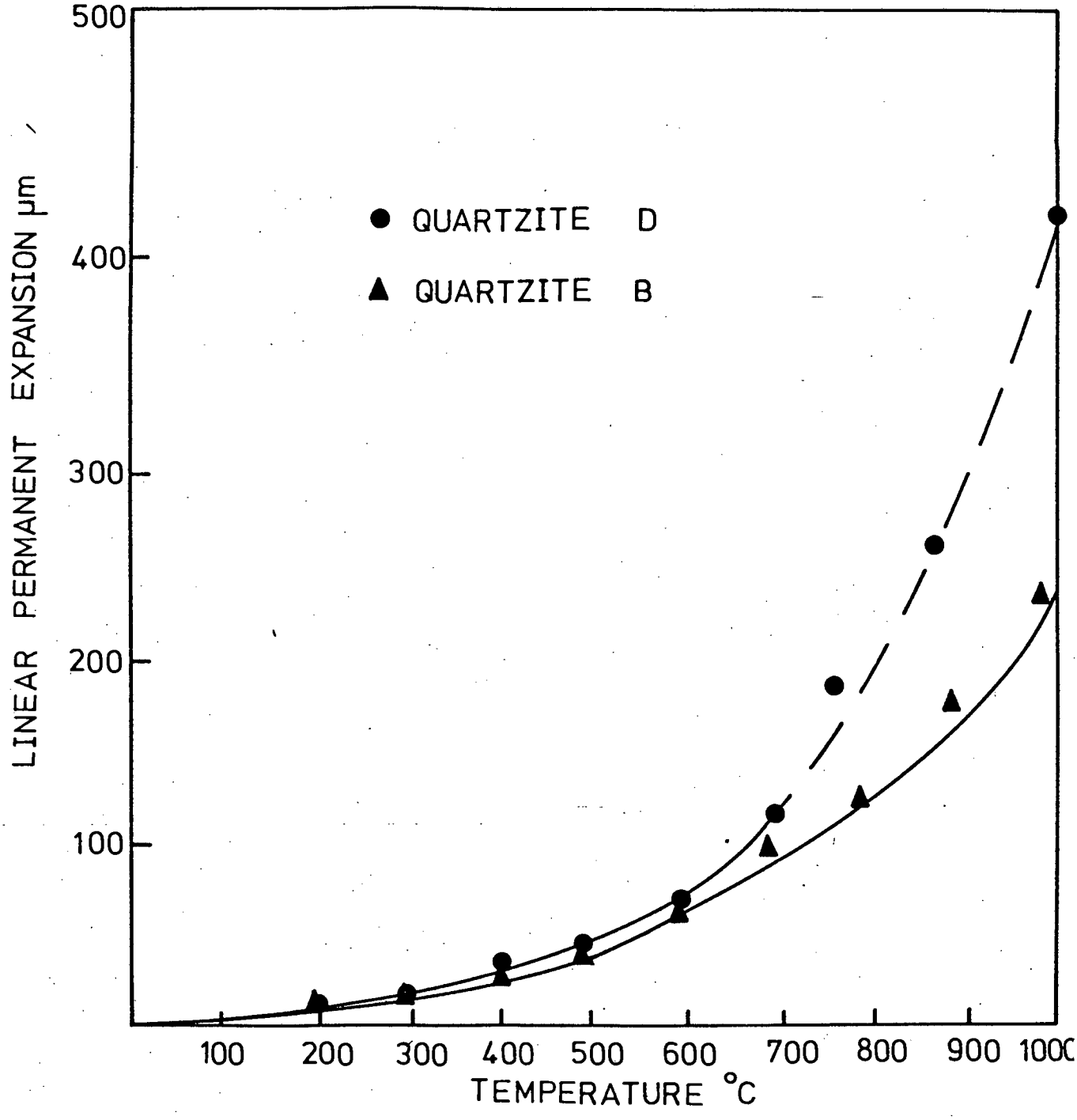

Figure 6

Relationship between permanent linear expansion and temperature for the petrographical types B and D of the Witwatersrand quartzite.

shape of cubes of 10 mm a side. The rock cubes were heated in a radiation furnace which had been set at given temperatures, from 400 to 800°C. The quenching of the heated specimens took place in a running water bath. The cubical specimens were comminuted by compression, between the two parallel plattens of the Instron Universal Testing machine. The product was dry-screened by a laboratory screen vibrator for standard volume of vibration with equal periodical intervals for total screening times of 20 minutes. The size distribution analysis of the comminution product of the compressed quartzite cubes is shown in figure 7, where the weight per cent retained on screen of stated size is shown. This way of presentation of the comminuted product, shows us that the heating at 400°C, 600°C, 700°C and 800°C and the subsequent quenching in water obtains a finer product than the untreated quartzite, and the comminution is improved as the treatment temperature rises. Presenting the size distribution of the thermally treated and comminuted quartzite specimens according to Rosin-Rammler (Appendix A), a slope of unity was found for the product of a single comminution event of both untreated and heat treated at 400°C and quenched in water rock specimens (figure 8). Different size distribution was presented by the product of rock specimens heated at temperatues higher than 400°C and quenched in water.

3.2.4. The reduction ratio and the number of particles produced by heating at various temperatures for increasing times and quenching in water

Run-of-mine quartzite rocks, (type D) of volume 200 ml (deviation ± 20 ml) were selected for this experiment. The heating of the rocks took place in a fluidised bath furnace for standard times and the quenching (< 30 seconds) in a water bath. For a limited number of experiments, the quenching took place in a vinegar bath. After each heat treatment the rock specimens became very friable and disintegrated with little or no applied stress. The particles of the product of each thermal treatment were measured and counted. The reduction ratio R, defined as the ratio of the diameter of the parent particle to the diameter of the largest daughter particle, and

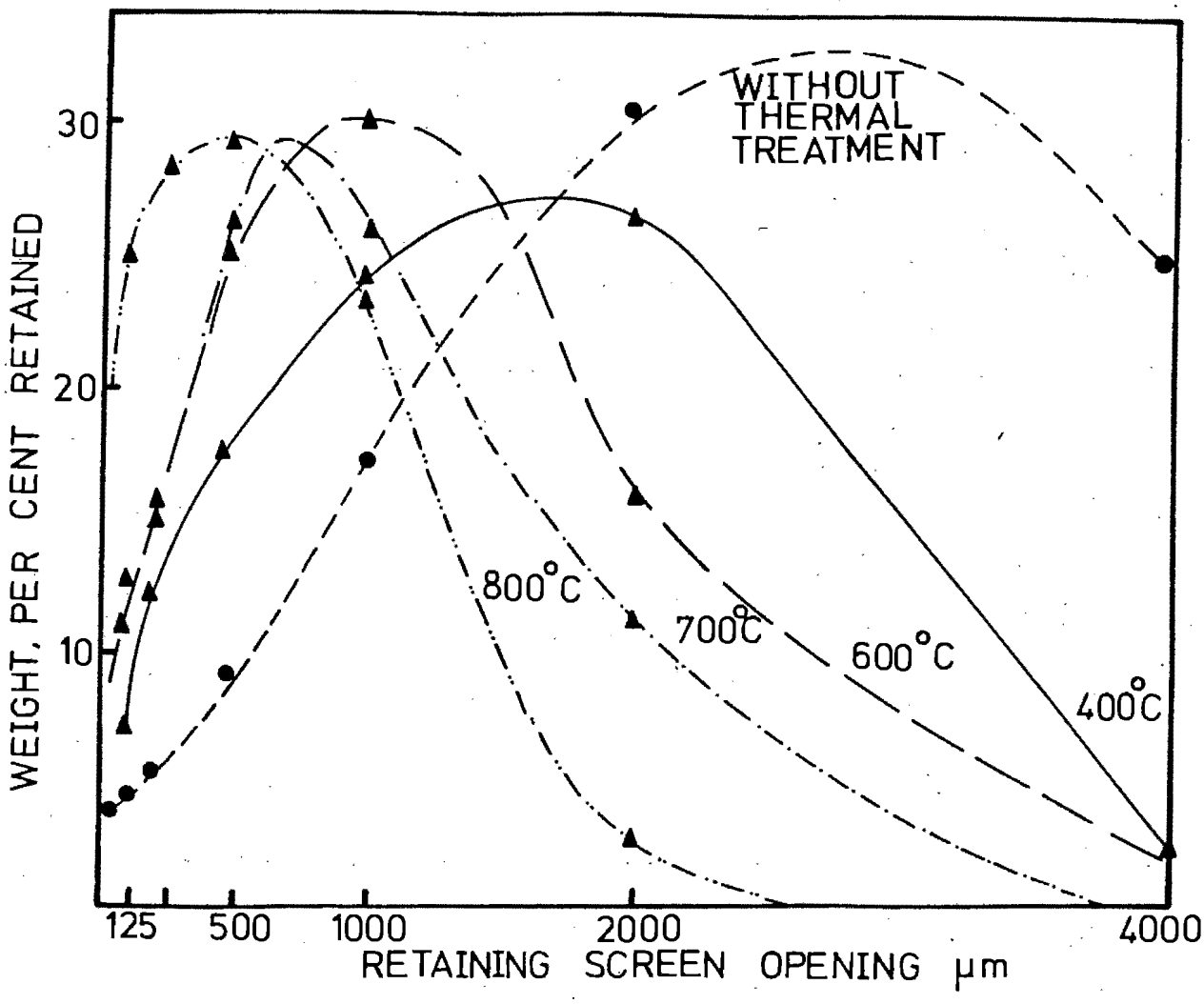

Figure 7

Size distribution of comminuted quartzite by compression, after prior heating at stated temperatures and quenching in water.

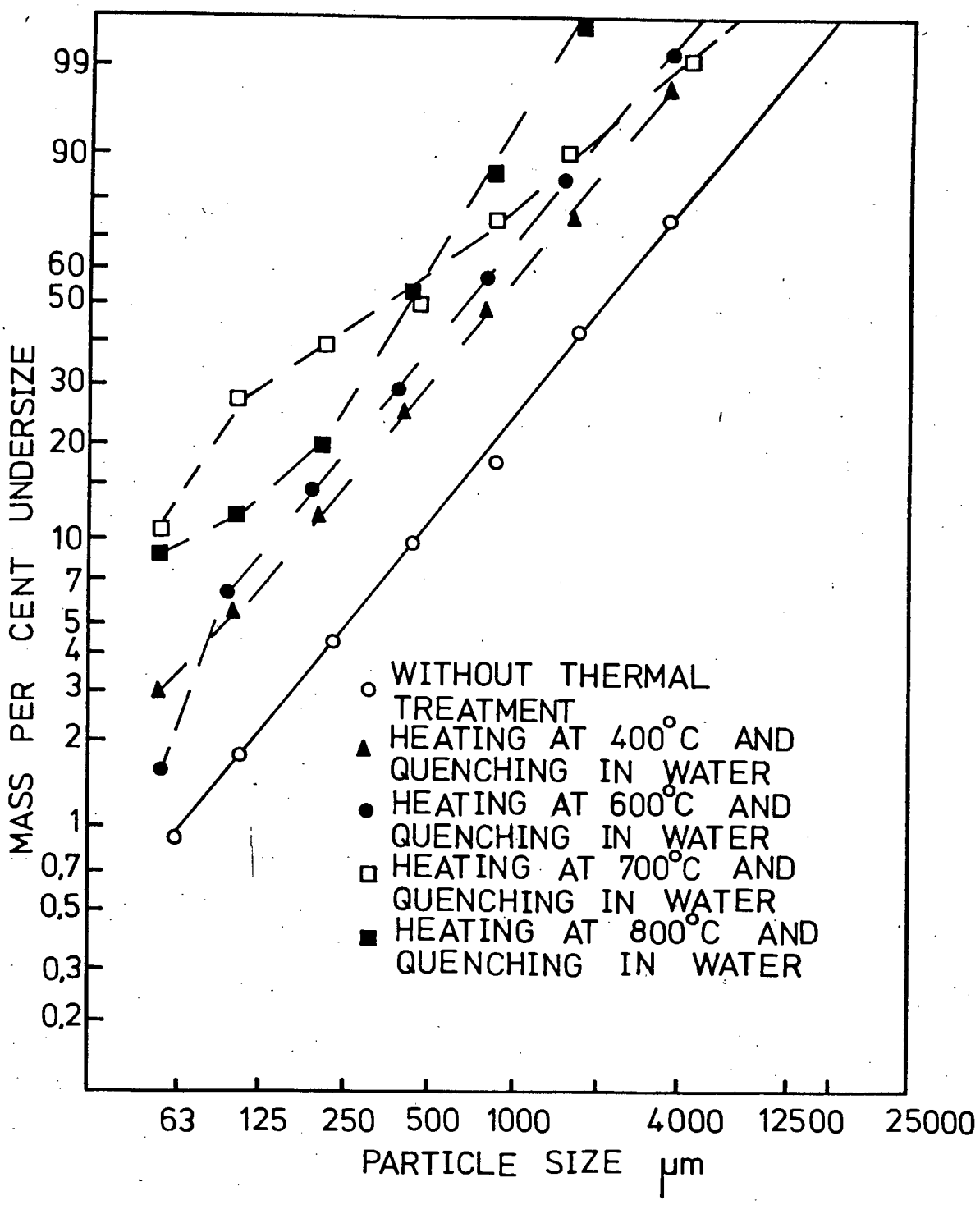

Figure 8

Rosin-Rammler presentation of comminuted quartzite by compression for rock specimens containing only inherent flaws and others containing inherent and thermally induced microcracks, after prior heating at 400°C, 600°C, 700°C and 800°C and quenching in water.

the number of new particles N were the variables selected to describe the fragmentation taking place due to thermal treatments.

The thermal disintegration due to heating and quenching alone was found to be influenced by both temperature and time at temperature. At 250°C, the reduction ratio R_R was practically equal to unity, although a small number of daughter rock particles were separated in a form of surface chipping (figure 9). Longer times of heating at 250°C did not obtain better comminution results. Thus it appears that the time of heating the rock specimen has little influence at 250°C, for periods 5 to 30 minutes. The low thermal stresses created at this temperature are not able to break the rock piece, but only to eliminate the irregularities and promote a spherical shape. When heating at 300°C, the thermal comminution also takes place in the form of a chipping actiong for heating periods up to 25 minutes (figure 9). After the rock piece had been heated at 300°C for 30 minutes, it divided into a number of daughter pieces from which two were large, approximately half of the size of the parent rock. The reduction ratio and the number of daughter particles were found to increase after heating at 450°C and 500°C (figures 9 and 10). The time dependence of the thermal stresses due to the thermal treatment at 450°C and 500°C seems to correspond with a linear function of time versus heating, since the quenching procedure remained the same. The difference between the product of the thermal comminution after heating at 450° and 500°C respectively and quenching in water was found to be negligible The heating at 550°C and 590°C and quenching in water, was found to produce higher thermal disintegration characteristics than the ones of lower temperatures of heating (figures 9 and 10). At the $\alpha \rightarrow \beta$ quartz transition point, 573°C, the disintergration characteristics were improved in a moderate manner. Plotting the reduction ratio after heating for a period of twenty minutes versus the temperature of heating (figure 11), an exponential type of curve is obtained. This relationship shows that for heating temperatures higher than 450°C, the thermal disintergration provides a reduction ratio higher than two. In other words, the thermal treatments technique itself, without any additional contribution in the form of mechanical energy i.e. impact or compression, can comminute each rock piece to daughter rock particles, to half or smaller, of its size, for treatment temperatures higher than 450°C.

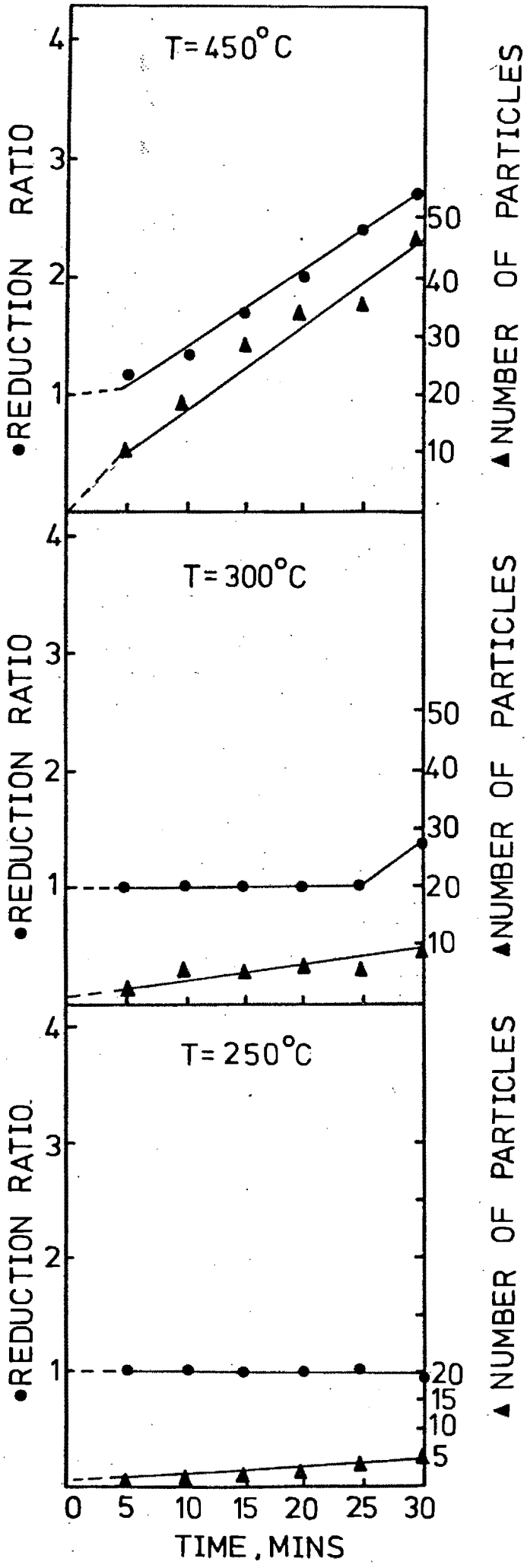

Figure 9

Thermal disintergration characteristics of quartzite D, after heating at 250°C, 300°C and 450°C for various periods and quenching in water.

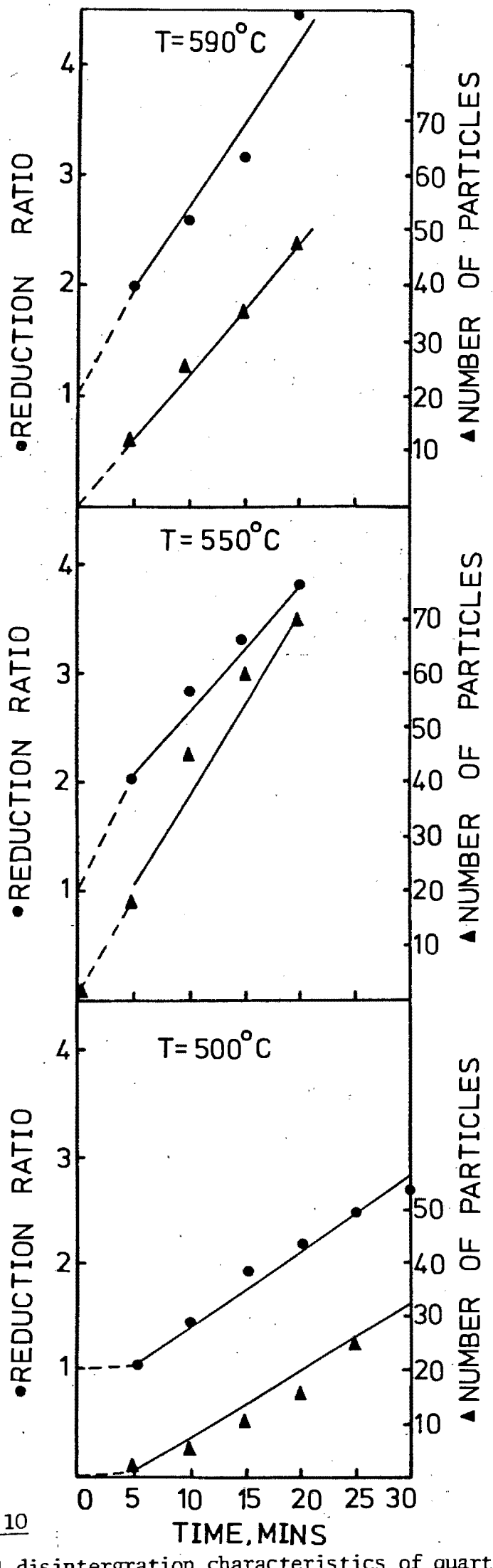

Figure 10

Thermal disintergration characteristics of quartzite D, after heating at 500°C, 550°C and 590°C for various periods and quenching in water.

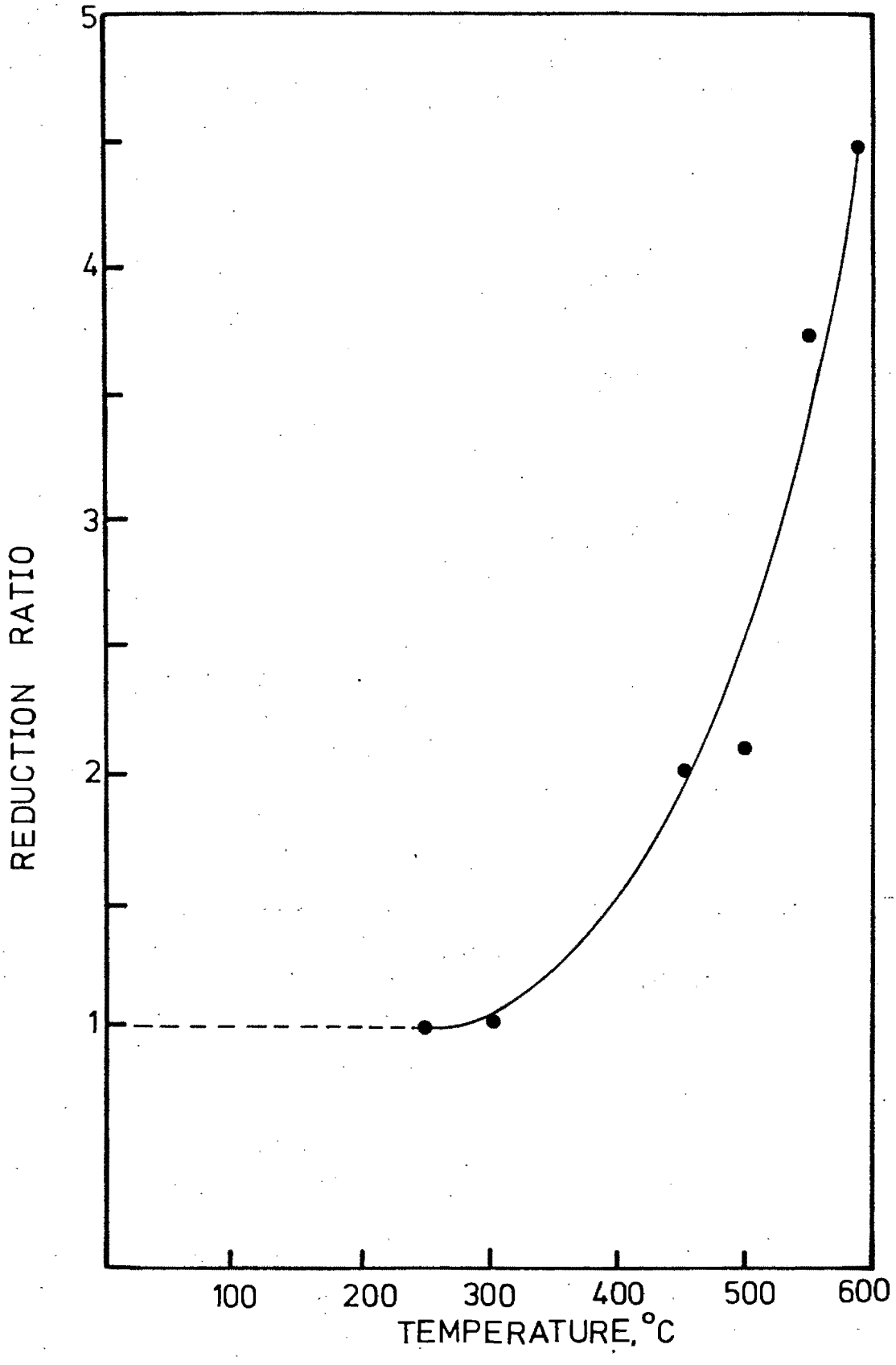

Figure 11

Relationship between reduction ratio and temperature of heating, for a 20 minutes heating of a quartzite D and quenching in water.

3.2.5. The detection of mineral liberation

The determination of the degree of liberation of the mineral constituents of quartzite, was performed for particles without any thermal treatment, and for particles which were the product of thermal treatments at temperatures 400°C and 600°C with subsequent quenching in water. The particles of quartzite comminuted by the thermo-mechanical treatments of section 3.2.3. were classified according to size, from +4 mm to -6μm, and examined by reflection microscopy in order to determine the degree of liberation of the mineral constituents of the Witwatersrand quartzite ore. A simple manual sampling of the comminuted ore was applied by coning and quartering twice. Using a flat glass plate, ten random areas of ten neighbouring particles were examined in order to determine their degree of liberation, D_L, defined as A_L/A_C+A_L with $A_L+A_C = 10$, where A_L is the number of the liberated particles (quartz, pyrites, phyllosilicates and A_C is the number of the composite particles.

The results of the mineral detection, which are shown in figure 12, indicate that the mineral liberation of quartzite is increased after the thermal treatments. For the particle sizes - 125 μm, which are the most important for the mineral processing, thermal treatments up to 400°C, can achieve higher recovery rates for the useful mineral than the ones obtained by the conventional methods of comminution. Plate 8 shows pyrite particles, magnetically separated, as an example of the mineral liberation due to heating at 600°C and quenching in water.

3.2.6. Fracture detection techniques

The following experiments were used to defect and measure the comminuting effects produced by thermal treatments.

Sections (6 mm thick) of quartzite rock and synthetic quartz were polished on both sides to a 6 μm finish. They were heated in a fluidized bath furnace to several temperatures up to 600°C for fifteen minutes and then quenched in a water bath. In addition, specimens of quartzite (type C) and specimens of synthetic quartz

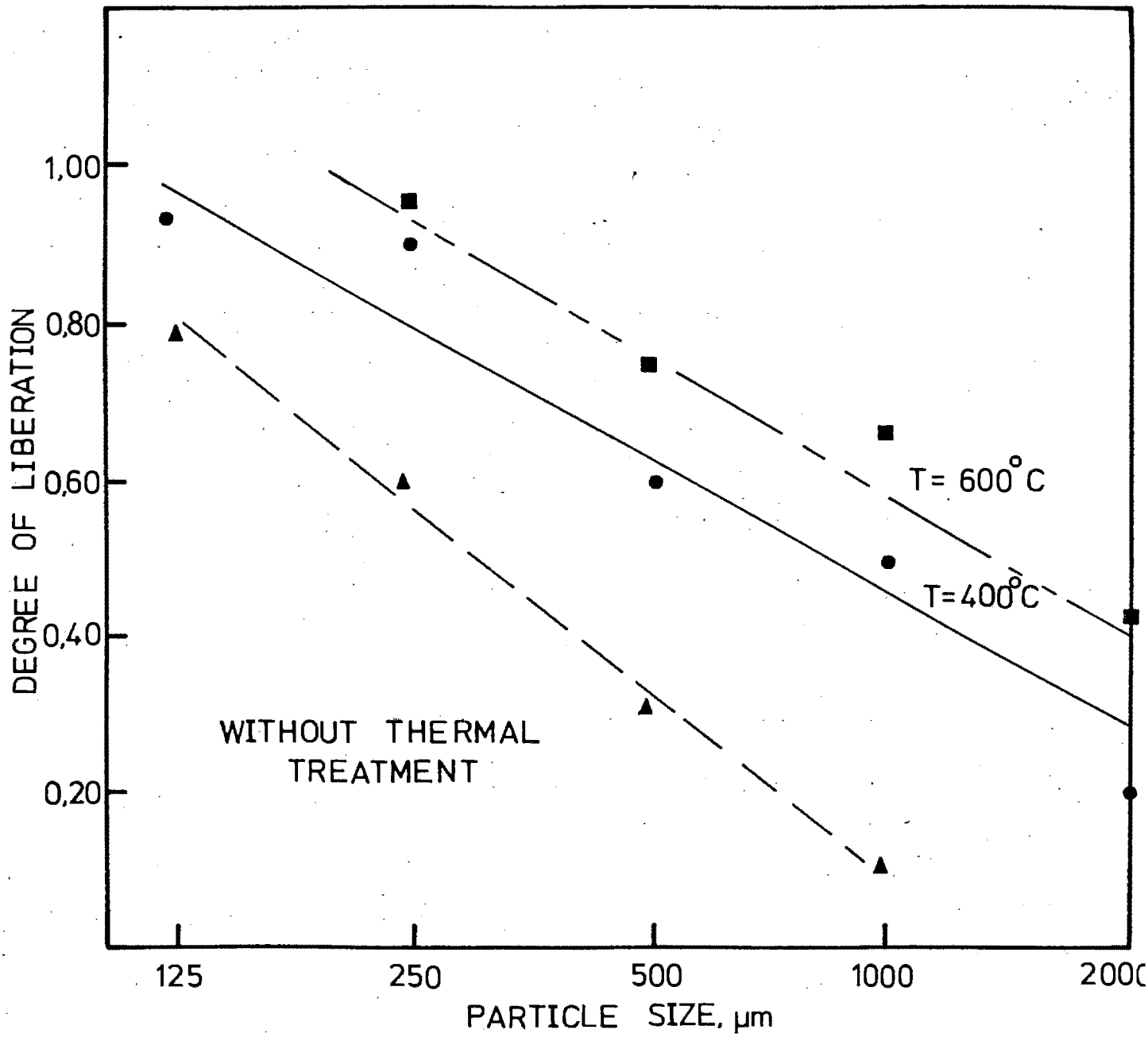

Figure 12

Relationship between degree of mineral liberation and particles for untreated and thermally treated quartzites.

were heated in the furnace at 550°C and then allowed to cool slowly in the fluidized bath, for a period of 4 hours. The specimens were then examined and photographed by reflection microscopy. The fracture density was an obvious function of the heat treatment parameters and many of the fractures seen in the rock samples appeared to be associated with inclusion particles. The density of microfractures was then determined by two different techniques, viz: the intensity of light from a fixed standard source transmitted through the specimen was measured by means of a photoresistant cell The recorded intensity will be a function of the number of internal fractures which disperse the light. A special technique was applied in order to use transmitted light microscopy. A polished thin section of quartzite, mounted on a glass slide with "Canada balsam" glue, was heated in a furnace at various temperatures in the range 20°C to 400°C, between two 20 mm thick brass plates, in order to achieve uniform heat transfer conditions and to avoid the breakage of the glass slide. The slide was examined after cooling to room temperature. The attenuation of an ultrasonic signal was then measured as a function of the temperature of the heat treatment. The specimens used in the above experiments were placed between a probe and a receiver and the signals were recorded on an oscilloscope. The attenuation is related to the density of the cracks within the specimens. Both techniques showed that a signigicant increase in the number of defects occurs in the specimens which had been heated to temperatures above about 425°C (figure 13). Specimens which had been cooled slowly, showed some reduction in microfracturing.

The transmitted light optical microscopy examination shows generation and/or propagation of cracks due to heating at various temperatures and quenching in water. Plate 9 shows the cracks formed due to heating at 200°C and quenching in water. Cracks in the quartz pebbles together with a system of minor cracks are shown. The quartzite thin section, shown in plate 10, was heated at 400°C and quenched in water. The mounting epoxy used, in this case, has "decorated" the cracks formed, because "burning" took place at the regions where cracks were formed. Plate 11 shows intragrain cracks, generated in a 30 mm quartz pebble, which was heated at 590°C in a fluidised bath furnace and slowly cooled in the sand bath. The treated quartz was etched by a low concentration HF.

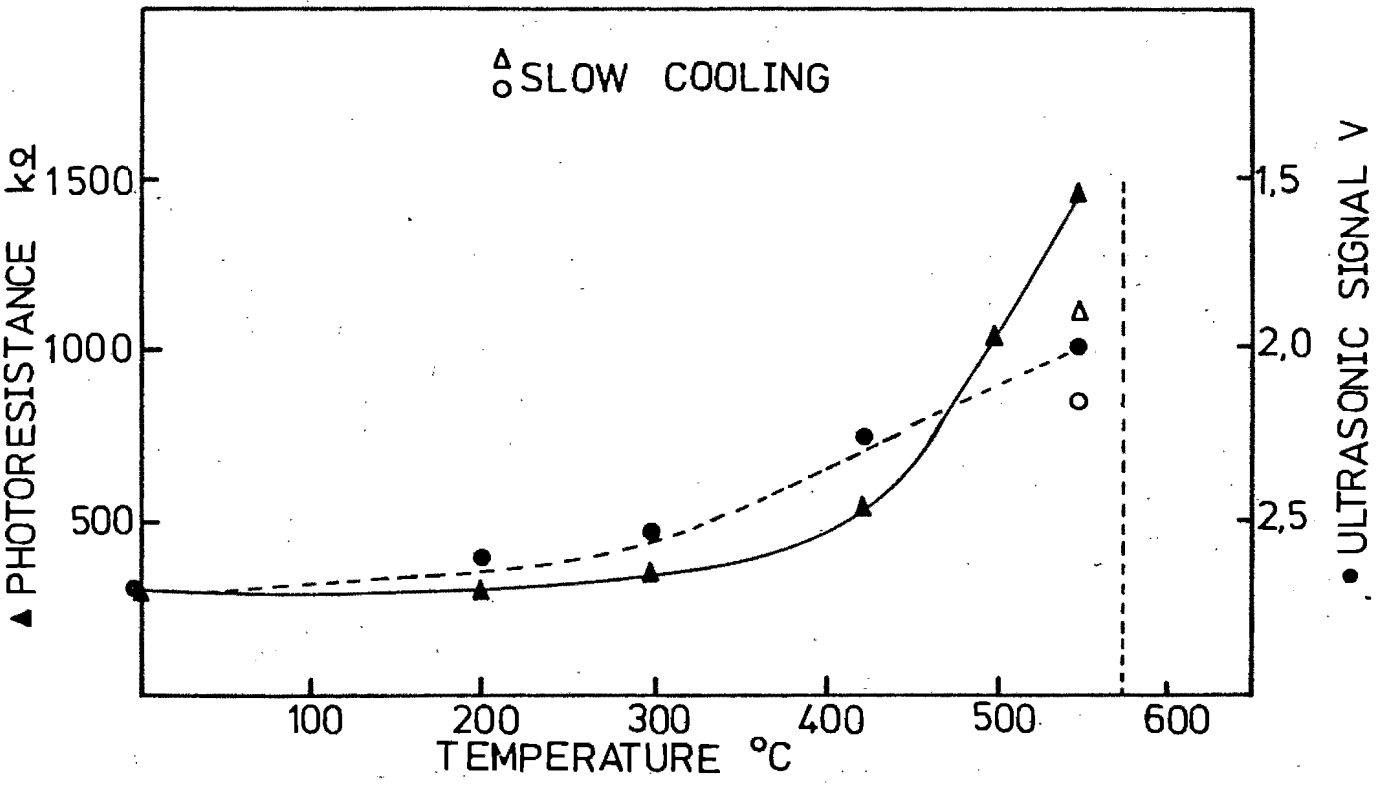

Figure 13

Fracture detection data on quartzite C, after prior heating at various temperatures.

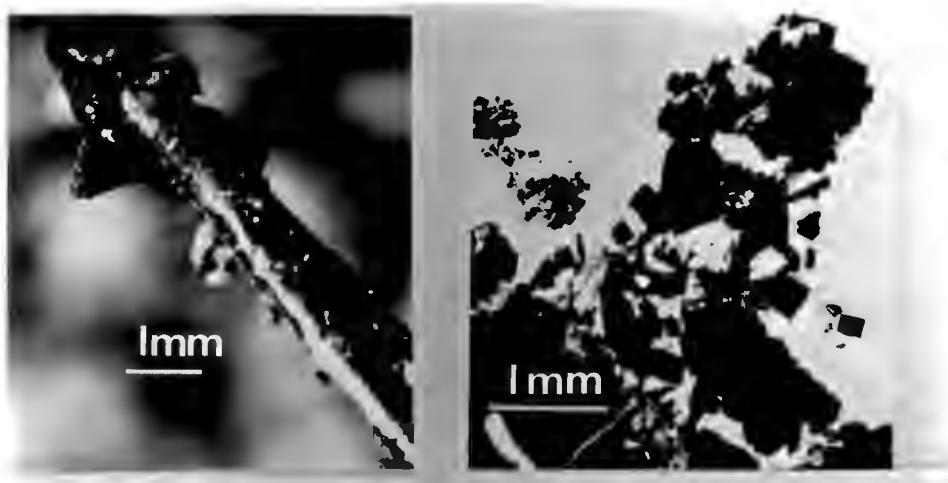

Plate 8

Liberated and magnetically separated particles taken from the comminuted product of compression test on quartzite D, after heating at 600°C and quenching in water.

Plate 9

Thermally induced microcracks in quartzite D after heating at 200°C and slow cooling.

Plate 10

Thermally induced microcracks in quartzite D after heating at 400°C and slow cooling.

Plate 11

Thermally induced microcracks in quartz 'pebble' taken from a Witwatersrand quartzite D, after heating at 590°C and quenching in water.

The quartzite particles, produced by the thermal comminution treatments at temperatures up to 800°C, were sampled by a coning and quartering and then prepared for SEM examination, according to the technique described in chapter 2. Microstructural features are shown in plates 12, 13. The shape of randomly selected thermally comminuted rock particles was examined and the shape factors of fourty different particles were been determined. These factors were found to be approximately equal to the ones for the particles taken from the Brazilian tests C (k_a = 0,5, k_o = 0,07). Sharp edges and cleavage facets were characteristic of the surface morphology of thermally treated particle (plates 12, 14) while conchoidal marking were also observed (plate 15).

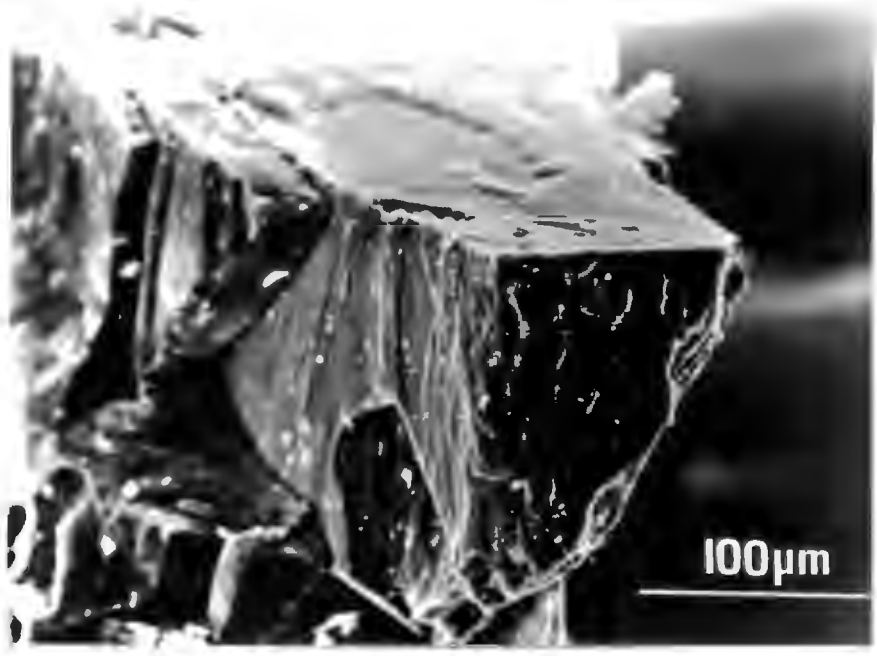

Plate 12

Fracture surface of a thermally comminuted quartzite D, by heating at 800°C and quenching in water.

Plate 13

Microstructural defects, thermally induced in quartzite D, by heating at 800°C and quenching in water.

Plate 14

Thermally comminuted particle of quartzite D, by heating at 700°C and quenching in water.
Size determined by sieve analysis:
-250 + 125 µm
Area: 30508 μm^2
Perimeter: 246,8 µm
k_a = 0,5
k_o = 0,066

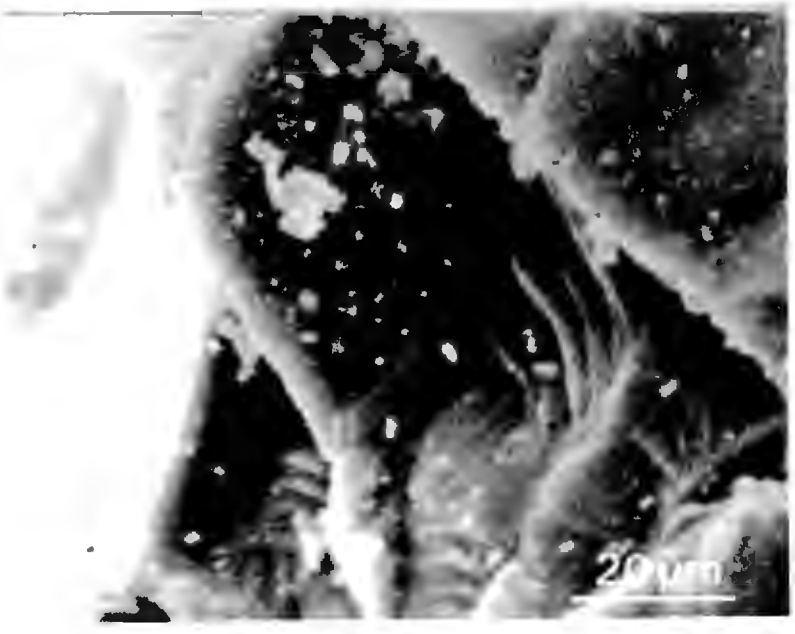

Plate 15

Fracture patterns indicative of transgranular comminution on the surface of a thermally comminuted particle by heating at 500°C and quenching in water.

CHAPTER 4

THE STUDY OF THE FRICTIONAL BEHAVIOUR OF THE WITWATERSRAND QUARTZITE

4.1. Introduction

4.1.1. General

Friction is the resistance to motion which exists, when an attempt is made to move or maintain motion of a solid object tangentially with respect to the surface with which it is in contact. The friction between two rock surfaces is very important in a wide spectrum of engineering applications. In engineering geology, the control of potential rock slides requires information concerning the frictional behaviour of rocks. In mining, friction is involved in many processes, from the first stage of excavation through to materials handling and processing. In the minerals processing stage, the frictional phenomena are very important, since the comminution process involves the mechanisms of abrasion and attrition.

An examination of the frictional behaviour characterised by the resistance in sliding under tangential action is aimed at in chapter 4. The experimental technique used is based upon the measurement of the magnitude of the frictional force at various conditions of normal load sliding speed, surface roughness and environment, while the wear effects of two sliding rock surfaces are examined in chapter 5, using different experimental apparatus.

4.1.2. The friction of inorganic non-metals

Although most friction studies have been done on metals, the frictional behaviour of some non-metallic materials has been investigated. Studies on the friction between two diamond surfaces (Wilks and Wilks 1959, 1972, Casey and Wilks 1973) as a function of the normal load, showed that the roughness theory of friction (Rabinowicz, 1965) is verified, since the frictional force was found to be linearly proportional to the normal load and independent of the contact area. According to this theory, when two surfaces slide

over each other, work is required to move the surfaces against the normal load as they are forced apart when asperities ride over each other. In the course of motion, particular asperities will eventually lose contact, and the load will then be carried on other asperities. Since the asperities are rough and jagged this transference of contact may take place abruptly and cause irreversible damage with some associated heat dissipation.

The surface flow of glass produced during the sliding of a diamond stylus was examined by Bowden and Scott (1958). They found that this flow occurs when the sliding speed exceeds a critical value, which depends on the type of the glass. The surface temperature produced (from 400 to 1200^{o}C) was also examined in relation to the softening behaviour of glass and the heavy wear of the sliding diamond (Jaeger 1942, Bowden and Thomas 1954). Marsh (1964) suggested that the brittle fracture theories are inadequate for an explanation of the frictional behaviour of glasses. He found that even at room temperatures glasses flow plastically if the load is high. The fatique free flow stress was determined by two method- viz. by hardness tests using very short loading times and by hardness measurements in liquid nitrogen environment (very low temperature). Typical flow stresses in a 10 seconds test were found to be 0,05 E, where E Young's modulus.

Bowden and Hanwell (1966) studied the frictional behaviour of magnesium oxide, sapphire and quartz crystals sliding on themselves in high vacuum. The authors suggested that the frictional behaviour of these non-metallic solids can be explained by theory expressed by Bowden and Tabor (1964). The frictional force between two sliding solids, according to this theory, is made up of two parts viz: the force required to shear the adhering junctions in the region of surface contact and the force required to deform the underlying crystal. They regarded that in the case of elastic solids the latter force is due to elastic hysteresis loss. However, if plastic deformation or fracture occurs, this force will represent the work required to produce this deformation i.e. to drag the surface irregularities through the solid and to plough out a track.

4.1.3. Changes in friction with sliding speed

Little work has been done on the role of the sliding speed upon the frictional properties of solids since Coulomb first noticed the speed dependence effects on the coefficient of friction in 1785 (Bowden and Tabor, 1950). Many empirical expressions have been proposed in order to describe this relationship, mainly for metal applications, such as railway brakes. The relationship between the frictional force and the duration of static contact was studied by Kragelskii (1965) for a wide range of metals and non-metals used in braking systems. He found that in general the frictional force increases, when the duration of contact increases, in a manner described by the empirical equation:

$$F_t = F_\infty - (F_\infty - F_o)\, e^{-ut}$$

where F_t is the frictional force for a given duration of contact t F_∞ is the frictional force for an infinitely long duration of contact and F_o, that of zero duration of contact and u constant. Assuming that F_∞ and F_o are characteristic for two surfaces in contact, Kragelskii's equation can be written as:

$$\log F_t = \lambda (e-ut)$$

Changes in the sliding speed were found to influence the frictional force fluctuations taking place during sliding. Kragelskii (1965) suggested that this oscillatory process involves periods in which the surfaces are at rest and periods in which they are in motion relative to each other and both static and sliding frictional characteristics contribute to the setting up of these relaxation oscillations.

4.1.4. Changes in friction with normal load

In 1699, Amontons stated that "friction produces double the amount of effort, if the weight is doubled" (Bowden and Tabor, 1966). The validity of the so called Amontons' law, which in other words states that the coefficient of friction of two sliding surfaces is independent of the normal load applied L, has been verified for some metals (Whitehead, 1950). The frictional force applied on a diamond stylus sliding on the (110) plane of diamond in air and for loads up to 0,1 N,

was found (Bowden and Young, 1951) to follow the equation:

$$F = k_1 L^{2/3}$$

where k_1 is constant related to properties of the sliding materials. A relationship of the form $F = k_1 L^m$ or $\mu = k_1 L^{m-1}$ was proposed by Gralen (1952) and Archard (1958) in order to describe the effect of the normal load upon the coefficient of sliding friction of two sliding surfaces. When purely plastic deformation is involved during friction, Archard (1953) using surface models involving the Hertz theory of deformation (Timesenko, 1934) suggested that $m = 1$, while $m = 2/3$ for purely elastic and brittle deformation. For an intermediate behaviour, Archard suggested that $2/3 < m < 1$.

4.1.5. The friction of rocks

The problem of rock stability and the understanding of the seismic faulting phenomena were the reasons for the enormous effort paid by researchers in the fields of rock mechanics and geophysics respectively. Spurr (1958) found that the coefficient of friction of loose particles between sliding parallel plates is approximately proportional to their Mohs hardness. The theory of tectonic friction assumes the validity of the roughness theory of friction, while Orowan (1958) proposed a mechanism of seismic faulting based on the brittle-ductile transition of the rocks which occurs at a particular high confining pressure, when frictional force along the fault surface exceeds the shear strength of the rock. Maurer (1965) found that friction does not vary significantly with rock type and verified Orowan's theory, using a triaxial testing machine at confining pressure up to 117,3 MPa.

The frictional characteristics of granite under high confining pressure were examined by slicing cylinders of the rock at various angles to their axes and stressing the resulting specimens in a triaxial testing machine (Byerlee 1967a, 1970). He suggested that the controlling friction mechanism for this rock, is based on the brittle fracture of the surface asperities. Byerlee (1967b) also presented a theory of friction based on the brittle fracture of the peaks of asperities of the rock surface. He calculated values of the coefficient of friction, μ, from the strength of asperities

of certain ideal shapes, such as cone and wedge, and correlated these different values with the observed changes of the frictional behaviour of geological materials with their surface roughness.

The frictional characteristics of gabbro, dunite and limestone were studied at different values of confining pressure by Byerlee and Brace (1968) and Byerlee (1968). The confining pressure at which the brittle-ductile transition occurs was found to be dependent upon the rock petrography. The presence of certain minerals in small fractions, for example less than 3 per cent serpetine, was found to lower the brittle-ductile transition values of confining pressure.

The brittle-ductile transition behaviour of limestone was suggested by Olsson (1974) to be dependent upon temperature, while a decrease in displacement rate from 10^{-4} to 10^{-8} ms^{-1} was found to have a little effect on the frictional properties of the rock examined.

The initial surface roughness and the sliding speed were found to influence the frictional behaviour of rocks such as granite, gabbro, trachyte sandstone and marble (Hoskins, Jaeger and Rosengren, 1968). The authors examined the friction between rock surfaces by sliding a block with plane parallel surfaces between two others in a testing machine, while the normal load was applied by flat jacks. Dieterich (1972), examined the friction of sandstone, quartzite and granite rocks in relation to the magnitude and the duration time of application of the normal stresses, using a similar apparatus to that used by Hoskins et al (1968) and found that the coefficient of static friction is proportional to the logarithm of the time that the adjacent blocks remain in stationary contact before movement. The author offered two possible explanations relating to the size and the strength of adhesive junctions across the slip surface. Time dependent localized plastic flow in the area of the contact points can increase the area of junction. Alternatively, the size of the adhesive junctions remains constant but the strength of junctions increases with time due to time controlled breakdown of surface films or diffusion across the junction interfaces.

Engelder (1976) examined the frictional tracks of granite and quartzite by a scanning electron microscope equipped for the energy

dispersion analysis of X-rays and suggested that the scratch hardness of the mineral constituents of the rocks influence their frictional properties while the "frictional instability" of these rocks is due to shearing of asperities. The study of the behaviour of rock under the influence of high stresses in relation to the strength characteristics of the material, may help the understanding of the deformation phenomena of the rock asperities, which make up the true points of contact of the rock surfaces. Indentation hardness tests were therefore performed by Brace (1960) for limestone, marble, anhydrite and artificial rock salt. The author found that the Vickers hardness of the rocks examined are proportional to their compressive strength, suggesting that the deformation of the rocks is due to a combination of gliding (relative movement of hard grains in soft matrix) and microfracturing. A similar model of rock behaviour under the influence of high stresses was also proposed by Hoek (1965).

The basic principles and practical applications of indentation fracture of solids were reviewed by Lawn and Wilshaw (1975), while the indentation fracture in granite rocks was examined by Swain and Lawn (1976). When the flat surface of a rock is loaded with a hard indenter, the rock experiences a complex stress field. The geometry of the indentetion determines to some extent the mechanical response of the rock. The authors analyzed the stress fields for a blunt and a sharp indenter respectively, and emphasised the importance of surface energy and hardness in the overall crack propagation process. They noted that the microstructure of a mineral can influence both of these parameters.

4.1.6. The influence of the environment on friction

A study of the influence of the environment on the coefficient of sliding friction of rocks may not only be useful for applications like the control of rock slides in the presence of water (Jaeger, 1971), but also for the control of the overall frictional behaviour during comminution. Lord Raleigh (1918) observed the effects of water on the frictional behaviour of glass. He studied paraffin oil lubri-

cation phenomena and suggested that these derive mainly from the presence of a monolayer of molecules. Hardy and Hardy (1919) and Doubleday (1922) examined the influence of some normal alcohols on the friction between a spherical glass slider and a polished glass plate. They found that the coefficient of static friction was independent of the normal load between 0,2N and 0,6N and the radius of curvature of the slider of 147,358 and 178 mm. They also found that the coefficient of static friction decreased when the number of carbon atoms in the molecules of the normal alcohols used increased from 2 to 11. Doubleday (1922) also examined the influence of alcohols of the formula $C_2H_5CH(OH)C_nH_{2n+1}$, for n values from 1 to 15. The coefficient of static friction was found to decrease linearly as n increased. Plotting the coefficient of static friction versus molecular weight (which is a linear function, of the carbon atoms contained in a molecule of each alcohol) he found a straight line, with the exception of methylpropylcarbinol ethylpropylcarbinol and ethyldodecylcarbinol. Doubleday could not explain this frictional behaviour, especially the one due to ethyldodecylcarbinol. Similar results were obtained for steel on steel plates, where the values for the coefficient of static friction were lower than the one of glass on glass. Plotting the values of the coefficient of static friction for steel on steel in the same manner as for the glass on glass results, Doubleday found two parallel lines, with the same discontuity points at n = 1,2 and 12, but he could not explain these frictional behaviours. The influence of surface films on the frictional behaviour of diamond was examined by Bowden and Young (1951). An adsorbed oxygen layer was found to reduce the coefficient of diamond from 0,5 to 0,05, for two sliding diamond surfaces under a normal load of 0,36 N. The frictional behaviour of a diamond sliding on glass, was also found dependent on the humidity of the atmosphere. A boundary lubrication mechanism for non-metallic solids, similar to the one proposed for metals (Tabor, 1952), was suggested by Bowden and Tabor(1964). Thus over the regions of contact the load is mainly supported by the boundary film. However, some interaction occurs through this film, with the formation of minute junctions. The presence of surface films, consisting of a few molecular layers, between the sliding diamond and magnesium oxide or sapphire crystal, was found

to reduce the friction by a factor of ten, in relation to the friction values in vacuo. The friction of water-saturated samples of sandstone gneis and granite was found to be smaller than the friction of dry samples (Jaeger, 1959, Byerlee 1967). Large changes from 0,2 to 0,8 coefficient of sliding friction of a sapphire ball sliding on glass surfaces and of the coefficient of friction of a diamond pyramid indenter on magnesium oxide crystals were measured by Macmillan, Huntington and Westwood (1974), in dimethyl sulphoxide of different concentrations and normal alcohols of increasing molecule chain length environments. The frictional behaviour of these materials was found to be influenced by the surfactant concentration and the numbers of carbon atoms per molecule of the normal alcohols. These phenomena were explained by the authors in terms of the zeta potential correlation theory (Westwood, 1974). The influence of normal alcohols on the frictional behaviour of glass spheres sliding on silicon carbide paper was also studied by Wiederhorn and Roberts (1975). The authors found that the coefficient of friction between these two materials decreased continuously as the number of carbon atoms per molecule of normal alcohol increases. This function was found to be non-linear, obtaining a minimum value for the coefficient of sliding friction for dodecyl alcohol, and for normal heptyl alcohol, as it was found by Macmillan et al (1974). The time dependence of the chemomechanical effects (Ahearn, Mills and Westwood, 1976) could explain the above differences in the influence of the normal alcohols on the frictional behaviour of the materials used, since sliding speeds of $8,33 \times 10^{-6}$ ms $^{-1}$ were used by Macmillan et al (1974), and those used by Wiederhorn and Roberts (1975) were not reported.

4.2. Experimental Technique

The experiments were designed to measure the friction between the circumference of a disk shaped upper slider and a cylindrical lower surface during controlled sliding at speeds from $4,23 \times 10^{-7}$ to $4,23 \times 10^{-3}$ ms^{-1} (Plate 16). The use of cylindrical surfaces moving with axes normal to each other, facilitated the study of the deformation of the lower surface by confining the damage to a narrow track.

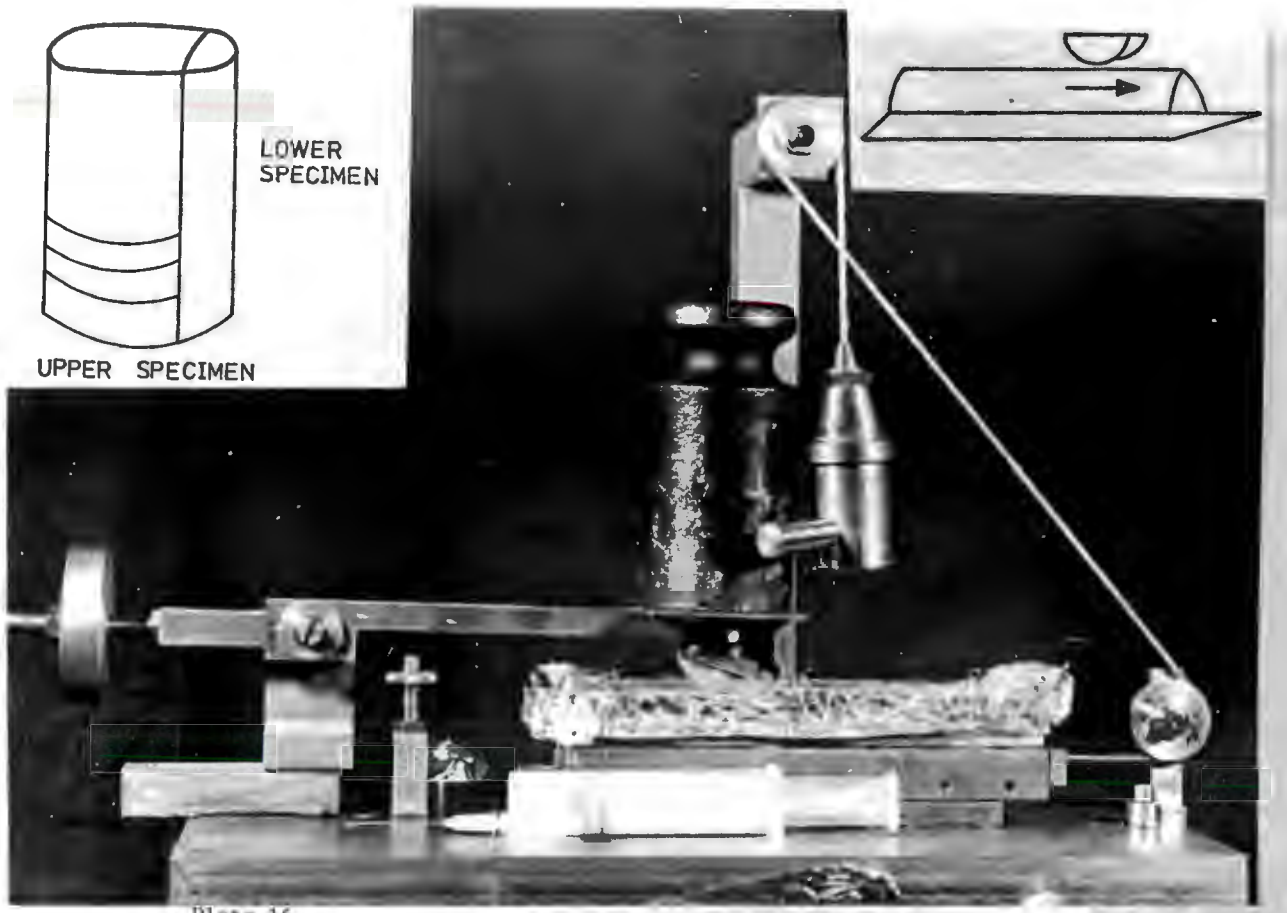

Plate 16

The sliding device used for the tests on the frictional behaviour of quartzite rock surfaces.

Each of the rock samples used for both upper and lower specimens was cut from the same drill core of quartzite C (Chapter 2).

For the experiments, which aimed to establish the role of the surface roughness of the rock specimens on their frictional properties, two flat surfaces were cut parallel to the axis of symmetry of the mother cylinder. The curved surfaces of these specimens were gently abraded under water on a succession of carborundum paper of decreasing roughness, ending with a grade which left irregularities on the surface of the order of 100 nm in height.

The arrangement of the apparatus for measuring friction is shown in plate 16.

The lower specimen was mounted on a table, which was moved at constant velocity on a carriage which was supported by two linear bearings. The upper specimen was clamped to a pivoted arm, which above the upper specimen had a centrally positioned load platform. Normal loads were applied to the upper specimen by placing dead weights on the platform. A counter weight, positioned at the other end of the pivoted arm, facilitated the accurate application of the normal loads. The whole device was mounted on the crosshead of the Instron Universal testing machine and the carriage was pulled along by a stiff cord which was attached via two pulleys to the load cell of the testing machine.

The frictional force generated during sliding caused a deflection of the base table and consequently of the cord connected with the machine load cell. Various precautions were taken to ensure that the frictional force was applied along the track of sliding and to minimize errors arising from torsion and asymmetry. The estimated maximum error in the measurement of friction force was ± 5 per cent.

The experimental variables considered were normal load, sliding speed and environment. To make a measurement, a known load was placed on the platform, which was then lowered gently to bring the upper rock specimen into contact with the lower one. Both of the friction surfaces were wetted iwth the particular liquid environment before the

beginning of each test. Then, the Instron Universal machine crosshead started pulling the table on which the lower specimen was mounted, at a selected speed. The Instron X-Y recorder was recording the frictional force as a function of the displacment of the crosshead (figure 14). For every experiment, the static frictional force and the mean value of the sliding frictional force were taken.

4.2.1. Examination of initial surface roughness

The term roughness refers only to relatively closely spaced surface irregularities produced by the drilling of Witwatersrand quartzite from the hanging wall, main reef and footwall ore. Every type of quartzite had a characteristic surface roughness, closely related to the grain size of the rock.

The "mean surface" is defined as the surface located so that volume of peaks above it is equal to the volume of valleys below. The "central line average" - (CLA) of the surface is the result of taking a great many uniformly spaced measurements of the distance of the actual surface from the mean surface and averaging them. The instrument used to measure surface roughness was a Talysurf. This instrument has a probe with a stylus which is traversed over the specimen. Vertical movement of the stylus is measured, averaged and displayed directly as the "central line average". Standard surfaces are furnished with the instrument and calculations were made on those before each set of measurements. An amplified recording of the surface profile, by the vertical movement of the stylus, is also provided by the "Talysurf" instrument. Typical surface profiles for each type of rock specimen used, were recorded (plate 17).

4.3. Results

4.3.1. Dependence on the sliding velocity

The results from the friction tests on quartzite surfaces, sliding at speeds from $4{,}23 \times 10^{-7}$ to $21{,}15 \times 10^{-4}$ ms^{-1} and under constant normal load of 20 N are shown in figures 15 to 17. These tests were performed in dry, distilled water, acetone, toluene, oleic

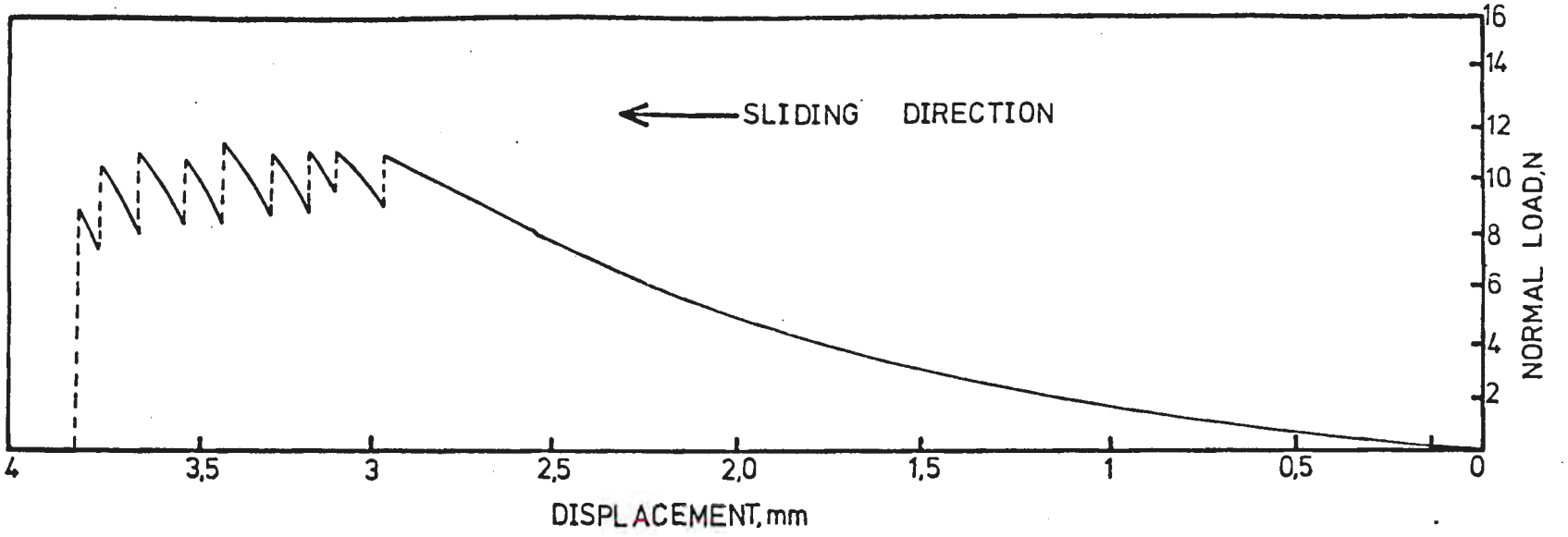

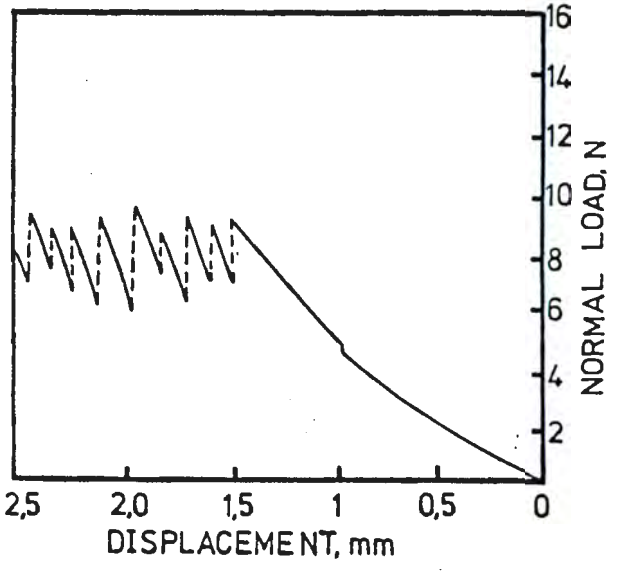

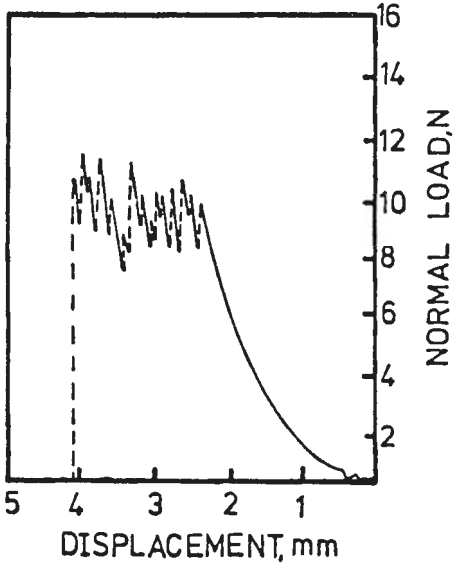

Figure 14

Relationship between normal load and frictional force indicative of the stick-slip phenomenon during the sliding of quartzite surfaces of 900 nm CLA.

Plate 17 (a)

Typical surface profile , as obtained by the Talysurf profilometer, for a polished quartzite surface
$\overline{CLA}$ = 93 nm

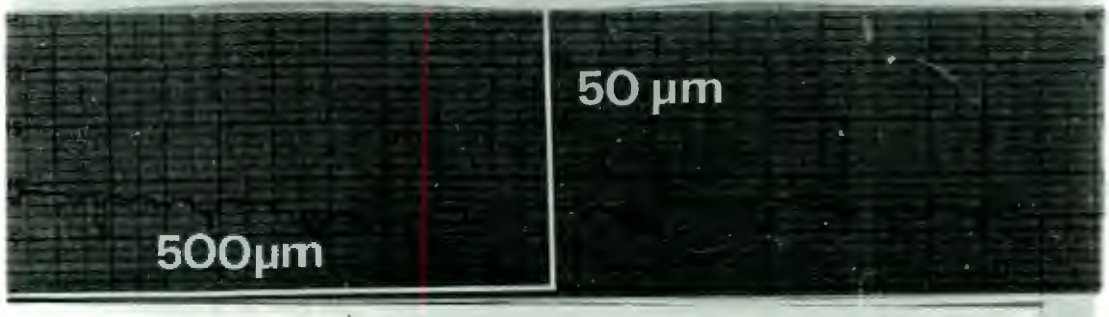

Plate 17 (b)

Surface profile as obtained by the Talysurf profilometer, for a friction track produced by a test at sliding speed of 8,46 x 10^{-5} ms^{-1} and under normal load of 20N.
Environment: Acetone
Initial: $\overline{CLA}$ = 900 nm.
$\overline{CLA}$: 190 nm.

Plate 17 (c)

Typical surface profile, as obtained by the Talysurf profilometer for "as received" quartzite surfaces used for the friction tests.

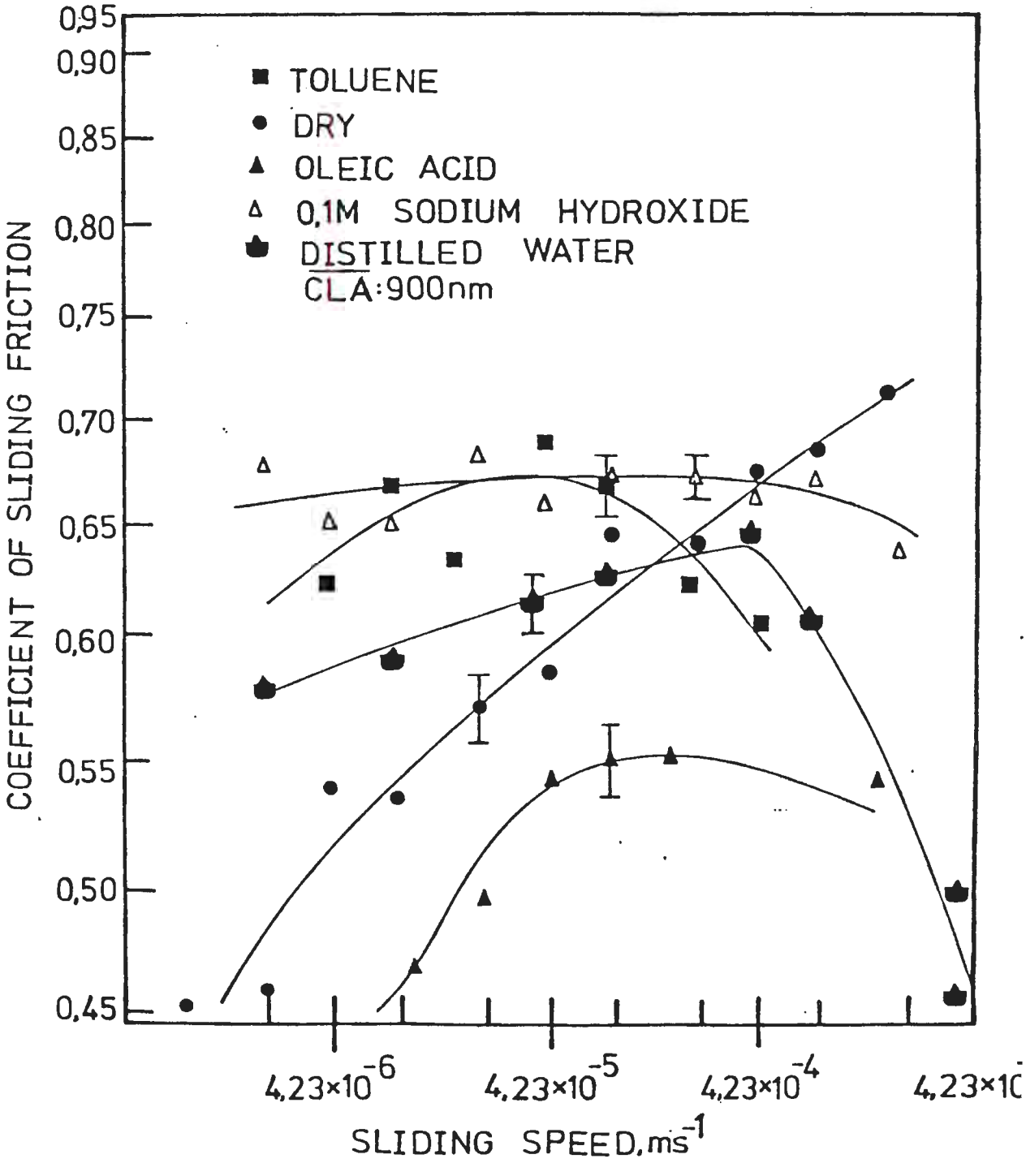

Figure 15

Relationship between coefficient of sliding friction and sliding speed in pure toluene, pure oleic acid, 0,1 M sodium hydroxide and distilled water environments.

Normal load applied 20 N (Logarithmic scales).

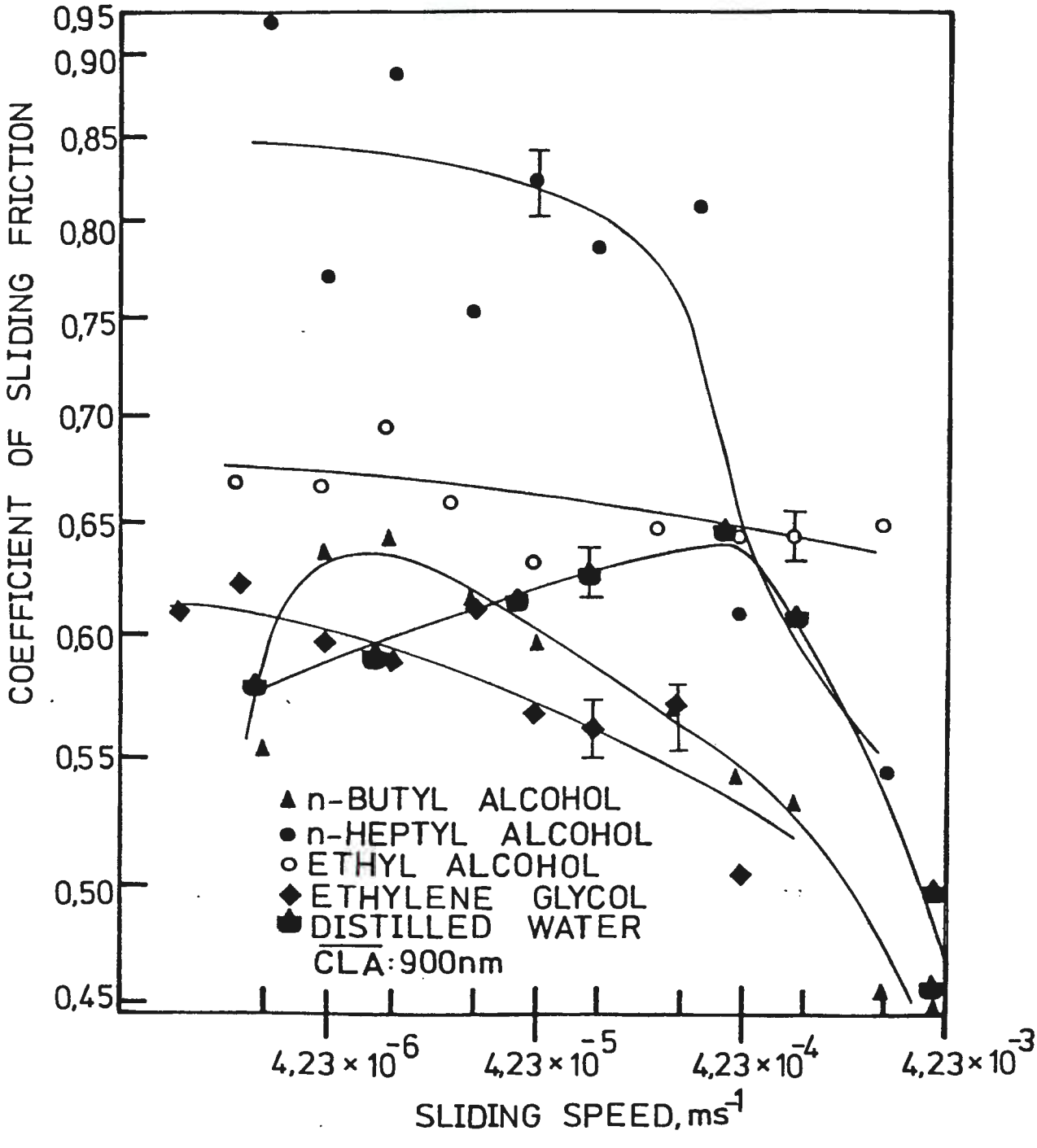

Figure 16

Relationship between coefficient of sliding friction and sliding speed in pure n-ethyl, n-butyl and n-heptyl alcohols, pure ethylene glycol and distilled water environments.

Normal load applied 20 N (Logarithmic scales).

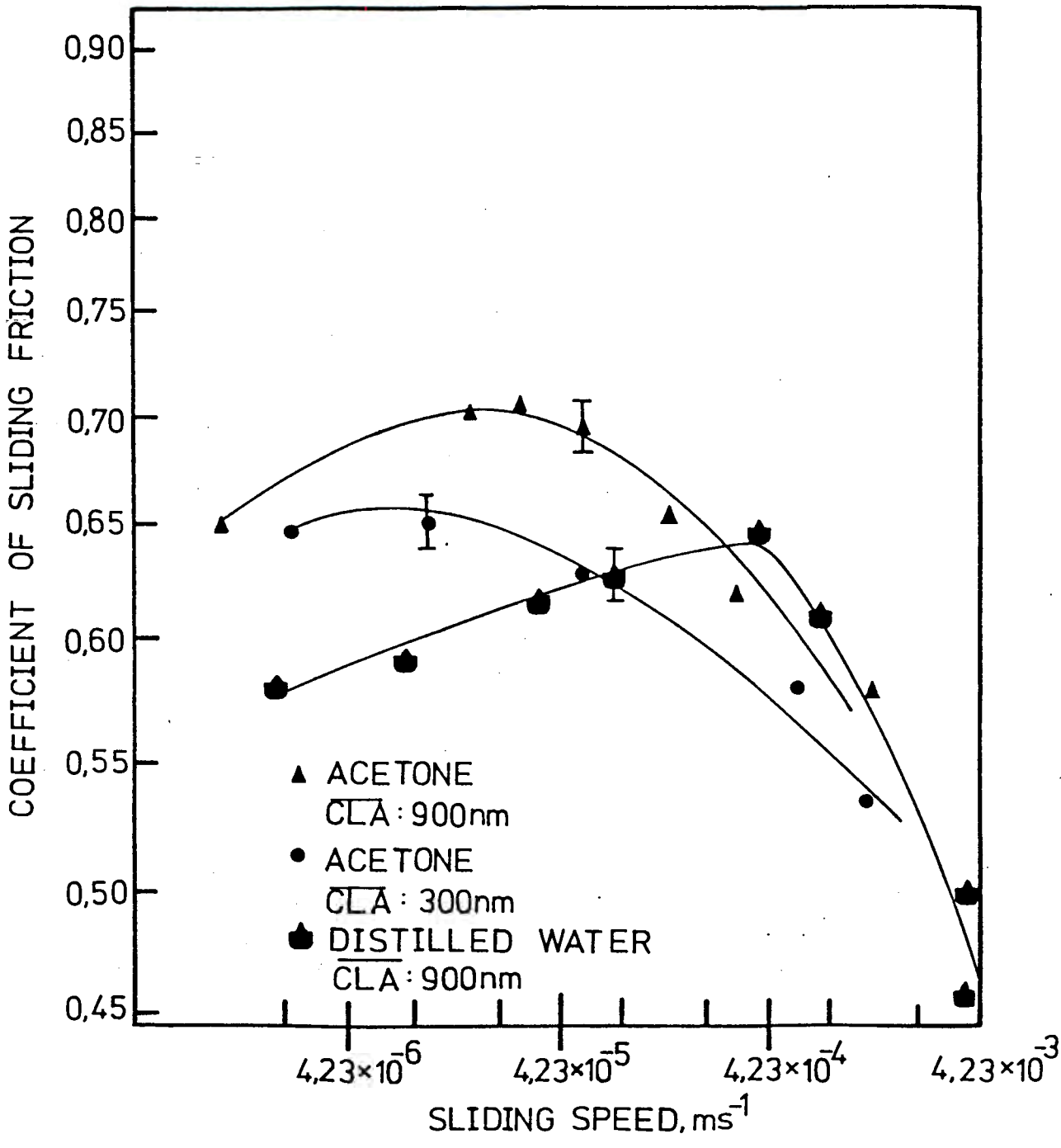

Figure 17

Relationship between coefficient of sliding friction and sliding speed in acetone for rock surfaces of different surface finish.
Normal load applied: 20N.
(Logarithmic scales).

acid, ethylene glycol, 0,1 M sodium hydroxide, n-butyl and n-heptyl alcohols respectively. The coefficient of friction for each of these environments was found to be dependent upon the sliding speed, in a different manner for each of them.

The coefficient of sliding friction was found to increase with the sliding speed in dry environment (figure 15), while a maximum value of this coefficient was obtained in the other environments used at sliding speeds from 4,23 x 10^{-6} to 4,23 to 10^{-4} ms^{-1}. Large values of the coefficient of friction were observed in n-heptyl alcohol environment, which at the sliding speed of 8,46 x 10^{-6} ms^{-1} was equal to 0,9, in comparison to the values 0,62 and 0,45 obtained in n-butyl alcohol and oleic acid at the same speed (figures 15 and 16).

4.3.2. Dependence on normal load

The frictional force was measured under normal loads in the range 5 N to 70 N, at a speed of 4,23 x 10^{-5} ms^{-1}. The tests were performed in dry, distilled water, normal butanol, normal heptanol and normal octanol environments. The dependence of the frictional force octanol on the normal load applied in dry and water environments is shown in figure 18 while the dependence of the coefficient of friction on the normal load applied is shown in figure 19. Similar relationships in figures 18 and 19 were obtained for the other environments used. The coefficient of sliding friction changes with the normal load presenting maximum and/or minimum values at different values of normal load in each of the used environments.

The frictional force F-normal load L relationship of two sliding quartzite surfaces was analysed graphically, in order to determine the values of the parameter m of the equation $F = kL^m$ or $\log F = \log k_1 + m \log L$. The graphical determination of the values of k (error $\pm$ 0,05 N) has given different values in each environment, which are listed in table IV. Using the graphically determined values of the parameter k, the values of the parameter m were determined, using the experimental values of nromal load and frictional force, and these are listed in table V. Although the change of the parameter m with the normal load was found to be different in each of the environments used, common characteristics can be observed at table V. When the magnitude of the applied normal loads is small m is smaller than the critical value of $^2/_3$ according to the analysis proposed by Archard (1958). As the applied normal load increases, the parameter m approaches the value of

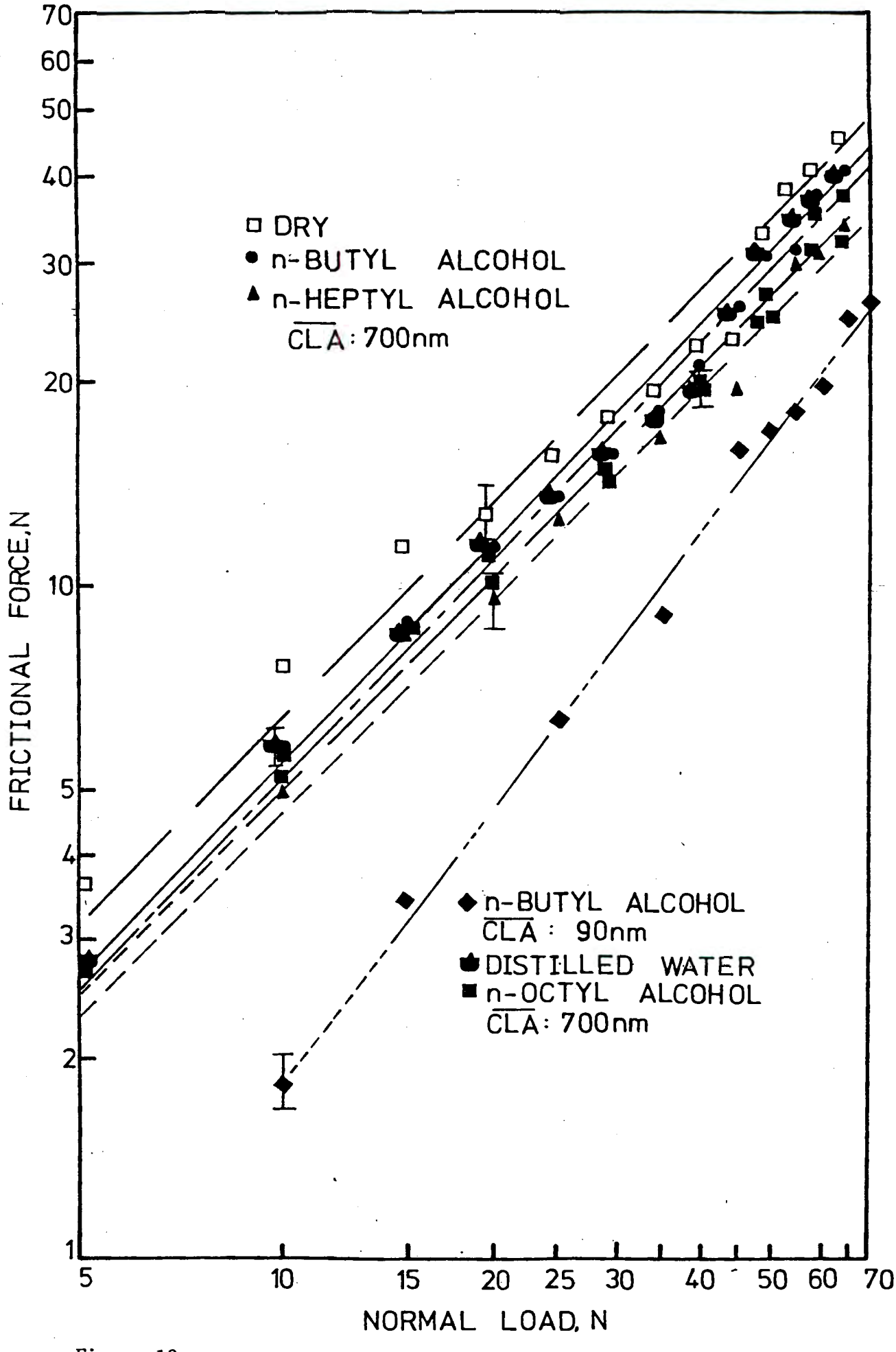

Figure 18

Relationship between frictional force and normal load in dry, distilled water and pure n-butyl, ... n-heptyl and n-octyl alcohols environments. Sliding speed: $4{,}23 \times 10^{-5}$ ms^{-1}. (Logarithmic scales).

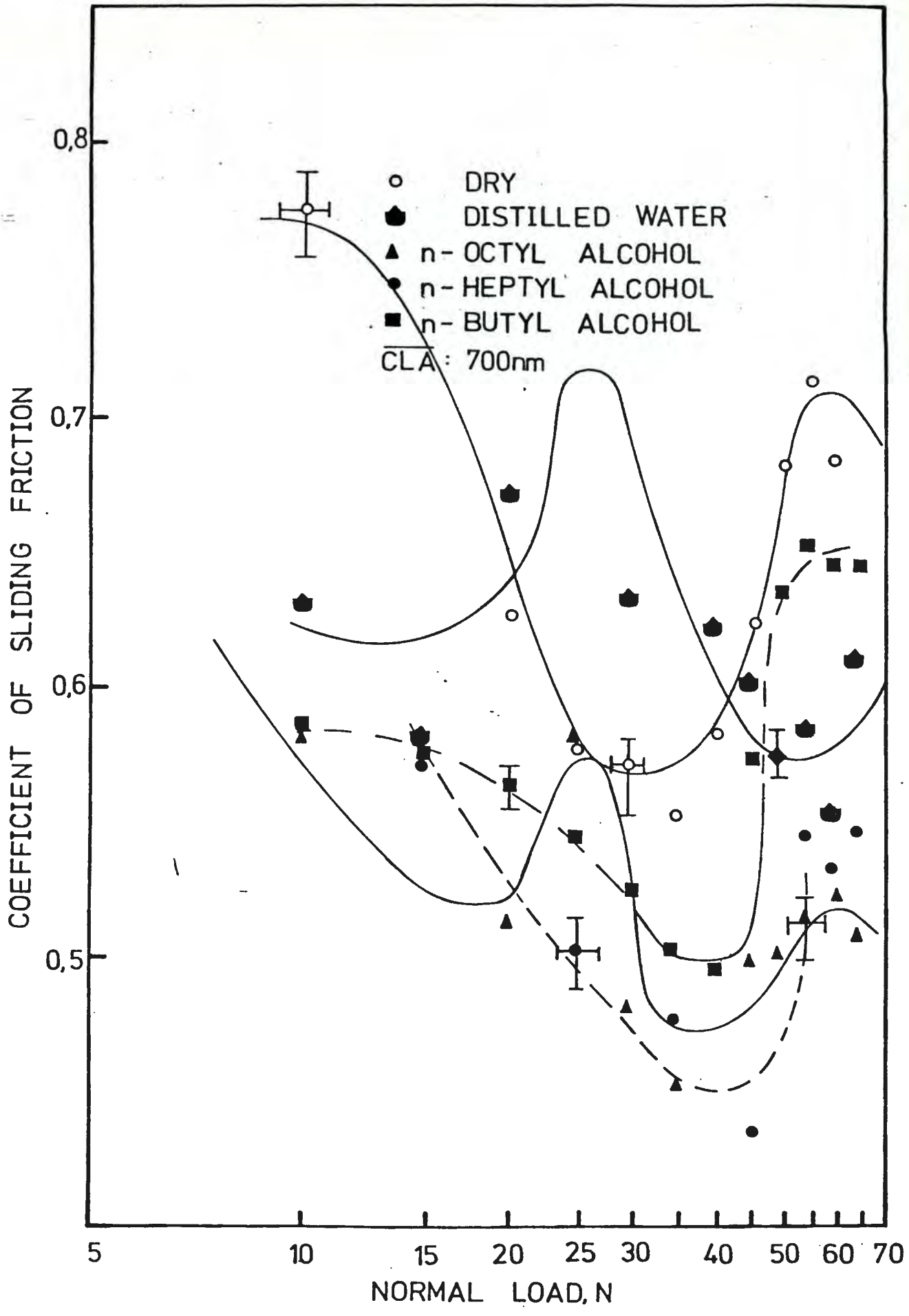

Figure 19

Relationship between coefficient of sliding friction and normal load in dry, distilled water and pure n-butyl, n-heptyl and n-octyl alcohols environments.
Sliding speed: $4{,}23 \times 10^{-5}$ ms^{-1}.
(Logarithmic scales).

0,66 and for loads higher than a critical value of load, which is different in each environment, m is equal to 0,66. For much larger normal loads m is larger than 0,66. In water environment, this change of m with the normal load in relation with the critical value of 0,66 is characterised by normal loads which are smaller than 20 N, between 20 and 50 N and larger than 50 N respectively. In dry environment these values of normal load are 50 and 65 N, while in n-butyl alcohol are 35 and 45 N.

4.3.3. Dependence on initial surface roughness

Friction measurements for rock surfaces of different surface roughness (900 nm and 300 nm CLA) were performed in an acetone environment, under a constant load of 20 N at sliding speeds $8,46 \times 10^{-5}$ to $8,46 \times 10^{-4}$ ms^{-1}. The obtained values for the coefficient of sliding friction are in figure 17. The coefficient of sliding friction was found to be smaller when the average height of the surface asperities is reduced while its dependence upon the sliding speed is expressed by a similar type of curve for both used types of surface roughness.

Friction measurements for surfaces of different surface roughness were also performed in n-butyl alcohol environment, under normal loads ranging from 5 to 70 N, at a constant speed of $4,23 \times 10^{-5}$ ms^{-1}. The results of these friction tests, using specimens of 700 nm and 90 nm CLA, are shown in figure 20. The values of the coefficient of sliding friction obtained by the polished quartzite surfaces were found to be much smaller than the 'as received' drill core surfaces. For example μ is smaller than 0,24 for the polished surfaces while the value of 0,58 is obtained by the as received surface at normal loads of 15 N. The dependence of the coefficient of friction upon the normal load is described by two different types of curves (figure 20). A maximum value equal to 0,4 is obtained at 60 N normal load for the 90 nm CLA surfaces, while a minimum value of 0,5 is obtained by the 700 nm surface at 35 N normal load.

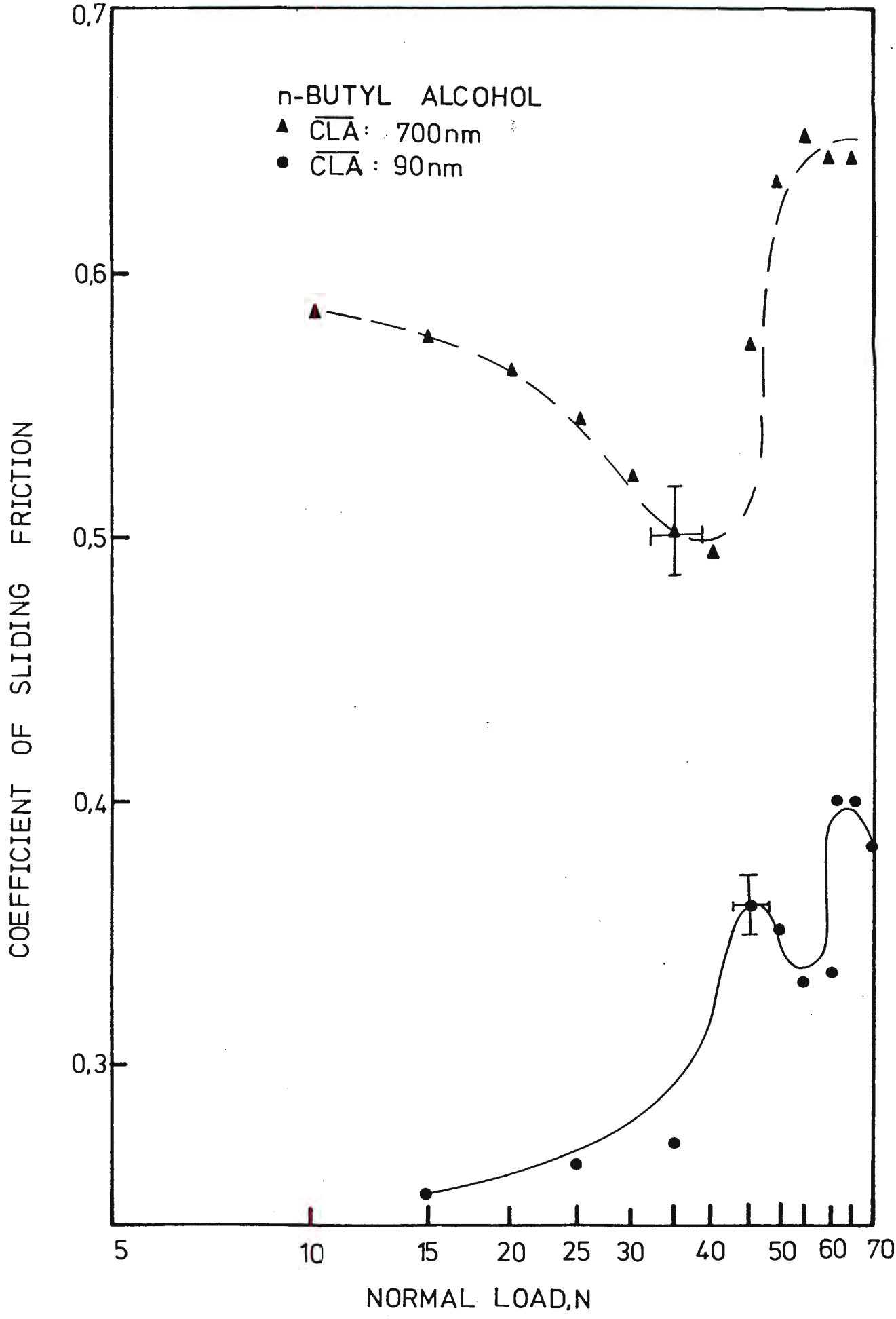

Figure 20

Relationship between coefficient of sliding friction and normal load in normal butanol environment for rock surfaces of different surface finish (700 and 90 nm CLA).
Sliding speed: $4{,}23 \times 10^{-5}$ ms^{-1}.
(Logarithmic scales).

4.3.4. Microscopic examination of the friction surfaces

The sliding surfaces produced were examined microscopically subsequent to the experiments and analysed as a function of the conditions of sliding speeds, normal load, initial surface roughness and environment.

No distinguishable surface damage on the sliding track was observed for tests performed under loads smaller than 15 N for a constant sliding speed of $8{,}46 \times 10^{-5}$ ms^{-1} or under normal load of 20 N for speeds lower than $4{,}23 \times 10^{-5}$ ms^{-1}, using Witwatersrand quartzite specimens of C type (Plates 18, 19). For loads between 15 and 40 N or sliding speeds between $4{,}23 \times 10^{-4}$ and $4{,}23 \times 10^{-5}$ ms^{-1} only the tips of the surface asperities fail by brittle cleavage fracture (Plates 20 to 31). For normal loads higher than 40 N or sliding speeds higher than $4{,}23 \times 10^{-4}$ ms^{-1} the formation of distinct friction grooves was found to take place (Plates 32 to 36). The width of these friction grooves was found to be 150 to 450 µm according to the experimental conditions. The size and friction debris observed by SEM, were found to be approximately 500 nm to 50 nm. The larger debris particles appeared to have angular edges as would expected for a brittle fracture product, while the fine gouge-debris were found to adhere on each other without possessing distinguishable angular edges.

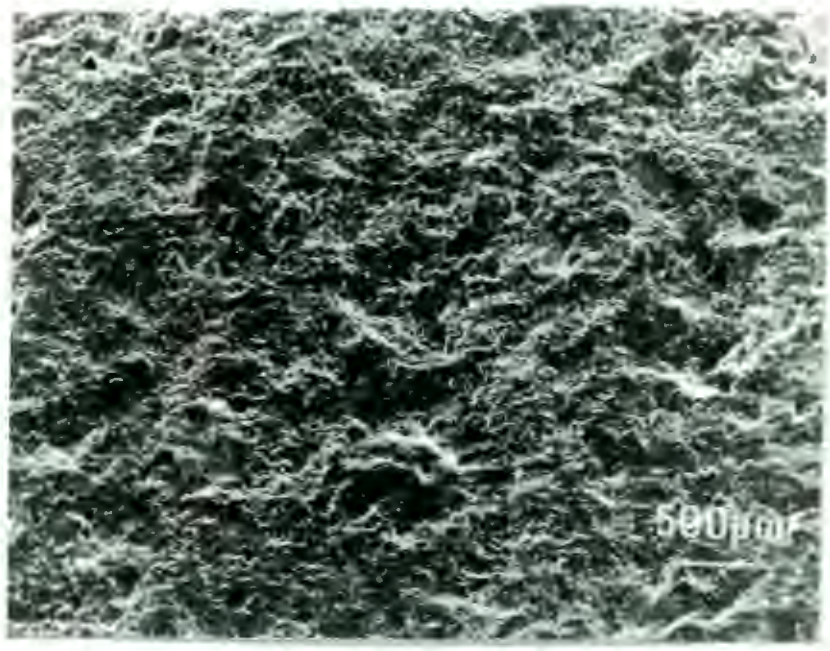

Plate 18

Surface morphology of a friction track taken from a test at sliding speed of $8,46 \times 10^{-7}$ ms^{-1} and under normal load of 20N.
Environment: water.
No surface damage is distinguishable.

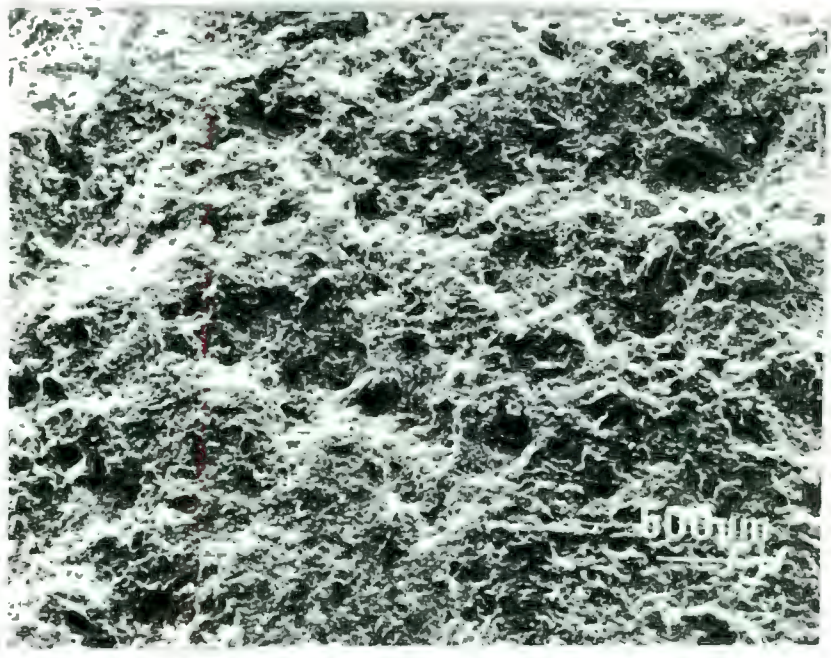

Plate 19

Surface morphology of a friction track taken from a test of sliding speed of $8,46 \times 10^{-5}$ ms^{-1} and under normal load of 10N.
Environment: water.
No surface damage is distinguishable.

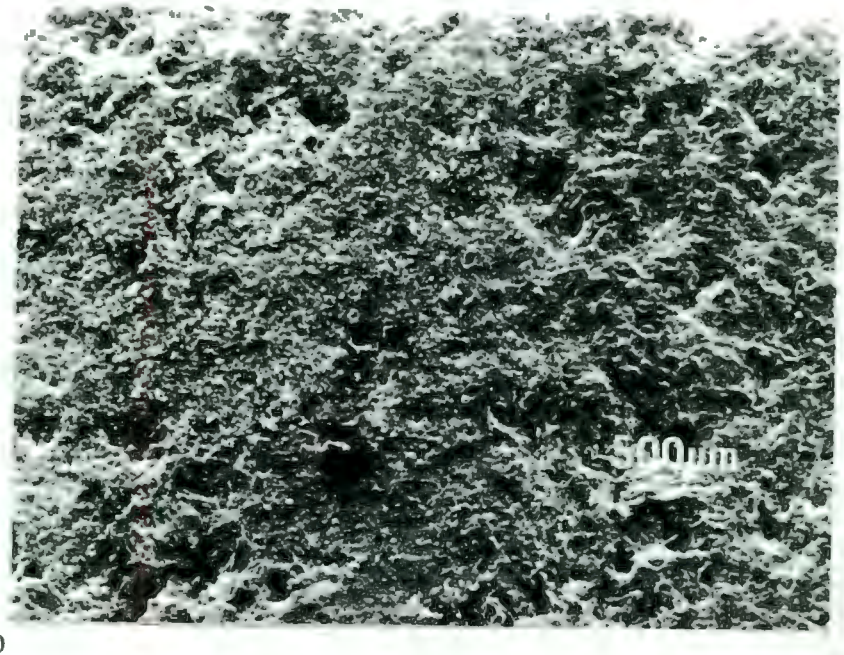

Plate 20

Surface morphology of a friction track taken from a test at sliding speed of 8,46 x 10^{-5} ms^{-1} and under normal load of 20N.
Environment: water.
Some surface damage is distinguishable.

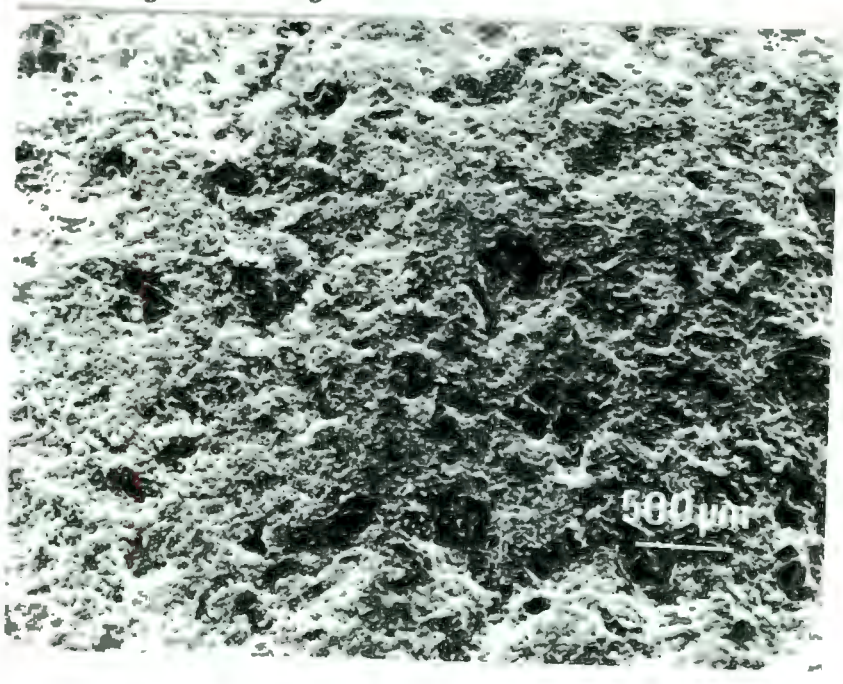

Plate 21

Surface morphology of a friction track taken from a test at sliding speed of 8,46 x 10^{-5} ms^{-1} and under normal load of 15N.
Environment: water.
A light surface damage is distinguishable.

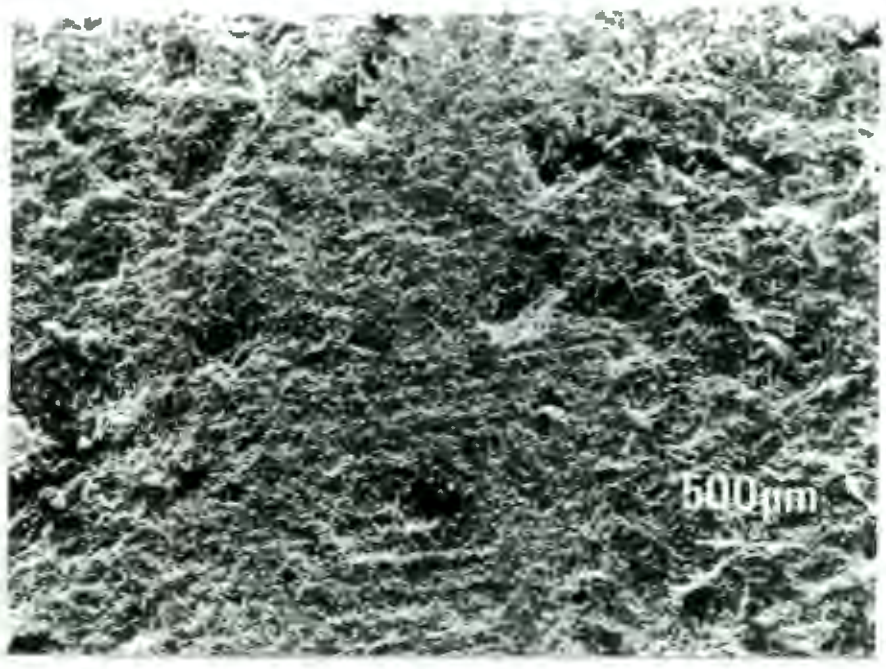

Plate 22

Surface morphology of a friction track taken from a test of sliding speed of 8,46 x 10^{-5} ms^{-1} and under normal load of 20N.
Environment: water.
Some surface damage is distinguishable.

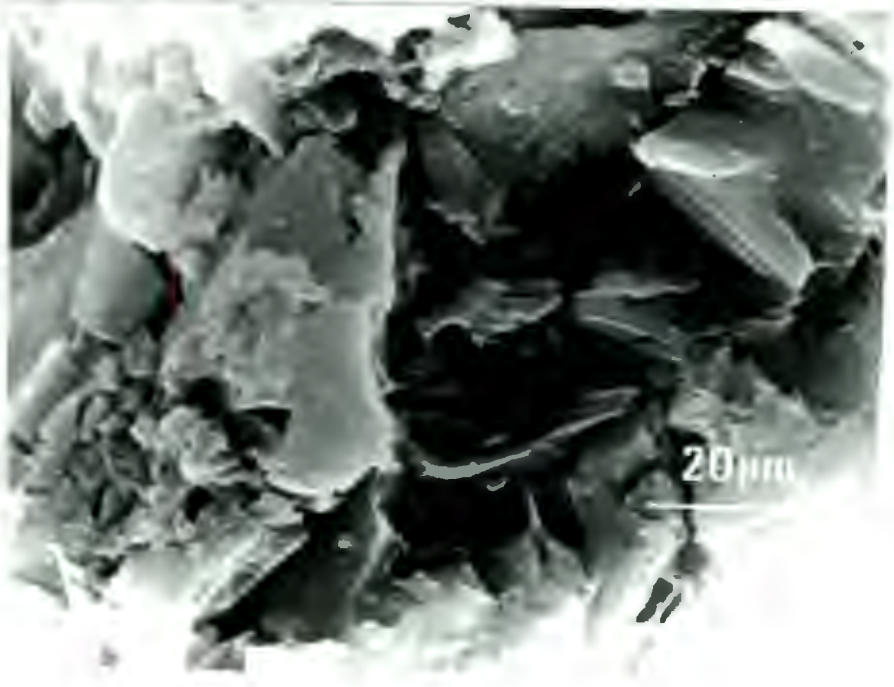

Plate 23

The same friction track, as at plate 22, at higher magnification.

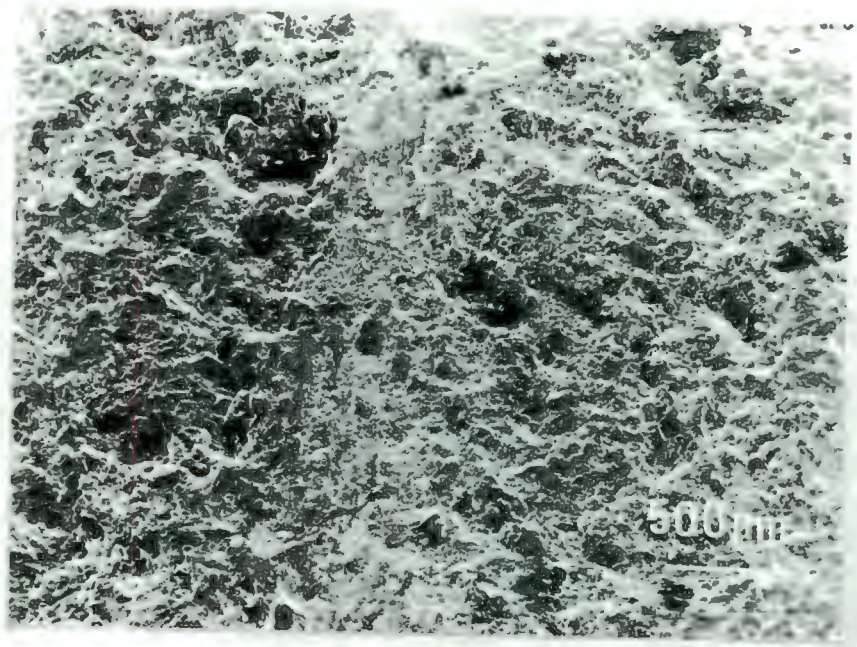

Plate 24

Surface morphology of a friction track taken from a test at sliding speed of 8,46 x 10^{-5} ms^{-1} and under normal load of 35N.
Environment: water.

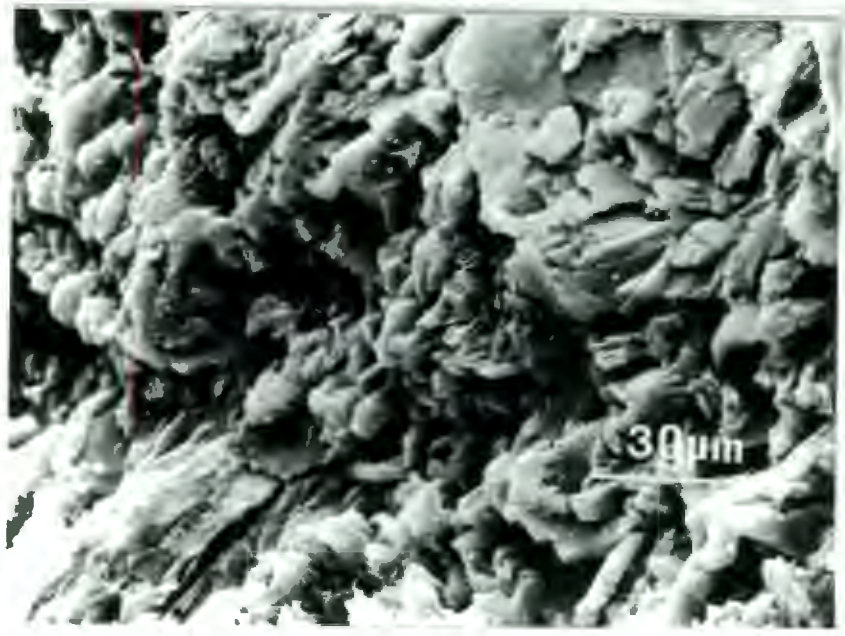

Plate 25

The same friction track, as at plate 24, at higher magnification.

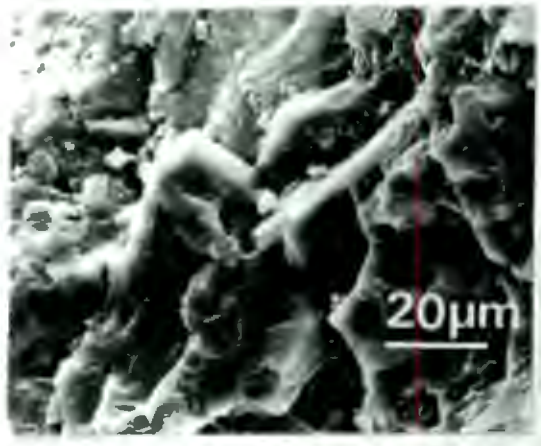

Plate 26

The same friction track, as at plate 24, at higher magnification.

Plate 27

The same friction track, as at plate 24.

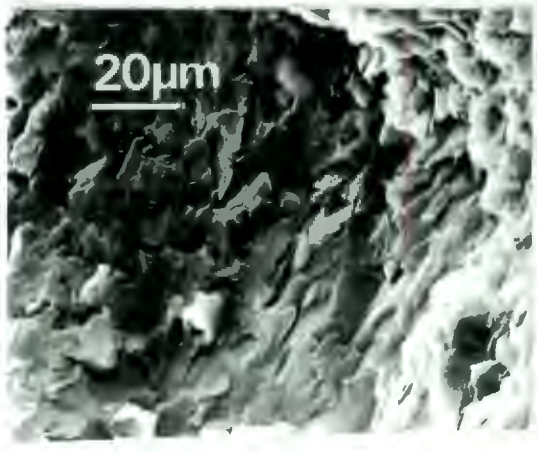

Plate 28

The same friction track as at plate 24.
A cavity, possibly resultant of a grain removal during friction.

Plate 29

The floor of the cavity shown in plate 28, under higher magnification.

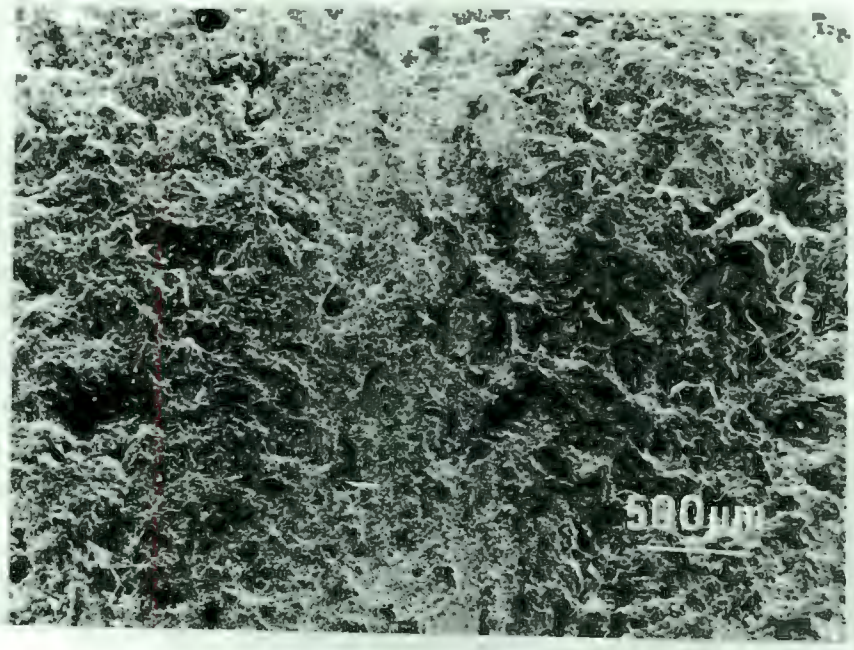

Plate 30

Surface morphology of a friction track taken from a test at sliding speed of $4,23 \times 10^{-5}$ ms^{-1} and under normal load of 20N.
Environment: ethylene glycol.

Plate 31

The same friction track, as at plate 30, under higher magnification.

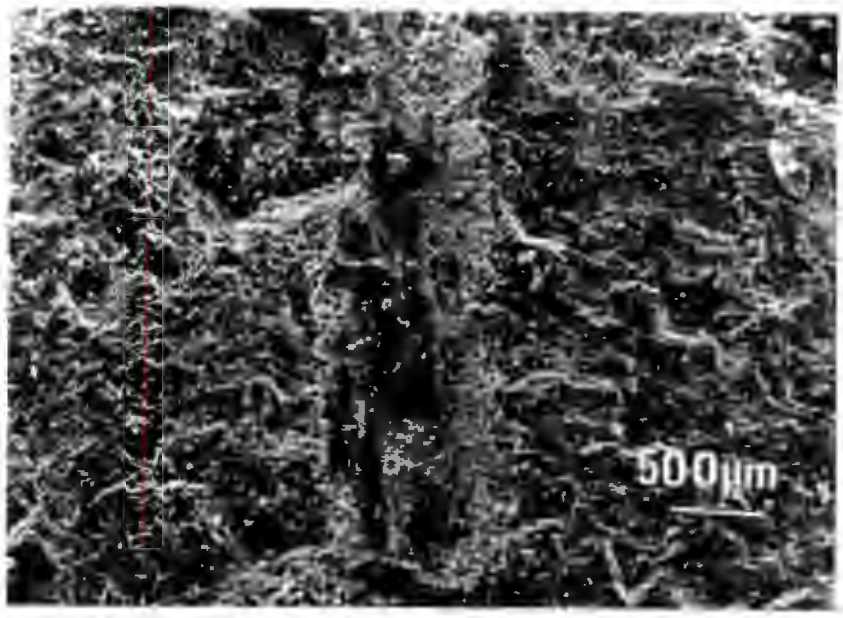

Plate 32

Surface morphology of a friction track taken from a test at sliding speed of $8{,}46 \times 10^{-4}$ ms^{-1} and under normal load of 20N.
Environment: water.
The groove formed is indicative of the occurence of both plastic flow (smooth finish) and brittle fracture phenomena (rough surface and presence of sharp, comminuted particles).

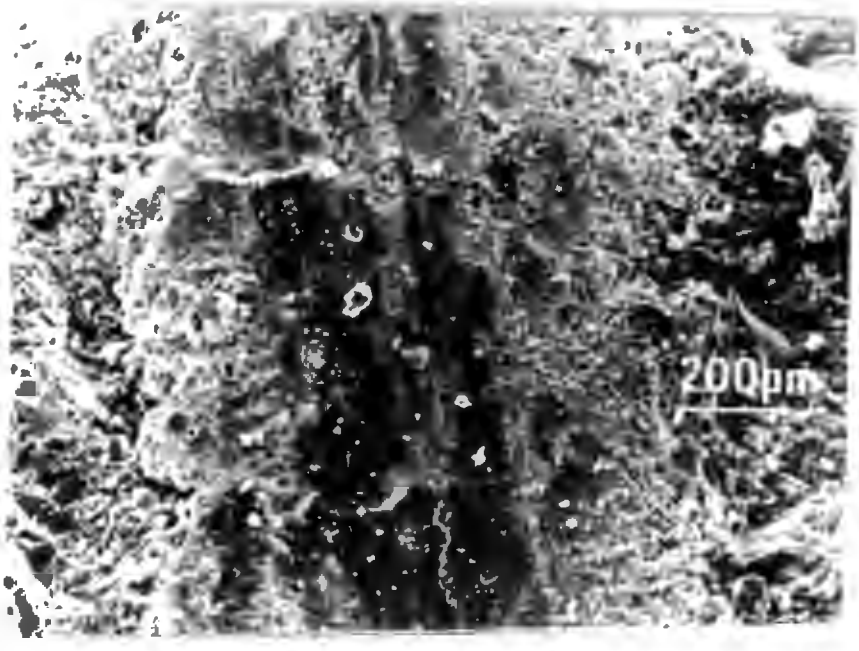

Plate 33

The same friction track, as at plate 32, at higher magnification. Sharp comminuted particles and microcracks are distinguishable on the formed friction groove.

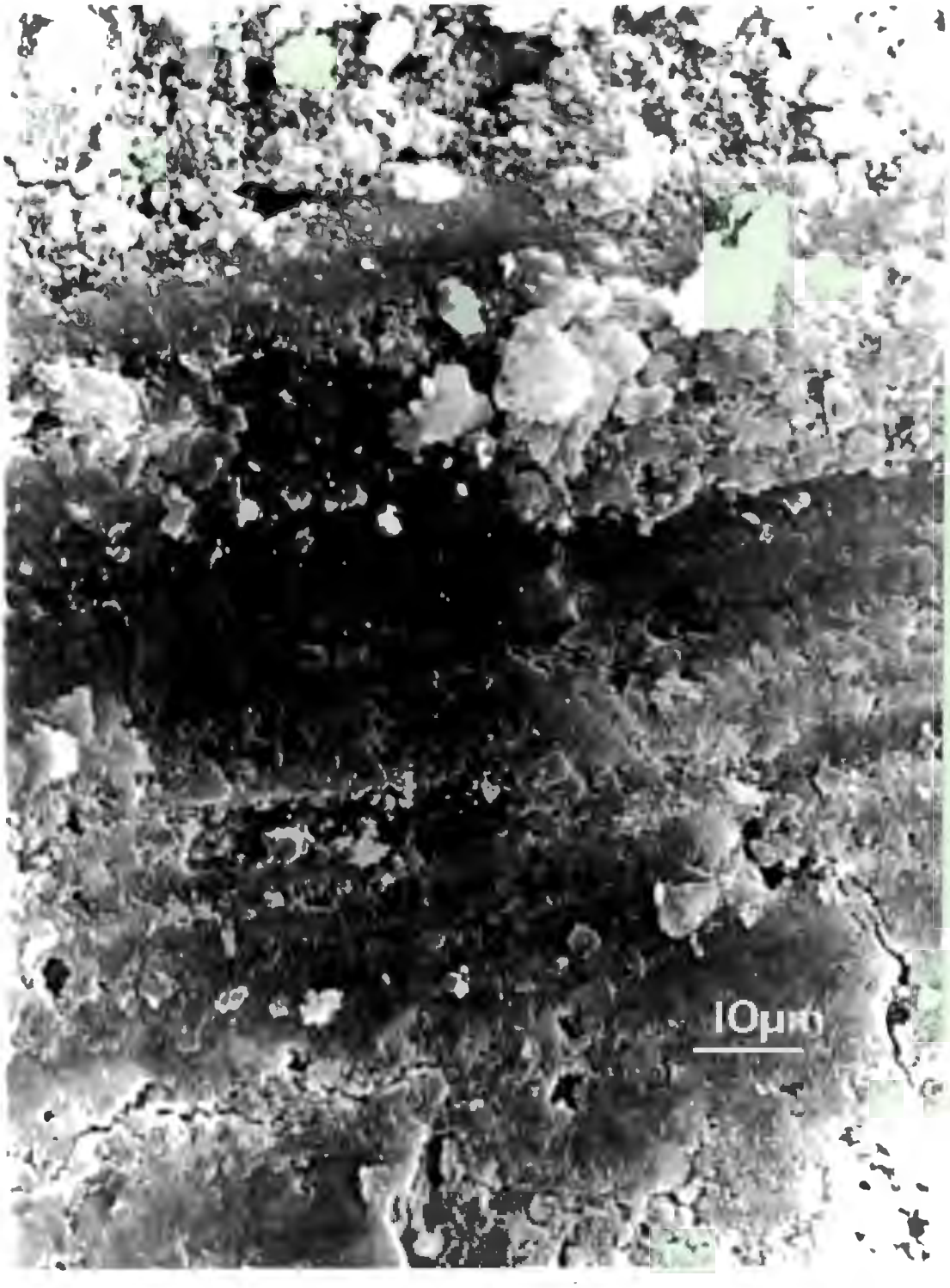

Plate 34

The same friction track, as at plates 32 and 33, under higher magnification.

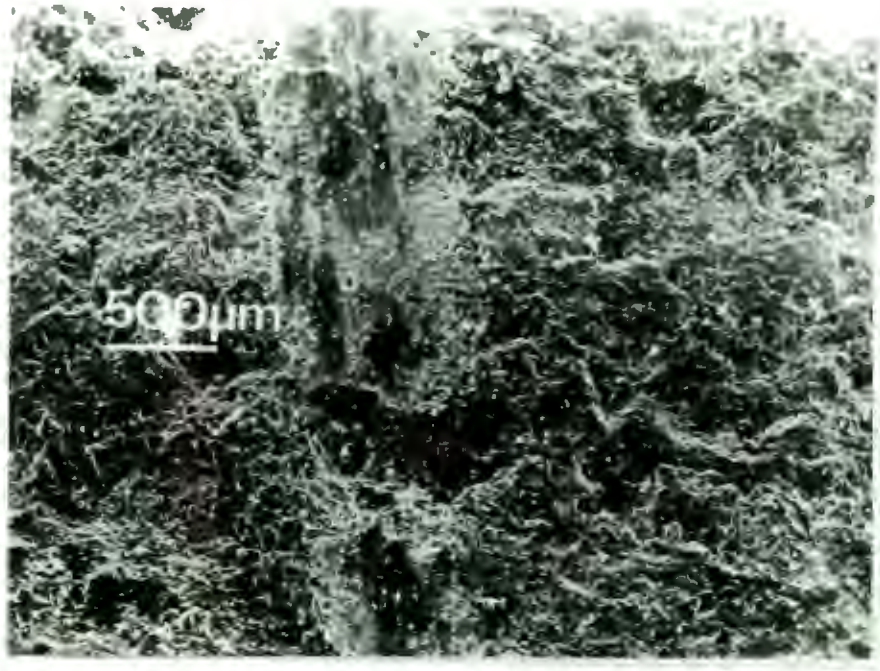

Plate 35

Surface morphology of a friction track taken from a test at sliding speed of 8,46 x 10^{-4} ms^{-1} and under normal load of 20N.
Environment: n-butyl alcohol.

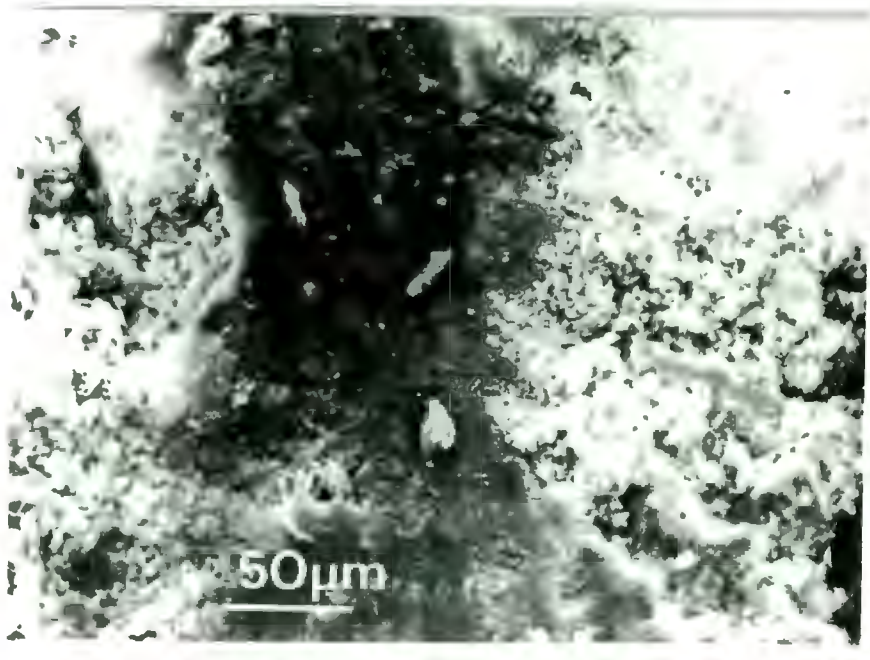

Plate 36

The same friction track, as at plate 35, under higher magnification.

TABLE IV

Values of the frictional parameter k_1 in different environments.

Environment	k_1, N
Dry	0,60
Water	0,47
Normal Octanol	0,45
Normal Heptanol	0,40
Normal Butanol	0,42

TABLE V

Values of the frictional parameter m in different environments and normal loads applied.

Normal Load N	Dry	Water	n-Butanol	n-Heptanol	m-Octanol
5	0,46	0,52			
10	0,55	0,56	0,57		0,54
15	0,58	0,58	0,60	0,61	0,60
20	0,57	0,63	0,62		0,60
25	0,58	0,65	0,63	0,63	
30	0,59	0,65	0,64		0,61
35	0,60	0,66	0,64	0,63	0,61
40	0,61	0,66	0,66		0,64
45	0,60	0,66	0,68	0,64	0,64
50	0,65	0,66	0,70		0,65
55	0,66	0,67	0,70	0,68	0,66
60	0,66	0,67	0,71	0,68	0,67
65	0,67	0,69	0,71	0,69	0,68

CHAPTER 5

THE STUDY OF THE ABRASION OF QUARTZITE SURFACES

5.1. Introduction

When two surfaces are rubbed against each other, frictional phenomena take place resulting in material removal. The wear mechanisms of friction between two brittle solids, despite the great interest in many engineering applications, are poorly understood. Glass and diamond are the materials, which were the subject of the early studies of abrasion. Preston (1922) investigated the structure of abraded glass surfaces and the flow produced in glass by stationary, rolling and sliding spheres. Tolkowsky (1920), (reference from Denning, 1953) proposed that abrasion of diamond on diamond proceeds by mechanical chipping on a microscopic scale. He found that the rate of material removal was proportional to the speed of rubbing. Denning (1953, 1955, 1957) also examined the abrasion of diamond surfaces, in relation to the orientation of the crystals, and found changes with the direction, in the cutting behaviour of diamond with the direction of cut Wilks & Wilks (1959, 1972) found great differences in the abrasion resistance on the various faces for different directions of abrasion of diamond. Seal (1958) also examined the abrasion of diamond on diamond. He found that, although the variations in the coefficient of friction with sliding direction were small, the resulting variation in the wear due to abrasion were large. Lawn and Komatsu (1966) and Frank, Lawn, Lang and Wilks (1967) studied the nature of surface damage suffered by the abrasion of diamond by X-Ray topographic means, and concluded that a microcracking mechanism is involved in the wear process. More work on the abrasion of diamond confirming Tolkowsky's postulation, was done by Wilks and Wilks (1972) and Wilks (1973).

Sapphire (Al_2O_3) has also been studied extensively in relation to it's abrasion behaviour. Steijn (1961) found that the wear of synthetic corundum (α-Al_2O_3) crystals was a function of crystallographic orientation with respect to plane of wear and rubbing direction. Evidence of plastic flow at the wear surface was also found. The plastic deformation of Al_2O_3 by abrasion was also studied by Hockey (1971, 1972). This author provided direct evidence, by transmission

electron microscopy, that this normally brittle material is deformed plastically at room temperature during abrasion. A model for the abrasion processes was proposed by Lawn, Swain and Phillips (1975), using the information derived from microfracture patterns produced beneath standard hardness indenters. According to this model, plastic deformation phenomena take place during the loading of the indenter or of any indenting sharp points, median vent cracks initiate and subsequently propagate radially. Upon unloading the indenter lateral vent cracks initiate and extend laterally from the deformation zone toward the specimen surface. The second type of cracking is the most important in terms of wear. The distribution of stresses at the boundary between the plastic deformation zone and the elastic matrix, during the indenter withdrawal is associated with the chipping fracture phenomena.

Lawn (1975) suggested that the wear during abrasion is related with the material "hardness", which is indicated by the width of the track produced by "plastic" deformation by a sliding particle. The "hardness" of the material, is a rate-dependent quantity, varying with the abrasion conditions for example environment or load rate (sliding velocity). Veldkamp and Klein Wassink (1976) investigated the energy required to remove a unit volume of brittle materials, such as SiC sintered alumina, glass or strontium hexaferrite. At very shallow penetration depths of a sharp scratching point the surface morphology was indicative of purely ductile grooving. For higher loads applied on this sharp scratching point, cracks are associated with the ductile ploughing resulting in chipping phenomena. The specific energy of the latter case was found to lower than the one of the ploughing action. The value of this energy was found to be $3{,}1 \times 10^{3}$ Jm^{-3} for sintered alumina.

The influence of the flushing fluid during diamond drilling was examined by Cooper and Berlie (1976) for marble and granite rocks using different feed force and rotation speed. The authors did not find any large differences in the measured penetration rates between surface active environments, such as normal alcohols and water.

5.2. Experimental Technique

5.2.1. Specimens

Quartzite drill cores* of 35,5 and 42,2 mm diameter and approximately 180 mm length were used. A selection of the drill cores was performed in order to maintain petrographical uniformity of the rocks used and to avoid surface flaws or included impurities. The samples selection was completed by petrographic observations in a reflected light optical microscope and initial surface roughness measurements were performed by a Talysurf profilometer. The rock samples, were washed with 50°C water and subsequently dryed in a 70°C drying cabinet, for 30 minutes. This procedure has been followed before and after each test in order to avoid errors in the mass loss determination. Abrasion tests were performed with Witwatersrand quartzite specimens of the four petrographical types, classified as A, B, C, and in the manner described in chapter 2.

5.2.2. Apparatus and procedure

The abrasion tests were performed, by rotating two quartzite drill cores, orthogonally against each other. Loads were applied normal to the axes of the rotating drill cores, by an ESH-Universal-testing machine via a pair of idler rollers, (Plate 37) while the rotation speed and torque was kept constant at the desired values by a pair of thyristor controlled DC-motors (Appendix F). The apparatus, shown in plate 38 consists of an L shaped rig, on which the two motors are fixed.. The power transmission from the motors to the rock specimen holders is effected by a pair of universal joints (Appendix G). The abrasion testing apparatus was mounted on the base table of the testing machine (Plate 39), for which both load actuator and load cell were aligned over the base table. The applied normal load is controlled by a closed loop signal system (Appendix F). A closed loop signal system is also applied to the motors by the thyristor control unit which maintains constant armature voltage and constant armature current. An additional instrumentation, consisting

---

*Kindly supplied by the Chamber of Mines Research Organization.

Plate 37

(a) Components of the power transmission system used from the motors to the rock specimens.

(b) Components of the clamping device used for the drill core quartzite specimens.

(c) A quartzite drill core specimen held by the clamping device.

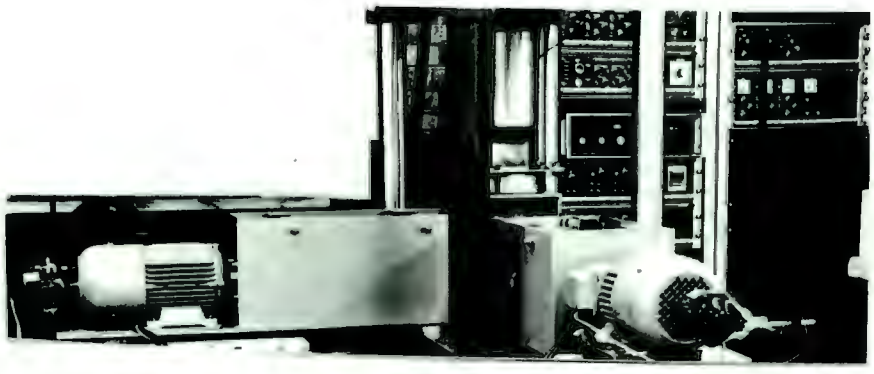

Plate 38

The abrasion testing apparatus housed in a mild steel waterproof frame and attached to the ESH machine.

Plate 39

The ESH servohydraulic universal testing machine.

of two DC-voltmeters and two DC-ammeters are attached in parallel and in series respectively, in order to monitor the feedback signal during the course of each test. The verification of the thyristor signal for the control of the constant rotation speed desired is maintained by a pair of DC-tachogenerators which monitor directly the rotation speed of motor shafts. RPM-meters, attached to the tachogenerators, give a continuous reading of the RPM of each motor. This signal is also recorded by time-based chart recorders. Another time-base recorder monitors the load applied by the ESH-machine. In this case it is necessary to amplify the load-signal, in order to observe the load fluctuations accurately. The flow of the liquid environments used was continuously applied on the abrading surfaces during each test by means of an adjustable tap, positioned in such a way, as to ensure the steady removal of the wear particles. A low pressure was applied by giving the liquid environment ahead of 0,8 m. In order to maintain uniform distribution of the surfactant reagents, some of which are immiscible at the concentration required, mechanical agitation was applied in the form of a rotating impeller. For better mixing conditions, water at $45^{o}C$ ($\pm$ $4^{o}C$) was used, during the course of all the abrasion tests performed. A continuous output of the flowing environment with the wear particles was maintained by housing the abrasion rig in a waterproof mild steel frame (plate 38) and samples were collected for microscopical examination.

Quartzite rock samples attached to the specimen holders were kept orthogonolly to each other via two pairs of idler rollers. Before the two rock surfaces come into contact, they were wetted with the test environment. Subsequently a constant flow of 2 ℓ min^{-1} was established. The two rocks were carefully brought into contact, by means of the displacement control of the ESH machine before the starting of their rotation. The selected load was gradually applied to the rock specimens, while the thyristor controls were used to select the rotation speed. A time-switch, connected in line with the AC power supply of the motors maintained the tests periods to an accuracy of $\pm$ 2 seconds. During each abrasion test, the test variables of load, rotation speed and torque were kept constant with the following deviations, monitored via the instrumentation units.

A deviation of ± 5 per cent for the load, was observed during each abrasion test and was due to the stick-slip of the interlocked surface asperities of the rubbing specimens. (Figure 21). A minor deviation on the load applied, ±2 per cent was due to an instrumentation error ("noise"). A deviation of ±4 per cent was observed for the rotation speed, during each abrasion test performed, while the torque was kept constant, with a ±5 per cent experimental error. The wear of the quartzite specimens was determined by two methods. The first was the measurement of the mass loss, i.e. the difference in mass before and after each test, determined by means of a balance with an accuracy of $\pm 1 \times 10^{-6}$ kg. The second was the measurement of the depth and the width of the wear groove, by means of a micrometer with an accuracy of ± 10 μm.

The reproducibility control for the abrasion testing apparatus, was performed by fifteen tests for each petrographical type of the Witwatersrand quartzite, presenting an experimental error ±2 per cent, for in the measured mass loss , the coefficient of linear wear φ and the width of the abrasion track w. The mass loss τ, expressed in 10^{-6} kg. represents the difference in mass, before and after the test and the coefficient of relative wear λ_τ is defined as: $\lambda_\tau = \tau_{environment} / \tau_{water}$. The coefficient of linear wear φ, is given by $10(D-D')/D$ where D is the initial specimen diameter and D' is the specimen diameter at the surface region of the abrasion track. The abrasion track width w is expressed mm. The values of $\tau, \lambda_\tau, \varphi$ and w represent the average of the values obtained from both the upper and the lower abrading specimens.

5.3. Results

5.3.1. The effects of the rock petrography

The petrography of the rock was found to influence the abrasion behaviour. The fine grained quartzite, designated as A, was found to wear at the rate of 560×10^{-6} kg per a 10 minutes test in a water environment under 100 N normal load and 240 RPM rotation speed.

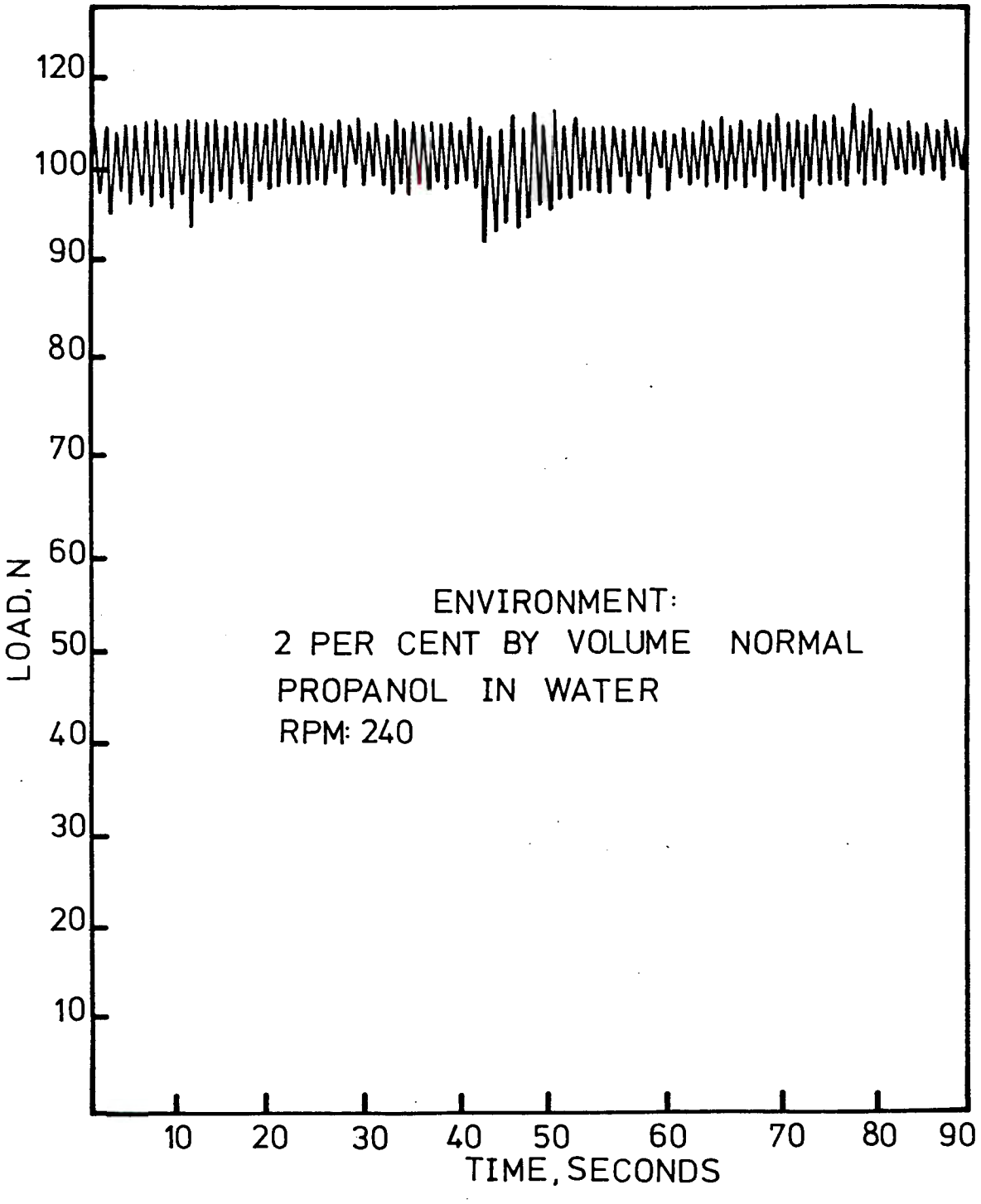

Figure 21

Relationship between normal load and time during an abrasion test. The occurence of the stick-slip phenomenon is indicated.

The fine to medium and the medium grained quartzites, designated as B and C respectively, were found to wear at the average rate of 600 and 710 x 10^{-6} kg per a 10 minutes respectively, under the same testing conditions. The argillaceous type of quartzite, designated as D, was found to behave in the same manner as the fine grained quartzite, when the abrasion was taking place into its fine grained matrix, while much higher wear rates were obtained when the abrasion involved the quartz "pebbles". The last case did not give reproducible results, since the size, orientation and relative position of the quartz "pebbles" were variable. For a total number of 24 tests on argillaceous quartzite, which presented coarse average grain size, the mean value of 690 x 10^{-6} kg, per a 10 minutes test, wear rate due to abrasion, under the above described testing conditions of load, speed and environment.

The results obtained from 15 representative drill core specimens of the Witwatersrand quartzite for a 10 minutes period abrasion tests in water environment under 100 N load and of 240 RPM speed and their respective values of the tensile strength, obtained via Brazilian tests, are shown in table VI. Figure 22 shows that the wear due to abrasion increases when the tensile strength of the rock decreases (Rock types A to C) and the grain size increased.

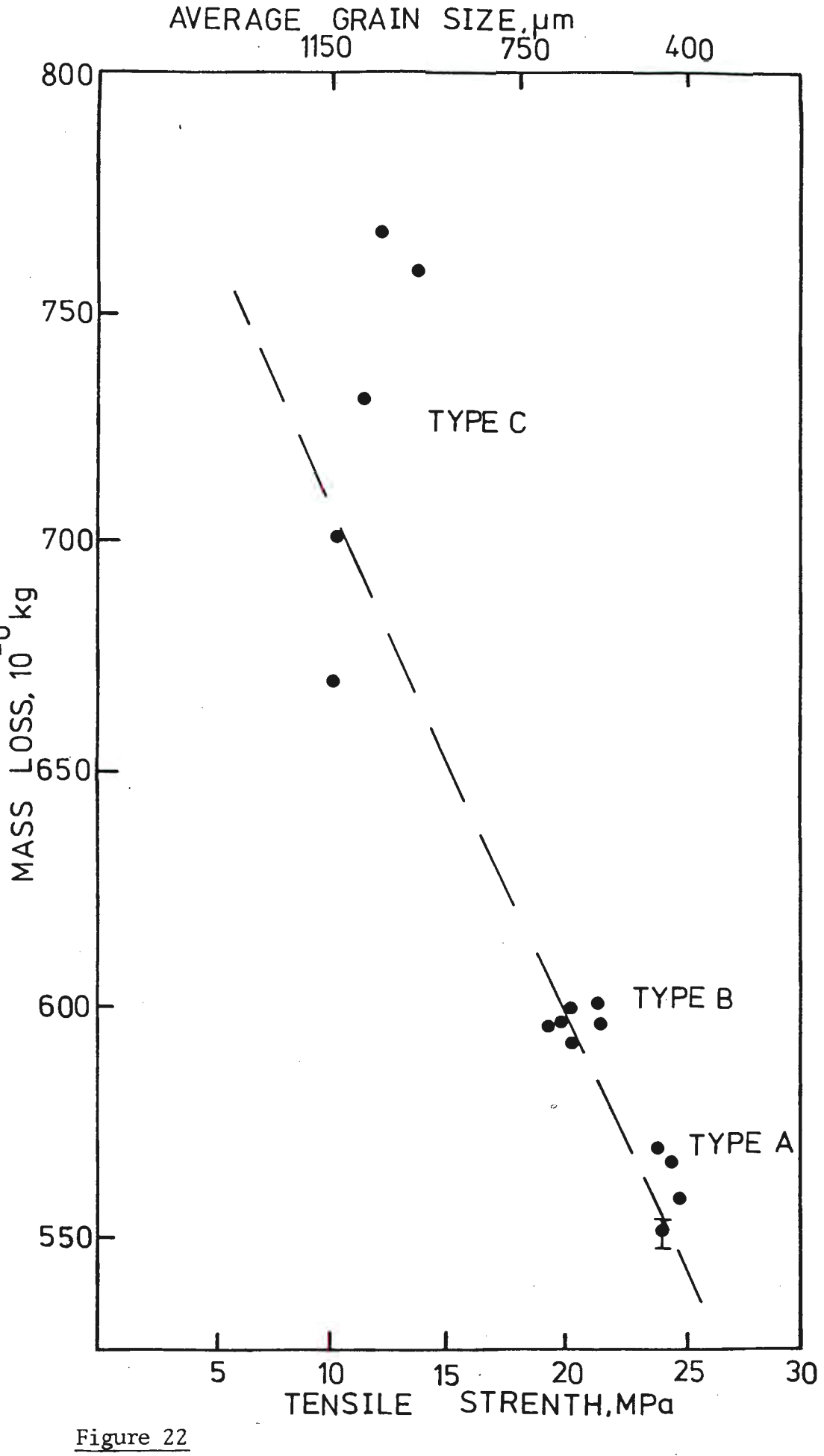

Figure 22

The influence of the rock petrography upon the mass loss due to abrasion for the types A, B and C of the Witwatersrand quartzite, expressed by the tensile strength of the drill core specimens. The role of the grain size upon the wear rate due to abrasion is also shown.

TABLE VI

Wear due to abrasion data for the A, B and C petrographical types of the Witwatersrand quartzite, classified via their respective tensile strength.

	Mass Loss, τ ,10^{-6} kg	Coefficient of Linear Wear, φ	Track Width, w, mm	Rock Type	Tensile Strength, σ_t, MPa
1	670	1,10	6,3	C	9,91
2	730	0,77	6,3	C	10,95
3	700	0,66	6,0	C	10,35
4	770	1,08	6,4	C	12,12
5	760	0,77	6,5	C	14,07
6	590	0,88	6,2	B	18,75
7	590	1,10	6,4	B	18,94
8	600	0,88	6,0	B	19,75
9	590	1,10	6,4	B	20,17
10	590	0,88	6,2	B	21,80
11	600	0,89	6,2	B	21,95
12	570	0,85	6,0	A	23,20
13	580	1,00	6,3	A	23,75
14	550	0,89	6,4	A	24,11
15	560	0,92	6,3	A	24,93

5.3.2. The effects of the environment

5.3.2.1. The effects of the chemical nature of the environment

Selected surfactants in aqueous suspension were used, in order to examine the role of the environment on the wear of the two quartzite cylindrical specimens rotating at 240 revolutions per minute under a 100 N normal load for a period of 10 minutes. Since variation in the petrography of each quartzite tupe (A, B, C and D) results in a small scatter of the wear values obtained, five tests for each drill core used, were performed. The first two tests were carried out in water and the following three in a particular environment. This sequence was followed for all the tests because chemisorption phenomena are not, in general, reversible under the cleaning and drying procedure, which was used. The results of a total of forty tests performed in n-methyl, n-ethyl, n-propyl, n-butyl, n-pentyl, n-octyl alcohols, in 0,05 M thallium chloride and in 0,05 M ammonium carbonate are shown in figure 23. The results are presented in terms of the coefficient of relative wear λ_τ , versus the number of carbon atoms of normal alcohol N_c, while the values obtained for water, thallium chloride and ammonium carbonate environments are shown separately. Each point represents the average of mass loss measurements obtained from three tests in the environment examined divided by the average of the mass loss obtained from two tests in water, for the same pair of rock samples positioned by the same way in the abrasion testing apparatus. The surfactant concentration in each environment used, was 2 per cent by volume in water.

The wear characteristics of abrasion were found to depend upon the chemical nature of the chemical reagent present. Although the concentration of the n-alcohols used was very small, 2 per cent by volume in water, their respective number of carbon atoms N_c was found to influence the comminution events of abrasion. A maximum of the wear characteristics was found for $N_c = 5$, while the smallest values were found in n-methyl and n-octyl alcohol environments.

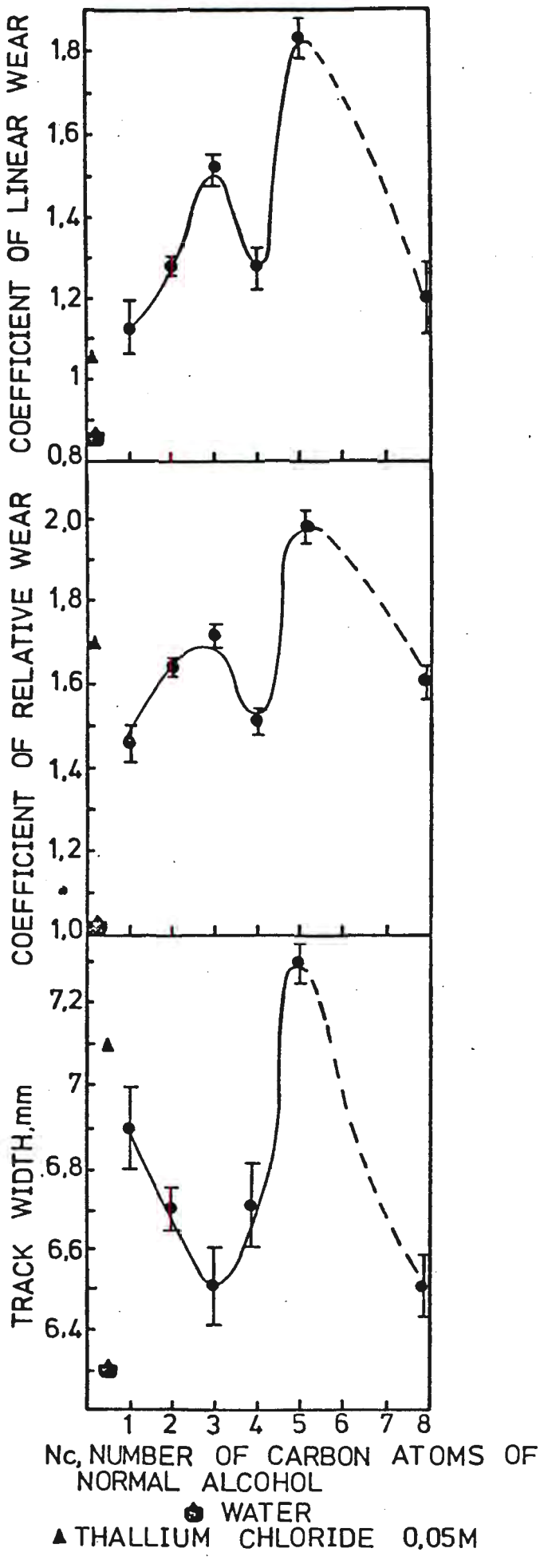

Figure 23

Relationship between coefficient of linear wear, coefficient of relative wear, track width of the abrasion groove and number of carbon atoms of normal alcohol.
Normal load: 100N.
Rotation speed: 240 RPM.
Concentration used: 2 per cent by volume in water
(0,05 M ammonium carbonate: λ_τ = 0,56, φ = 0,74 and w = 6,3 mm).

and n-pentyl alcohols. The presence of 0,05M thallium chloride was found to enhance comminution during abrasion in relation to water to a similar extent as in n-propyl alcohol, while poorer comminution results in relation to water were obtained in the presense of 0,05M ammonium carbonate ($\lambda_\tau = 0,56$, $\varphi = 0,74$ and $w = 6,3$ mm).

5.3.2.2. The effect of the concentration of the surfactant used

The effects of the concentration of the surfactant in the aqueous environment on the wear of the two rock samples was examined for a range of concentrations of ethyl alcohol in water. Ethyl alcohol was selected because it has a wider range of solubility than the other normal alcohols examined. Additionally, the test operation conditions maintained during the use of ethyl alcohol at high concentrations in water at 45°C, were the best in comparison with the other alcohols examined, in terms of safety. The results of the abrasion tests are shown in figure 24 where the coefficient of relative wear λ_τ and the coefficient of linear wear φ versus the percent by volume concentration of ethanol on a logarithmic scale are presented respectively. An approximately 9 per cent error on the concentrations used, was found by density determinations. For all the experiments of this series the rotation speed of the rock specimens was 240 ($\pm$ 10) revolutions per minute, while load of 100 N ($\pm$ 5 N) was applied. Maximum wear characteristics were obtained by concentrations of 1 per cent by volume in water.

5.3.3. The influence of the applied load

The magnitude of the load applied on the rotating rock specimens, was varied both in water and in 1 per cent by volume of n-pentyl alcohol in water environments in order to establish its influence on the abrasive wear. The results of tests performed under loads of 25, 50, 75, 100 and 125 N are shown in figure 25 where the mass loss and track width are plotted as a function of load. Force fluctuations introduced an error of approximately $\pm$ 5 per cent on the desired load value. The rotation speed of the rock specimens in this series of

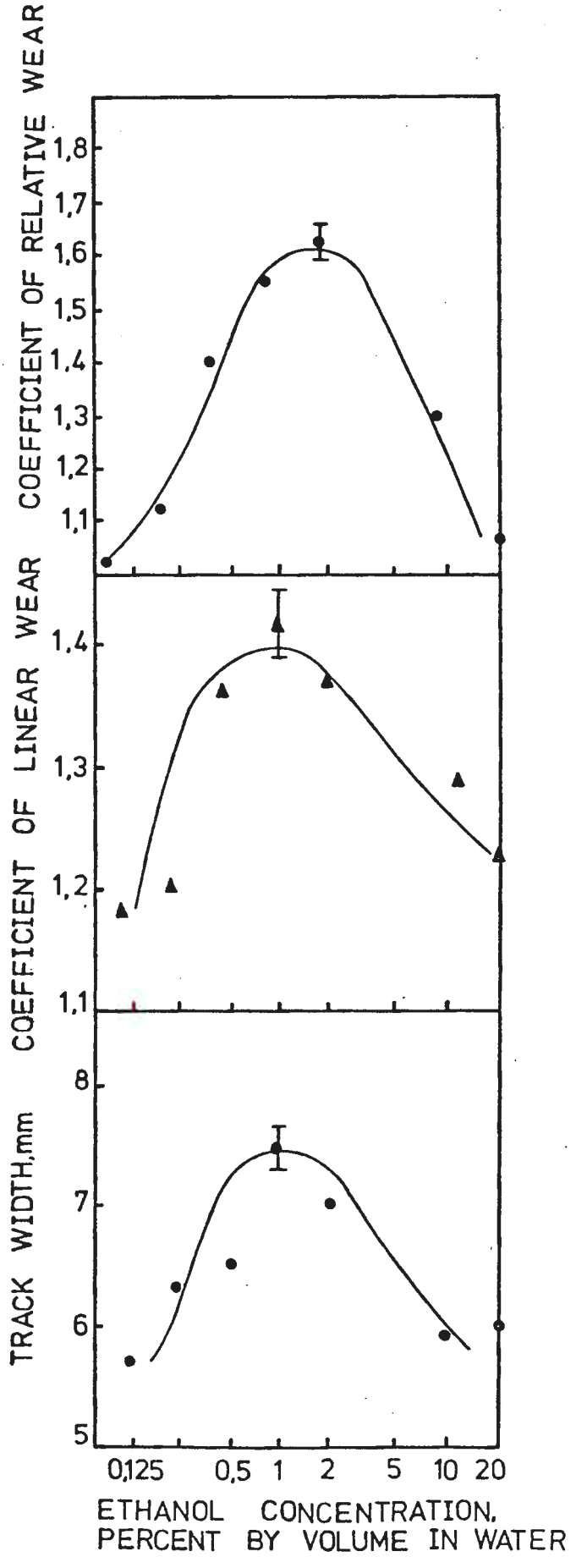

Figure 24

Relationship between coefficient of relative wear, coefficient of linear wear, track width of the abrasion groove and ethyl alcohol concentration.
Normal load: 100N
Rotation speed: 240 RPM

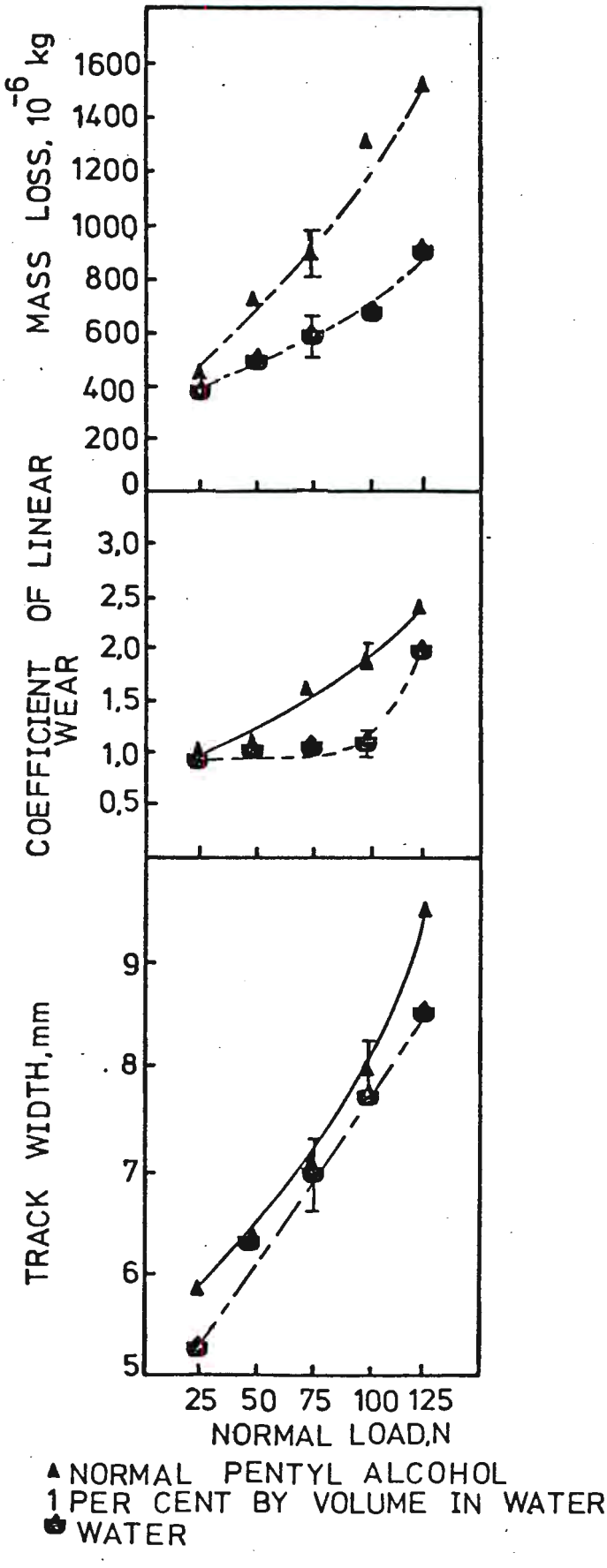

Figure 25

Relationship between mass loss, coefficient of linear wear, track width of the abrasion groove and normal load.
Environments used: Water and n-pentyl alcohol 1 per cent by volume in water.
Rotation speed: 240 RPM.

experiments was kept constant at 240 revolutions per minute. The power capacity of the motors (0,7kW for each motor) did not allow us to perform tests for higher values of load applied, at the constant rotation speed of 240 revolutions per minute.

The wear rates due to abrasion were found to increase with the normal load in both environments of the used environments and the rate of increase of wear characteristics obtained by the environment containing n-pentyl alcohol was found to be larger than the one of water environment.

5.3.4. The influence of the rotation speed and the process time

The rotation speed of the rock specimens was varied in water and in 2 per cent by volume normal propyl alcohol in order to establish the influence of speed on the wear due to abrasion and to assess the rate dependence of the effects of a surfactant. The results of the abrasion tests performed at rotation speeds between 100 and 600 revolutions per minute (i.e. speeds between 0,22 and 1,33 ms^{-1}) are shown in figure 26. These results are presented in the form of mass loss per revolution, coefficient of linear wear per revolution and track width per revolution versus the revolutions per minutes for tests of 10 minutes.

An error of $\pm$ 5 per cent was introduced in the above values due to the presence of the load fluctuations of the abrasion process. For power capacity reasons, it was not possible to achieve higher rotation speeds under the load of 100 N.

No significant change in the wear effects of abrasion was observed within the range of the used rotation speeds in both of the environments.

The wear characteristics of abrasion tests, in water and 1 per cent by volume n-butanol in water environments were examined for test periods of 10, 20, 30, 40 and 50 minutes, while the applied normal load was kept constant at 100 N. Figure 27 shows the wear characteristics of these tests expressed as mass loss per minute,

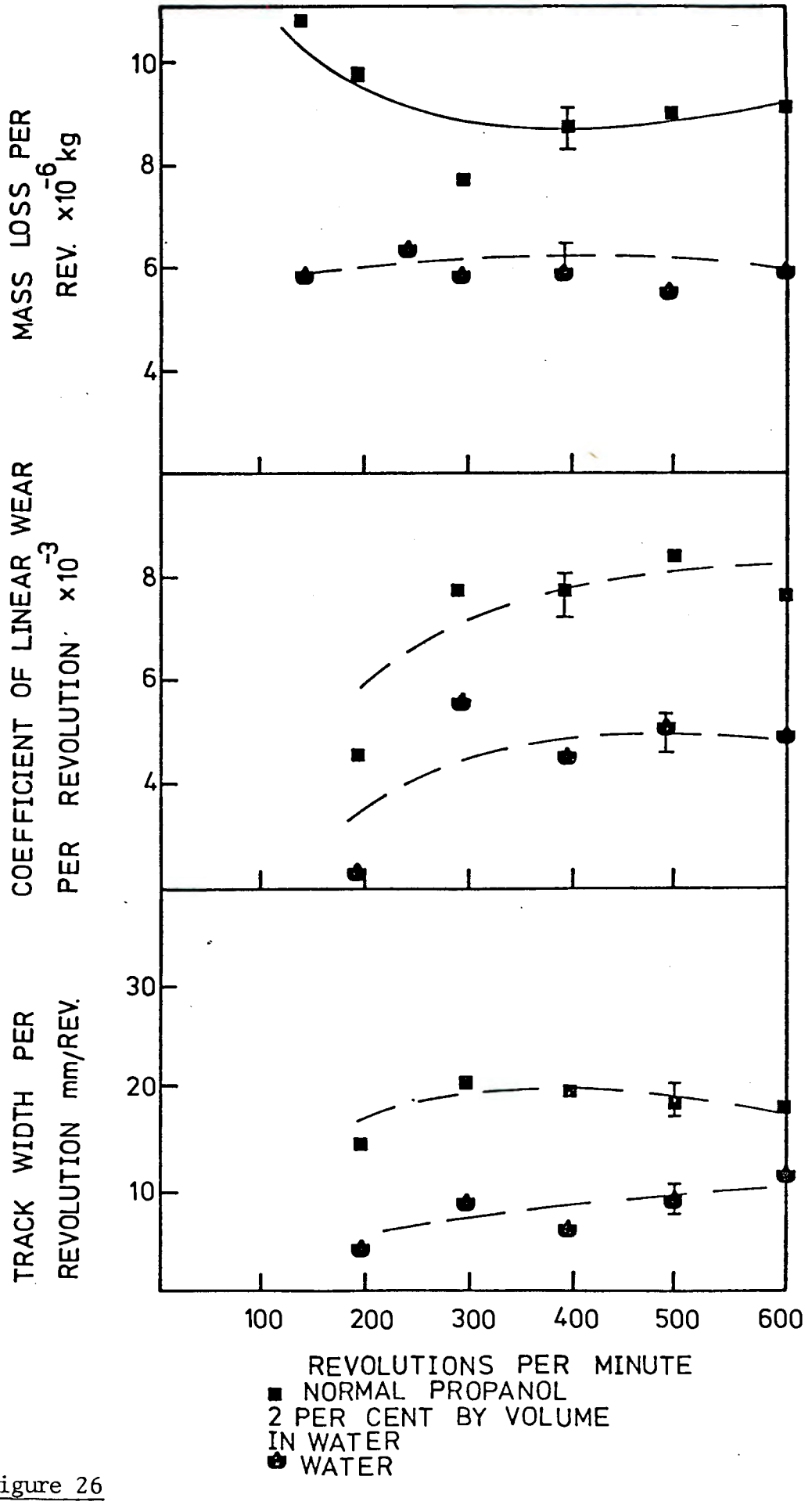

Figure 26

Relationship between mass loss per revolution, coefficient of linear wear per revolution, track width of the abrasion groove per revolution and revolution per minute of the rock specimens.
Environments used: Water and n-propyl alcohol 2 per cent by volume in water.
Normal load: 100N.

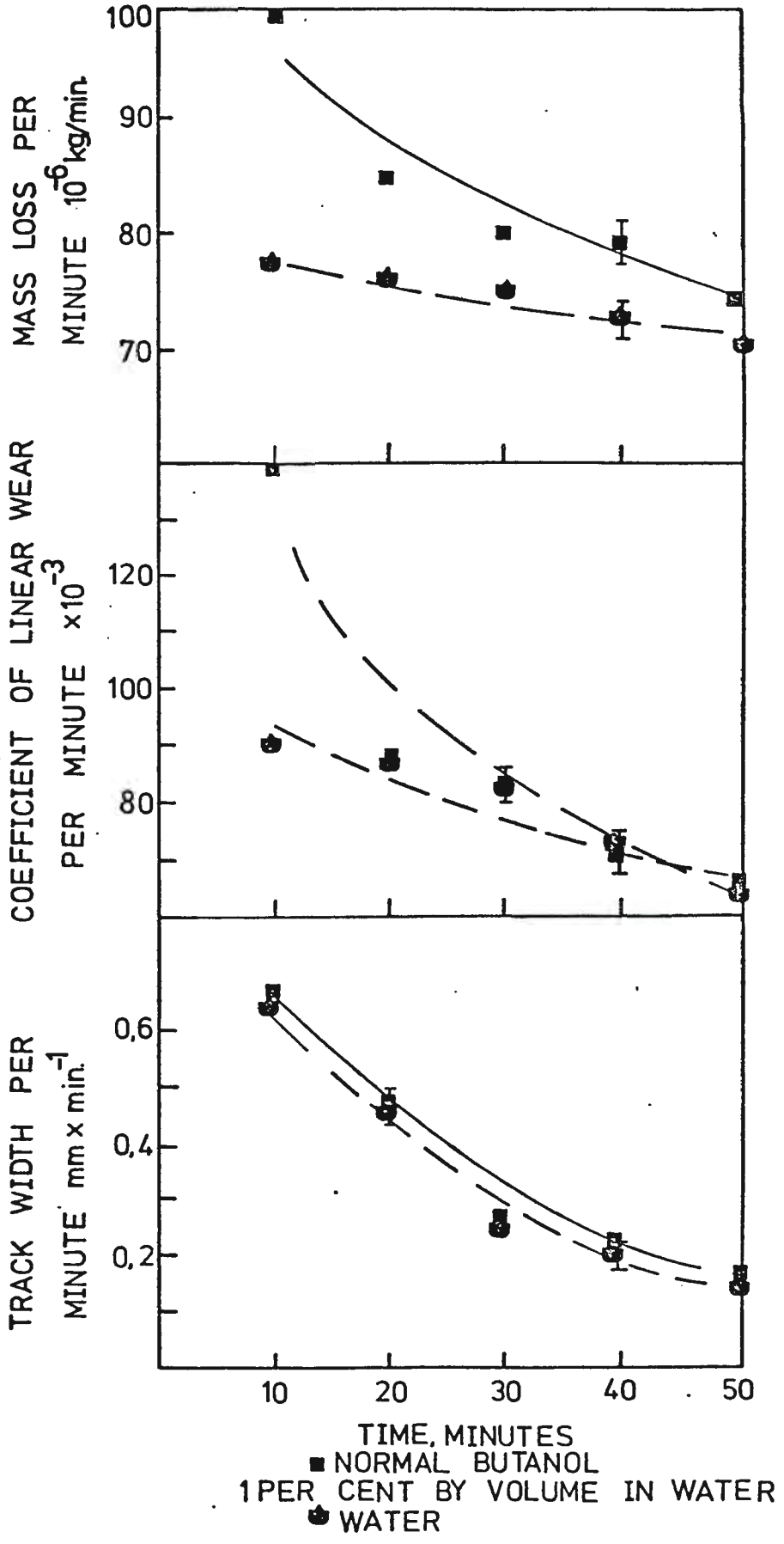

Figure 27

Relationship between mass loss per minute, coefficient of linear wear per minute, track width of the abrasion groove and abrasion time.
Environments used: Water and n-butyl alcohol 1 per cent by volume in water.
Normal load: 100N.

coefficient of linear wear per minute and track width per minute. A small decrease of the wear rates per unit time was observed for increasing process times as might be anticipated from geometrical changes. The mass loss per unit time of the abrasion tests performed in the n-butyl alcohol aqueous environment was found to be larger than the mass loss per unit time in water, for all of the times used.

5.3.5. Scanning Electron Microscopy examination of the abrasion surface and wear particles

The surface morphology of the abrasion grooves is characterised by sections with smooth extruded appearance and others with rough finish. (Plates 40 to 49.) The abrasion grooves look similar to the metal bearing surfaces, such as roller bearings, fall by surface spalling fatigue. The ploughing tracks are indicative of the occurence of plastic flow, while fracture facets and patterns indicate the occurence of brittle fracture. The ratio of the total area indicative of plastic flow to the total area showing brittle fracture sections was found to change with the conditions of the abrasion process, such as environment, speed or normal load. The surface morphology of the abrasion grooves, compared to the surface morphology of an "as received" drill core specimen (Plate 50) and the one of the same specimen taken after cutting by a diamond-cutting wheel (Plate 49) shows the complexity of the process.

The quartzite particles taken from the product of the abrasion were found to have angular and irregular shape, while very fine coagulated particles were also found to be present (Plates 51, 52). The abrasion detritus was found to be very similar to the particles observed on the friction tracks of the plates 33, 34, and 36.

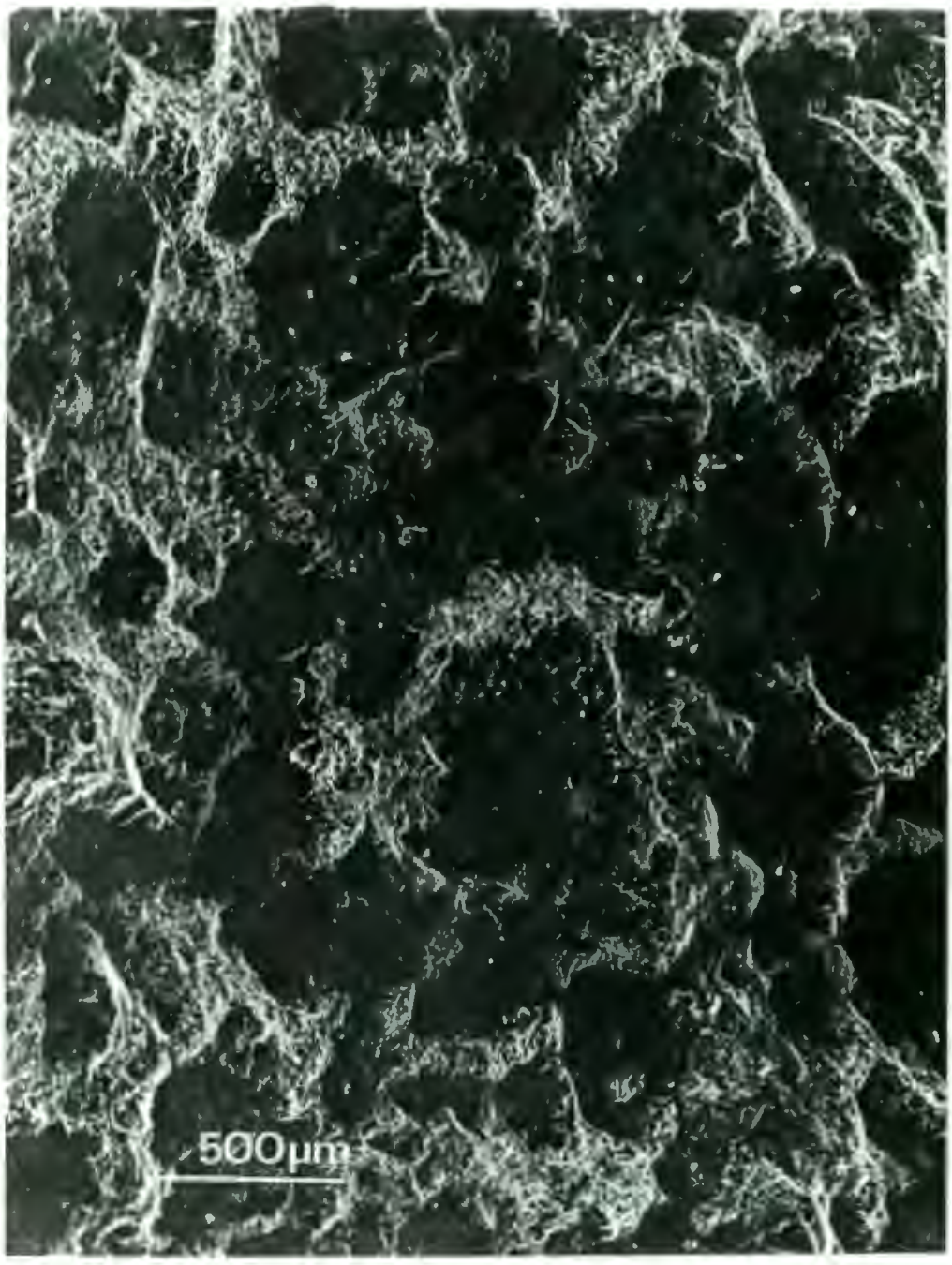

Plate 40

Surface morphology of an abrasion groove taken from a test in 1 per cent by volume n-pentyl alcohol in water.
Normal load: 50N.
Rotation speed: 200 RPM.
Both plastic flow and brittle fracture phenomena are indicative by the ploughing tracks, similar to the ones of the abrasion of metals and the fracture surfaces respectively.

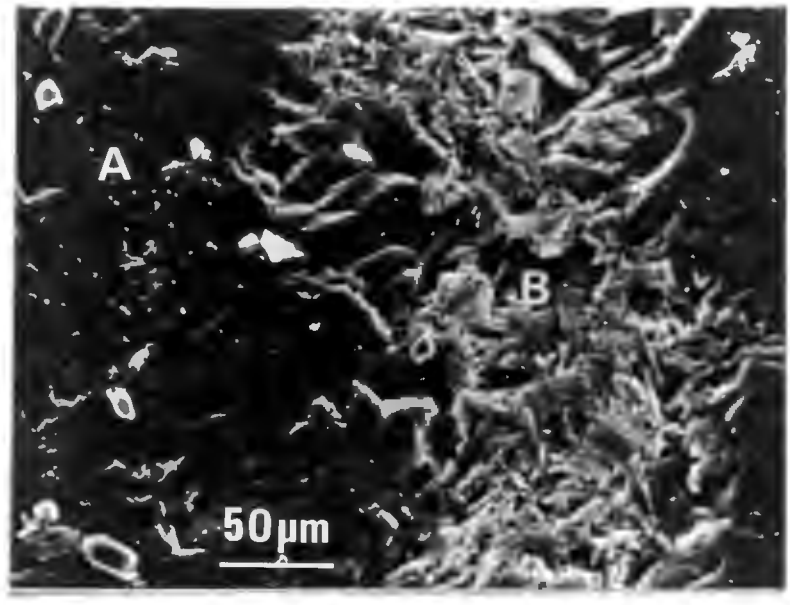

Plate 41

A region of the abrasion groove shown in plate 40, under higher magnification. On the plastic flow section of the groove (A) the presense of very fine abrasion detritus is indicative of the so called 'shaving' action (Bowden and Tabor, 1964).
On the brittle fracture section of the groove (B) the phyllosilicates flakes present at the floor of the groove cavity are indicative of a grain removal by intergranular fracture.

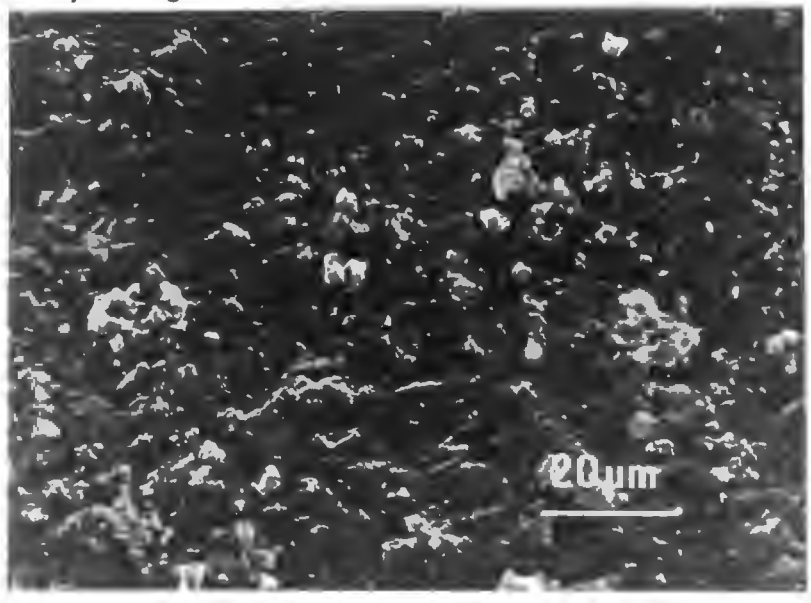

Plate 42

A region of the abrasion groove shown in plates 40 and 41. The presence of detritus of colloidal dimensions is indicative of plastic flow phenomena.

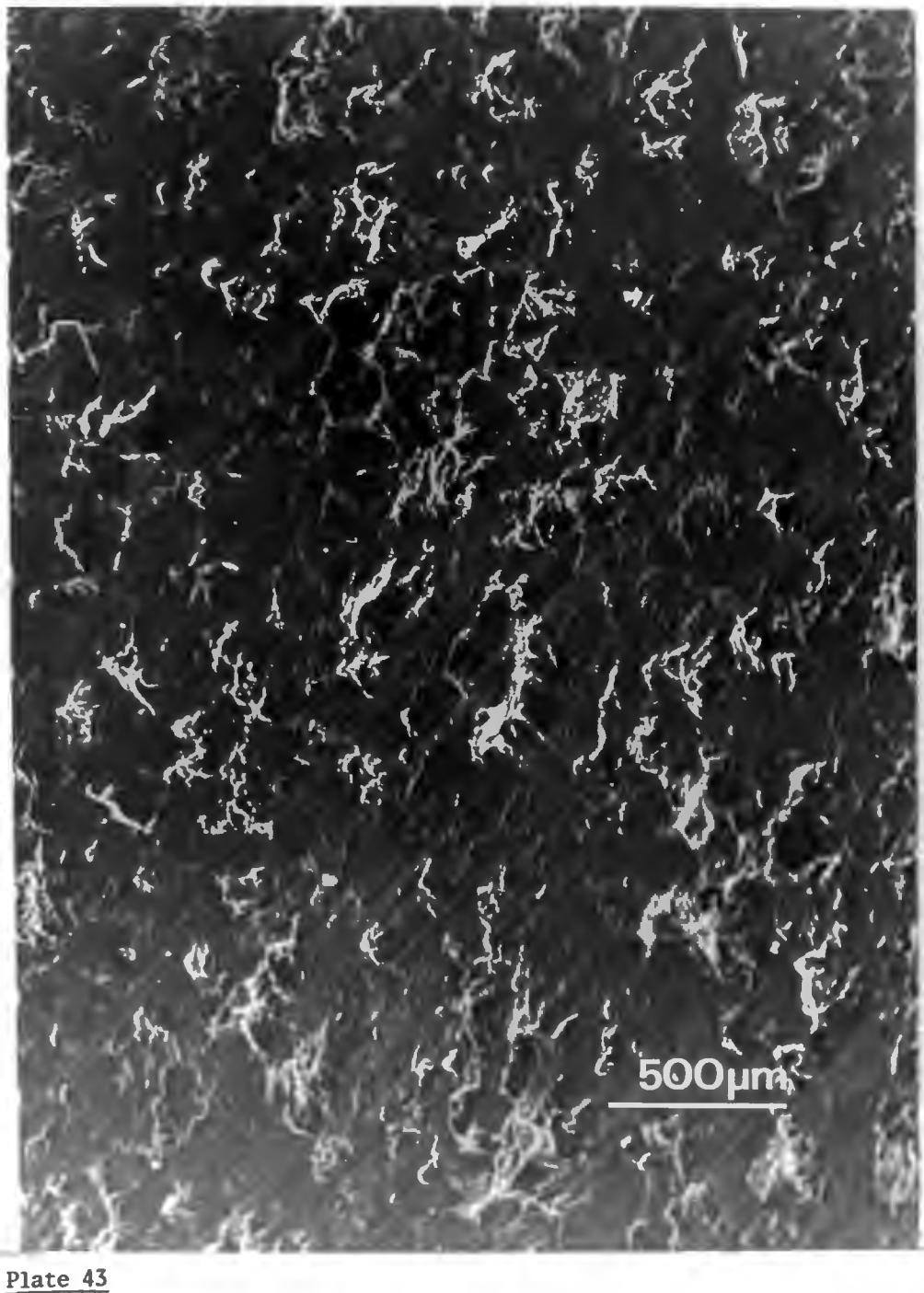

Plate 43

Surface morphology of an abrasion groove taken from a test in 2 per cent by volume normal propyl alcohol in water.
Normal load: 100N.
Rotation speed: 400 RPM.
Both plastic flow and brittle fracture are indicated, in the same manner as in plate 40 but in different state of equilibrium between the two occuring mechanisms.

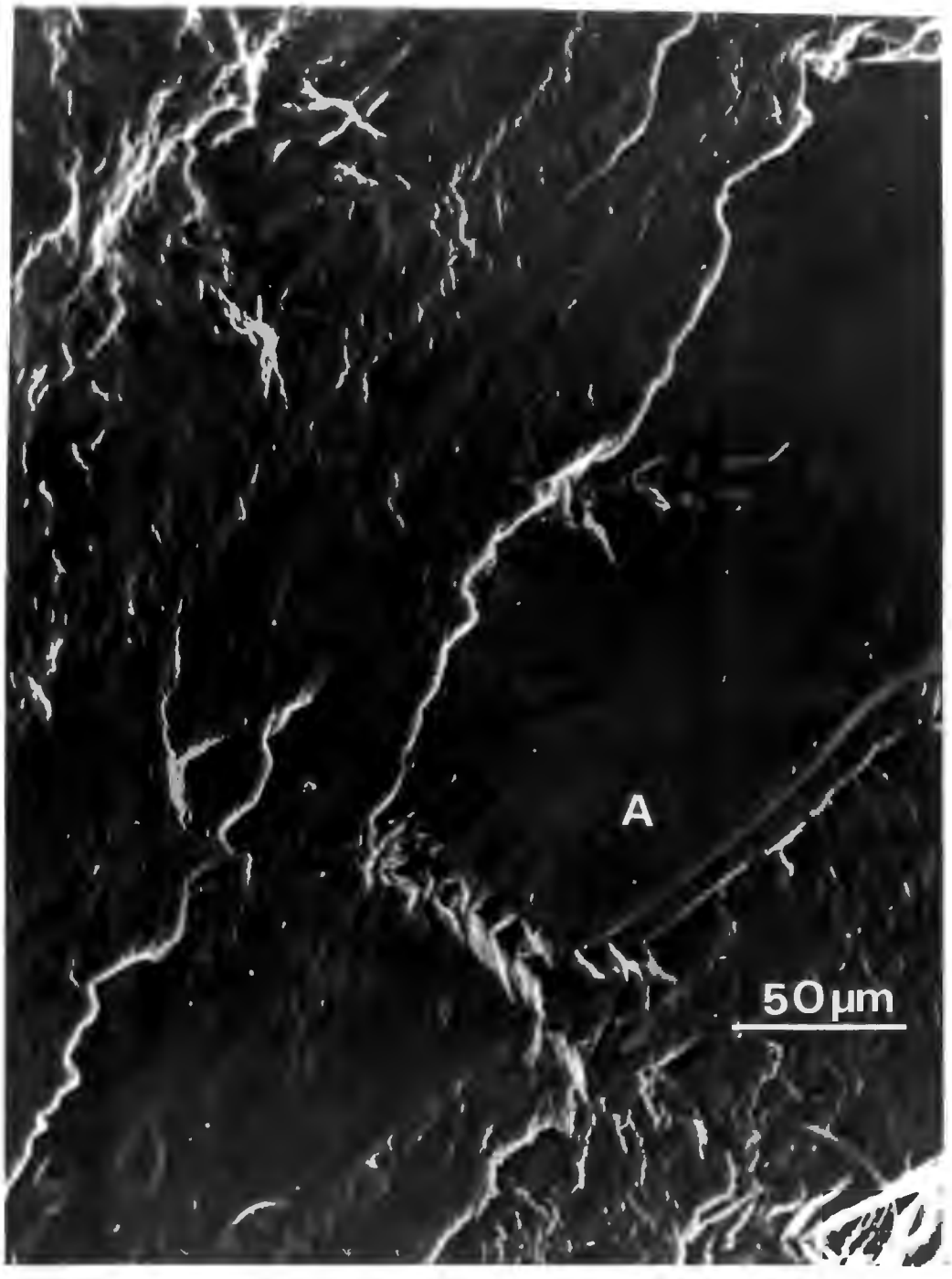

Plate 44

A region of the abrasion groove shown in plate 43, under higher magnification.
Transgranular fracture is indicative by the cleavage facet (A).

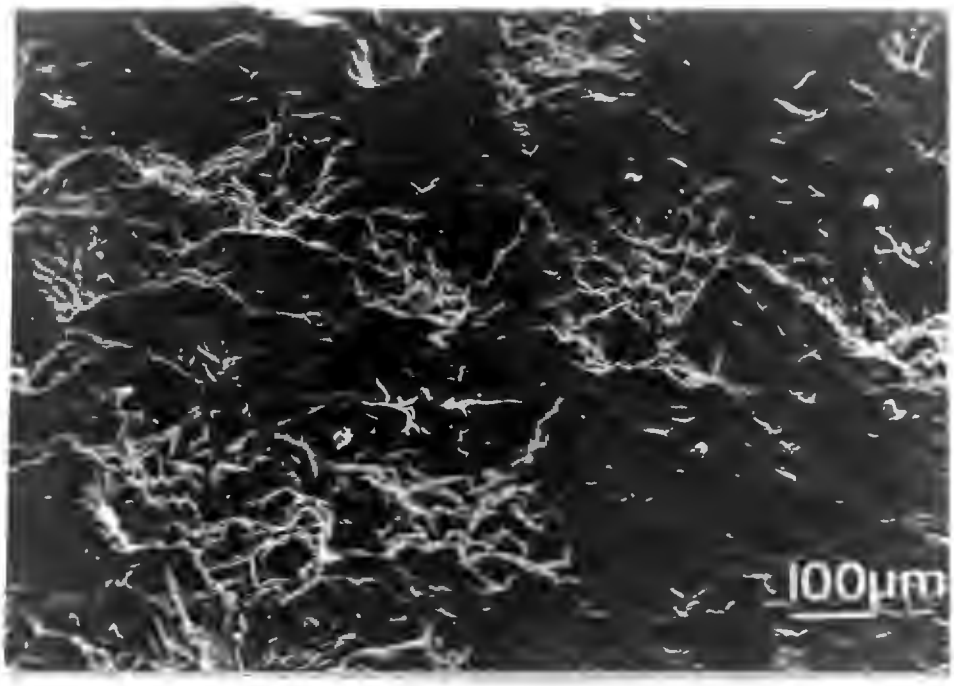

Plate 45

Surface morphology of an abrasion groove taken from a test in water.
Normal load: 50N.
Rotation speed: 200 RPM.

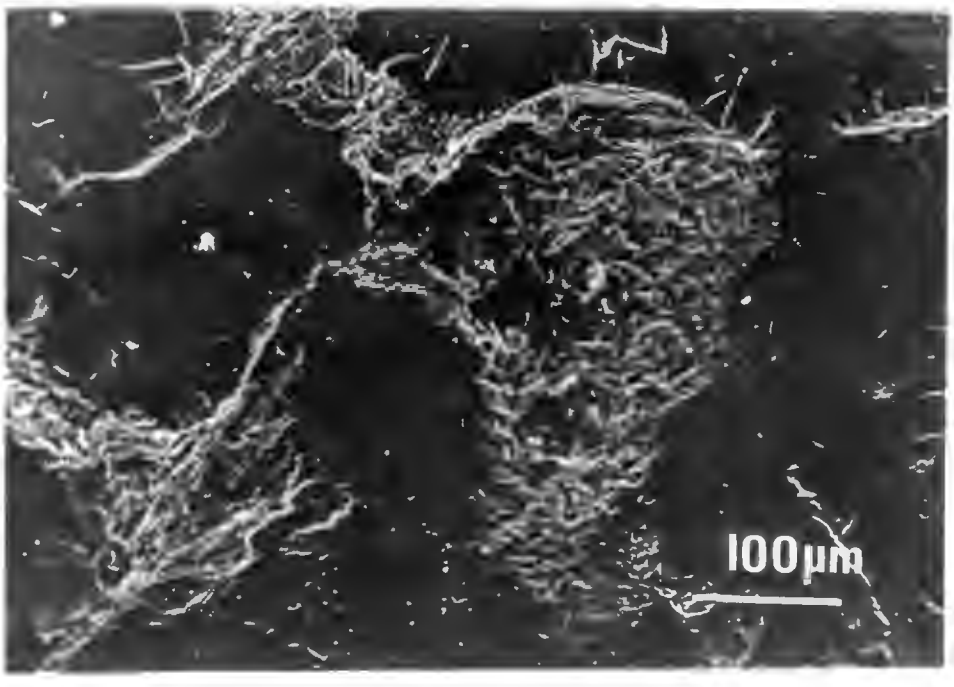

Plate 46

A region of the abrasion groove shown in plate 45.

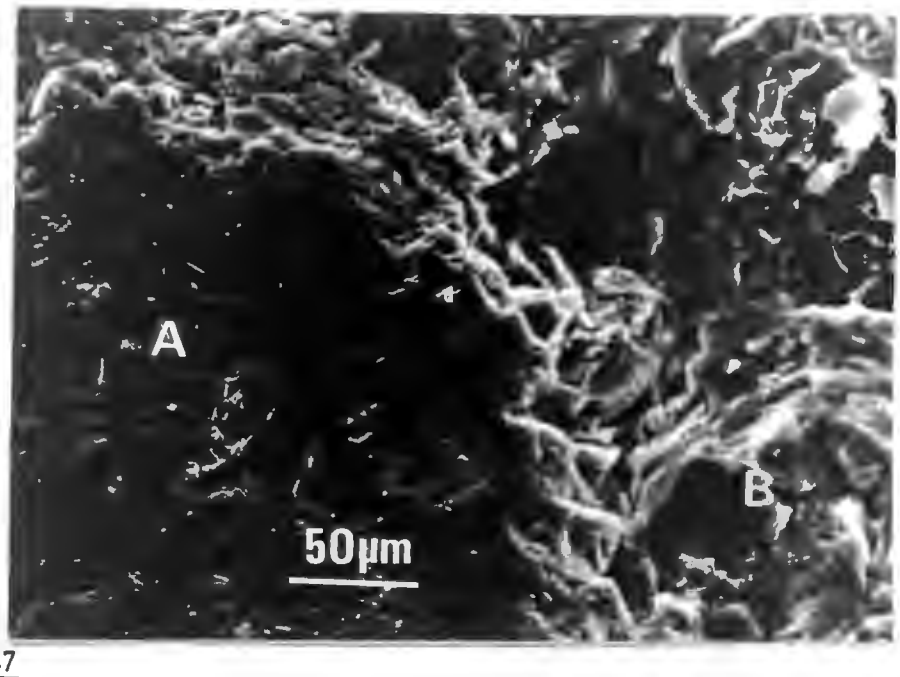

Plate 47

A region of the abrasion groove shown in plate 45, under higher magnification.
The surface morphology and the presence of very fine detritus are indicative of plastic flow phenomena (A) while the fracture surfaces are indicative of removal of material via brittle fracture (B).

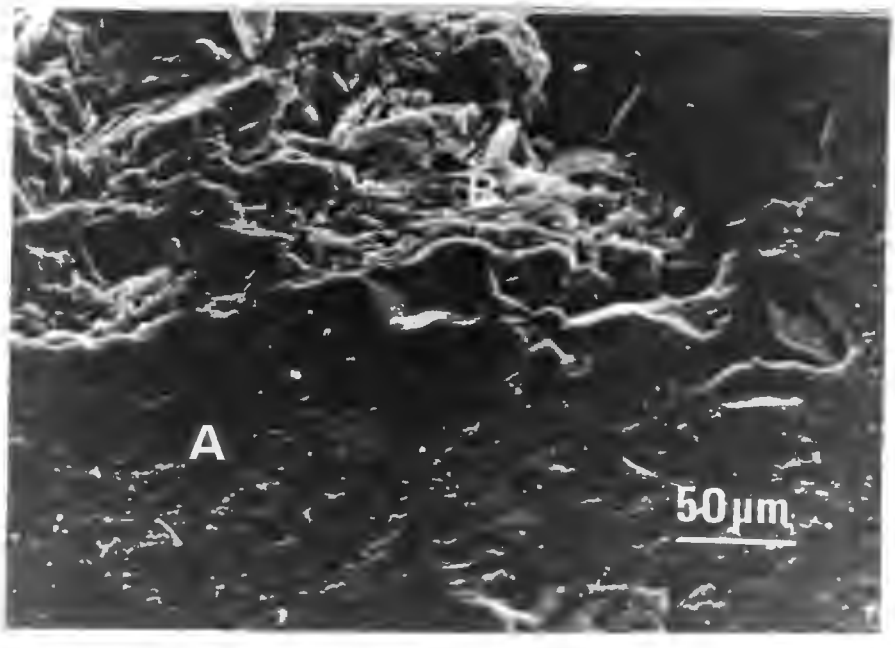

Plate 48

As plate 47.

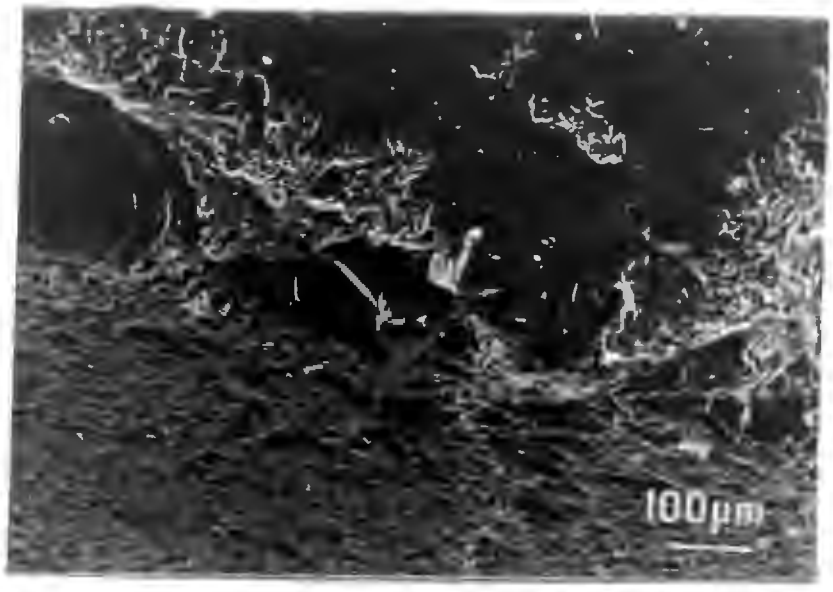

Plate 49

A : Surface morphology of an abrasion groove taken from a test in 1 per cent normal pentanol by volume in water.
Normal load: 50N.
Rotation speed: 200 RPM.

B : A plane cut orthogonally to the abrasion groove by a "Rimlock Diamond Cut-Off" blade of 203,2 mm diameter, rotating under 1425 RPM by a 233,3 W - 220 V AC motor, in water environment.

The morphology of the cutting surface is indicative of the occurence of comminuting mechanisms employing only fracture phenomena in comparison with the surface morphology of an abrasion groove which employs both fracture and plastic flow phenomena.

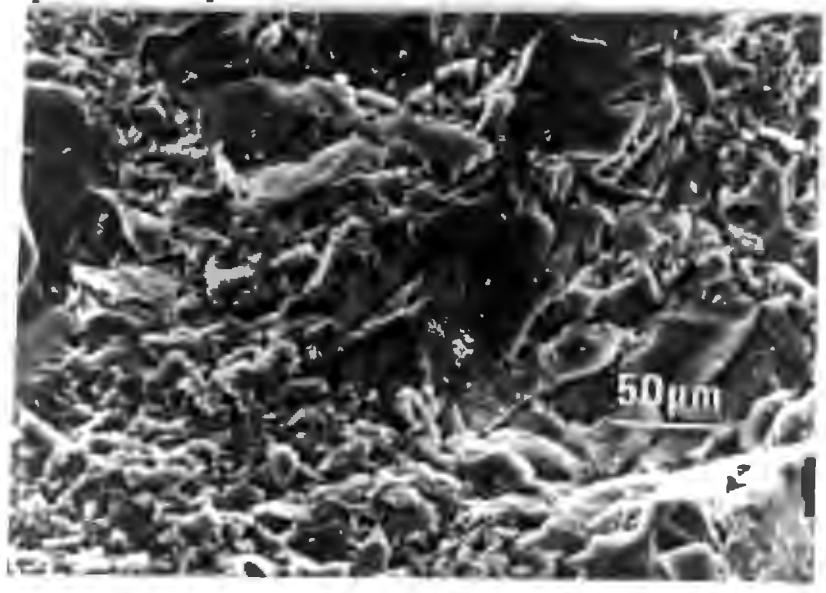

Plate 50

Typical surface morphology of an as received quartzite drill core. (Quartzite of type C. Tensile strength 12,15 MPa).

Plate 51

Abrasion detritus taken from a test in water.
Normal load: 50N.
Rotation speed: 200 RPM.
The size distribution of the abrasion detritus falls within the range of 11 µm to 0,5 µm, while their shape is irregular.

Plate 52

Abrasion detritus taken from a test in 2 per cent by volume ethanol in water.
Normal load: 100N.
Rotation speed: 200 RPM.
The size distribution of the abrasion detritus falls within the range of 34 to 99 µm, while their shape is irregular.

CHAPTER 6

THE AUTOGENOUS MILLING BEHAVIOUR OF THE ROCK

6.1. Introduction

Milling is generally treated as a physical process controlled by the mill geometry, speed, type of liners and wear media. The milling environment, particularly for wet milling is examined usually in terms of pulp density. This is used as an empirical indication for the mill performance. The control of the milling environment, as a primary variable of a milling system has not been undertaken and little attention has been given to the physical and chemical properties of the environment.

Schweyer (1942) investigated the effect of the viscosity of the fluid medium on the milling efficiency of a batch scale ball mill using dry, water, 49,7 per cent, 75 per cent and 95,4 per cent glycerol in water for milling times of 4 to 164 hours. He suggested that the function of the fluid is to separate the particles and thus to prevent "cushioning" by the finely comminuted mass. However, the fluid also tends to absorb the shock of impact when the wear media fall and to lubricate the action when the balls roll over one another. He detected changes in the ball milling behaviour, but he could not derive any quantitative relationship between the milling efficiency and the liquid environment. Similar work was done by Hockings, Volin and Mular (1965), for the milling of quartzite in a batch scale rod mill in a corn syrup and water environments of varying viscosity. The authors found that the milling efficiency was independent of the viscosity up to the level of 20 cP, while poorer comminution results were obtained for higher viscosities. They suggested that this difference in milling behaviour was mainly due to the liquid flow characteristics, viz. turbulent flow for low viscosities and laminar flow at the higher viscosities. Kapur, Mular and Fuerstenau (1965) observed that the density of the environment results in a preferential comminution of the heavy mineral components. Clarke and Kitchener (1968) using glycerol-water mixtures and fine mineral powders in suspension observed an influence of the rheology of the mill contents upon the milling efficiency. They agreed with the theory of Schweyer (1942),

but they also mentioned that a decrease in the coefficient of sliding friction may be involved when the viscosity of the milling environment increases thus suggesting that more work should be done on this aspect. Most authors have tried to explain the influence of the environment upon milling via a single physical property of the environment. For example, Clarke and Kitchener (1968) observed that the fine solids dispersed in the liquid environment may enhance comminution, but they tried to explain this phenomenon only in terms of physical properties of the liquid environment. However, the system is complex and dynamic and the mechanisms of comminution must first be studied individually as a function of the many variables.

The study of the agglomeration phenomena which occurs during comminution mainly in dry environments, is another field in which the influence of the environment has been examined. Rumpf (1958, 1959, 1973) stated that the presence of the fresh fracture is very important in terms of milling efficiency, due to the adhesion of the fine comminuted particles to each other and to wear media and liners and the resultant cushioning effects. Gregg (1968) suggested that the surface activity of the freshly comminuted flaky particles of sub-sieve size results in the occurence of a "coagulation process" which hinders further comminution. Papadakis (1960) suggested that agglomeration activity reduces the new surface area produced, in a manner, that is dependent upon the geometry of the wear media and the mill, while Beke (1964) found that agglomeration is a function of temperature. Locher and von Seeback (1972) measured the forces of adhesion between cement clinker particles in various environments, and found that while these forces are strong in a dry environment they are reduced in the presence of organic liquids like ethylene glycol and butylamine. The surface activity of the fine comminuted particles, in the milling environment was found in general to reduce the milling efficiency. The above workers tried to study the agglomeration phenomena in order to avoid the disadvantages of the presence of fines during dry milling. They were unable to propose a mechanism explaining agglomeration, although they postulated that van der Waals and electrostatic forces are involved.

Electrokinetic phenomena are utilized in mineral seperation techniques by the use of a wide range of surface active reagents, while systematic studies of the zeta-potential of dispersed fine solids in pure aqueous and organic liquids-aqueous environments have been performed, (Yousef, Arafa and Boulos, 1971, Yücesoy and Yarar, 1974). From the time that Rehbinder (1947) found that the speed of penetration of a drill into hard rocks could be increased by the presence of various environments, experimental milling tests have been performed (Snow, 1970) in electrolytes and in pure and diluted organic liquids in order to improve milling efficiencies of quartz and quartzite. For example, Frangiskos and Smith (1957) also used environments described as "hardness reducers" for laboratory stamp milling tests of quartz and limestone. The authors found that in comparison with pure water, certain surfactants enhanced comminution in a manner which is influenced by the concentration of the surfactant used and the impact magnitude and frequency of their comminuting device. In trying to explain these results in terms of Rehbinder's hypothesis, Pryor (1957) suggested that the enhancement may derive from changes of pH and viscosity of the mill charge and the resultant variations in the flocculation or the dispersion of the solids in the milling environment. Kuznetsov and Taube (1969) suggested that the enhancement in comminution may be due to a preferential weakening of the mineral constituents from the rock matrix. They also found that the dispersed solids influence the comminution efficiency, with a considerable increase in comminution during the synchronous presence of the solids and surfactants. Snow (1970) reported a number of industrial milling applications, particularly in cement comminution, where enhancement up to 50 per cent may be achieved by the use of surfactants in the milling environment.

From the work reported, it appears that the enhancement of comminution by the control of the milling environment is certain, to the extent that patents on the use of additives have already been established (Bartha, 1969). The mechanism of enhancement seems to be more complex than Rehbinder's theory which is based on the reduction of the effective surface energy of the solid. From the milling results reported and from the separate examination of the main comminuting mechanism of abrasion (chapter 5) it appears that the

environmental effects on comminution are dependent upon the relative speed of the comminuted particles, the load applied on the particular particles in contact, the concentration of the aqueous environment, the petrography of the rock and the chemistry of the environment used.

The intention to overcome a disadvantage of autogenous milling (the suitability problems of a given ore for a sufficient application) by the control of the milling environment requires an assessment of its role under the complex conditions which occur in the mill. The results of these tests will be analysed in combination with those of the more idealised fracture, friction and abrasion tests of chapters 2, 4 and 5.

6.2. Experimental techniques

In the first series of the laboratory testing for autogenous milling, we aimed at the establishment of conditions similar to the ones of a production scale mill. Rounded "pebbles" and a finer mill feed were used to represent a portion of the contents of an autogenous mill, during an intermediate phase of the industrial process. In the second series of laboratory tests for autogenous milling, the mill charge size distribution was scaled to be as a typical run-of-mine feed of a production scale mill of the South African gold industry (Stanley, 1977, 1975). In the third series of experiments, the mill charge was similar to the one of the second series, but it consisted of two milling periods, while three milling periods were employed in water and dry environments.

6.2.1. Material

Witwatersrand quartzite rocks, of the type B and C taken from the run-of-mine product of the Leslie Mine, Union Corporation were comminuted to smaller sizes by small scale jaw crushers. The product of the jaw crusher was classified by means of a laboratory screen vibrator to the sizes -25+12,5 mm, -12,5+9,51 mm for the coarser particles and to the sizes -9,51+4,00 mm, -4,00+2,00 mm and -2,00+1,00 mm for the finer particles. The screening was dry and

during the size classification an effort to control the uniformity of the rock particles classified was attempted by manual removal of the particles having irregular flaky shapes (British standards, 1959, 1970, 1975). Quartzite particles of -25+12,5 mm, rounded by a 50 hours dry milling session (of a 50 per cent of the mill volume charge of rock particles of -50+25 mm) were used in the first series of the laboratory autogenous tests.

6.2.2. Milling Apparatus

The milling was carried out by a batch type mill having internal diameter 166 mm and internal volume 3,21 litre and smooth ceramic internal surface. The rotation of the milling tube was performed by a pair of rubber coated idler rollers and the rotation speed of the drive roller was monitored by a tachogenerator. The mill tube was rotated at 99 revolutions (± 2 revolutions) per minute and an electronic timer was used to control the milling periods of the tests performed.

6.2.3. Milling procedure

In the first series of the milling experiments performed, a mass of 1,000 kg (± 1,5 per cent) of rounded quartzite particles of -25+12,5 mm size was milled with a mass of 4,500 kg (± 0,4 per cent) of quartzite particles of 4 mm size, taken from the product of the laboratory jaw crusher used. A volume of 1 litre of each liquid environment was used in each test. The charge was milled for 120 minutes. In the second series of experiments a mill charge of volume representing 30 per cent of the internal mill volume was used, consisting of 1 kg (± 1,5 per cent) of -25+12,5 mm particles, 1 kg (± 0,4 per cent) of 9,51 mm particles, 0,250 kg (± 0,4 per cent) of 4,00 mm particles, 0,150 kg (± 0,4 per cent) of 2,00 mm particles and 0,1 kg (± 0,4 per cent) of 1,00 mm particles of quartzite taken from the product of the laboratory jaw crusher. The volume of the liquid environment used for each test was 0,250 litre.

In the third series of the milling tests performed, the feed consisted of the +1 mm product of a milling test from the second series of tests. Additionally mass equal to that of the 1 mm

product was added, with a size distribution analogous to the one of the second series, in order to maintain the 30 per cent by volume mill charge conditions. The milling was performed for a period of 120 minutes. In water and dry environments, the above procedure was repeated for one more cycle, resulting in a total milling time of 360 minutes. The volume of the liquid environment used for every milling period was 0,250 litre.

After every milling period of 120 minutes the milling tube was tipped forward and the pulp was collected. The contents were wet-screened in the first stage in order to remove the +9,51 mm coarse material. The -9,51 mm milling product was dried and then subjected to screen analysis. The screening was performed by a laboratory screen vibrator for a standard volume of vibration with equal periodical intervals. The total screening time was 40 minutes, while the size classification procedure was assisted by a 40 kPa vacuum. After the screening, all size fractions were weighed and the size distribution of the milled product was computed.

6.2.4. Reproducibility of results in relation to the milling periods

The relatively long milling periods were used in order to ensure the reproducibility of the milling results. Four milling tests were carried out for each of the periods of the 10, 30, 45, 60, 75 and 120 minutes. For periods longer than 60 minutes, the deviation of the size distribution of the mill product between the three tests performed in the same liquid environment was found to be acceptable since it included the same values for each size as the ones of the mill feed.

6.2.5. Milling environments

The milling environments used can be classified into the following three categories:

(a) Single phase environments, with characteristic physical and or chemical properties.

(b) Environments of liquids with characteristic physical and or chemical properties in aqueous suspension and inorganic salts diluted in water.

(c) Environments of dispersed fine solids in water or in aqueous environments containing liquids or inorganic salts as above. Table VII shows the environments used and classified into the above categories for each series of the tests performed.

TABLE VII

Milling environments used

(a) Single environments

First series of tests Milling time: 120 minutes	Second series of tests Milling time: 120 minutes	Third series of tests Milling time: 240 minutes
Distilled water	Distilled water	Distilled water
Methyl alcohol	Dry air	Dry air
Toluene	n-Butyl alcohol	n-Butyl alcohol
	iso-Propyl alcohol	**iso**-Propyl alcohol
	n-Octyl alcohol	
	iso-Pentyl alcohol 50 per cent by volume in ethylalcohol	

(b) Organic liquids and inorganic salts in aqueous suspension

First series of tests Milling time: 120 mins	Second series of tests Milling time: 120 mins
n-Propyl alcohol 50 per cent by volume	n-Octyl alcohol 10 per cent by volume
n-Butyl alcohol 10 per cent by volume	Oleic acid 10 per cent by volume
Ethylene Glycol, 50 per cent by volume	
0,1 M Ammonium carbonate	
0,5 M Ammonium carbonate	
0,5 M Sodium chloride	

TABLE VII (Continued)

(c) Dispersed solids in liquid environments

Second series of tests Milling time: 120 mins	Third series of tests Milling time: 240 mins
Distilled water with 9 per cent by weight of -45 μm solids	Distilled water with 26 per cent of -45 μm solids
Distilled water with 21 per cent by weight of -63+45 μm solids	
Distilled water with 26 per cent by weight of -45 μm solids	
iso-Pentyl alcohol 10 per cent by volume in water with 14 per cent by weight of -45 μm wolids	
iso-Pentyl alcohol 10 per cent by volume in water with 14 per cent by weight of -63+45 μm solids	
Oleic acid 10 per cent by volume in water with 14 per cent by weight of -63+45 μm solids	
Thallium chloride 1 per cent by weight with 14 per cent by weight of -63+45 μm solids	

6.2.6. Scanning electron microscopy study of comminuted particles

Rock particles were taken from both test and laboratory autogenous mills. These particles represent various stages of the milling procedure for the test plant and various milling times for the laboratory mill. A coning and quartering technique was used for the sampling of the particles to be examined by SEM. The techniques used for the preparation of the SEM specimens were the same as described in chapter 2.

An analysis of the scanning electron micrographs, was performed in order to evaluate the shape characteristics of the rock particles examined, in relation to the comminution conditions involved. The variables used to characterise the two dimensional image of the particles were, the particle image area A, the perimeter P and the maximum diameter D_m. A planimeter, a chart-odometer and a micrometer respectively were used for these measurements.

Two shape factors were used viz. the surface shape factor k_a defined as $A/_D2$ and the outline area shape factor k_o, defined as $A/_P2$. (For a sphere $k_a = 0,785$ and $k_o = 0,0796$).

The particles examined were randomly selected from the micrographs and for each particle image, two surface, three perimeter and three diameter measurements were performed. Ten particles were examined for each of the following categories:

(1) Run-of-mine fine particles (Leslie mine, Union Corporation).

(2) Fine particles taken from the interior of an "Aerofall" test autogenous mill (in two series of samples).

(3) Fine particles taken from the cyclone overflow of the same mill, as at (2).

(4) Fine particles, taken from the product of our laboratory autogenous milling tests, in aqueous environments and for a milling period of 120 minutes.

(5) Fine particles, taken from the product of the laboratory mill in environments containing surface active environments such as normal alcohols.

(6) Fine particles, taken from the product of the same mill as at (4), in aqueous environment and for a milling period of 240 minutes.

(7) Fine particles, taken from the product of the laboratory mill in aqueous environment and for a milling period of 360 minutes.

6.3. Results

6.3.1. The first series of the milling tests

The milling efficiency (i.e. the mass of fines found by the size distribution analysis of the product) obtained from tests in inorganic salts and organic reagents was found to be larger than the milling efficiency of water. Ammonium carbonate 0,1M in water, was found to contribute to the production of a larger quantity of fines (figure 28), than the other environments used in this series of tests. Higher concentrations of the same salt was not found topromote enhanced comminution. Ammonium carbonate 0,5 M, presented lower comminution efficiency than the previous environment (figure 28). The enhancement of the comminution characteristics in 0,5 M sodium chloride in comparison to the water environments was found to be smaller than the ones in 0,1 and 0,5 ammonium carbonate (figure 28). Pure methyl alcohol was found to obtain better milling efficiency than pure toluene (Figure 29) while n-propyl alcohol 50 per cent by volume in water and n-butyl alcohol 10 per cent in water were found to enhance autogenous comminution in a better manner than ethylene glycol 50 per cent in water.

6.3.2. The second series of the milling tests

The results obtained in our batch scale autogenous milling tests of the second series, the feed of which is shown in figure 30, show that there are significant differences among the size distributions of the products comminuted in different environments.

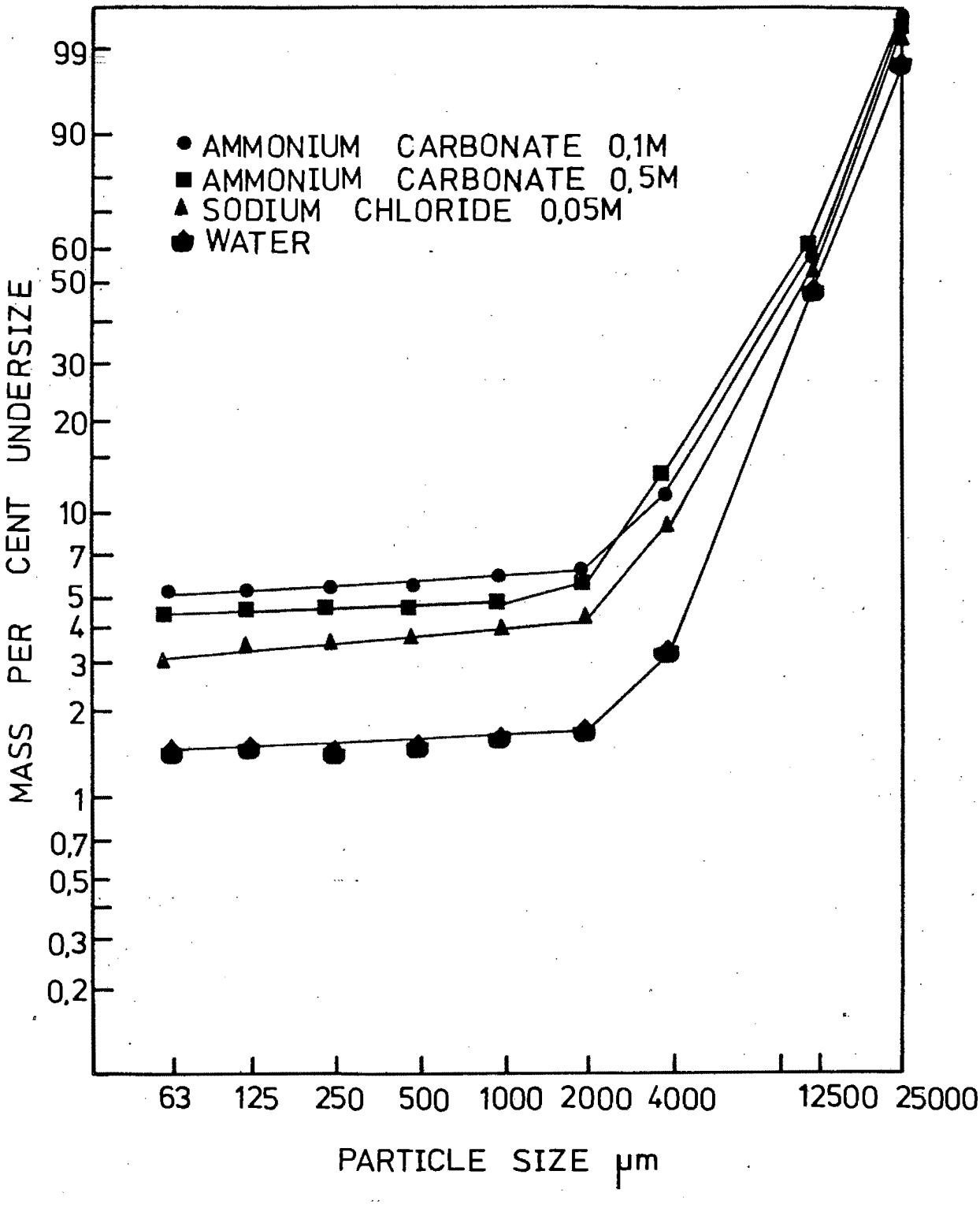

Figure 28

Size distribution of the product of laboratory autogenous milling tests of the first series, presented according to the Rosin-Rammler method.
Milling environments used: Ammonium carbonate 0,1 M and 0,5 M, sodium chloride 0,05 M and water.

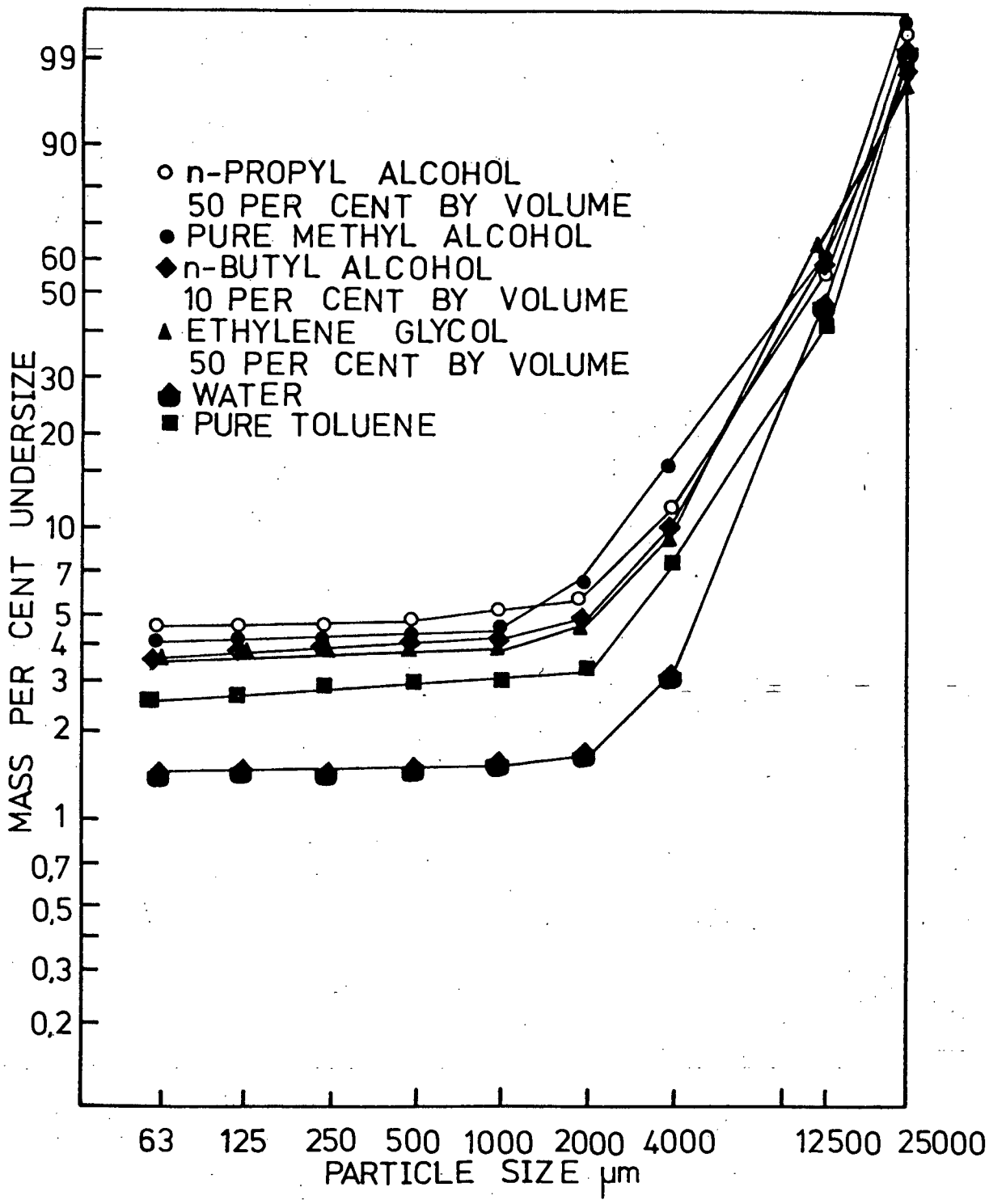

Figure 29

Size distribution of the product of laboratory autogenous milling tests of the first series, presented according to the Rosin-Rammler method.
Milling environments used: Pure methyl alcohol, pure toluene, water, n-propyl alcohol 50 per cent by volume in water, n-butyl alcohol 10 per cent by volume in water and ethylene glycol 50 per cent by volume in water.

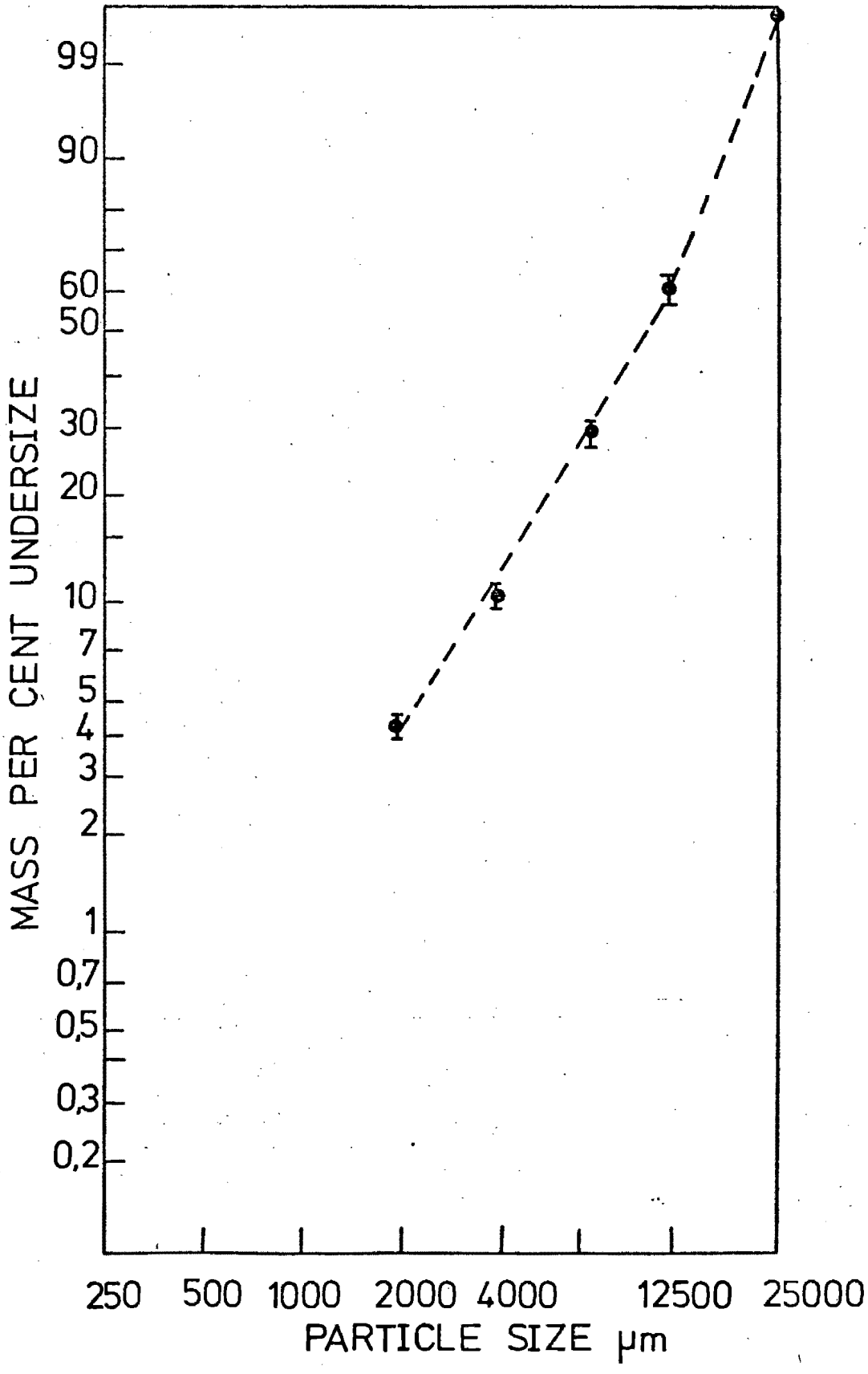

Figure 30

Typical size distribution of the feed used for the second series of the laboratory autogenous milling tests.

Milling environments consisting of pure liquid reagents, viz. n-butyl alcohol, water, iso-propyl alcohol and n-octyl alcohol (figure 31) were found to obtain better milling efficiency, according to the order of their reference, than the dry environment. The milling environment consisting of 50 per cent by volume of iso-propyl alcohol in ethyl alcohol (figure 31) was found to obtain approximately the same milling efficiency as the one of pure n-butyl alcohol

Dilute surface active reagents, viz. n-octyl alcohol (figure 32) were found to present different milling behaviour than their similar behaviour in their pure form. The presence of comminuted quartzite particles in water was found to result in chances in milling efficiency, as it is shown in figures 33 and 34, in a manner dependent upon the quantity (per cent by weight in water) and the size of these solids.

Composite environments, consisting of both organic reagents and comminuted particles in aqueous suspension were found to enhance comminution in a considerable manner. The presence of 14 per cent by weight of -63+45 μm particles in an environment of 10 per cent by volume oleic acid in water, was found to improve comminution (figure 34). The largest comminution efficiency found to be obtained in an environment consisting of 10 per cent by volume iso-pentyl alcohol and 14 per cent by weight of -45 μm comminuted solids in water (figure 34). Larger particles, of -63+45 μm, in an environment with the same characteristics, i.e. 10 per cent by weight solids and 10 per cent by volume iso-pentyl alcohol were found to obtain slightly smaller milling efficiency. The presence of an inorganic salt, such as thallium chloride together with solids, 14 per cent by weight of -63+45 μm, was also found to produce a large milling efficiency (Figure 34).

6.3.3. The third series of the milling tests

The results obtained from our batch scale autogenous milling tests show that the dependence of the comminution efficiency on the milling time is different for each environment used. Although the milling efficiency obtained by water was found to be smaller than the one obtained in n-butyl alcohol for milling time of 120 minutes the

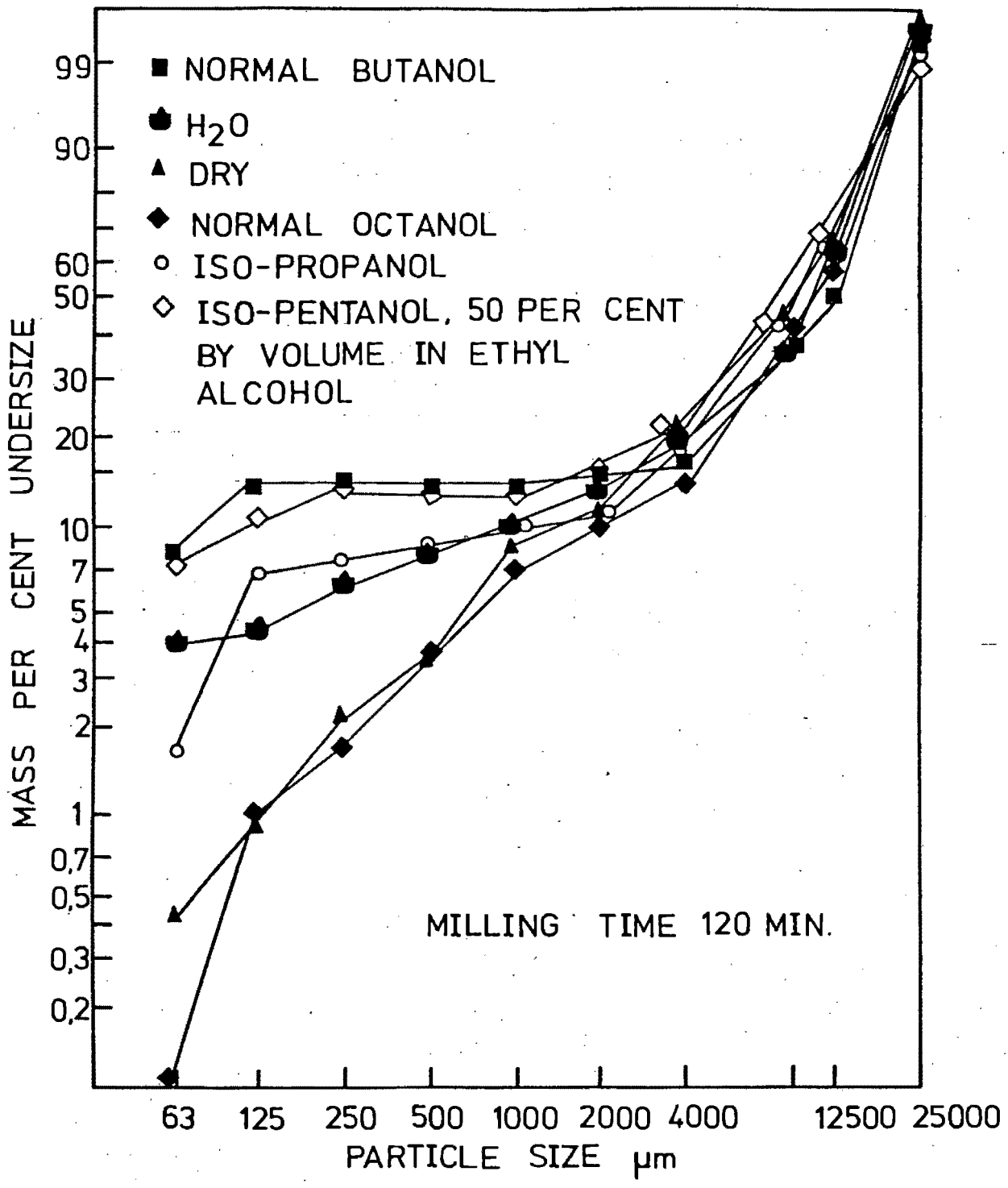

Figure 31

Size distribution of the product of laboratory autogenous Milling tests of the second series, presented according to the Rosin-Rammler method.

Milling environments used: Water, dry, pure iso-propyl alcohol, n-octyl, n-butyl alcohols and iso-pentyl alcohol 50 per cent by volume in ethyl alcohol.

Milling time: 120 minutes.

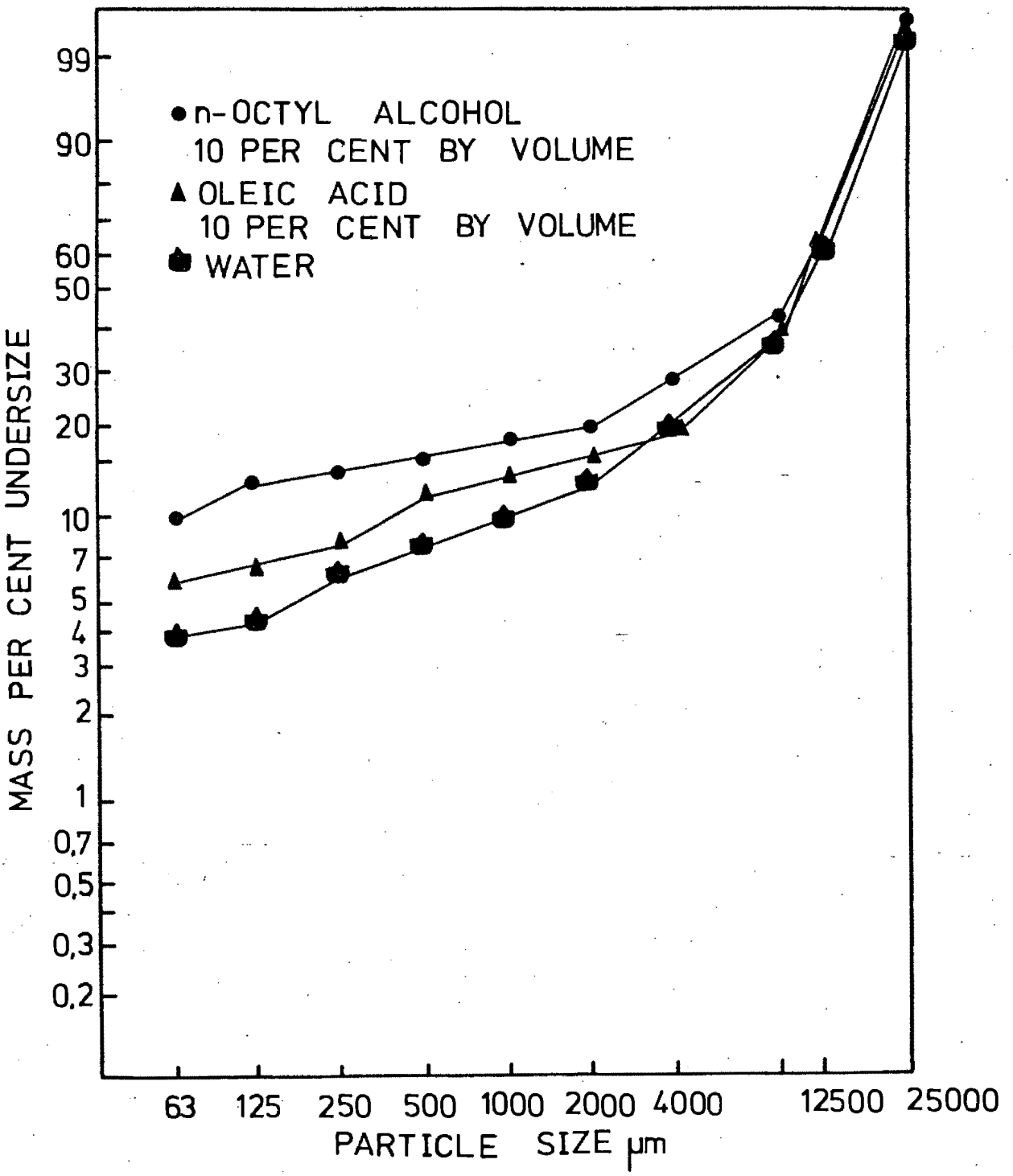

Figure 32

Size distribution of the product of laboratory autogenous milling tests of the second series, presented according to the Rosin-Rammler method.
Milling environments used: n-octyl alcohol 10 per cent by volume, oleic acid 10 per cent by volume and water.
Milling time: 120 minutes.

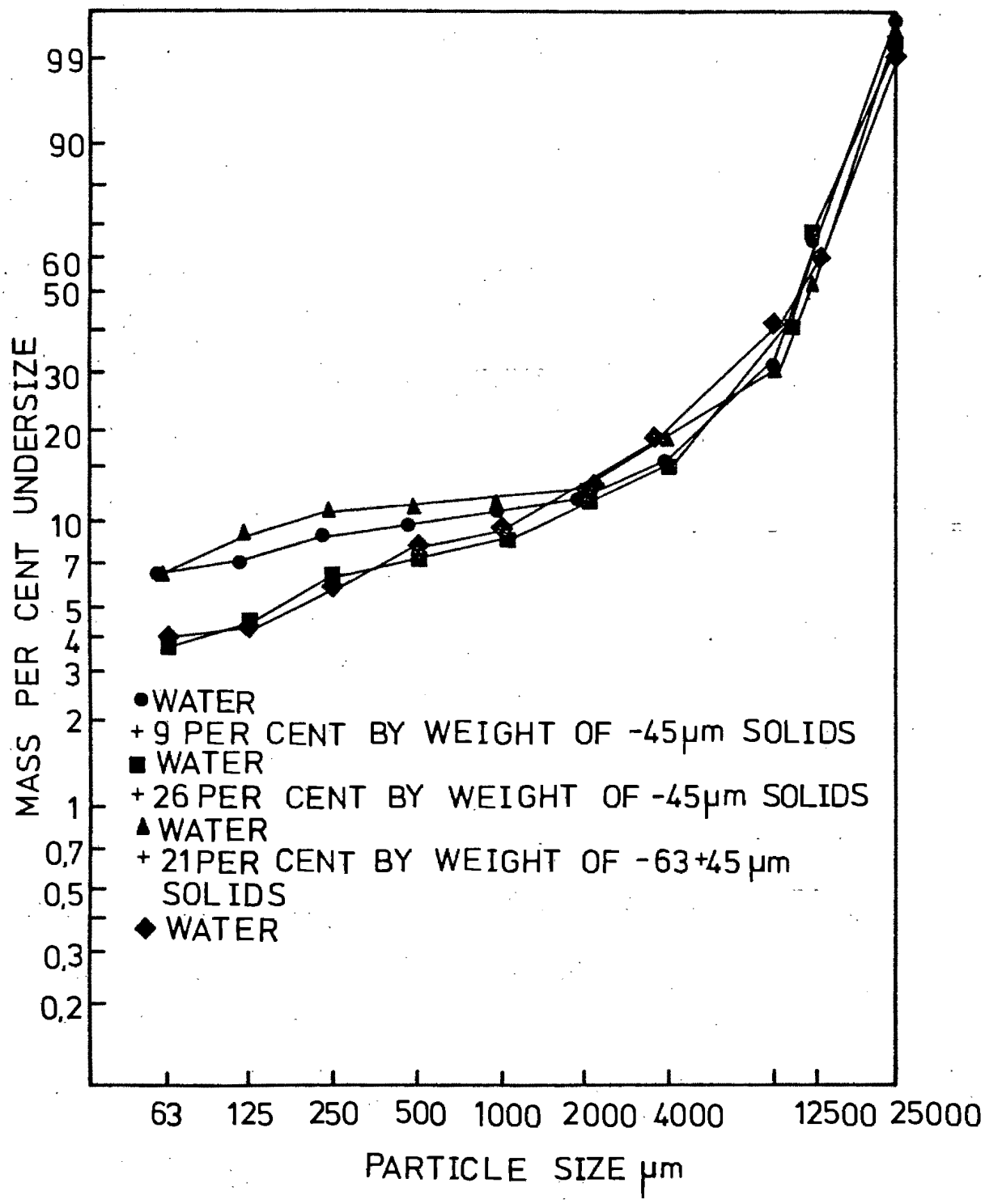

Figure 33

Size distribution of the product of laboratory autogenous milling tests of the second series, presented according to the Rosin-Rammler method.
Milling environments used: Water with 9 per cent by weight of -45 µm, water with 26 per cent by weight of -45 µm solids, water with 21 per cent by weight of -63 + 45 µm solids and pure water.
Milling time: 120 minutes.

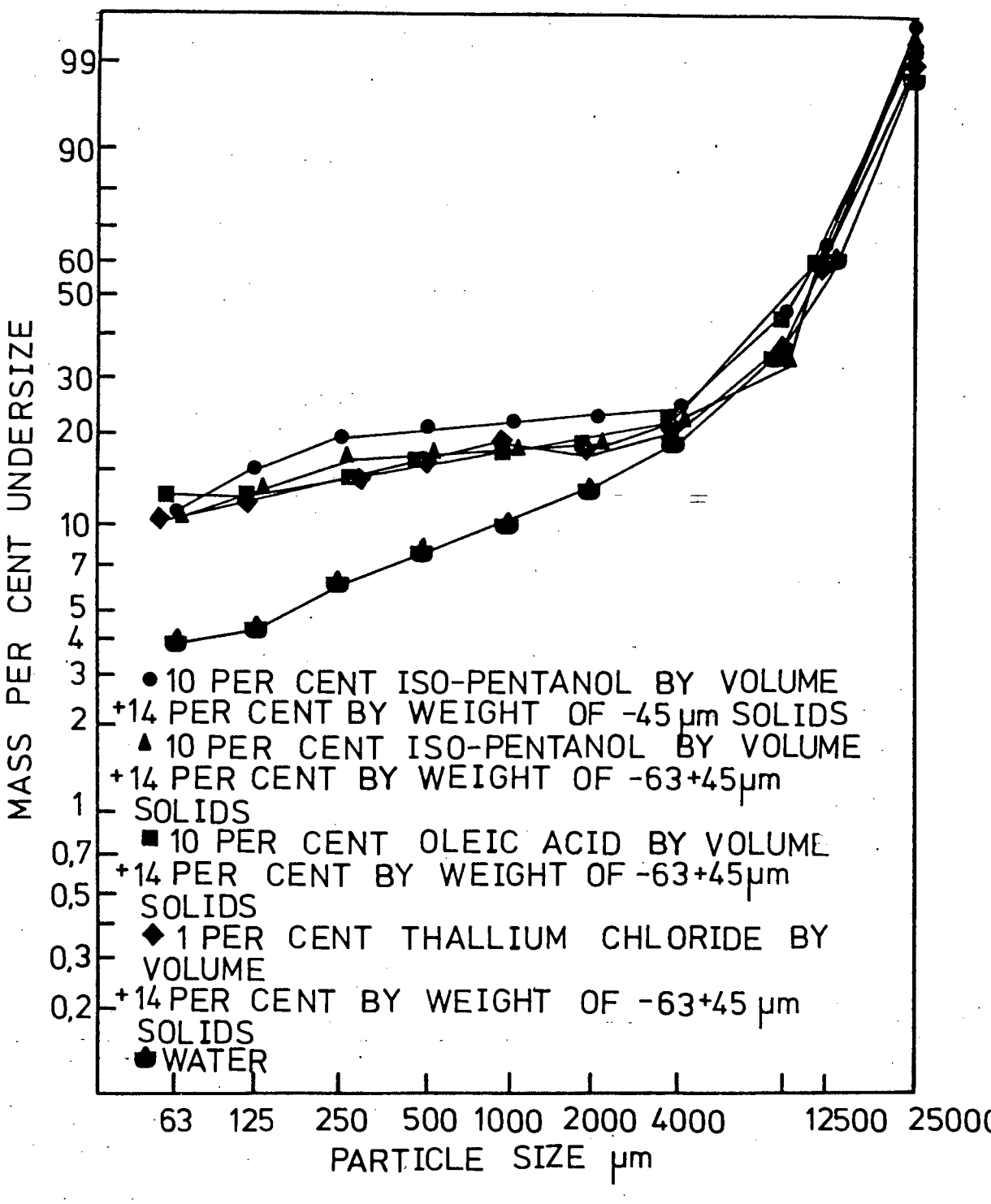

Figure 34

Size distribution of the product of laboratory autogenous milling tests of the second series, presented according to the Rosin-Rammler method milling environments used iso-pentyl alcohol 10 per cent by volume in water with 14 per cent by weight of -45 µm solids, iso-pentyl alcohol 10 per cent by volume in water with 14 per cent by weight of -63+45 µm solids, oleic acid 10 per cent by volume with 14 per cent by weight solids of -63+45µm, thallium chloride 1 per cent by weight with 14 per cent by weight of -63+45 µm solids, and pure water. Milling time: 120 minutes.

opposite was found to occur for total milling time of 240 minutes (figure 35). The milling efficiency obtained in iso-propyl alcohol was found to be approximately the same as the one in n-butyl alcohol environment (figure 35), while a significant difference in comminution characteristics was observed for 120 minutes milling. The fine particles which are present in water n-octyl alcohol and dry environments was found to influence the comminution efficiency in a similar manner with the one observed at the second series of milling tests (figure 34). Figure 36 shows that the milling efficiency in water is also larger than the one in dry environment for total milling time of 360 minutes.

6.3.4. Surface morphology of autogenously milled particles

The run-of-mine particles used for the experiments were found to be angular with smooth surfaces, indicating the influence of the material transfer and storage from the excavation to the mill, upon the character of the particles shape (Plate 53). Very fine particles were also found to adhere on the surface of the run-of-mine particles (Plate 54).

The fine particles taken from the mill interior of the "Aerofall" mill were characterised by cleavage fracture facets and fracture patterns, having sharper edges than the run-of-mine particles (Plates 55 to 58). The surface morphology of the particles taken from the output of the "Aerofall" mill was also indicative of the occurence of cleavage fracture in the mill (Plates 59, 60).

The surface morphology of particles, randomly selected from the product of laboratory autogenous milling tests for periods of 120 minutes (Plates 61, 62), 240 minutes (Plates 63, 64) and 360 minutes (Plates 65, 66) were found to be similar to that of the particles taken from the interior and output of the "Aerofall" mill. The surface morphologies of particles comminuted in surface active environments are similar to those of the particles obtained in water (Plates 67, 68).

Microcavities and microcraks were present on the surface morphology of particles autogenously milled (Plates 69 to 70). Particles of colloidal dimensions adhering to the surface of the

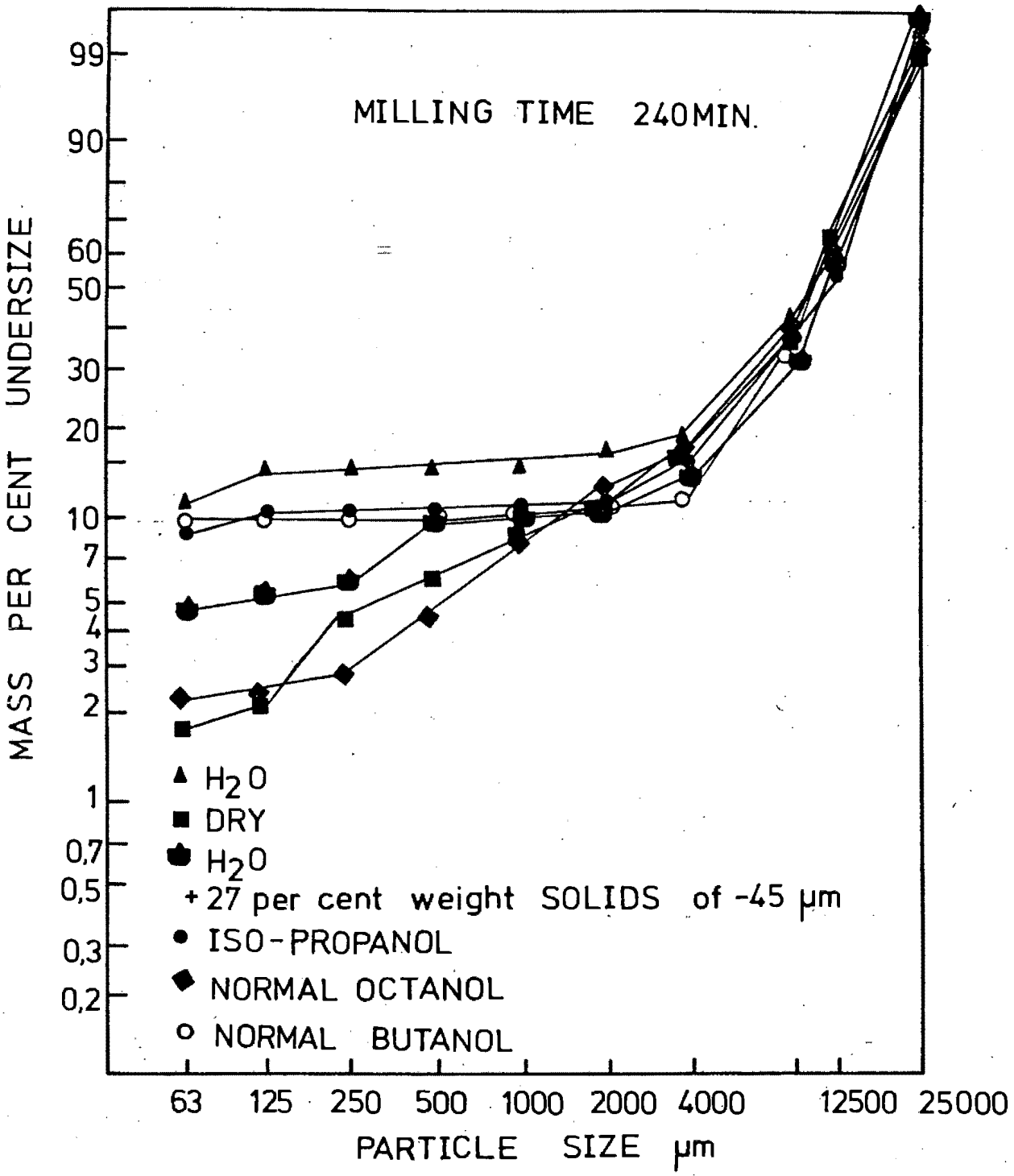

Figure 35

Size distribution of the product of laboratory autogenous milling tests of the third series, presented according to the Rosin-Rammler method.

Milling environments used: Water, dry, water with 27 per cent by weight solids of -45 µm, pure iso-propyl alcohol, n- octyl-alcohol, n- butyl alcohol.

Milling time: 240 minutes.

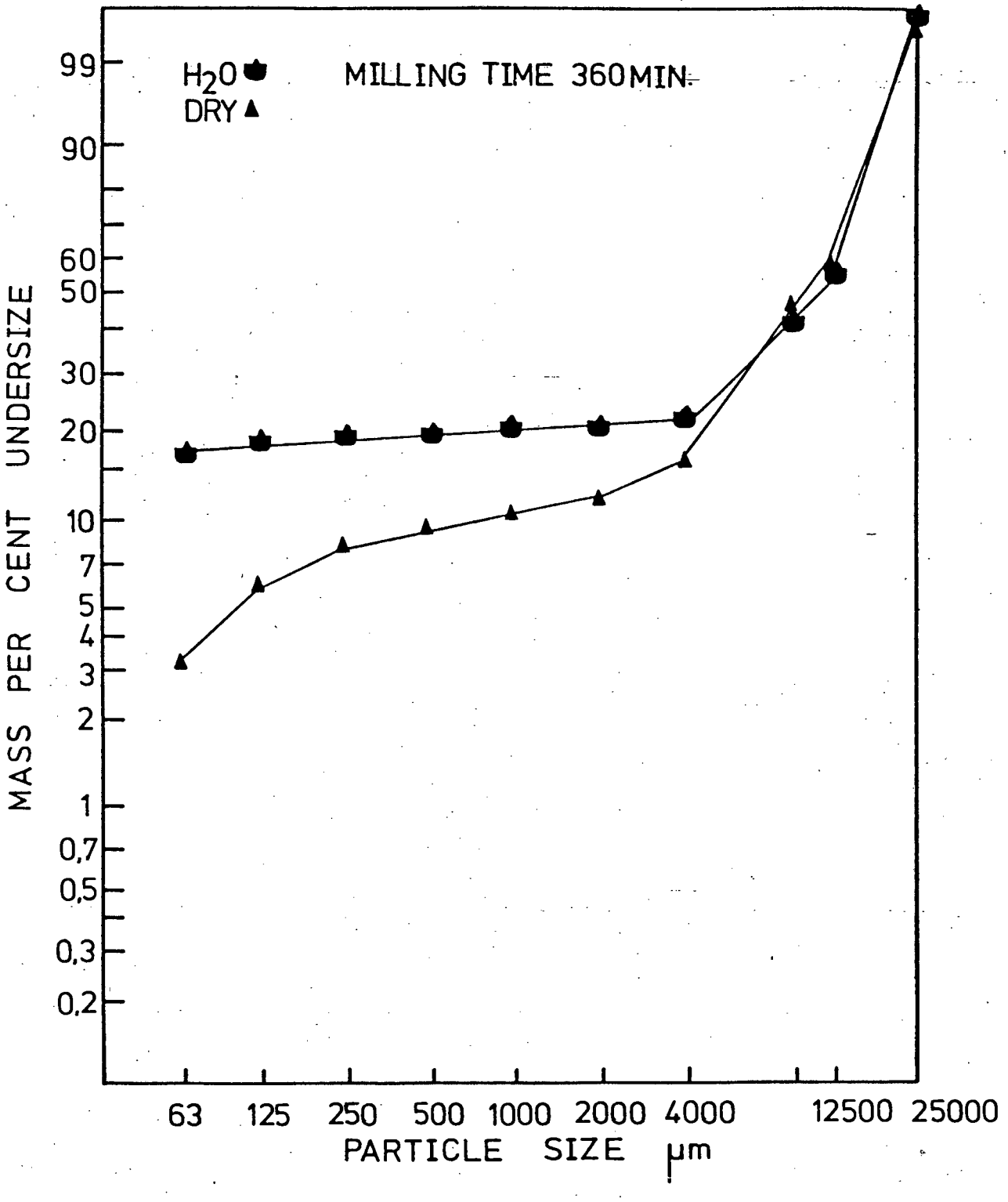

Figure 36

Size distribution of the product of laboratory autogenous milling tests of the third series, presented according to the Rosin-Rammler method.
Milling environments used: dry and water.
Milling time: 360 minutes.

Plate 53

Run-of-mine quartzite particles, showing the influence of the material handling on their surface morphology.
Sieve distribution analysis size: -500 + 250 µm
k_a = 0,3881
k_o = 0,0679

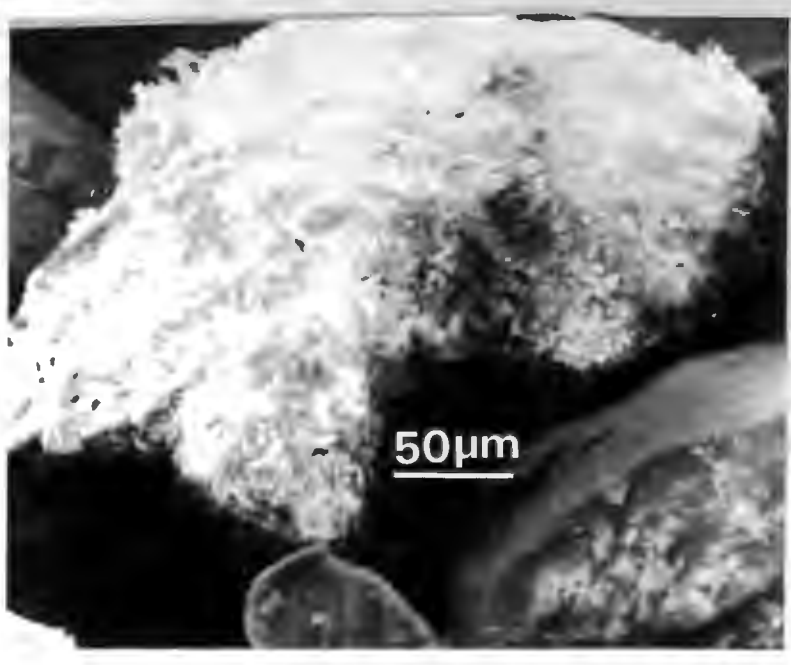

Plate 54

Run-of-mine quartzite particles, showing adhering fine particles on its surface.
Sieve distribution analysis size: -250 + 125 µm

Plate 55

Particles taken from the interior of a fully autogenous wet 'Aerofall' mill.
Sieve distribution analysis size: -250 + 125 µm

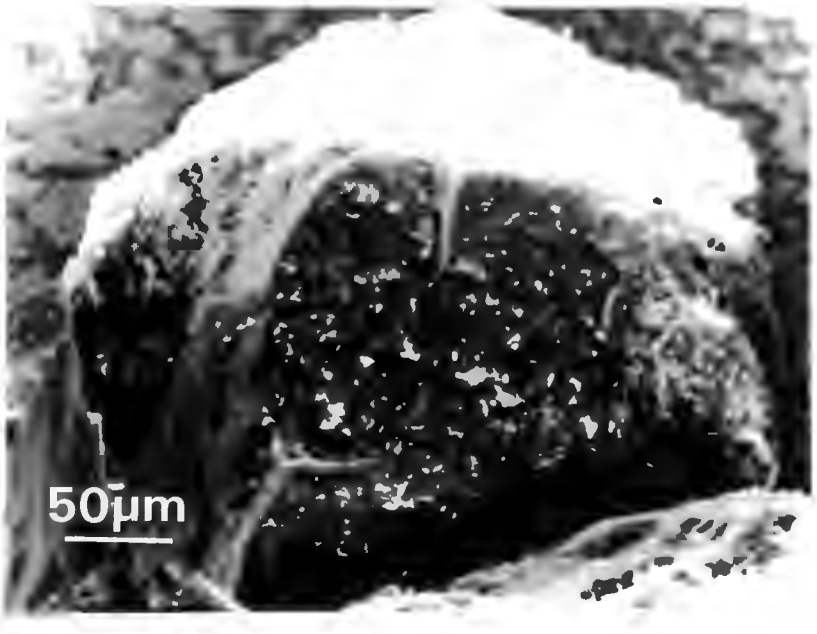

Plate 56

Particle taken from the interior of a fully autogenous wet 'Aerofall' mill.
Sieve distribution analysis size: - 250 + 125 µm
k_a = 0,5698
k_o = 0,07013

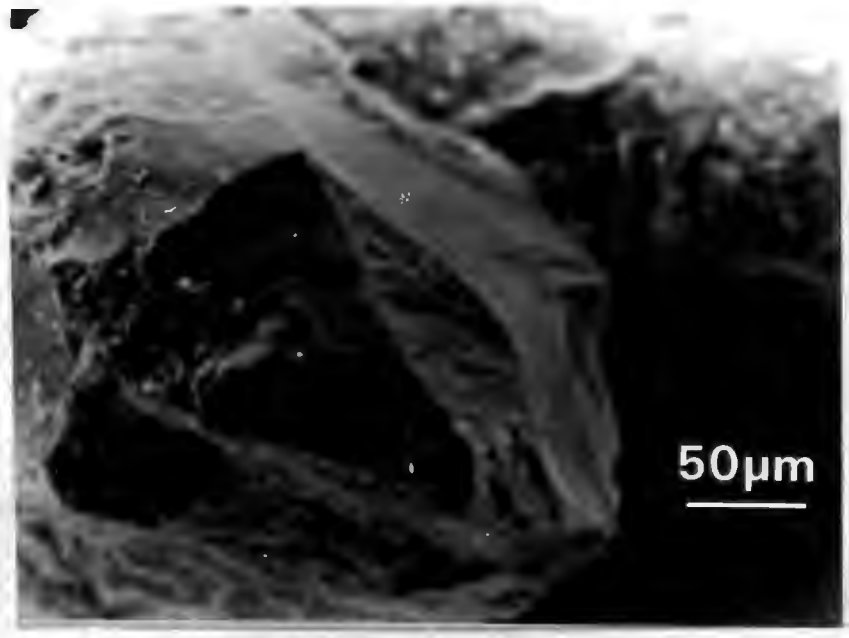

Plate 57

Surface morphology of a particle taken from the interior of a fully autogenous wet 'Aerofall' mill, showing fracture patterns indicative of transgranular comminution.
Sieve distribution analysis size of the particle: -500 + 250 µm

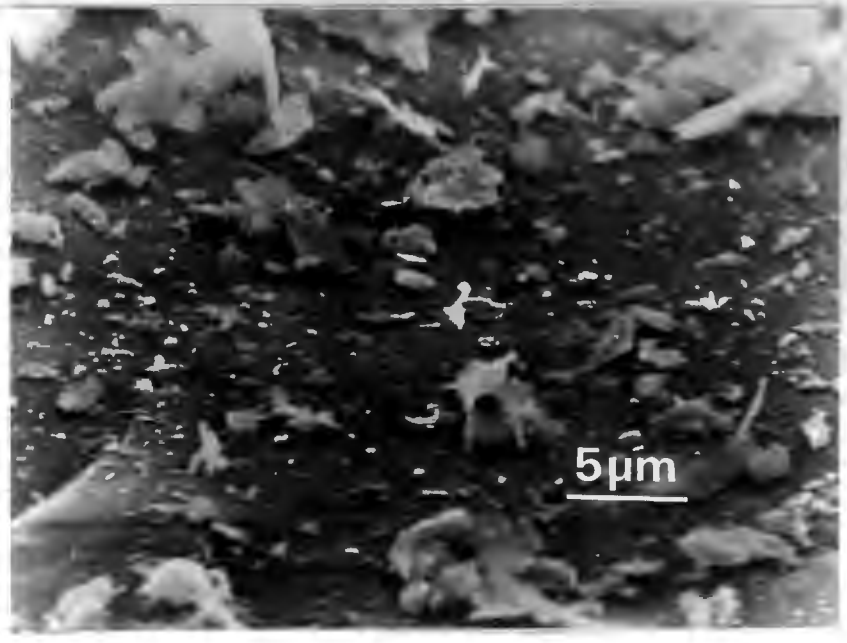

Plate 58

Very fine particles adhering on the surface of a -500 + 250 µm particle, taken from the interior of a fully autogenous wet 'Aerofall' mill.

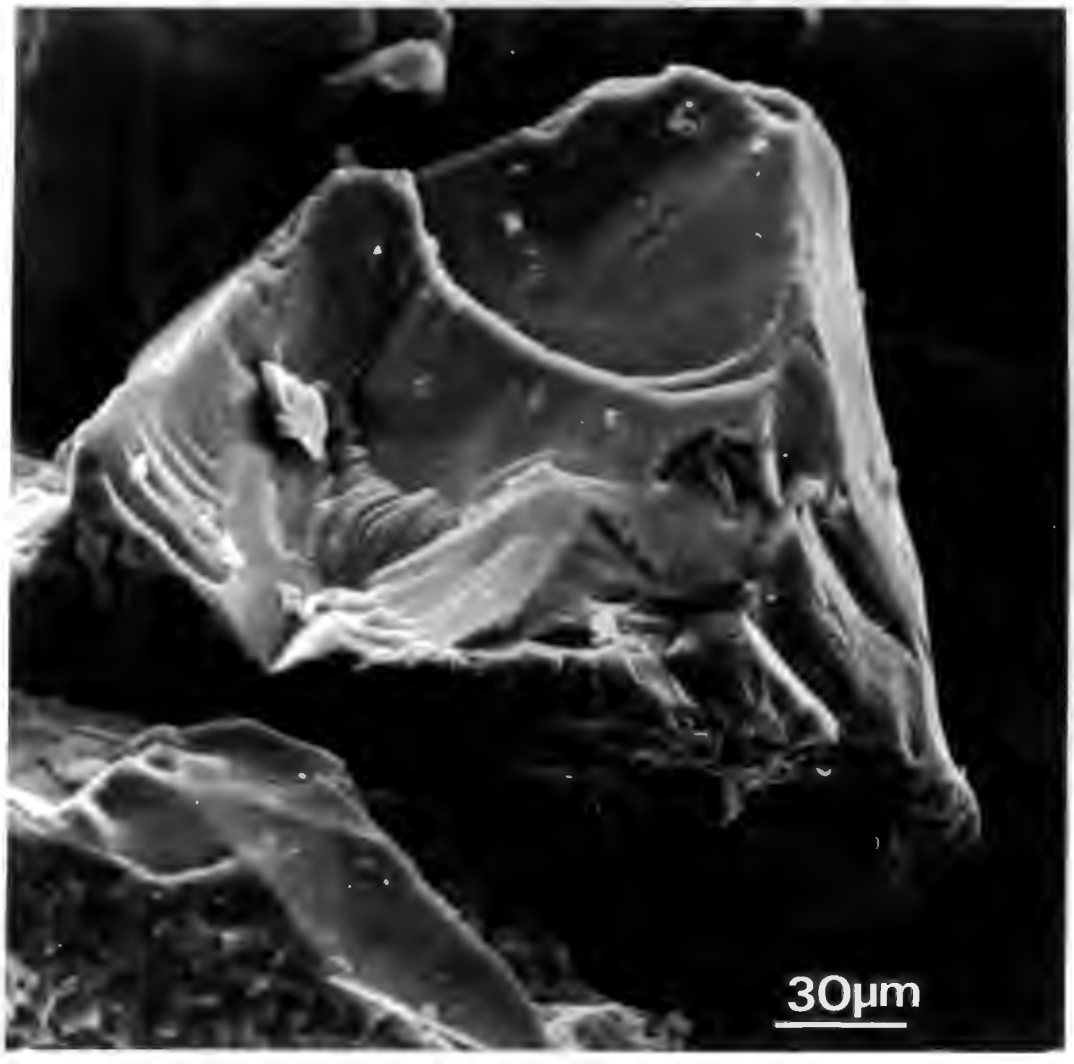

Plate 59

Particle taken from the cyclone overflow of a fully autogenous wet 'Aerofall' mill.
Sieve distribution analysis size: -250 + 125 µm
k_a = 0,542
k_o = 0,0970

Plate 60

Particle taken from the cyclone overflow of a fully autogenous wet Aerofall mill.
Surface morphology indicative of transgranular comminution.
Sieve distribution analysis size: -125 + 63 µm
k_a = 0,4836
k_o = 0,07305

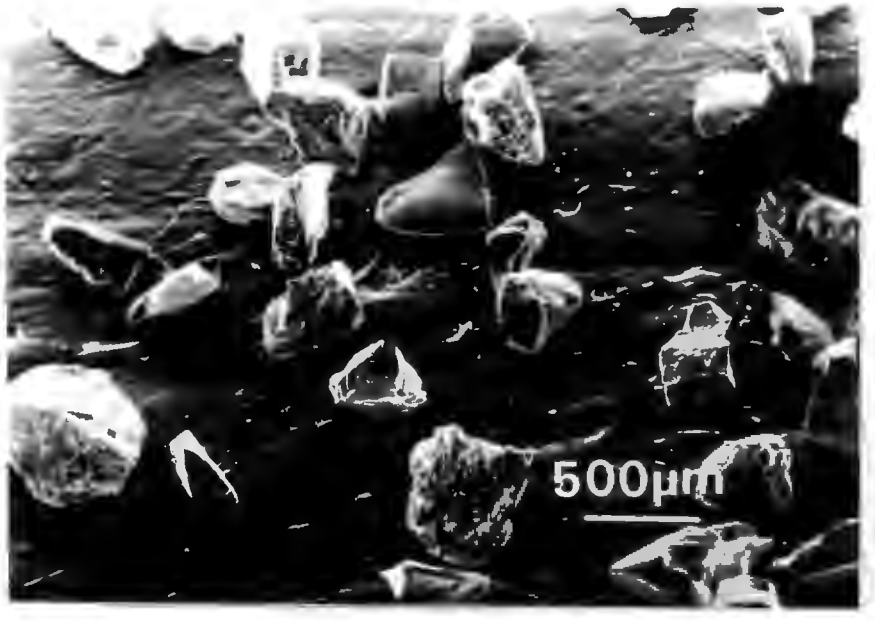

Plate 61

Particles taken from the -500+250 µm product of a laboratory autogenous milling in water environment after 120 minutes milling.

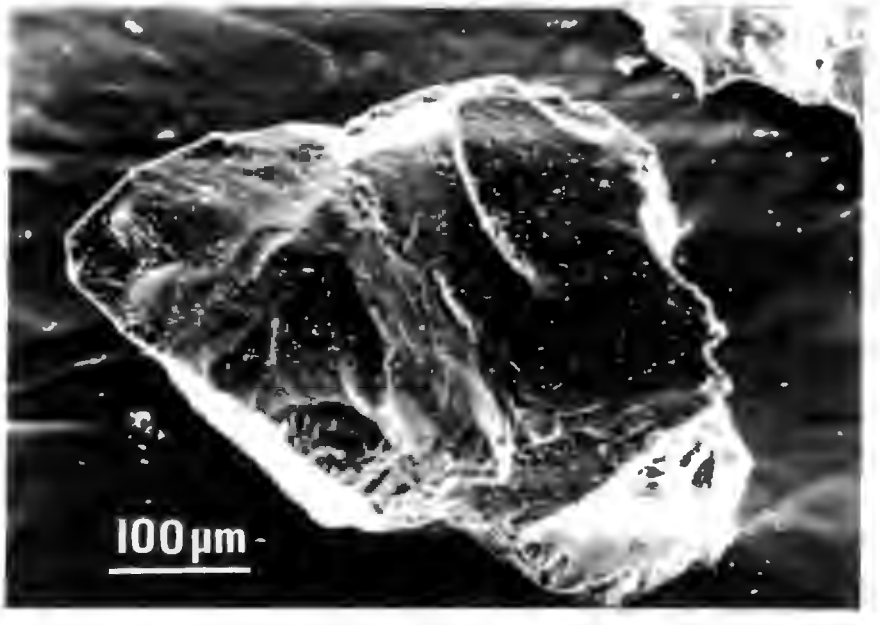

Plate 62

Particle taken from the -500+250 µm product of a laboratory autogenous mill, after 120 minutes of milling.
k_a = 0,0955
k_o = 0,0140

Plate 63

Particles taken from the -250+125 µm product of a laboratory autogenous mill, after 240 minutes milling.
Environment: water.

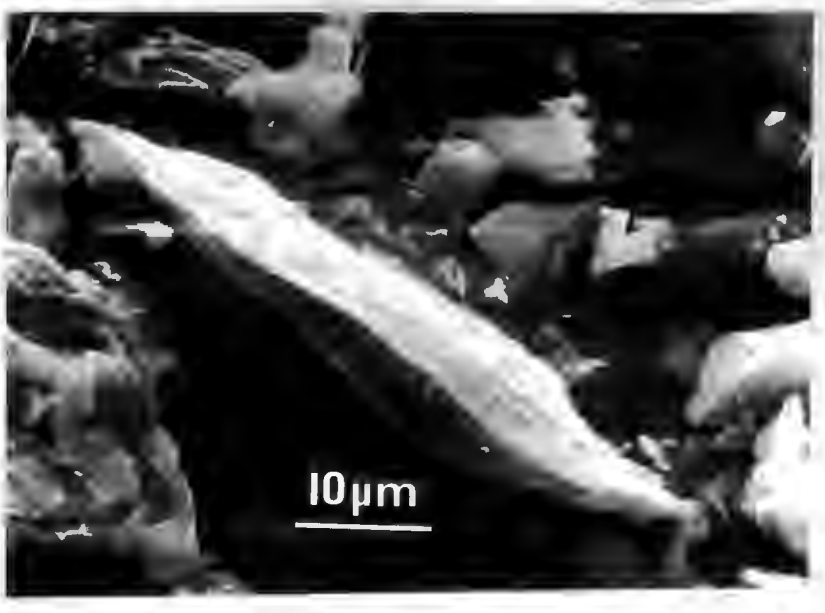

Plate 64

A flaky particle taken from the -63 µm product of a laboratory autogenous mill, after 240 minutes milling.
Environment: water.
The thickness of the particle is less than 10 µm.
k_a = 0,1150
k_o = 0,0431

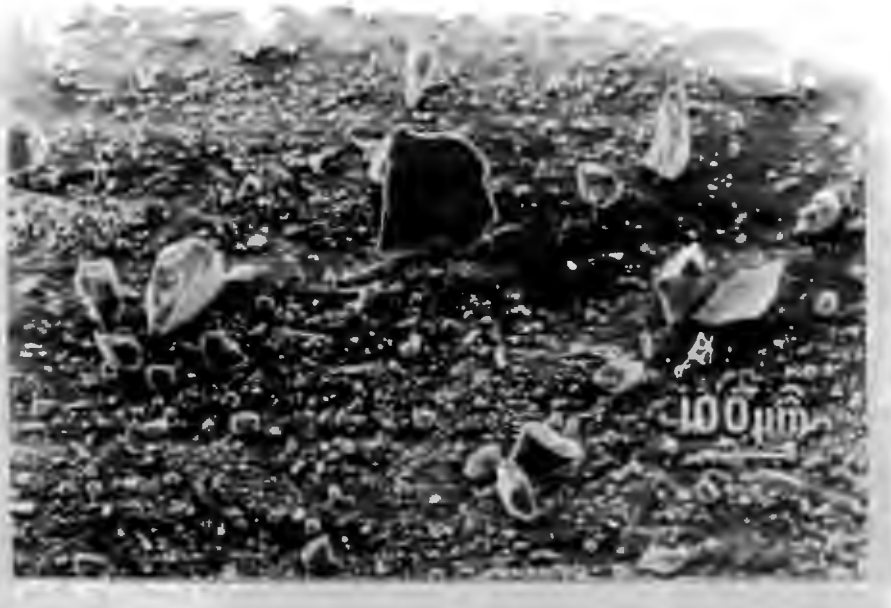

Plate 65

Particles taken from the -125+63 µm product of a laboratory autogenous mill after 360 minutes milling.
Environment: water

Plate 66

Particle taken from the -125+63 µm product of a laboratory autogenous mill, after 360 minutes milling.
Environment: water.
Adhering particles on the surface of the particle.
k_a = 0,2687
k_o = 0,0497

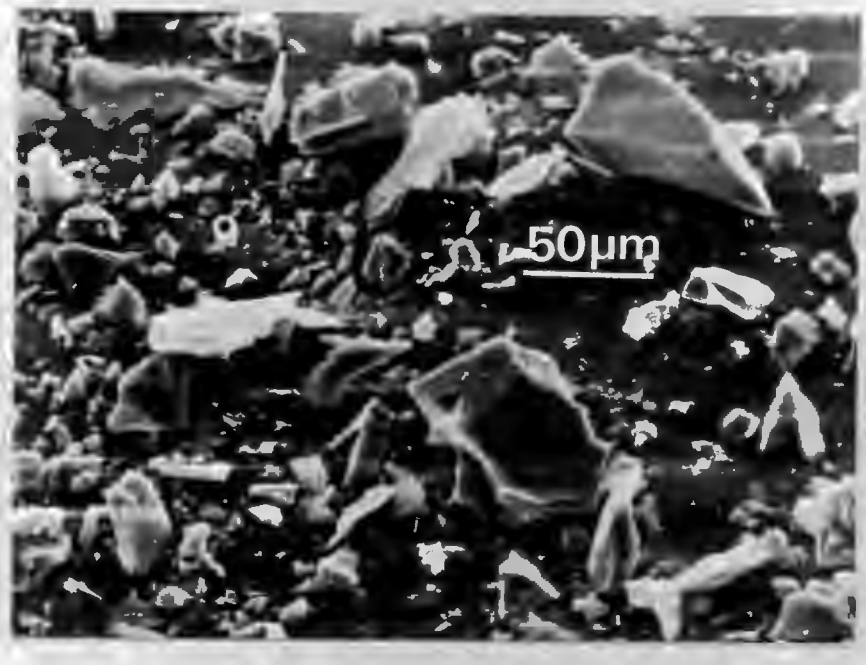

Plate 67

Particles taken from the -63 µm product of a laboratory autogenous mill, in n-butyl alcohol environment, after 120 minutes milling.

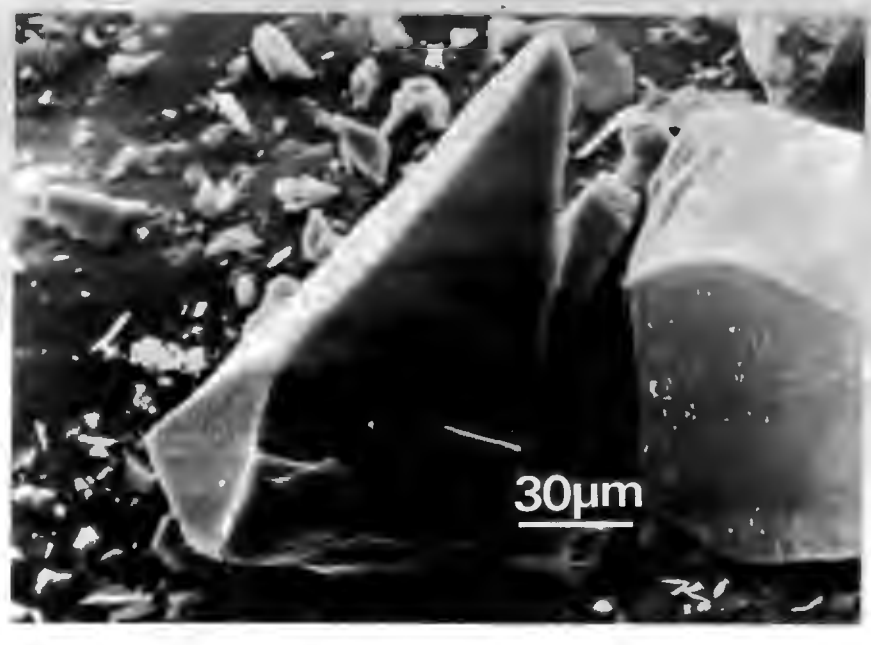

Plate 68

A particle taken from the -63 µm product of a laboratory autogenous mill in n-butyl alcohol environment, after 120 minutes milling.

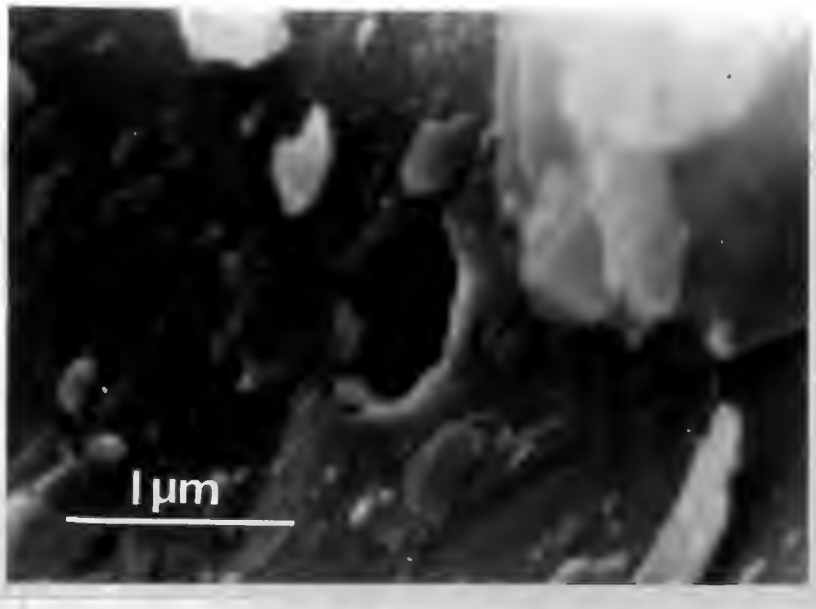

Plate 69

A microcavity on the surface of a -63 µm particle, taken from a laboratory autogenous milling test. Very fine adhering particles are also shown.

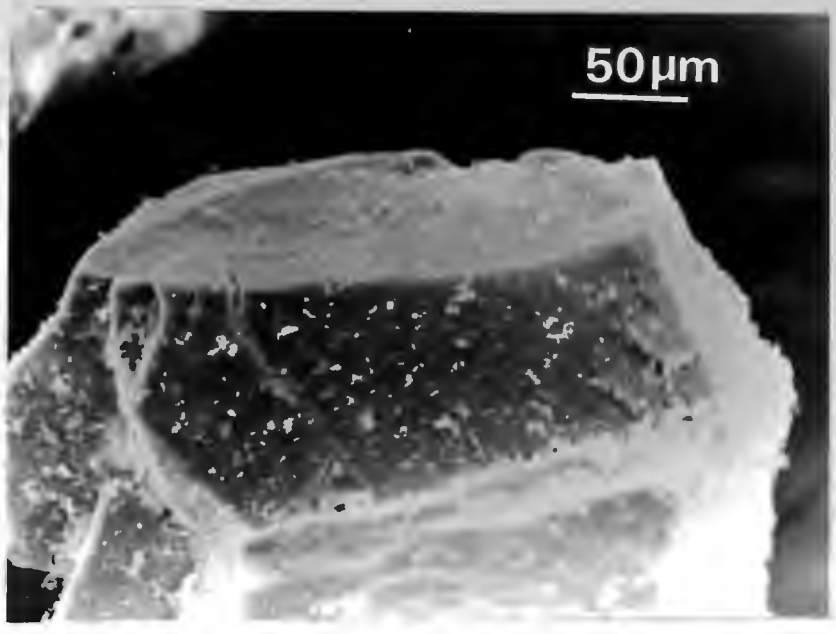

Plate 70

Microcrack on the surface of -500+250 µm particle taken from the interior of a fully autogenous wet Aerofall mill, indicative of trangranular fracture.

examined particles (Plates 55, 56, 57, 58, 66, 69, 70, 71) were also observed. Most of these particles were found to have sharp edges, and flaky platelike appearance, but some of them, and particularly the ones of sizes of the order of 100 nm, appeared in "round" shapes (Plate 70).

The comparison of the surface morphology of particles comminuted autogenously under different conditions of total milling time or environment cannot provide information related to the milling efficiency of these tests, because of the existing similarities of particles belonging to the product of different tests. This comparison can only be achieved by a systematic analysis of the shape characteristics of the examined particles, such as the SEM image analysis of these particles.

6.3.5. SEM image analysis of comminuted quartzite particles from autogenous mills

The arithmetic mean values obtained by each group of particles are shown in table VIII. The deviation of the values of the shape factors from the mean value of their respective group was found to be large (Appendix H). For example the flaky particles seen in plate 58 have very small shape factors.

Particles taken from the mill interior of the "Aerofall" mill were found to have larger "angular roundness" than the run-of-mine particles. The particles taken from the output of the same mill were found to be "rounder" than both of run-of-mine and mill interior particles.

As anticipated the milling time of the laboratory autogenous milling tests in water was also found to influence the shape characteristics of the examined particles. The milling environment was also found to influence the shape characteristics of the examined particles. Milling in n-butyl alcohol for 120 minutes obtained particles of much larger "angular roundness" the particles milled

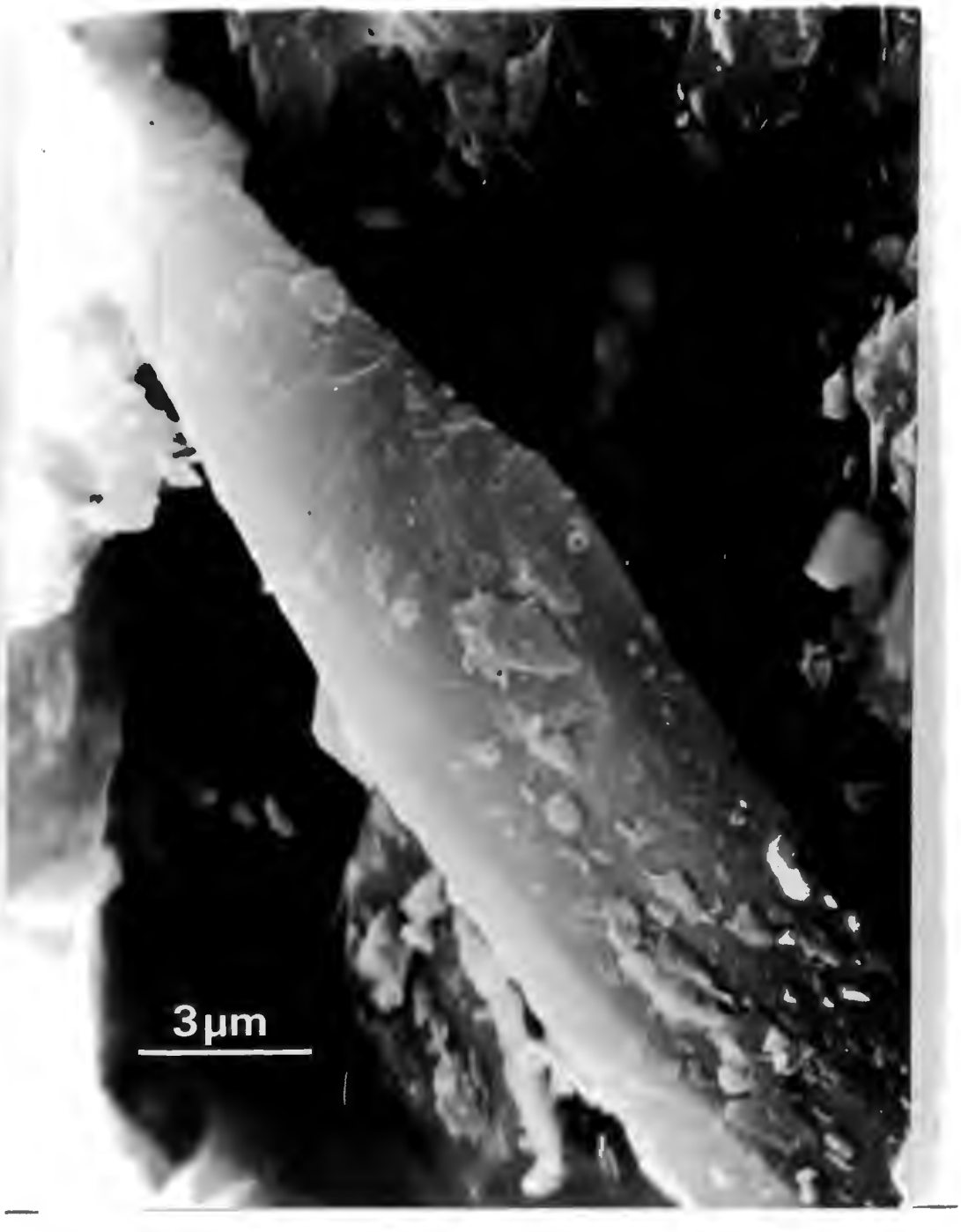

Plate 71

Phyllosilicate particle taken from the interior of a fully autogenous wet Aerofall mill, adhering on particles of -125+63 µm.
Sieve distribution size
k_a = 0,1722
k_o = 0,04272

in water for the same time (Table VIII). The shape characteristics of the particles milled in n-butyl alcohol can be compared to the ones of the milling test in water with total milling time of 360 minutes.

The increase of the "angular roundness" of the particles with the milling time in combination with the size distribution data obtained in figures 31, 35, and 36, for the laboratory tests performed in water environment is indicative of the importance of the breakage of the edges and corners of the particles in relation to the milling efficiency of the comminution system. The similar increase of the "angular roundness" due to the presence of a surface active environment is indicative of changes in the brittle fracture behaviour of the mill charge.

TABLE VIII

Arithmetic mean values of surface and outline area shape factors of each class of particles examined.

MILL	CLASS	k_a	k_o
"AEROFALL"	RUN-OF-MINE FEED	0,398	0,0610
"AEROFALL"	MILL INTERIOR	0,414	0,0630
"AEROFALL"	CYCLONE OVERFLOW	0,488	0,0717
LABORATORY	120 minutes, water	0,378	0,0567
LABORATORY	240 minutes, water	0,399	0,0608
LABORATORY	360 minutes, water	0,447	0,0648
LABORATORY	120 minutes, n-Butyl alcohol	0,455	0,0659
	Sphere	0,785	0,0796

CHAPTER 7

GENERAL DISCUSSION

7.1. General

Autogenous comminution is associated with the presence of a complex and varying stress field upon each consituent of the mill charge. The understanding of the physical processes involved during this type of milling requires a detailed analysis of the mechanics of the brittle fracture and plastic deformation phenomena which are resultant of the mill stress field.

The results of the experimental program described herein have brought to light the following general comments.

Rocks are polycrystalline aggregates composed of highly anisotropic mineral constituents. The mineralogy of the rock is related to the effective surface energy of the rock γ_{eff} (different values of γ_{eff} have been measured for rock of different mineralogy, Friedman et al, 1972) in terms of the Griffith fracture criterion, according to which the critical stress for fracture σ_f is proportional to $\gamma_{eff}^{1/2}$. The grain size of the rock also influences the fracture behaviour of the rocks since, in general, grain boundaries are areas of weakness. The grain size and the geologically inherent microstructural defects, such as microcracks and microcavities are associated with the flaw distribution in the material. The length C and the sharpness of these defects, characterised by the radius of the tip r, are of importance for the initiation and the propagation of these flaws. Sharp and long cracks favour fracture initiation since according to the Orowan criterion the critical stress for fracture is proportional to $(r/C)^{\frac{1}{2}}$. The intragranular or transgranular flaws show a tendency to be very sharp, since they are in general regions of microcleavage. Their length will in general be equal to the grain size because of the ease of cleavage across the complete grain (see figure 37). Microporosity, consisting of short and blunt intragranular defects, is not very important for the fracture behaviour of a rock, since the magnitude of the stresses which are required to initiate fracture is very large in comparison with the similar critical stresses of the sharper and longer flaws. The length C of the intergranular microstructural

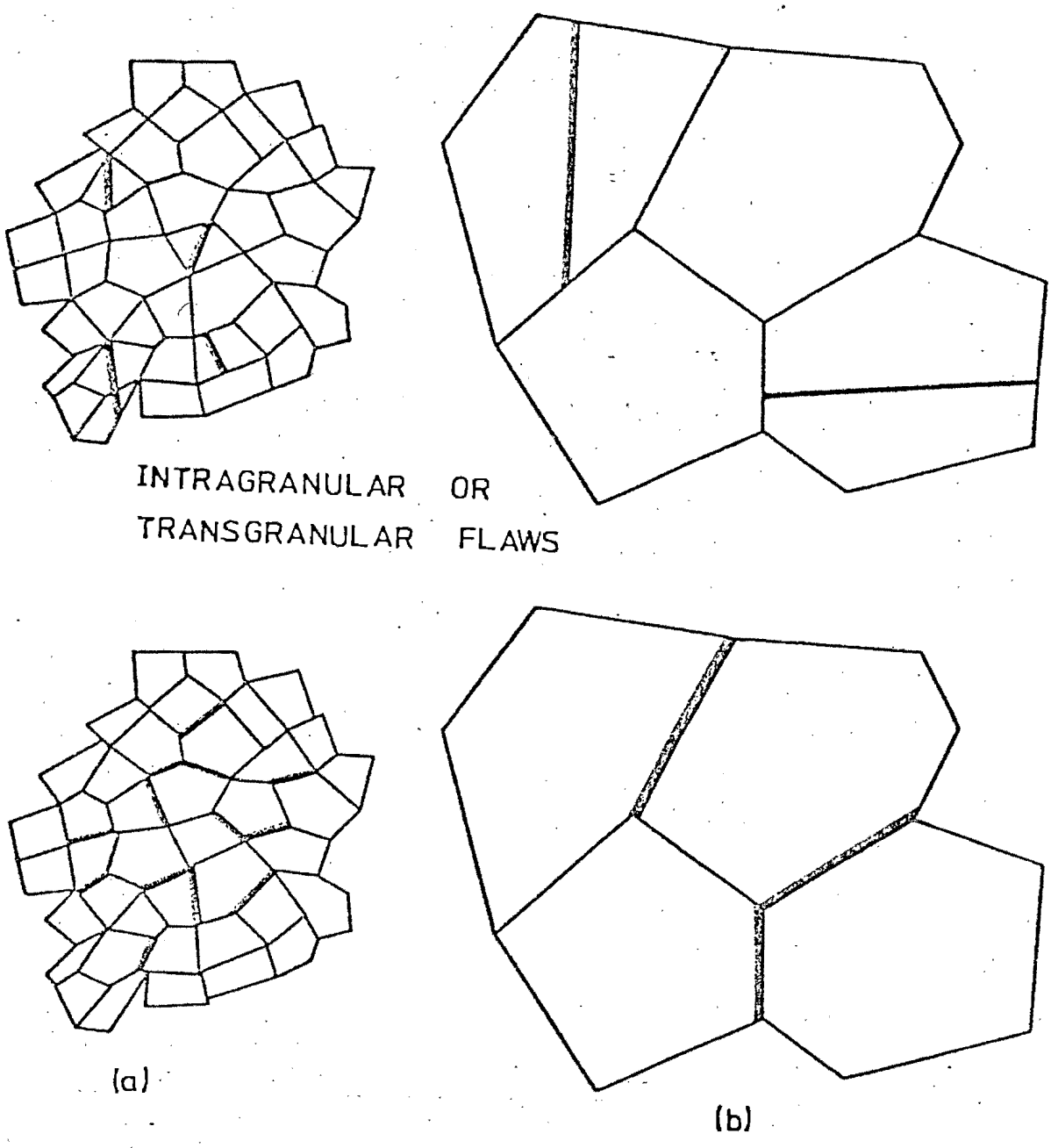

Figure 37

Relationship between the grain size of the rock and the length C of the intragranular (or transgranular) flaws and the intergranular flaws. Influence of the grain size upon the length C of the intergranular micro-structural defects. A rock of a relatively small grain size (a) has shorter intergranular flaws than that of a rock of a relatively large grain size (b) due to smaller total area of grain boundary area of the first type of rock than the total grain boundary area of the second type.

defects is proportional to the grain size, as is shown in the schematic of the figure 37.

The crack propagation in a brittle solid such as quartz will occur by cleavage fracture at very high speeds. During the propagation, a crack may be "arrested" by a weak grain boundary interfaces or particles lying orthogonal to the moving crack. The total area of the crack propagation is influenced by the grain size, presenting larger values when the grain size decreases, as it is schematically shown in figure 38. The velocity of crack propagation is influenced by the geometry of the crack; blunt cracks propagate at higher stress level than sharp cracks of the same length, since this process takes place at higher stresses for the blunt cracks. When the velocity of crack propagation is higher than a critical value, the phenomenon of bifurcation occurs (Payne and Ball, 1976). Blunt notches propagate at higher velocities than the relatively sharp ones. Bifurcation, therefore, is favoured by blunt initiating notches. Bifurcation is associated with the production of small fragments of the comminuted rock, which is in general desirable in comminution.

When two rock surfaces are sliding on each other, under the influence of a normal load, both plastic deformation and fracture may occur. The relative amount of these two competing processes will be determined by various factors. At the area of contact of the two surfaces (figure 39) the resulting high hydrostatic pressure favours plastic deformation at this region (Lawn and Wilshaw, 1975). In addition, since plastic flow is a thermally activated process, it is favoured by high temperatures (i.e. low values of sliding speeds). The surrounding stress field which is present during the sliding of the rock surfaces consists mainly of tensile and shear stresses and the magnitude of the shear stresses will influence the possibility of dislocations activity.

The fracture initiation, which is associated with the tensile stresses of the stress field, is influenced by the dislocation mobility, in terms of changes of the geometry of the near surface flaws. These inherent microstructural defects of the rock surface

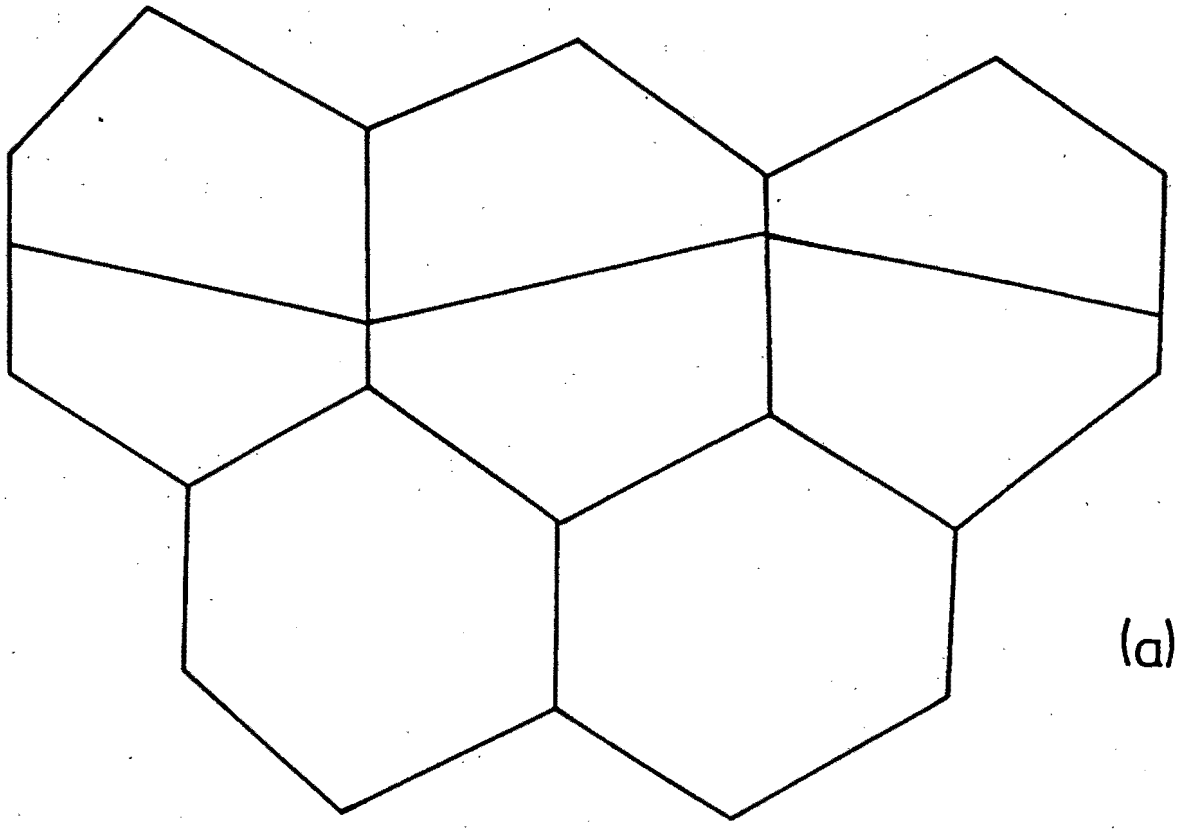

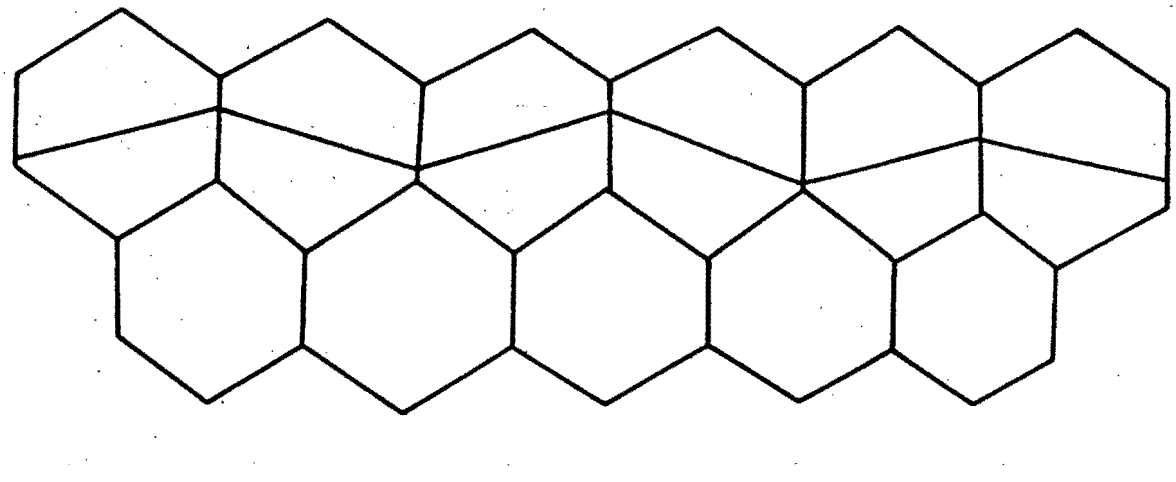

Figure 38

Influence of the rock grain size upon the total area of crack propagation. This area is smaller for a rock of relatively large grain size than that of a rock of a relatively small grain size.

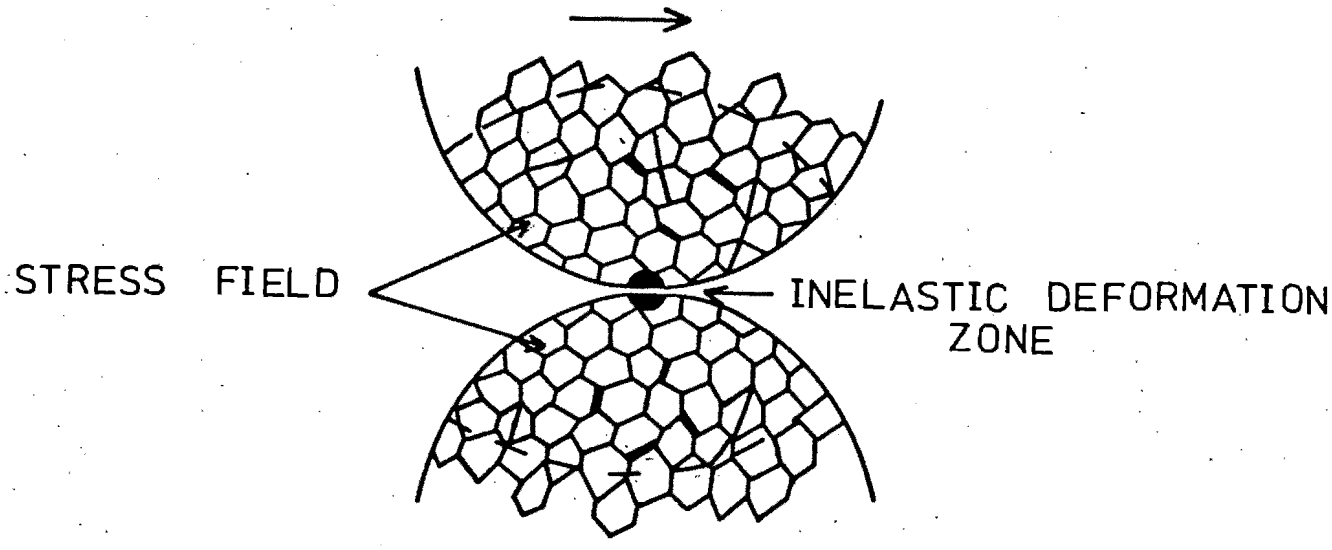

Figure 39

The development of the "inelastic" deformation zone and of the stress field during the sliding of two rock surfaces of a given grain size. Dotted line marks the area in which fracture initiation and propagation can take place.

can be propagated in a manner governed by the conditions of crack length and geometry of the flaw.

The rock surfaces consist of grain asperities which are interlocked during contact. During sliding these asperities may climb each other without any surface damage, or break only their tips by brittle fracture, or result in extensive surface damage involving both brittle fracture and plastic flow phenomena. The climbing of the surface asperities without any surface damage is favoured by low values of normal load and sliding speeds. The area which is influenced by the stress field is small, while the magnitude tensile stresses in this field are too small for fracture initiation from microstructural surface defects. Low sliding speeds favour the occurence of this model of friction, since the time necessary for the climbing the surface asperities is provided. This required time is dependent upon the surface roughness, grain size and rock mineralogy, because the geometry of a typical rock asperity ("model of asperity", Byerlee, 1967 a) is influenced by these parameters. The brittle fracture of tips of the surface asperities occurs at sliding speeds, which do not allow the necessary time for the climbing over the asperities, while the stress field which is present influences a small region below the sliding rock surfaces. High sliding speeds are associated with a stronger interlocking action than the two previous cases, since the time provided for a "smooth" sliding of the surface asperities on each other is very small. Similarly high normal loads are associated with the presence of a larger stress field, which influences a large portion of the near surface regions of the sliding rocks. Extensive fracture and plastic deformation is therefore anticipated. Plastic deformation will be particularly extensive when a large difference in Mohs hardness characterises the mineral rock constituents in contact.

7.2. Fracture characteristics of the rock in relation to its suitability for autogenous milling

The differences in compressive and tensile strength between the various petrographical types of the Witwatersrand quartzite (Figure 2,

Table III, Plates 1 to 4) can be explained in terms of the fracture initiation and propagation of the geologically inherent microstructural defects in the rock. The effective surface energy of the rock changes with the chemical composition. Friedman, Handin and Alani (1972) found values of γ_{eff} to range from 19 to 68 Jm^{-2} for Chilhowee quartzites, while the value of 2 Jm^{-2} was obtained by Ball and Payne (1976) for quartz crystals fractured in tension. The size of the grain boundary microstructural defects, such as those associated with phyllosilicates flakes, is proportional to the grain size. This follows because, for a rock of given impurity content the total area of grain boundary is reduced when the grain size of the rock increases, and subsequently a rock of a relatively large grain size will contain longer intergranular defects than a fine grained rock (Figure 37). The decrease of the "Brazilian" tensile and uniaxial compressive strength with the increasing grain size of the petrographical types of the Witwatersrand quartzite, from A to D, is explained by the increase of the length c of the geologically inherent microstructural defects of the rock. The distribution and the character (intra- or inter-grannular) (see Figure 37) of those microstructural defects is very important, since they will determine the comminution behaviour of the rock. Since the minerals to be exploited from the Witwatersrand quartzite are mainly distributed along grain boundaries intergranular comminution events are desirable in comminution.

The relationship between the fracture load P and the diameter D, which was found by Brazilian tests on specimens of various diameters (Figure 1), and can be described by an equation of the form: $P = \lambda_D D^{1,7(\pm 0,05)}$, where λ_D is a constant. These results show that the fracture resistance of rock pieces in slow compression increases with their diameter. An analysis of this relationship based upon specific energy E_s, per unit volume, and geometrical and

elastic characteristics of the material* comminution shows that for the Witwatersrand quartzite of the petrographical type B, the comminution of the rock by slow compression is governed by the Bond energy concept** (Arbiter and Harris, 1965). Bergstrom et al (1964) found from an analysis of experimental results on the fracture load versus geometrical characteristics of quartz crystals, that the Rittinger's energy concept is followed. The granular nature of rock in combination with the geologically inherent microstructural defects can explain the difference in fracture energy requirements between quartz crystals.

The size distribution of the product of uniaxial compression fracture, tests shown in figure 8, is compatible with the hypothesis expressed by Gilvarry (1961) concerning the distribution of the activated micro-structural defects within the mass of a rock, which is under stress. The results of these tests can be expressed in terms of the Rosin-Rammler equation $Y = 1 - \exp(-(^{X}/k)^{n})$ (Appendix A). The value of the parameter n was found to be approximately unity. The parameter k of this equation describes in a statistical manner the average spacing between the activated micro-structural defects of the rock. The presence of a large number of activated micro-

---

*For materials obeying Hooke's law and for point contact, the specific energy E_S (i.e. energy per unit volume, Jm^{-3} or Nm^{-2}) is given by the equation $E_s = C_1(L/M^{2/3})^{5/3}$ where L is the fracture load, M the specimen mass and C constant dependent upon the elastic properties of the material. The value of C_1 is a function of physical properties only, viz:

$C_1 = 4/5(3/4)^{5/9}(1 - v_1^2)/E_1 + (1 - v_2^2)/E_2^{2/3}(\rho\pi)^{1/9}$ where v_1, v_2 and E_1, E_2 is the Poisson's ratio and modulus of elasticity for the specimens and the pattens respectively (Bergstrom, 1965). For a cylindrical rock specimen and for line contact Bergstrom (1965) reported the following relationship, based upon Roesler (1956) and Porisky (1950) analyses: $E_s = C_2(L/D^2)^2$

**A general form of the specific energy-size relationship, summarising the Rittinger-Kick-Bond equations has given by Holmes (1957), $E_S = \lambda_1 \frac{1}{D^r}$ where λ_1 is constant dependent upon the comminution material characteristics and the comminuting device for a large reduction ratio and r is 0, 1 and 1/2 for the Kick's, Rittingers and Bond's Law respectively. Thus: $L = \lambda_2 D^{(4-r)/2}$ or $L = \lambda_{2_K} D^2$ for Kick's law, $L = \lambda_{2_R} D^{3/2}$ for Rittinger's law and $L = \lambda_{2_B} D^{7/4}$ for Bond's law.

structural defects, like the ones induced by heating at 400°C and quenching in water (Chapter 3) correspond with smaller values of the parameter k. The thermally induced flaws are easily be activated due to their sharpness. This analysis can explain the fracture load-grain size relationship in terms of the higher statistical probability of flaws of a relatively large length than the similar one of shorter flaws which appear in a higher frequency and possess similar sharpness.

The stress conditions occuring in an autogenous mill will vary over a wide range of values. This, in combination with the inhomegeneity in the material, does not allow any easy or accurate establishment of milling suitability criteria for a given rock. The results obtained for the tensile strength σ_t of the rock specimens examined by the Brazilian method, using the equation $\sigma_t = 2P/\pi Dl$, where P the fracture load, D the diameter and l the length of the rock specimen (Figure 2), were found to be more reproducible, than those obtained from the tests on the compressive strength (Table III). The different action of the packing strips used, in terms of distribution of the applied stresses, was found to be responsible for the small increase of the measured value of the tensile strength, when the diameter of the test specimens increases.

Brazilian tests can provide information about the ability of a given ore to "survive" as wear media during autogenous milling. Assuming that the slow compression of a drill core maintains stresses, the distribution of which is not different than that of free-fall impact and considering that the increase of the fracture load P for increasing loading rates (John, 1972) is very small, the Brazilian testing technique can provide usuful information about the prediction of the impact behaviour of a given ore, during autogenous milling. The same testing procedure can be used for the selection of the optimum size distribution of the mill feed.

The reproducibility of the results of the free fall tests was found to be very poor (figure 3). This behaviour can be explained by the different impact conditions deriving from the existence of different sharp edges of each specimen and by the inhomogeneity in

microstructural defects within the mass of the rock and particularly at the near to its surface region.

7.3. The thermal weakening of the rock

The heating of the rock and the subsequent quenching was found to reduce the tensile strength of the rock (Figure 4), due to thermally induced microstructural defects, such as the microcracks and microcavities shown in plates 12, 13. The distribution of these defects, produced by heating temperatures up to 400°C, is similar to the one of the geologically inherent flaws, since the slope of the Rosin-Rammler presentation is similar to that of the as received rock (Figure 8). The thermal microfracturing appears in a higher frequency when the heating temperature is higher than 425°C (Figure 13). The high incidence of microstructural defects within the mass of the rock is expected to result in interaction between two neighbouring defects. The longer flaws produced by thermal treatments compared with the ones in run-of-mine rock, require smaller loads for fracture propagation.

The differences in thermal expansion characteristics between the various petrographic types of the rock and quartz, shown in figure 5, is due to the differences in their mineral composition. The $\alpha \rightarrow \beta$ quartz transition, 573°C, can also develop thermal stresses (Figures 5 and 6), while chemical reaction of pyrites, the occurence of which can be observed at the thermal expansion characteristics of the quartzite of type D for temperatures higher than 640°C, is also important for the thermal comminution.

The dependence of the thermal comminution upon the time of heating (Figures 9 and 10) and the detected increasing amount of microfracturing taking place for heating temperature higher than 450°C (Figure 13) indicates that a time dependent process occurs at this temperature. Considering that the time necessary for a uniform heating of the mass of the used rock specimens cannot be longer than three minutes, this microfracturing process cannot be dependent on temperature gradients. The dehydration of the

phyllosilicates group of minerals, which occurs at temperatures approximately 430°C (Deer et al, 1962) will be time dependent, and the liberated water will produce increasing pressures in pores and cavities and subsequent microfracturing will ensue. The heating of the rock thus results in the weakening of the rock, while further improvement, from the comminution point of view, is achieved by a fast cooling of the hot material (Figure 13).

Such thermal treatments, although more effective in terms of comminution efficiency with increasing heating temperatures (Figure 11) are not directly applicable due to their high energy requirements. Quartzite has a specific heat capacity of about 10^3 J kg^{-1} $^oC^{-1}$, at temperatures 20°C to 400°C and the energy required for the one tonne of ore to reach 400°C is approximately 4×10^8 J. The increased finess of the comminuted product of a thermally treated quartzite due to the increased presence of microstructural defects (Figures 8 and 13) and the enhanced degree of mineral liberation of the same material (Figure 12, Plate 8) can offer large benefits, from the total production point of view, than the cost of the energy required for thermal treatments. The relative toughness of a given ore, which does not allow high values of efficiency of an autogenous milling system and the possible availability of a low cost heating fuel can offer a successfull application for the partial heat treatment of a run-of-mine ore.

It should be noted that the local temperature rises developed during the sliding of two rock surfaces or between a rock surface and the mill liners may cause local thermal weakening of the material, similar to the one achieved by an external heating source. A large fraction of the kinetic energy activities in a mill is transformed into heat by this manner. Although measured temperatures are only about 40°C, local temperatures can be sufficiently high, higher than 400°C, to create flaws, with a subsequent contribution in the comminuting action of the mill.

7.4. The frictional behaviour of rock

The magnitude of the frictional force and the surface morphology

of the friction track were used to study the mechanisms involved during the sliding of two rock surfaces. The variables of the normal load, sliding speed and initial surface roughness for a given environment can establish the conditions necessary for the occurence of distinctive modes of friction.

The geometrical characteristics of the surface asperities of sliding rocks and the magnitude of the applied normal load govern the interlocking of these asperities. The "climbing" of the interlocked asperities is a process which requires a given time which is dependent upon the surface roughness and the applied normal load. The change of the relative velocity of the two sliding surfaces is associated with changes in the time which is provided by the relative movement of the sliding surfaces for each "pair" of interlocked asperities. Thus for a given value of normal load and surface roughness the coefficient of friction will be dependent upon the relative velocity of the moving surfaces. The time necessary for the "climbing" over the surface asperities is provided when the sliding speeds are low. This process takes place in a "smooth" manner and is associated with small values of frictional force and subsequently small values of coefficient of sliding friction while the surface damage involved is negligible (Figure 15, water, for speeds smaller than $4{,}23 \times 10^{-5}$ ms^{-1} and Plate 18). This behaviour is indicative of the occurence of the roughness theory of friction (see section 4.1.2.)

When the relative velocity of the sliding rock surfaces increases to values which correspond with duration of contact slightly shorter than the necessary period for the "climbing" of one asperity over another, stress concentration at the tips of the rock surface asperities results in the brittle fracture of these tips. The coefficient of sliding friction obtains higher values, while a distinguishable surface damage is involved across the friction track (Figure 15, water, for a sliding speed between $8{,}46 \times 10^{-5}$ and $8{,}46 \times 10^{-4}$ ms^{-1} and Plate 20). This frictional behaviour is indicative of the occurence of the theory of friction proposed by Byerlee (1967 a).

For increasing values of sliding speed the corresponding values of "duration of contact" becomes very small and the climbing over of the surface asperities is very difficult in the time available. As a result strong interlocking conditions are developed. Fracture initiation and propagation occurs under the influence of the stress field which is developed by the applied normal load while plastic flow can also occur when the sliding surfaces consist of minerals of different scratch hardness. Brittle fracture and plastic flow take place at high sliding speeds in a manner similar to one proposed by Bowden and Tabor (1964) for the friction of metals, and result in the formation of a very distinctive surface damage along the friction track (Plate 32).

The frictional force and consequently the coefficient of sliding friction (since the applied normal load is constant), obtain their maximum values when the sliding speed allows the brittle fracture of the tips of the asperities, i.e. in the mid-range of sliding speeds. The higher value of the frictional force at these speeds can be explained by the interlocking action of the tips of the asperities. The frequency of these interlocking events is high, since the surface damage which caused the breakage of the tips is very small. The value of the measured frictional force is relatively high, representing the average of the values of the frictional force. This is indicated by "stick-slip" variations of the recorded frictional force (Figure 14). The frictional force obtains lower values (Figure 15, water, at sliding speeds higher than $8{,}46 \times 10^{-4}$ ms^{-1}) when the sliding speed increases, causing the occurence of both brittle fracture and plastic flow phenomena. The large surface damage which is caused at these sliding speeds reduces the number of the interlocking events and subsequently the measured average value of the frictional force.

The changes of the frictional force with the sliding speed are dependent upon the surface roughness, (Figure 17), presenting smaller values for smaller magnitude of surface roughness (CLA). This can be explained by the decrease of the magnitude of the interlocking action when the average height of the asperities decreases.

A change in the load normal to sliding surfaces of standard roughness and moving with constant relative velocity also results in

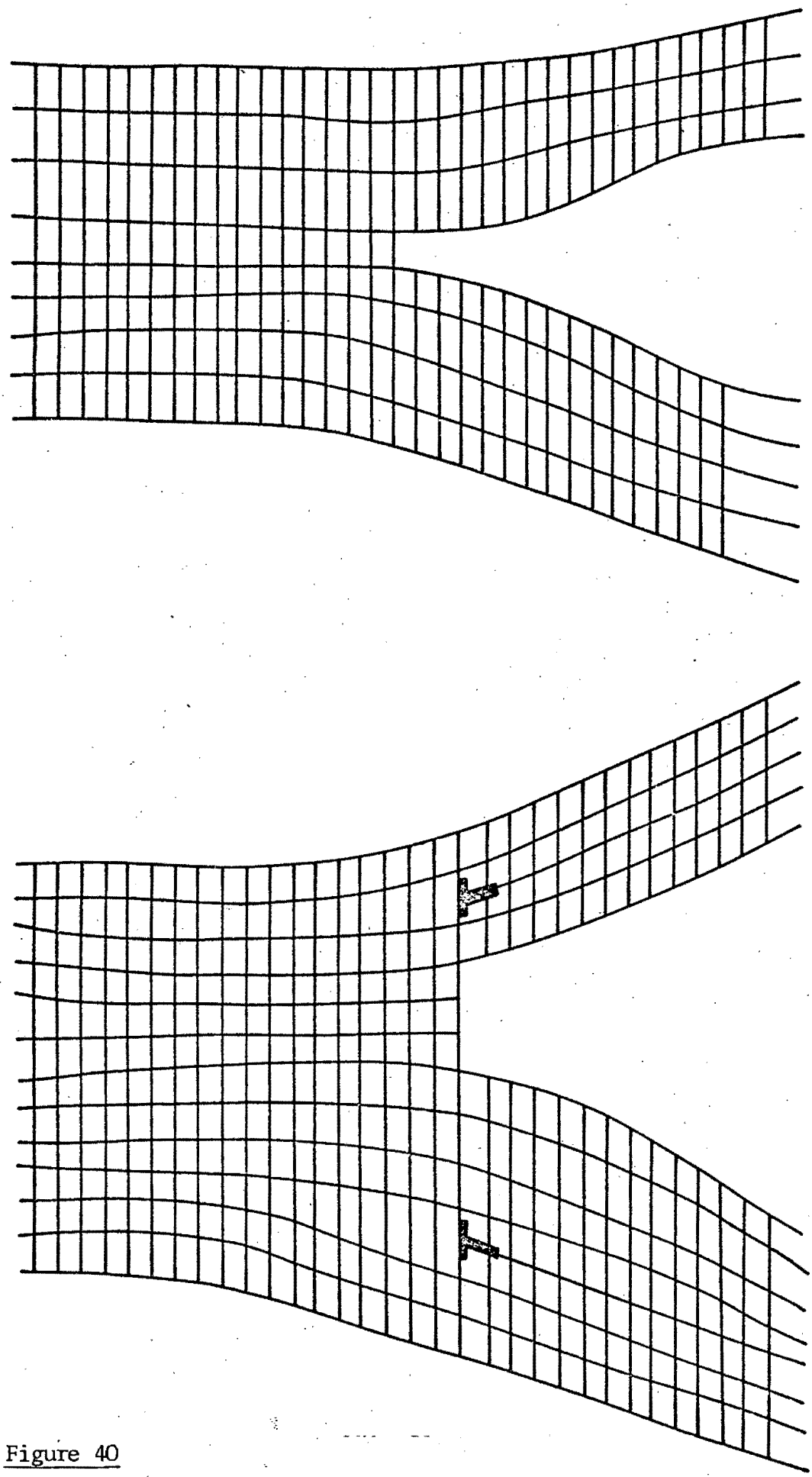

Figure 40

The blunting of an atomically sharp crack via two mobile dislocations.

the occurence of different modes of friction. For relatively low values of the applied normal load, the parameter m of the equation $F = kL^m$ (Archard 1953, 1957), was found to be smaller than 0,66, the limiting value for pure elastic deformation (Table V). These relatively small values of the parameter m are indicative of the occurence of the "climbing" of the surface asperities, in a manner similar to the one described when the sliding speed is very small (Plate 19). The critical value of 0,66 is obtained for relatively high values of the applied normal load indicating the brittle fracture of the tips of the surface asperities, according to the mode of friction proposed by Byerlee (1967 a).

The parameter m increases at values up to 0,69 when the normal load further increases (Table V), showing that plastic flow is also involved during sliding under these conditions. This is also confirmed by the smooth extruded appearance of the grooves, observed by SEM means (Plates 32 to 36). The ploughing of a relatively hard mineral (e.g. quartz with Mohs hardness 7 or pyrite with $6\frac{1}{2}$) into a softer one (e.g. muscovite with Mohs hardness 3 or serpetine with $2\frac{1}{2}$) results in the formation of a such groove, while at the same time fine adhering gouge-debris are produced (Plates 34 and 36). The relatively soft mineral constituents of the sliding rock surfaces can also cover the asperities of the relatively hard minerals in a manner described as "shaving" action by Bowden and Tabor (1964). Plastic flow phenomena are concurrent with brittle fracture, which occur during sliding when the minerals in contact have similar scratch hardness and subsequently promote the state of "adhesion".

The parameter m and the mode of friction change with load in a different manner (Figure 18) for different surface roughnesses since the geometry of the interlocked asperities changes with the values of central line average.

7.5. The wear due to abrasion

The wear effects associated with the sliding of two rock surfaces, studied by the abrasion testing apparatus, have shown that they are influenced by changes of the rock petrography, the normal load applied, the relative speed and the abrasion time.

The rock petrography influences the wear rates since both fracture and plastic flow phenomena are affected by the type of rock. The fracture initiation is favoured by the increase of the grain size and the corresponding reduced values of the tensile strength (Figure 22). The distribution of the soft mineral constituents such as phyllosilicates, in larger quantities along the quartz grain boundaries in large grain size quartzites will also permit the plastic flow which takes place during the ploughing of a relatively soft mineral by a relatively hard grain asperity.

The increase of the wear rates due to abrasion with the increase of the normal load L (Figure 25) is explained by the changes in the stress field between the rock specimens. The fracture initiation and propagation which occurs during abrasion (Figure 39) is enhanced, since the magnitude of the generated tensile stresses increases, while the increase of the magnitude of the rock mass, which is affected by the stress field, is statistically associated with an increase in the number of the incipient fracture nuclei. The mass removed by plastic flow, which takes place during the abrasion also increases with the normal load.

The wear by plastic flow is not favoured by the increase of the sliding speed, since slow speeds (i.e. strain rates) promote plastic deformation. On the contrary the development of local high temperatures due to the increase of the sliding speed (Jaeger, 1942, Bowden and Thomas, 1954) favours the occurence of plastic flow phenomena. The development of these local temperatures can also influence the fracture initiation and propagation during abrasion. Since high temperatures favour plastic deformation, changes at geometry of the tip of the microstructural defects present i.e. increase of the tip "bluntness", the fracture initiation of these defects will become more difficult while their propagation will occur at higher stresses and subsequently will be more rapid. A similar situation applies to the wear by plastic flow, which although favoured by high friction temperatures decreases with the higher loading rates. These counteracting conditions for wear by both brittle fracture and plastic flow finally maintain approximately constant wear rates when

the sliding speed increases within the one order of magnitude range of sliding speeds examined (Figure 26). Contrary to expectations therefore, an increase in rotation mill speed does not neccessarily lead to an increase of comminuting by wear processes.

The wear rate due to abrasion, observed in our experiments, is a function of the total process time since the area of contact of the sliding surfaces increases with the time. This results in the decrease of the load per unit area, which reduces the total mass removed per unit time by abrasion for the conditions of the experiments performed (Figure 27).

Brittle fracture and plastic flow coexist and interact in the manner outlined above during abrasion. Other industrial processes, such as cutting or drilling employ mainly fracture phenomena as indicated by the nature of the surfaces of quartzite rocks (Plates 49 and 50).

7.6. The role of the environment

The environment present between two sliding rock surfaces can influence their friction and abrasion behaviour, resulting in a possible enhancement of the comminution process. Possible influences of the environment include:

(a) Change of the heat transfer between the sliding surfaces during the development of high local temperature rises.

(b) Change in lubrication between the sliding rock surfaces.

(c) Change of the fracture surface energy.

(d) Promotion or reduction of the plastic work.

(e) Changes in the crack tip geometry by plastic flow and hence the energy required for fracture.

Each of the possible influences will be discussed separately.

(a) If the coolant properties of the various environments used in the friction, abrasion and milling test are responsible for the observed differences in the parameters of frictional force, mass loss

due to abrasion and the size distribution of the milled product, a relationship between these parameters and the environmental heat transfer properties should explain these differences. The similar values of the thermal conductivity of ethyl and n-butyl alcohol, which are 169 and 168 x 10^{-3} $Wm^{-1}K^{-1}$ at 20°C respectively will be expected to obtain similar values for the coefficient of sliding friction. On the contrary the different values of 0,55 and 0,65 were found for the coefficients of sliding friction in ethyl and n-butyl alcohols respectively (Figure 16) obtained under the same experimental conditions of load and at a given sliding speed. Large differences in the values of the thermal conductivity between water and toluene environments, which are 631 and 131 x 10^{-3} Wm^{-1} °K respectively will be expected to obtain proportionally different values for the coefficient of sliding friction. On the contrary, figure 15 shows a similarity in the relationship between v and μ in these environments. The respective values of 627, 204 and 131 x 10^{-3} Wm^{-1} °K of the thermal conductivities of water, methanol and toluene (at 20°C) also did not give an increase in milling efficiency in corresponding order (Figure 29).

(b) The regimes of lubrication developed by the environment as a function of its chemical composition, the sliding speed, the normal load and the surface roughness influence the friction and wear effects of the sliding rock in a manner which can be analysed into hydrodynamic, elastohydrodynamic and boundary lubrication (Bowden and Tabor, 1966). But the theoretical study of the role of each liquid-lubricant present, in a way similar to the one proposed by Korovchinskii (1962) for metals, requires many assumptions for the sliding materials concerned, e.g. homogeneity in composition, ideal surface finish or curvature, which can be difficult to obtain and therefore are misleading when they are applied to rocks.

The viscosity of the environments used can be employed as a simple measure of the different lubrication effects obtained in the friction, abrasion and milling tests. The difference in the values of the viscocities of toluene and ethylene glycol (0,586 and 17 cP respectively,

at atmospheric pressure and 20°C) cannot explain the similarity in frictional behaviour (Figures 15, 16). The very small differences in viscosity of the alcohols used (aqueous concentrations used are only two per cent by volume) in the abrasion tests cannot explain the large differences in the measured wear rates (Figure 23, Appendix E).

Changes in the viscosity or flow characteristics in the mill interior (i.e. change in pulp density with time) cannot be considered as a main factor affecting the milling efficiency of the system, since resulting changes in the values of the viscosity do not correspond with similar changes in the size distribution of the mill product. This can be considered by the milling results shown in figure 29, where the milling efficiencies found from tests performed in water, pure toluene and ethylene glycol (50 per cent by volume in water) environments do not correspond in the same order as their respective values of viscosity viz. 1, 0,59 and 2,5 cP.

(c) The brittle fracture phenomena which occur during the friction, abrasion and autogenous milling tests can be influenced by the environment present through a change in the chemical free energy of the new surfaces produced on account of chemical reactions at the broken bonds at the tip of incipient crack and consequent crack growth (static fatigue). Stress activated chemical reactions would be expected to employ the -OH of the alcohols. The length of the chain length influences the chemical activity in terms of the polarity of the molecule of the normal alcohol. The differences in the measured values of the coefficient of sliding friction during tests in ethyl n-butyl and n-heptyl alcohol shown in figure 16, cannot be explained on the basis of this assumption. Indeed figure 23 shows that the wear due to abrasion is not affected continuously in a monotonic manner by the alcohol chain length. The -OH of the 0,1M sodium hydroxide is expected to be more active than alcohols and hence promote fracture in a better manner than for example ethyl alcohol. Figures 15 and 16 show that the measured values of the coefficients of sliding friction are approximately equal in the environments of ethyl alcohol and 0,1M sodium hydroxide.

The above experimental results indicate that it is difficult to explain the difference in the behaviour of quartzite during friction, abrasion and autogenous milling only on the basis of changes in the fracture behaviour due to chemical attack at the crack tip or reduction of the surface energy. But this does not mean that the fracture behaviour is not affected by such phenomena, since other experimental results show that the occurence of stress activated reaction (i.e. stress corrossion phenomena) is possible. The increase of the normal load during friction can influence the reaction kinetics of a stress activated reaction of incipient surface flaws, resulting in different fracture behaviour of the sliding materials.

If the experiments, the results of which are shown in figures 18, 19 and 25, were carried in an inert environment, then the coefficient of friction will increase continuously with load. The observed maxima and minima may denote the occurence of stress activated reactions at the tips of near surface flaws. Similarly inorganic reagents such as ammonium carbonate and sodium chloride present in the aqueous milling environment were found experimentally (Figure 28) to influence the milling efficiency of the system by the possible occurence of stress activated chemical reactions.

In addition to the chemical interactions described above adsorption induced changes may also influence the fracture behaviour of rocks during the friction, abrasion and milling tests. The reduction of the effective surface energy of the rock due to the presence of adsorbed layers of the present environment, such as normal alcohols reduces the critical stress for fracture initiation, since the latter is proportional to $\gamma^{\frac{1}{2}}$ according to the Griffith criterion. But as already mentioned in the introduction (Chapter 1) the magnitude of the reduction of effective surface energy cannot adequately account for the effect of the environment on the fracture behaviour of the rocks.

(d) During sliding, plastic deformation takes place according to a "shaving" action (Bowden and Tabor, 1964) when the "slider" has higher scratch hardness that the material of the "sliding surface".

This mode of plastic deformation is of importance for sliding rock surfaces, since they contain mineral constituents with large differences in their scratch hardness. A sharp indenter also causes plastic deformation in a material, when there is large difference in their scratch hardness (Lawn and Swain, 1975, Swain 1977). The environmental effects upon the plastic flow behaviour may be explained by the adsorption induced changes in the electronic structure of the material, and for the particular case of a rock by changes in the electronic structure of each mineral of the solid. Changes in the scratch (Mohs) hardness of the mineral constituents of the rock are associated with changes in the ploughing of a relatively soft mineral by a relatively hard one. The adsorption induced changes in the electronic structure of a solid affect its indentation or scratch hardness in a manner, according to Westwood theory (1974), that this hardness reaches its maximum value when the zeta potential of solid-environment is zero. For every material, according to this theory, the selection of the right environment can obtain mechanical surface properties identical to those of the bulk of the solid. An increase in the magnitude (positive or negative) of the zeta potential of each mineral constituent environment present result in a decrease of the scratch (Mohs) hardness and indentation hardness since they are related via simple mathematical expression (Bowden and Tabor, 1964, 1966). If the relative difference between the hard and the soft minerals is increased, then wear by plastic flow will be increased. If the difference in scratch hardness is reduced the wear by plastic flow will be reduced.

(e) The changes in electronic structure, which are induced into the solid by adsorption, may markedly increase the mobility of near surface dislocations and hence under the influence of the stress field the geometry of a crack tip can be changed by plastic flow. As indicated in figure 40, a limited motion of small number of dislocations can have a dramatic effect on the geometry of the crack tip. The blunting of a crack is shown schematically. Such changes in the sharpness of the near surface flaws, results in larger critical stress

for fracture initiation. Subsequent crack propagation is also influenced by these changes, since a "blunter" crack will propagate at a higher stress and subsequently of a higher velocity than a sharp crack. The notch-brittleness of each mineral component of the rock can change in this manner, resulting in a different fracture behaviour of the rock during sliding and hence in a large change in the wear rates and comminution.

It appears that from the five possible influences discussed above, the latter three present some basis for an understanding of the influence of the environment. The following discussion attempts to interpret in detail the results of the friction, abrasion and milling tests. The effects of the environment are separately discussed for each of the experimental parameters used viz: (i) nature of the environment (ii) concentration characteristics of the environment (iii) sliding speed and (iv) normal load.

(i) The large differences in the value of frictional force in the different alcoholic environments measured as a function of sliding speed and normal load and the irregular dependence on the number of carbon atoms in the alcohol chain (N_C) may be explained by the different values of zeta-potential between each mineral constituent and environment. This follows, since the zeta-potential is a non-linear function of N_C (as for example for quartz, Westwood and Mills, 1976). The differences in the measured wear rates of the abrasion tests in environments of normal alcohols in aqueous suspension for N_C = 1, 2, 3, 4 and 8 (Figure 23) also show a non-linear dependence on the value of N_C.

The measured effects of the presence of the freshly comminuted solids in aqueous suspension (Figure 33) is also indicative of adsorption induced changes in the electronic structure of the mill charge. The new surface possesses broken chemical bonds and on account of the aqueous environment and/or the molecules of the surfactant present they are surrounded by a double adsorption layer, which is characterised by its own zeta-potential. The zeta-potential of the large rock pieces is therefore affected by the presence of these particles. The value of zeta-potential, resulting from both surfactant (or water) and freshly comminuted solids is different than the one of the

surfactant alone. The interaction between two surfactants and between a surfactant and freshly comminuted solids results in different values of zeta-potential in a manner similar to the one demonstrated by Westwood (1974) for binary solutions. For example iso-pentyl alcohol with solids and iso-pentyl alcohol with ethyl alcohol show different results in terms of milling efficiency. The size of the solids which are dispersed in the milling environment also influences the milling efficiency. For example, particles of -45 μm, present in an aqueous environment of iso-pentyl alcohol maintain better milling efficiencies than that of particles of -63 + 45 μm (Figure 34).

(ii) The influence of the aqueous concentration of ethanol upon the measured wear rates due to abrasion, which is shown in figure 24 is similar to the changes in the zeta potential with the concentration of the surfactant in that they show a maxima (Somasundaran, Healy, Fuerstenau, 1964, Somasundaran, Agar 1967) and hence the occurence of chemomechanical phenomena is indicated. The differences in the size distribution of the autogenously milled product in pure n-octyl alcohol (Figure 31) and in 10 per cent by volume n-octyl alcohol in water (Figure 32) also indicates that the milling enhancement effects are dependent on the concentration of the surfactant in a manner that the 10 per cent concentration obtains better milling efficiency than the pure reagent. This can be explained by the obtained values of zeta-potential in relation to the optimum scratch hardness and notch brittleness of the mill charge by each of the two environments. Similar are the effects of the by weight concentration of the fine solids of the same size (Figure 33).

(ii) The changes in the sliding speed influence the frictional behaviour, the wear due to abrasion and the size distribution of the autogenously milled product in a manner which may also be explained by the adsorption induced changes in the notch brittleness and the scratch hardness of the rock. The three different mechanisms of friction described in section 7.4, namely the mechanisms of roughness, brittle fracture of the tips of the asperities and of (the simultaneous) brittle fracture and plastic flow, take place at different sliding

speeds in each environment, because the material possesses different mechanical properties in each of these environments. The same may apply for the very small influence of the relative speed upon the wear due to abrasion (Figure 26) in a different manner in each of the two used environments.

Since the relative speed of the tumbling rocks in an autogenous mill changes with position in the mill, the mill type (i.e. dimensions) and rotation speed, the influence of the environment upon the efficiency of comminution is expected to change with the above variables.

(iv) The irregular and unsystematic changes of the frictional force with the normal load in each of the environments may also be due to adsorption induced changes in the electronic structure of the material. Differences in the brittle fracture and plastic flow behaviour are associated with different values of the measured frictional force (Figure 18), and the values of the parameter m of the Archard equation (and the associated frictional mechanisms). Similar are the effects of the normal load upon the enhancement of the measured wear rates in n-pentyl alcohol in comparison to those in water (Figure 25). Considering that the loads applied on the rocks in an autogenous mill cover a wide range of values for each mill, the environmental enchancement effects will also be expected to vary in an predictable manner.

7.7. Surface morphology and shape characteristics of autogenously comminuted quartzite particles

In addition to the influence of the environment on the size distribution of the milled product, which has been discussed in section 7.5., changes in the angular roundness of the autogenously milled particles with the milling environment and time, show independently the influence of the environment. These effects must originate from the influence of the environment on the notch brittleness and scratch hardness of the particles.

The sharp edges and the irregular angular shape of the particles show the importance of the transgranular cleavage fracture in autogenous comminution (section 6.3.4. and 6.3.5.). Adhering particles of colloidal dimensions show that a limited amount of plastic flow also occurs during comminution in an autogenous mill.

The similarity in the surface morphology of the autogenously comminuted particles and the detritus produced during the abrasion tests also confirms the conclusions based upon size distribution data viz: that abrasion is the main comminuting mechanism of autogenous milling. In view of the fact that it has been shown that abrasion occurs by brittle fracture and that it is the major mechanism of the autogenous milling, the design and operation of the mill should optimise conditions promoting the process.

7.8. The thermodynamics of the autogenous mill

The energy input of an autogenous mill mainly consists of the kinetic energy introduced by the driving motors. This kinetic energy input is transfered to either the mill charge or the milling device itself. The elastic strain energy, introduced into the rock by impact and contact, changes into other forms of energy, viz:

(1) New surface energy created by chipping and abrasion.

(2) Internal elastic stresses developed by local temperature differentials associated with abrasion.

(3) Plastic work during microplastic deformations. This dissipation will be influenced by the conditions of relative speed, temperature and environment in the mill interior.

(4) Changes in the rock structure produced by adsorption, phase transformations, or formation of amorphous mass.

Interaction of the above forms of energy affects their magnitude and subsequently the comminution process of the mill.

The friction between the mill charge and the internal surface of the mill ("liners") consumes a part of the energy input, producing

heat and/or wear of the rock and the "liners". Acoustic energy is another form of energy which appear in the mill, originating from the kinetic energy input. It can be seen that the forms of energy which are involved in the interior of an autogenous mill are larger in number and more complicated than that of a slow compression comminuting device such as a jaw crusher.

The output of the energy balance of an autogenous mill can be divided into two parts viz: the useful new surface energy of the comminuted product of a size distribution required by the mineral processing and, the non-useful energy. The non-useful energy output of the mill can be carried out by the rock product or via the comminution device. Comminuted particles finer than that required by the mineral processing size represent wasted energy. Wasted energy is carried by the comminuted product in the form of electrical charge (piezoelectricity, broken chemical bonds, electrons exchange), plastic deformation or structural changes (for example formation of amorphous mass). The non-useful energy is dissipated through the mill in the form of heat, sound (acoustic waves) plastic work (deformation of the "liners") and new surface area on the worn "liners".

The input, 'flow' and output of an autogenous mill is summarised in Table IX.

The useful energy output of an autogenous mill, (i.e. the new surface energy of the comminuted product with a size distribution according to the mineral processing requirements) can be estimated via the measured value of surface energy of quartz, 2 Jm^{-2} (Ball and Payne, 1976). The energy required for the comminution of one tonne of Witwatersrand quartzite of an assumed cubic shape into cubic particles of -75 μm is of the order of 60kJ. The South African gold mining industry requires an energy input (kinetic energy of the driving motors) ranging from 30 to 100 MJ per tonne of -75 μm product. Thus the energy utilization, which is obtained by the autogenous mill of industrial scale is less than 0,1 per cent of the energy input.

In order to emphasise that the major proportion of the energy output is dissipated in the form of heat energy, the following cal-

culations have been performed.

The heating of one tonne of the rock, which occupies 30 per cent of the volume of the mill interior, may result in the development of a temperature differential DT, assuming that no heat losses take place to the mill and the surroundings, is governed by the equation: $Q_{\Delta T} = m_1 c_1 \Delta T + m_2 c_2 \Delta T$ where $Q_{\Delta T}$ is the heat necessary for the development of the temperature differential ΔT, m_1 and m_2 the mass of the rock and of the water in the mill interior (equal to 1 and 0,86 tonnes respectively), and c_1 and c_2 heat capacities of the quartzitic ore and water (equal to 1 kJ kg^{-1} $^oC^{-1}$ and 4,18 kJ kg^{-1} $^oC^{-1}$ respectively). The development of a temperature differential of 10°C requires an energy of the order of 46 MJ while the development of a differential of 20°C requires 92 MJ. For T = 30°C and T = 40°C the necessary heat required is of the order of 138 and 184 MJ respectively. That means that for the assumed ideal heat insulation conditions, the development of a temperature differential of 20°C requires an amount of heat of the order of 92 per cent of the energy input or more. The heat transfer may take place via the mill output or the drum itself, and hence the actual temperature differential will be smaller than that of our calculations.

The low magnitude of the energy utilisation of the autogenous milling is indicated by the easy dissipation of the thermal energy, for a temperature differential of the order of 10°C. Similar calculations on ball milling (Lowrison, 1974) have shown that these heat losses represent the 84,4 per cent of energy input, while an amount of the order of magnitude of 10,7 per cent of the energy input represents energy dissipation in the form of gear losses and bolt friction.

Factors favouring the presence of large values of relative velocity of the constituents of the mill charge should, therefore, be avoided, since the development of local temperature differentials during abrasion, the main comminuting mechanism of the process, increases with speed.

TABLE IX

Energy Flow Characteristics of an Autogenous Mill

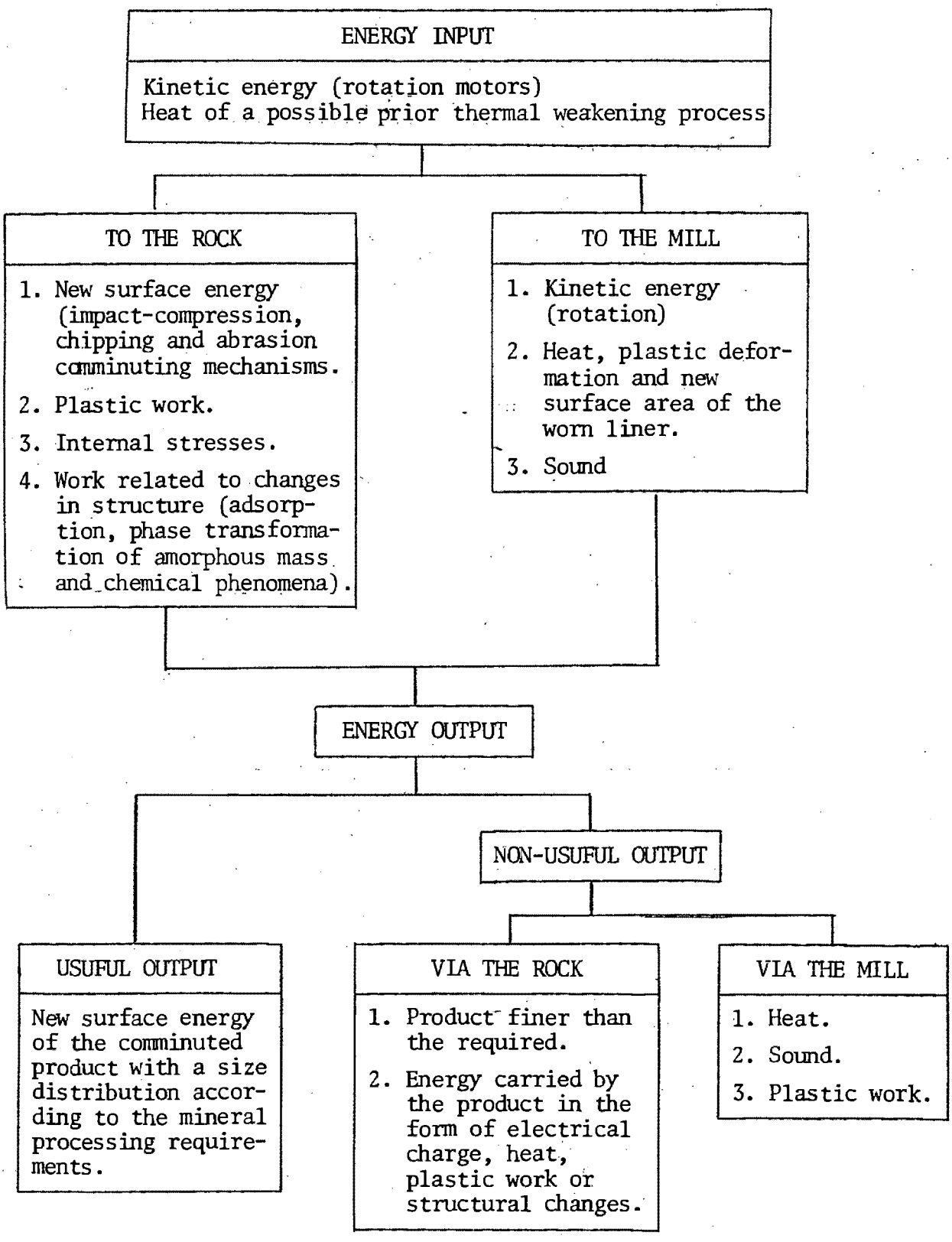

CHAPTER 8

CONCLUSIONS AND RECOMMENDATIONS

It has been established that the fracture load of the rock is a function of the rock minerology, grain size and specimen diameter.

Three mechanisms of friction have been found to take place during the sliding of two rock surfaces and their operation is a function of the applied normal load and the relative speed and the initial surface roughness.

The main comminuting mechanism of the autogenous milling has been found to be abrasion and this has been shown to consist of brittle cleavage fracture phenomena. A limited amount of plastic flow is also involved.

The nature and the concentration characteristics of the environment has been found to affect the frictional, abrasion and milling behaviour of the rock in a manner which can be explained by changes of the magnitude of the zeta-potential between each mineral constituent and the environment.

Surface heating and quenching have been found to cause microfracturing and consequently to increase the fragility of the rock.

In view of these results the following general recommendations can be made.

The suitability of a given rock for autogenous milling can be related to its mineral composition, grain size, size to strength relationship and wear rates during abrasion. These factors can be tested in a convenient fashion by the employment

of drill cores as specimens for Brazilian and abrasion tests.

For example Brazilian tests on drill cores of different diameters may allow the prediction of the optimum size distribution at which pebbles-wear media are able to survive during autogenous comminution in a given type of mill. Tests on the abrasion behaviour of a rock can be employed by testing apparatus similar to the one designed and used in the present work. Orthogonally rotated drill cores, under controlled conditions of angular velocity, normal load and torque will allow a prediction of the abrasion behaviour.

Autogenous milling can be enhanced by the use of surface active additives. The selection of the optimum environmental conditions during autogenous milling, can be performed by the abrasion testing apparatus described herein. Further tests on the nature and concentration of the additive to be used should be conducted using laboratory, pilot plant and test autogenous mills.

The energy requirements of the thermal treatments are relatively high, as for example the heating of one tonne of the Witwatersrand quartzite at 400^{o}C requires 400 MJ in comparison with the 100 MJ required for the autogenous milling of one tonne of the same ore. The application of thermal treatments may be considered only on a portion of the run-of-mine feed of a mill, when that rock offers relatively poor autogenous milling results, with energy requirements higher than 100 MJ per milled tonne. The total energy requirements of such thermal and mechanical process are expected to be reduced to the values of 300 or 200 MJ per comminuted tonne, a figure which does allow the application of this process of continuous basis. This method may be useful in terms of flexibility of the use of the existing size reduction equipment when the run-of-mine ore is occasionally consisting of relatively tough

rocks and particularly when coal, natural or hot waste gas are available at relatively low cost. The expected reduced amount of wear of the liners and of the used steel balls in semi-autogenous milling must also be considered in this case.

In view of the fact that abrasion is the main comminuting mechanism of the autogenous milling the design and operation of a mill should be aimed at creating conditions which increase the wear by abrasion. The increase of the mill diameter must not exceed certain limits since the survival of the necessary amount of pebbles-wear media may be disturbed, with negative effects upon the suitability of the process for the given ore. Considering that a large amount of the energy losses in the form of heat, any increase in the mill diameter or the mill speed cannot be recommended, particularly where the cost of the available energy is high.

The wide variety of experiments which have been carried out during this study has enabled an appreciation of the importance of the abrasion in autogenous milling, while the use of surface active additives was found to be another step towards the direction of the optimisation of the process. The results of these basic studies can now be used to advantage autogenous comminution on industrial scale, with the subsequent positive effects upon the extraction metallurgy of low-grade ores. However, the energetics of the autogenous milling also indicate the necessity for the establishment of novel comminution methods with a better energy utilisation than that of this method or of other tumbling processes. Future comminution research, should therefore be directed towards the design of systems which minimise the use of kinetic energy and its subsequent loss in the form of heat.

NOMENCLATURE LIST

a	Lattice parameter
A	Particle image area
A_c	Number of composite particles
A_L	Number of liberated particles
b	radius of a sphere
c	Specific heat
C	Crack length
CLA	Central line average characterising the specimen surface roughness, taken by the "TALYSURF" profilometer
D	Initial specimen diameter
D'	Specimen diameter at the region of an abrasion track
D_m	Maximum diameter of the particle image
D_L	Degree of liberation
E	Elastic modulus
E_s	Specific energy (energy per unit volume)
F	Frictional force
F_t	Frictional force for a given duration of contact
F_o	Frictional force for a zero duration of contact
k	Parameter of the Rosin-Rammler presentation of the size distribution of rock particles
k_1	Constant related to the properties of the sliding materials when the applied normal load changes
k_a	Surface shape factor (equal to A/D_m^2)
k_o	Outline area shape factor (equal to A/p^2)
k_{th}	Thermal conductivity
K	Mass of the adsorbed environment per mass unit of the adsorbent
l	Specimen length
L	Normal load

m	Parameter of the Archard (1957) equation
M	Molecular weight
M_p	Probability of formation of a particle of sieve size x
n	Parameter of the Rosin-Rammler presentation of the size distribution of rock particles
p	Equilibrium pressure
P	Fracture load
r	Radius of the crack tip
R	Gas constant
R_R	Reduction ratio
S_m	Specific surface of the adsorbent
t	Time
u	Constant for two sliding surfaces, when the relative velocity changes
v	Sliding speed
w	Track width
x	Particle size
y	Mass fraction undersize x
α	Mean coefficient of linear thermal expansion
β	Number of adsorbed molecules per surface area unit
γ	Surface energy per unit area or surface tension
γ_e	Effective surface energy in an environment
γ_{eff}	Effective surface energy
γ_o	Effective surface energy in vacuum

ΔT	Temperature change
η	Viscosity
λ	Constant related to the duration of contact of two sliding surfaces
λ_τ	Coefficient of relative wear (in an environment/z in water)
μ	Coefficient of friction
ν	Poisson's ratio
ρ	Density
σ_f	Stress required for fracture
σ_c	Compressive strength
σ_t	Tensile strength
τ	Mass loss (Initial weight - Weight after an abrasion test)
φ	Coefficient of linear wear $(^{D-D'}/_{D'} \times 10^2)$

REFERENCES

Ahearn J.S., Mills J.J., Westwood A.R.C.
Short-time Chemomechanical Effects in Lithium Fluoride.
Philos. Mag. 34, (1976), 391

Agricola G.
De Re Metallica (1556).
(Transl. by H.C. Hoover).
London (1912)

Arbiter N, and Harris C.C.
Particle Size Distribution/Fine Relationships in Comminution.
Br. Chem. Eng., 10, (1965), 240.

Arbiter N., Harris C.C., Stamboltzis G.A.
Single Fracture of Brittle Spheres.
Trans. Soc. Min. Eng., AIME, 244, (1969), 118.

Archard J.F.
Elastic Deformation and the Contact of Surfaces.
Nature, (London) 172, (1953), 918.

Archard J.F.
Elastic Deformation and the Laws of Friction.
Prof. R. Soc., London, Ser. A., 243, (1957), 190.

Ball, A., Payne, B.W.
The Tensile Fracture of Quartz Crystals.
J. Mater. Sci., 11, (1976), 731.

Bartha, B.
Improvement of Grinding.
Hungarian patent 155.524 (Jan. 25, 1969).

Beke, B.
Principles of Comminution.
Akademiai Kiadó, Budapest. Publishing House of the Hungarian Academy of Sciences, (1964).

Bergstrom, B.H., Crabtree, D.D., Sollenberger, C.L.
Feed Size Effects in Single Particle Crushing.
Trans. Soc. of Mining Eng., AIME, 226, (1963), 433.

Bergstrom, B.H.
Crushing of Single Brittle Particles in Fracture (Osborn, C.J. Ed.)
University of Melbourne, (1965), 329.

Bieniawski, Z.T.
Mechanism of Brittle Fracture of Rock.
Council of Scientific and Industrial Research, Pretoria, (1967).

Bieniawski, Z.T.
Mechanism of Brittle Fracture of Rock.
Int. J. Rock Mech. Min. Sci., 4, (1967), 395.

Bowden, F.P., Hanwell, A.E.
The Friction of Clean Crystal Surfaces.
Proc. R. Soc., London, Ser. A., 295, (1966), 233.

Bowden, F.P., Scott, H.G.
The Polishing, Surface Flow and Wear of Diamond and Glass.
Proc. R. Soc., Ser. A., 248, (1958), 368.

Bowden, F.P., Tabor, D.
The Friction and Lubrication of Solids. Part I.
Clarendon Press, Oxford, (1950).

Bowden, F.P., Tabor, D.
The Friction and Lubrication of Solids. Part II.
Clarendon Press, Oxford, (1964).

Bowden, F.P., Tabor, D.
Friction, Lubrication and Wear: A Survey of work during the last decade.
Brit. J. Appl. Phys., 17, (1966), 1521.

Bowden, F.P., Thomas, P.H.
The Surface Temperature of Sliding Solids.
Proc. R. Soc. London, Ser. A., 223, (1954), 29.

Bowden, F.P., Young, J.E.
Friction of Diamond, Graphite and Carbon and the Influence of Surface Films.
Proc. R. Soc., London, Ser. A., 208, (1951), 311.

Brace, W.F.,
Behaviour of Rock Salt, Limestone, and Anhydrite during Indentation.
J. Geophys. Res., 65, (1960), 1773.

British Standard.
Glossary of Terms Relating to Powders.
BS 2955, (1958).

British Standard.
Sampling and Testing of Mineral Aggregates, Sands and Fillers.
Part 1: Sampling, size, shpae and classification.
BS 812, Part 1, (1975).

British Standard.
Methods for Determination of Specific Surface of Powders.
Part 3: Calculation from the particle size distribution.
BS 4359 (1970).

Brown, J.H., Gaudin, A.M., Loeb, C.M., Jr.
Intergranular Comminution by Heating.
Trans. AIME, 199, (1958), 490.

Burton, T.G.
Chages in the State of Solids Due to Milling Processes.
Trans. Instn. Chem. Engrs., 44, (1966), 137.

Byerlee, J.D.
Theory of Friction based on Brittle Fracture.
J. Appl. Phys., 38, (1967), 2928.

Byerlee, J.D.
Frictional Characteristics of Granite under High Confining Pressure.
J. Geophys. Res., 72, (1967), 3639.

Byerlee, J.D.
Brittle-Ductile Transition in Rocks.
J. Geophys. Res., 73, (1968), 4741.

Byerlee, J.D.
Static and Kinetic Friction of Granite at High Normal Stress.
Int. J. Rock Mech. Min. Sc., 7, (1970), 577.

Byerlee, J.D., Brace, W.F.
Stick Slip, Stable Sliding, and Earthquakes - Effect of Rock Type,
Pressure, Strain Rate, and Stiffness.
J. Geophys. Res., 73, (1968), 6031.

Carneiro, F.
Une Nouvele Methode D'Essai Pour Determiner La Resistance Á La
Traction Du Beton.
Reunion Des Laboratoires D Essai De Materiaux, Paris, (1947).

Casey, M., Wilks, J.
The Friction of Diamond Sliding on Polished Cube Faces of Diamond.
J. Phys. D., 6, (1973), 1772.

Chakravarti, A., Jowett, A.
Aspects of Comminution by Heating.
Zerkleinern Dechema-Monographien, 57, (1967), 583.

Clarke, B., Kitchener, J.A.
The Influence of Pulp Viscosity on Fine Grinding in a Ball Mill.
Br. Chem. Eng. 13, (1968), 991.

Colback, P.S.B., Widd, B.L.
The Influence of Moisture Content on the Compressive Strength of Rocks.
Proc. of the Rock Mech. Symp.
University of Toronto, (1965).

Cooper, G.A., Berlie, J.
On the Influence of the Flushing Fluid during Diamond Drilling.
J. Mater. Sci., 11, (1976), 1771.

Crabtree, D.D., Kinasevich, R.S., Mular, A.L., Meloy, T.P., Fuerstenau, D.W.
Mechanisms of Size Reduction in Comminution Systems.
Part 1: Impact, Abrasion and Chipping Grinding.
Trans. Soc. Min. Eng., AIME, 229, (1964), 201.

Denning, R.M.
Directional Grinding Hardness in Diamond.
Am. Mineral, 38, (1953), 108.

Denning, R.M.
Directional Grinding Hardness in Diamond. A Further Study.
Am. Mineral., 40, (1955), 186.

Denning, R.M.
The Grinding Hardness of Diamond in a Principal Cutting Direction.
Am. Mineral., 42, (1957), 362.

Deer, W.A., Howie, R.A., Zussman, J.
Rock Forming Minerals.
Longmans, London, (1962).

Dieterich, J.H.
Time-Dependent Friction in Rocks.
J. Geophys. Res., 77, (1972), 3690.

Digre, M.
Wet Autogenous Grinding in Tumbling Mills.
AIME Annual Meeting, Denver, Colorado, Feb. 15-19, (1970).

Diodorus Siculus.
Βιβλιοθήκης Ἱστορικῆς τά Λείψανα
Aedibus B.G. Teubneri, Lipsiae, (1887).

Dogan, Z.M.
Autogenous Milling Practice in Turkey.
Fourth European Symposium on Comminution , European Federation of Chemical Engineering, Nürnberg, (1975), 297.

Doubleday, I.
Boundary Lubrication and Chemical Constitution. The Optically Active Carbinols of the Formula C_2H_5. CH (OH). C_nH_{2n+1}.
J. Chem. Soc., 121, (1922), 2875.

Elgelder, J.T.
Effect of Scratch Hardness on Frictional Wear and Stick-Slip of Westerly Granite and Cheshire Quartzite in Sterns R.G.J. (Ed.)
The Physics and Chemistry of Minerals and Rocks.
John Wiley & Sons, London - New York - Sydney - Toronto, (1976), 139.

Fahlstrom, P.H.
Autogenous Grinding.
World Mining, 15, (1962), 28.

Fahlstrom, P.H., and staff
CIM Bulletin, 67, (1974), 128.

Frangiskos, A.Z., Smith, H.G.
The Effect of Some Surface Active Reagents on the Comminution of Limestone and Quartz.
Proc. Int. Min. Dressing Cong., Stockholm, (1957), 67.

Frank, F.C., Lawn, B.R., Lang, A.R.
A Study of Strains in Abraded Diamond Surfaces.
Proc. R. Soc., Ser. A., 301, (1967), 239.

Friedman, M., Handin, J., Alani, G.
Fracture-Surface Energy of Rocks.
Int. J. Rock Mech. Min. Sci., 9, (1972), 757.

Geller, L.B., Tervo, R.O.
Grinding of Preheated Rocks.
Trans. Instn. Min. Metall. (Sect. C.), 84, (1975), 25.

Gilvarry, J.J.
Fracture of Brittle Solids I. Distribution Function for Fragment Size in Single Fracture (Theoretical).
J. Appl. Phys., 32, (1961), 391.

Graham, K.L.
Notes on Some Recent Improvements in Tube Mill Practice.
J. Chem., Metall. and Mining Soc. of S.A., 7, (1907), 317.

Gralen, N.
Friction Between Single Fibres.
Proc. R. Soc., London, Ser. A., 212, (1952), 491.

Gregg, S.J.
Surface Chemical Study of Comminuted and Compacted Solids.
Chem. Ind., (1968), 611.

Griffith, A.A.
The Phenomena of Rupture and Flow in Solids.
Phil. Trans. R. Soc., London, Ser. A., 221, (1921), 163.

Hallbauer, D.K., Wagner, H., Cook, N.G.W.
Some Observations Concerning the Microscopic and Mechanical Behaviour of Quartzite Specimens in Stiff, Triaxial Compression Tests.
Int. J. Rock Mech. Min. Sc. & Geomech. Abstr., 10, (1973), 713.

Hardie, D., Petch, N.J.
Lowering of Surface Energy by Adsorption on Alumina.
Proc. Br. Ceram. Soc, 5, (1965), 85.

Hardy, W.B., Doubleday, I.
Boundary Lubrication - The Paraffin Series.
Proc. R. Soc., London., Ser. A., 100, (1922), 550.

Hardy, W.B., Hardy, J.K.
Note on Static Friction and the Lubricating Properties of Certain Chemical Substances.
Philos. Mag., 38, (1919), 32.

Hatschek, E.
The Viscosity of Liquids.
G. Bell and Sons Ltd., London, (1928).

Hobbs, D.W.
A Study of the Behaviour of a Broken Rock under Triaxial Compression, and its Application to Mine Roadways.
Int. J. Rock Mech. Min. Sci., 3, (1966), 11.

Hockey, B.J.
Plastic Deformation of Aluminum Oxide by Indentation and Abrasion.
J. Am. Ceram. Soc., 54, (1971), 223.

Hockey, B.J.
Observations by Transmission Electron Microscopy on the Subsurface Damage Produced in Aluminium Oxide by Mechanical Polishing and Grinding.
Proc. Br. Ceram. Soc., 20, (1972), 95.

Hockings, W.A., Volin, M.E., Mular, A.L.
Effect of Suspending Fluid Viscosity on Batch Mill Grinding.
Trans. Soc. of Min. Engrs., 232, (1965), 59.

Hoek, E.
Rock Fracture under Static Stress Conditions.
University of Cape Town, 1965.

Holman, B.W.
Heat-Treatment as an Agent in Rock Breaking.
Trans. I.M.M., 36, (1926), 219.

Holmes, J.A.
A Contribution to the Study of Comminution.
Trans. Inst. Chem. Engrs., London, 35, (1957), 125.

Hoskins, E.R., Jaeger, J.C., Rosengren, K.J.
A Medium Scale Direct Friction Experiment.
Int. J. Rock Mech. & Min. Sci., 5, (1968), 143.

Jackson, O.A.E.
Autogenous and Composite Load Milling Practice in the South African Gold Mines.
VII International Mineral Processing Congress (1968), 560.

Jaeger, J.C.
Moving Sources of Heat and the Temperature at Sliding Contacts.
J. R. Soc. N.S.W., 76, (1942), 203.

Jaeger, J.C.
The Frictional Properties of Joints in Rock.
Geofis. Pura Appl., 43, (1959) 148.

Jaeger, J.C.
Friction of Rocks and Stability of Rock Slopes.
Géotechnique, 21, (1971), 97.

Jaeger, J.C. and Hoskins, E.R.
Rock Failure under the Confined Brazilian Test.
J. Geophys. Res., 71, (1966), 2651.

John, M.
Time-Dependence of Mechanical Properties and Fracture Processes of Rock Materials.
Zeitabhangighkeit der Mechanischen Eigenschapten und Brüchvorgänge von Gesteinen.
Fakultät für Bauingenieeurwesen und Architectur der Technischen Hochule, Graz, (1972).

Kanellopoulos, A.C., Ball, A.
The Fracture and Thermal Weakening of Quartzite in Relation to Comminution.
J. S.A. Inst. Min. Met. 76, (1975), 45.

Kapur, P.C., Mular, A.L., Fuerstenau, D.W.
The Role of Fluids in Comminution.
Can. J. Chem. Eng. (1965), 119.

Kidybinski, A.
Heat Resultant of Uniaxial Stress Field in Rock.
Int. J. Rock Mech. Min. Sci. & Geomech. Abstr., 10, (1973), 727.

Korovchinskii, M.V.
Certain Problems of Elastorheology as Applied to the Theory of Friction and Wear in Machinery, 17, (1962).
Translation by the American Society of Mechanical Engineers, New York, (1965), 114.

Kragelskii, I.V.
Friction and Wear.
(Transl. Ronson, L. and Lancaster, J.K.)
Butterworths, London, (1965).

Kuznetsov, Y.S. and Taube, P.R.
Strength Decrease due to Adsorption in Coarse Grinding of Brecciated Rocks.
Colloid J. USSR, 31, (1969), 59.

Lawn, B.R.
A Model for the Wear of Brittle Solids Under Fixed Abrasive Conditions.
Wear, 33, (1975), 369.

Lawn, B.R. and Komatsu, H.
The Nature of Deformation around Pressure Cracks on Diamond.
Phil. Mag., 14, (1966), 689.

Lawn, B.R. and Swain, M.V.
Microfracture Beneath Point Indentations in Brittle Solids.
J. Mater. Sci., 10, (1975), 113.

Lawn, B.R., Swain, M.V. and Phillips, K.
On the Mode of Chipping Fracture in Brittle Solids.
J. Mater. Sci., 10, (1975), 1236.

Lawn, B.R., Wilshaw, R.
Review, Indentation Fracture: Principles and Applications.
J. Mater. Sci., 10, (1975), 1049.

Lawrison, G.C.
Crushing and Grinding the Size Reduction of Solid Materials.
Butterworths, London, (1974).

Livy, (Livius Titus).
Ab Urbe Condita Libri.
Weidmannsche Buchhadlung, Berlin, (1875).

Locher, F.W., Von Seebach, H.M.
Influence of Adsorpsion on Industrial Grinding.
Ind. Eng. Chem. Proc. Des. Dev., 11, (1972), 190.

MacMillan, N.H., Huntington, R.D., Westwood, A.R.C.
Chemomechanical Control of Sliding Friction Behaviour in Non-Metals.
J. of Mater. Sci., 9, (1974), 697.

Marsh, D.M.
Plastic Flow in Glass.
Proc. R. Soc., London, Ser. A., 279, (1964), 420.

Maurer, W.C.
Shear Failure of Rock under Compression.
J. Soc. Petrol. Engrs. AIME, 5, (1965), 167.

McCammond, D., Newmann, A.W., Natarajan, N.
Strength of Glass Rod in Polar and Non-polar Liquids.
J. Am. Ceram. Soc., 58, (1975), 15.

McPherson, R.
Transient Temperatures Produced by Abrasion of Aragonite.
Wear, 23, (1973), 83.

Mills, J.J., Huntington, R.D., Westwood, A.R.C.
Environment - Sensitive Wedge Indentation Behaviour of Granites.
Int. J. Rock Mech. Min. Sc. & Geom. Abstr., 13, (1976), 289.

Moore, H.E. and Sibson, R.H.
Experimental Thermal Fragmentation in Relation to Seismic Faulting.
Dept. of Geology, Imperial College, London, (1977).

Moulson, A.J., Roberts, J.P.
Water in Silica Glass.
British Ceram. Soc., Trans., 59, (1960), 388.

Myers, W.M.
Calcining as an Aid to Grinding.
Am. Ceram. Soc., 8, (1925), 839.

Niggli, P.
Rocks and Mineral Deposits.
(Transl. by R. Parker).
W.H. Freeman and Co., San Francisco (1954).

Olsson, W.A.
Effects of Temperature, Pressure and Displacement Rate on the Frictional Characteristics of a Limestone.
Int. J. Rock Mech. Min. Sci. & Geomech. Abstr, 11, (1974), 267.

Orowan, E.
Fracture and Strength of Solids.
Rep. on Progr. in Phys., 12, (1948), 185.

Orowan, E.
Mechanism of Seismic Faulting.
Bull. Geol. Soc. Am., 69, (1958), 465.

Papadakis, M.
Contribution A L' Étude
Des Broyeurs A Boulets Industriels
Revue Des Materiaux De Construction No. 542, (1960), 295.

Payne, B.W. and Ball, A.
The Determination of Crack Velocities in Anisotropic Materials by the Analysis of Wallner Lines.
Phil. Mag., 34, (1976), 917.

Perry, J.H. (Ed.)
Chemical Engineers' Handbook.
McGraw-Hill Book Company - Kogakusha Company Ltd., Tokyo, (1963).

Pliny (Plinius Secundus).
Historia Naturalis (Natural History).
Harvard University Press, Cambridge Mass.
Heinemann Ltd., London, (1938).

Poritsky, H.
Stresses and Deflections of Cylindrical Bodies in Contact with Application to Contact of Gears and Locomotive Wheels.
J. Appl. Mechanics (Trans. Asme), 17, (1950), 191.

Preston, F.W.
The Structure of Abraded Glass Surfaces.
Trans. Octical Soc., 23, 1922, 141.

Pryor, E.J.
Discussion on the Effect of Some Surface Active Reagents on the Comminution of Limestone and Quartz.
Proc. Int. Min. Dressing Cong., (1957), 82.

Rabinowicz, E.
Friction and Wear of Materials.
John Wiley and Sons Inc., New York - London - Sydney, (1965).

Raleigh, Lord.
On the Lubricating and Other Properties of Thin Oily Films.
Philos. Mag., 35, (1918), 157.

Rehbinder, P.
New Physico-Chemical Phenomena in the Deformation and Mechanical Treatment of Solids.
Nature, 159, (1947), 866.

Rose, H.E.
On the Comminution Process in a Ball Mill.
Proc. Fourth European Symposium on Comminution, European Federation of Chemical Engineering, (1975), 253.

Rose, H.E. and Sullivan, R.M.E.
Vibration Mills and Vibration Milling.
Constable and Co., London, (1961).

Roesler, F.C.
Indentation Hardness of Glass as an Energy Scaling Law.
Proc. Phys. Soc., (London), 69B, (1956), 55.

Rumpf, H.
Grundlagen und Methoden des Granulierens.
Chemie-Ing-Techn., (1958), No. 3, 144.

Rumpf, H.
Entwicklungsgeschichte der Physik der Brucherscheinungen.
Chem.-Ing-Techn., (1959), No. 11, 697.

Rumpf, H.
Physical Aspects of Comminution and New Formulation of a Law of Comminution.
Powder Technology, 7, (1973), 145.

Schönert, K., Umhauer, H. and Klemm, W.
The Influence of Temperature and Environment on the Slow Crack Propagation in Glass.
International Conference on Fracture, 2nd, Brighton, Proceedings, April 1969 (Paper 41).

Schuhmann, R.J.R.
Energy Input and Size Distribution in Comminution.
Amer. Inst. of Min. Metal. & Petrol. Engs. Trans., 21, (1960), 22.

Schuhmann, R.
Energy Input and Size Distribution in Comminution.
Trans. AIME, 217, (1960), 22.

Schweyer, H.E.
Effect of Viscosity of Medium on Rate of Grinding in Pebble Mills
Ind. Eng. Chem., 34, (1942), 1060.

Seal, M.
The Abrasion of Diamond.
Proc. R. Soc., London, Ser. A., 248, (1958), 379.

Snow, R.H.
Size Reduction.
Ind. Eng. Chem., 62, (1970), 36.

Somasundaran, P. and Agar, G.E.
The Zero Point of Charge of Calcite.
J. Colloid Interface Sci., 24, 1967, 433.

Somasundaran, P., Healy, T.W. and Fuerstenau.
The Aggregation of Colloidal Alumina Dispersions by Adsorbed Surfactant Ions.
J. Colloid Interface Sci., 22, (1966), 599.

Sosman, R.B.
The Properties of Silica.
The Chemical Catal. Co., New York, (1927).

Spurr, R.T.
The Friction of Mineral Particles.
Brit. J. of Appl. Phys., 9, (1958), 486.

Stanley, G.G.
Mechanisms in the Autogenous Mill and their Mathematical Representation.
J. S.A. Inst. Min. Met., 75, (1974), 77.

Stanley, G.G.
Considerations in the Application of Autogenous Milling.
J. Inst. Min. Met., 76, (1975), 53.

Steijn, R.P.
On the Wear of Sapphire.
J. Appl. Phys., 32, (1961), 1951.

Swain, M.V.
Microcracking Associated with the Scratching of Brittle Solids.
Physics and Chemistry of Solids Section, Cavendish Laboratory, Cambridge, (1977).

Swain, M.V. and Lawn, B.R.
Indentation Fracture in Brittle Rocks and Glasses.
Int. J. Rock Mech. Min. Sci. & Geomech. Abstr., 13, (1976), 311.

Tabor, D.
Mechanism of Boundary Lubrication.
Proc. R. Soc., Ser. A., 212, (1952), 498.

Talbot, J.H. and Kempis, E.B.
Finely Ground Quartz: Evidence Against a 'Disturbed' Layer.
Nature, 188, (1960), 928.

Talbot, J.H. and Kempis, E.B.
Effect of Grinding on Quartz Particles.
Nature, 197, (1963), 66.

Thirumalai, K., Cheung, J.T.
Combined Thermal Energy Processes for Hard Rock Fragmentation.
Proc. 3rd Cong. Internat. Soc. for Rock Mech., Denver, Colo. Sept. 1-7, 1974.
National Academy of Sciences, Washington D.C., II, (1974), 1460.

Thirumalai, K., Demou, S.G.
Effect of Reduced Pressure on Thermal-Expansion Behaviour of Rocks and its Significance to Thermal Fragmentation.
J. Appl., Phys., 41, (1970), 5147.

Timoshenko, S.
Theory of Elasticity.
McGraw Hill, London and New York, (1934).

Veldkamp, J.D.B. and Klein Wassink, R.J.
Grindability of Brittle Materials: A Theoretical and Experimental Investigation.
Philips Res. Repts., 31, (1976), 153.

Westwood, A.R.C.
The Rebinder Effect and the Adsorption of Dislocations in Lithium Fluoride.
Philos. Mag., 7, (1962), 633.

Westwood, A.R.C.
Tewksburgy Lecture: Control and Application of Environment - Sensitive Fracture Processes.
J. Mater. Sc., 9, (1974), 1871.

Westwood, A.R.C., Goldheim, D.L.
Mechanism for Environmental Control of Drilling in MgO and CaF_2 Monocrystals.
J. Am. Ceram. Soc., 53, (1970), 142.

Westwood, A.R.C., Mills, J.J.
Application of Chemomechanical Effects to Fracture Dependent Industrial Processes.
Proc. NATO-ASI, Surface Effects in Crystal Plasticity, Leiden-Holland, (1976).

Whitehead, J.R.
Surface Deformation and Friction of Metals at Light Loads.
Proc. Roy. Soc., Ser. A, 201, (1950), 109.

Weiderhorn, S.M.
Influence of Water Vapor on Crack Propagation in Soda-Lime Glass.
J. Am. Ceram. Soc., 50, (1967), 407.

Wiederhorn, S.M. and Roberts, D.E.
Influence of Normal Alcohols on the Abrasive Wear of Glass.
Wear, 32, (1975), 51.

Wilks, E.M. and Wilks J.
The Resistance of Diamond to Abrasion.
Philos. Mag., 38, (1959), 158.

Wilks, E.M. and Wilks, J.
The Resistance of Diamond to Abrasion.
J. Phys. D: Appl. Phys., 5, (1972), 1902.

Wilks, J.
Experiments on Polishing of Diamond.
Nature, 243, (1973), 15.

Wright, P.J.F.
Comments on an Indirect Tensile Test on Concrete Cylinders.
Mag. of Concrete Res., (1955), 87.

Yates, A.
Effect of Heating, and Heating and Quenching Cornish Tin Ores Before Crushing.
Trans. I.M.M., 28, (1918), 41.

Yousef, A.A., Arafa, M.A. and Boulos, T.R.
Influence of Manganese Dioxide Slimes on Quartz Flotation.
Trans. I.M.M., C80, (1971), 223.

Yücesoy, A. and Yarar, B.
Zeta-Potential Measurements in the Galena-Xanthate Oxygen Flotation System.
Trans I.M.M., C83, (1974), 96.

A C K N O W L E D G E M E N T S

It is a great pleasure to express my appreciation to those who have been helpful during the course of this work.

I am greatly indepted to Professor A. Ball for his invaluable assistance, his interest and encouragement, as well as the many stimulating discussions, during my research.

Thanks are also extended to the National Institute for Metallurgy and to the Chamber of Mines for providing the financial support, without which this investigation would not have been possible.

The University of Cape Town is acknowledged for the facilities provided and the Electron Microscopy Unit at U.C.T. for experimental assistance.

Many thanks are also due to Miss T.R. Barrow, Miss E. Lewis and Mr. B. Greeves for their help in the final stages of this thesis.

- - - - - - -

APPENDICES

APPENDIX A

THE ROSIN-RAMMLER PRESENTATION OF THE DISTRIBUTION OF THE COMMINUTED QUARTZITE PRODUCT

The equation $y = 1-\exp(-(x/k)^n)$ or $Y=100(1-e^{-(x/k)^n})$ describes the Rosin-Rammler presentation of the size distribution for a comminuted product, where y and Y are the fraction and the precentage of the mass undersize x and n and k constants. The above equation may be rearranged in the following manner:

$$1-y = e^{-(x/k)^n} \quad \text{or} \quad 1/(1-y) = e^{(x/k)^n} \quad (\text{for } y<1) \text{ or}$$

$$\log_e(1/(1-y)) = (x/k)^n \quad \text{and for } 0<y<1$$

$$\log_e \log_e (1-(1-y)) = n(\log_e x - \log_e k).$$

Special Rosin-Rammler graph paper with log particle size as abscissa and with 100 (log log reciprocal), from 0,1 to 99,9 as ordinate, was used for the presentation of the size distribution of the comminuted produced by compression or antogenous milling. The parameter n of this presentation is the geometrical slope of the interpolated curve of the product size distribution points. The parameter k has the dimensions of length, with a value which can be determined by the interpolated curve on the Rosin-Rammler chart for $y=0,632$ (or $y= 1-e^{-1}$).

APPENDIX B

DIODORUS SICULUS (1st Century B.C.)
BIBLOTHECA HISTORICA
BOOK III, Chapter 12
Trans. from ancient greek

.....The very hard rocks, which contain gold, are crushed by means of a strong fire, according to the following procedure. The rock is heated and then impacted by iron bars, like the ones which are used in quarries[1]. Thousands of miners[2] break the hot rock, without any great effort, under the guidance of a technician. The rocks are extracted from the ore deposit by iron hamers, which are manipulated by the strongest of the miners. This extraction takes place in the form of galleries, which are mined not in a straight line, but according to the direction of the gold ore deposit. The rocks which are extracted in these galleries, are carried with great efforts to the section, where the (secondary) comminution takes place. The product of the thermal comminution, which is of small size, is carried to the surface by young boys, because of the small size of most of the mine galleries[3]. A further comminution of these rocks is performed by fall[4] and iron bars impact. A process of milling follows, which is very similar to the baking powder preparation. The size of the final product is very small[5].

1. Unfortunately, Diodorus does not describe these quarry iron bars elsewhere.

2. Diodorus extrapolates the number of the mine workers to lots of "ten thousands". He specifies that they are poor, but not slaves.

3. The rock transportation difficulties arise, according to Diodorus, mainly because of the limited space and sharp angles of the galleries. He also mentions that lamps were used, without specifying their type or way of handling them.

4. Diodorus describes this process as easy, because it is performed by men "older than thirty years" - old miners by the ancient measures.

5. Diodorus, then interrupts the description of the comminuting process, expressing his sorrow about the conditions in which the miners are working.

APPENDIX C

SURFACE TEMPERATURE DEVELOPED DURING SLIDING

The mean temperature , difference with respect to ambient, developed between two sliding surfaces, at a range of sliding speeds between $4{,}23 \times 10^{-7}$ and $4{,}23 \times 10^{-3}$ ms^{-1}, is given by the equation (Jaeger, 1942, Bowden and Thomas (1954):

$$\Delta\theta = 0{,}II8\ \mu\ L\ v\ /l\ k_{th}$$

where it is assumed that the contact area is small in comparison with the mass of the rock and is the coefficient of sliding friction, L the applied normal load, v the sliding speed, 21 is the length of the side of an assumed square area of contact between the rock specimens and k_{th} is the thermal conductivity of the material.

The values of the parameters used in the above equation are:

μ: from 0,45 to 0,94

L: from 5 to 70 N

v: from $8{,}46 \times 10^{-7}$ to $4{,}23 \times 10^{-3}$ ms^{-1}

21: from 100 to 500 m

k: from 0,72 to 12 W m deg^{-1} *

The values of $\Delta\theta$ are:

$6{,}24 \times 10^{-4}$deg $^{o}C < \Delta\theta < 18{,}17$ deg ^{o}C

*The thermal conductivity of the mineral constituents of quartzite and some rocks is given as (in W m^{-1} deg $^{-1}$):

mica (muscovite) for 100°C 0,72 Quartz: ∥ c axis for 0°C: 12

for 300°C 0,65 ⊥ c axis 6,8

for 600°C 0,69

Rocks: (at 20°C) granite 2,2; sandstone 1,3; shale ⊥ axis; shale ∥ axis 2,5).

APPENDIX D

PRESSURE APPLIED AT THE CONTACT AREA OF TWO ROCK SPECIMENS DURING THE FRICTION EXPERIMENTS

The values of the contact area A can be estimated from the friction grooves shown in the scanning electron micrographs. The width of the friction grooves, which are dependent on the sliding speed and the normal loads applied, varies from 100 to 500 μm. Assuming that the contact area A between the two rock specimen falls in a circle, of diameter D_g the estimated width of the grooves, the contact area $A = \pi D_g^2/4$ would be:

$$25 \times 10^{-10}\ m^2 < A < 625 \times 10^{-10}\ m^2$$

For normal loads from 5 to 65 N, the applied pressure $p = L/A$ would be: $80\ MPa < p < 2{,}6 \times 10^4\ MPa$

APPENDIX E

PHYSICAL PROPERTIES OF THE USED ENVIRONMENTS

The values of the viscosity, thermal conductivity and specific heat of some of the environments used are shown in table E.

The values of the compressibility of the same reagents at the stated temperatures and pressures are also shown in table E together with data related to their solubility in water (Perry, 1963). The dependence of the viscosity of ethyl alcohol on its aqueous concentration at temperatures from 0^{o} to 40^{o} is shown in figure (E1), while the dependence of the viscosity of ethylene glycol on its aqueous concentration at $20^{o}C$ is shown in figure (E2). (Hatschek, 1928).

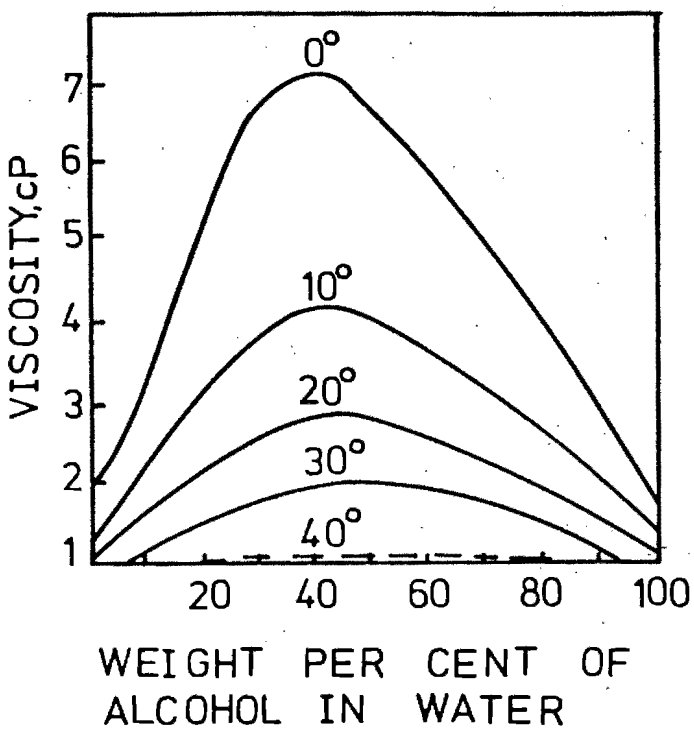

FIGURE E1

Influence of the temperature upon the viscosity of aqueous environments of ethyl alcohol of various concentrations.

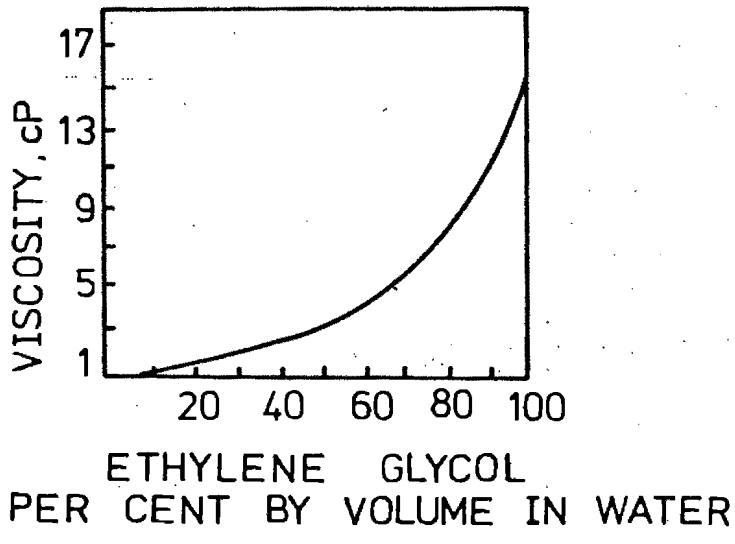

FIGURE E2

Influence of the concentration of ethylene glycol in water upon the viscosity of the system.

TABLE E

REAGENT	VISCOSITY cP at 20° and 1 atm	THERMAL CONDUCTIVITY mW.m^{-1} K^{-1} at 20°C	SPECIFIC HEAT Jkg^{-1} C^{-1}		SOLUBILITY*** IN 100 PARTS OF WATER		COMPRESSIBILITY*** Per Pa x10^6			DENSITY kg m^{-3}	MOLECULAR WEIGHT
					COLD	HOT	Temp. °C	Pressure Pa			
			Temp. °C								
METHANOL	0,571*	204***	5-10	462	SOLUBLE		15	230	10,3	792	32
ETHANOL	1,192*	168***	0-98	2842	SOLUBLE		14	230	10,0	790	46
PROPANOL	2,255*	172***			SOLUBLE		20	2000	7,7	800	60
ISO-PROPANOL	2,369*	158***	0-19	2353	SOLUBLE		-	-	-	-	60
BUTANOL	2,947*	169***	21-115	2872	9	SOLUBLE	-	-	-	810	74
PENTANOL	5,091*		22-125	2971	2,7	SOLUBLE	20	5000	6,1	820	88
HEPTANOL	-	-	-	-	0,18	SOLUBLE	-	-		874	116
OCTANOL	-	-	-	-	0,054	SOLUBLE	-	-		827	130
ETHYLENE GLYCOL	17,0*	243***	0-20	2395							
TOLUENE	0,586*	136***			0,05	SOLUBLE	20	2000	7,4	860	92
ACETONE	0,50*	162***	12-99	1839	SOLUBLE	SOLUBLE	14	230	11,1	792	58
WATER	1,0*	597**	3-22	2148			20 20 20	130 2000 5000	4,9 4,3 3,9	1000	18

*HATSCHEK, 1928 ***PERRY (Ed), 1963

APPENDIX F

DESIGN OF THE CONTROL SYSTEM OF THE MOTORS USED FOR THE ROTATION OF THE ROCK SPECIMENS IN THE ABRASION TESTING APPARATUS

In view of the constant conditions of angular velocity and torque required for the abrasion testing procedure, the motors used had to maintain a constant torque for a given range of rotation speeds. Since sufficiently constant speeds are maintained only by DC motors, two 0,72 W DC-motors (Plate 38) were selected. The change of speed for a DC-motor takes place by the application of a variable DC-voltage, but the voltage control itself cannot maintain constant torque for different speeds. This problem was solved by the sychronous control of the voltage and current input of the motors used, by a Thyristor (Plastelect (Pty) Ltd., Johannesburg) bridge card (figure F1). This system of control, had a single phase 220V AC input and maintained adjustable current and voltage in a wide range for torque and RPM output of a given DC-motor. The schematic of the controls system layout for a 0,7 W DC motor, is shown in figure (F2).

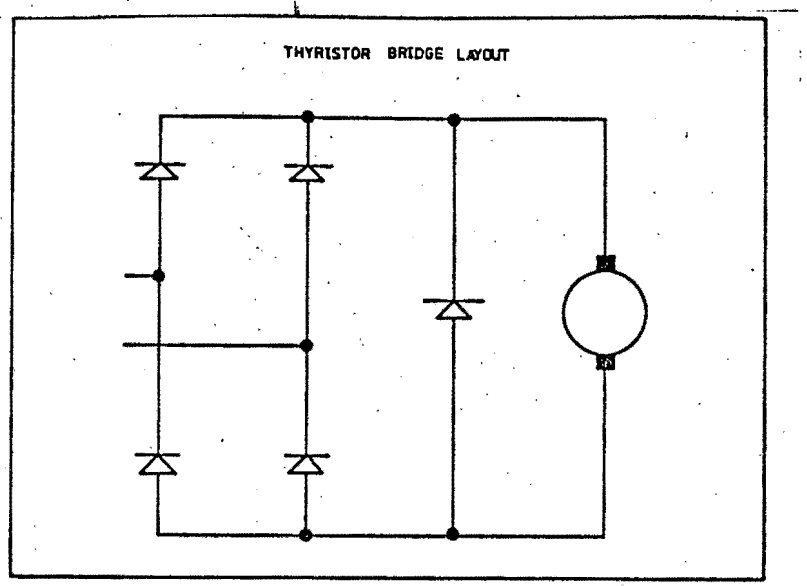

INPUT		OUTPUT	
VOLTS	220	ARMATURE VOLTAGE	200
MAX CURRENT	7·5	ARMATURE CURRENT	5
PHASE	1	KW	0·7
		FIELD VOLTS	190
		FIELD AMPS	0·7

FIGURE F1

Layout of the Thyristor bridge used for the control of the rotation motors of the abrasion testing apparatus.

FIGURE F2

Layout of the circuit of the control system used for the rotation motors of the abrasion testing apparatus.

APPENDIX G

DESIGN ASPECTS OF THE CLAMPING DEVICE FOR THE ROCK SPECIMENS, THE POWER TRANSMISSION JOINTS AND THE IDLER ROLLERS OF THE ABRASION TESTING APPARATUS

The testing on the abrasion behaviour of the drill core specimens required an efficient way of holding the cylindrical rock pieces in a manner which would not cause damage on the rock surfaces and allow multiple use of the same pair of specimens. The clamping device used consisted of the three items A, B, and C, (Plate 37 a, b, c and figure G1). The rock was successfully gripped and the setting up procedure did not present particular problems. Rotation at a range of selected constant speeds and torque was required while a relative vertical change of position of the two rock specimens (or a change of the vertical position of the specimens in relation to the rotation axes of the motors), was necessary. A pair of universal joints was selected in order to meet these requirements, connected with intermediate shaft (200 mm long, 25,4 mm diameter) maintaining a working angle larger than the one required by speeds 25 to 1000 RPM (5^{o}) and torque 46 to 922 Nm for the type of the used specimens (Plates 37a and 38).

The idler rollers, required for the application of the normal load from the testing machine to the rotating rock specimens, consisting of the housing frame, the rotation shaft with bearings and the coated rollers, (Figure G2) were attached directly to loading platten of the testing machine.

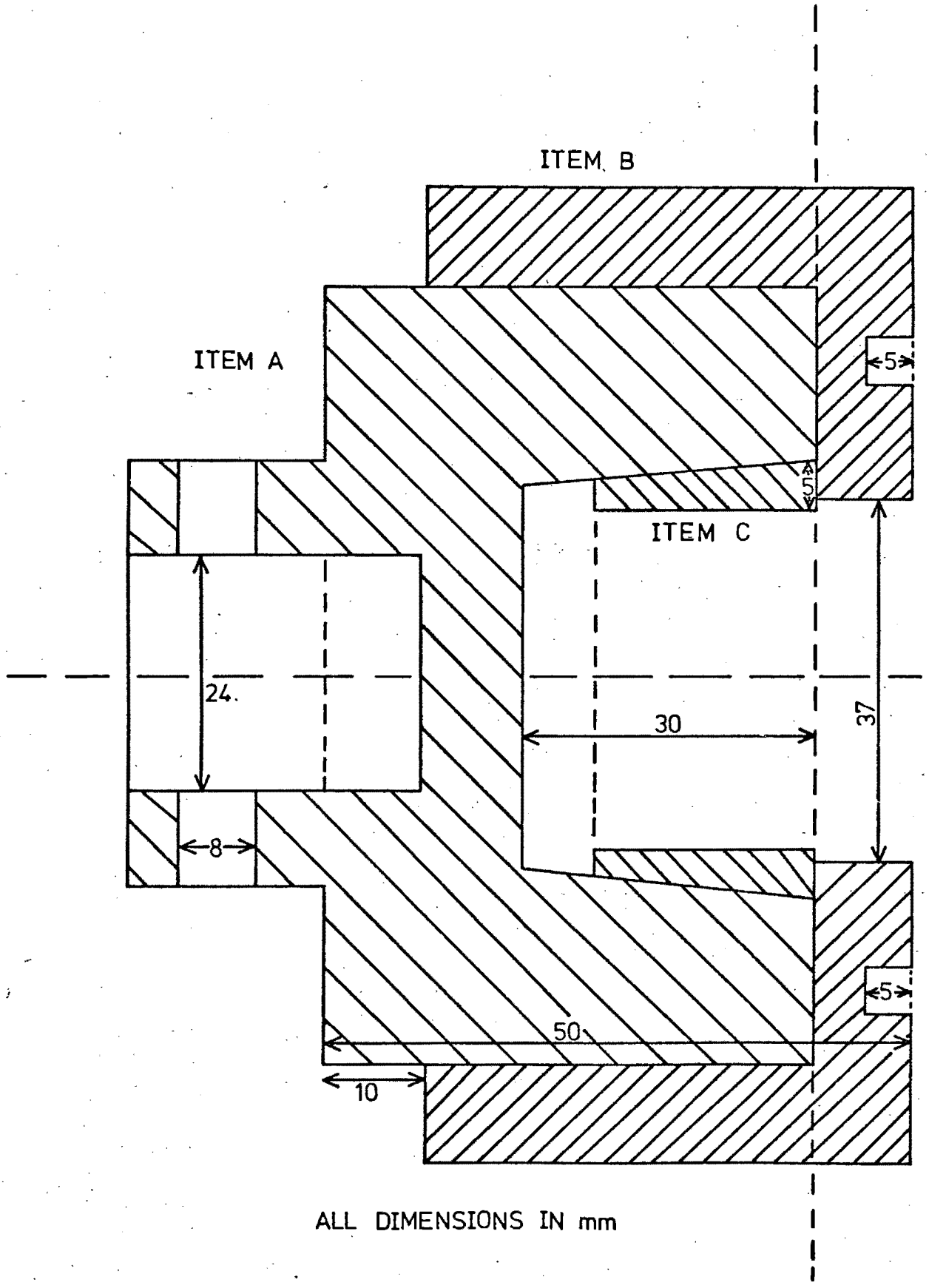

FIGURE G1

The clamping device used for the rotation of the abrasion testing drill core specimens, consisting of three items, viz. A, B and C.

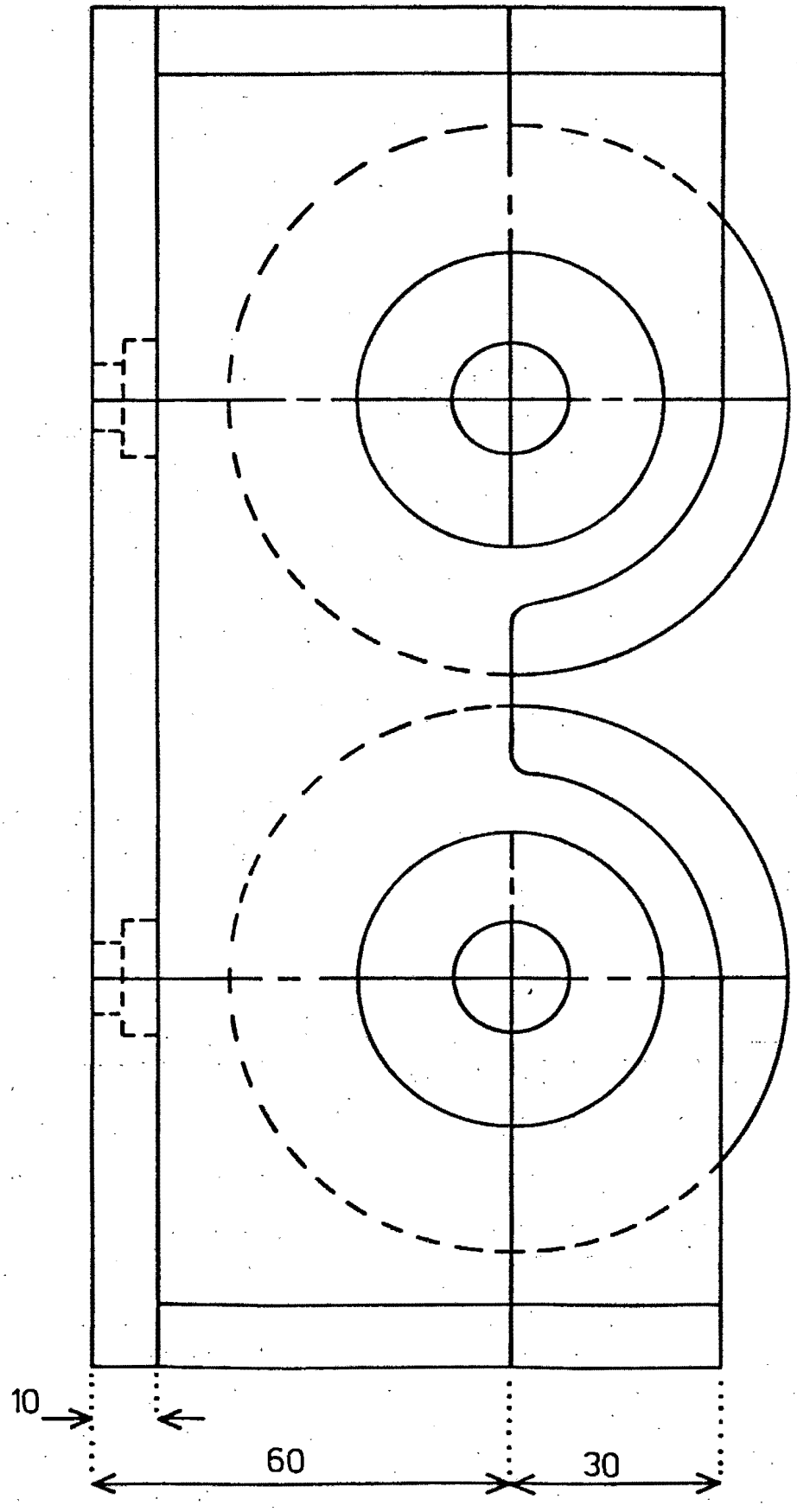

FIGURE G2

The idler rollers used for the application of the normal load on the rotating abrasion testing specimens. The rollers consist of fare parts.

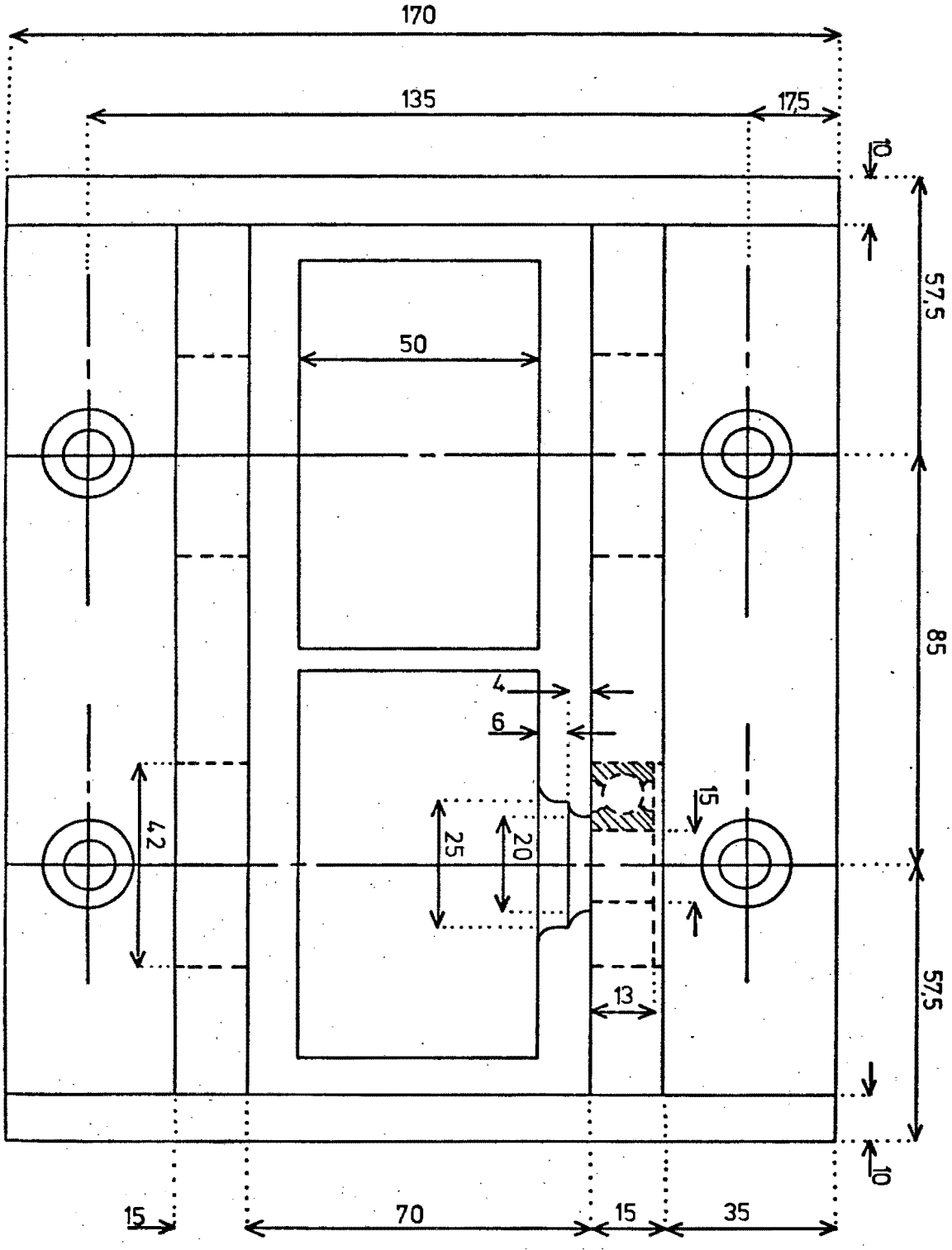

FIGURE G2a

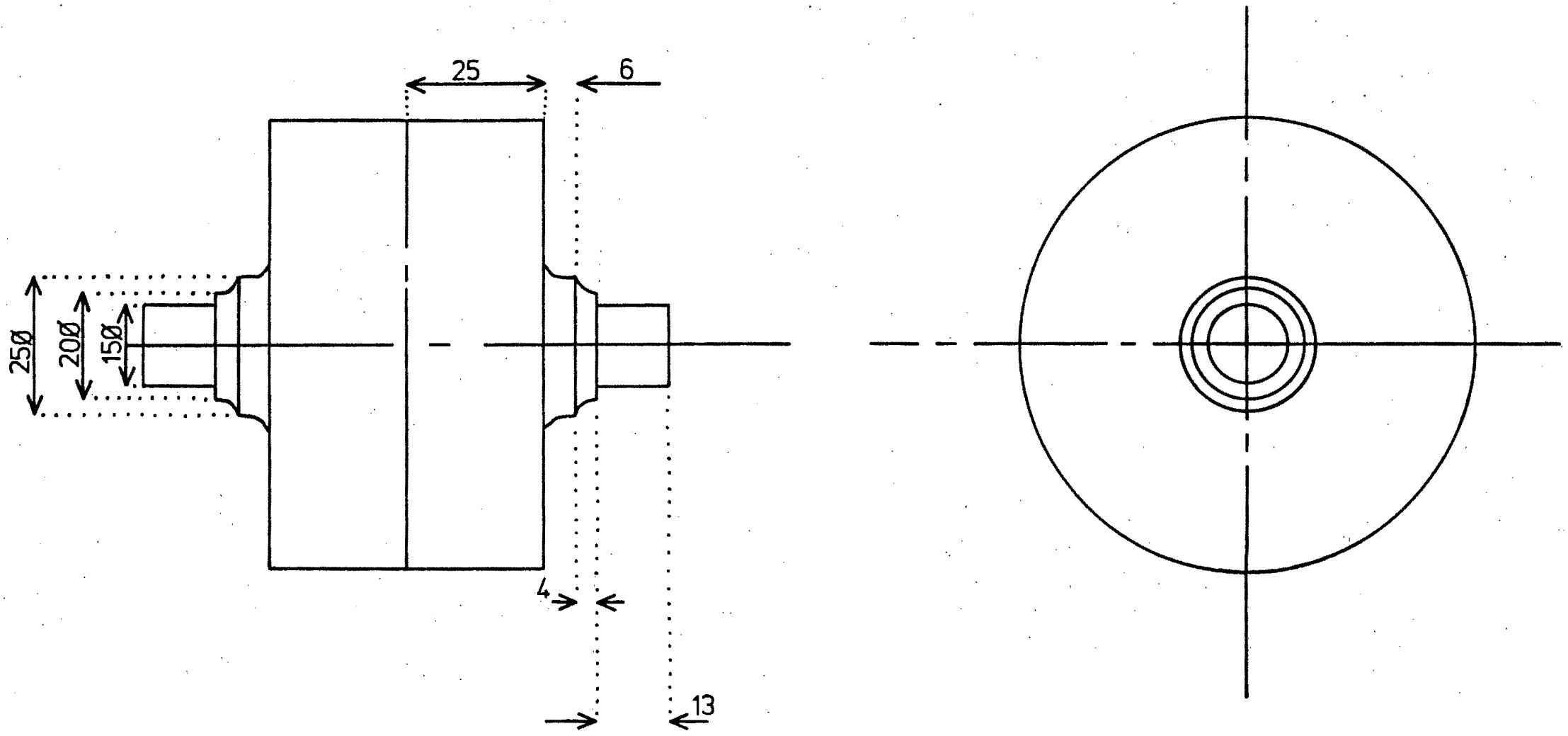

PART NO.3

FIGURE G2b

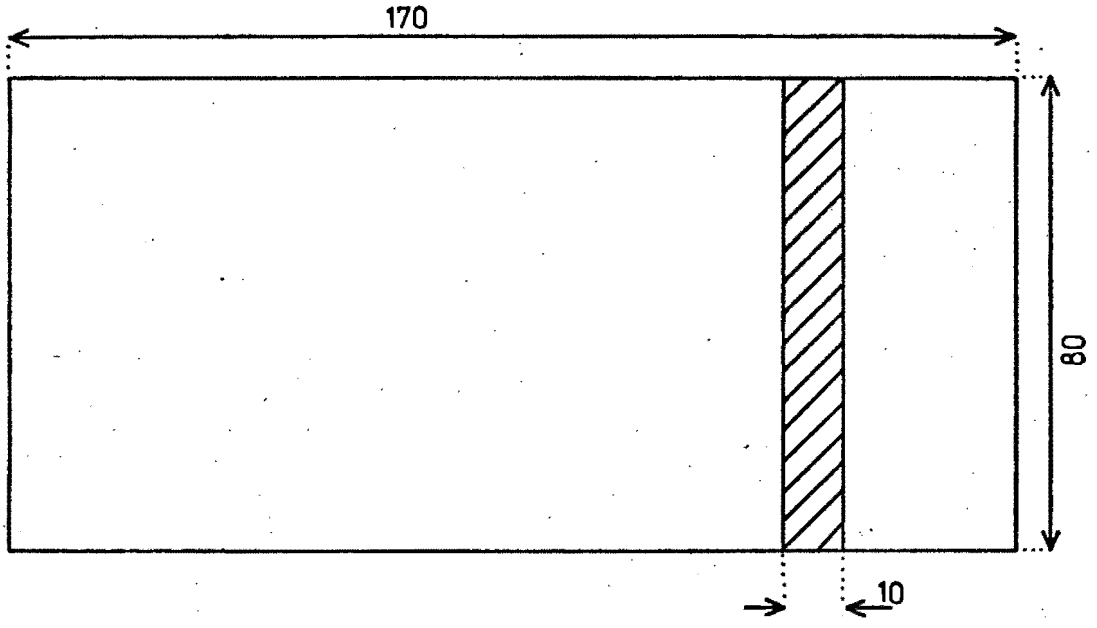

PART NO.2

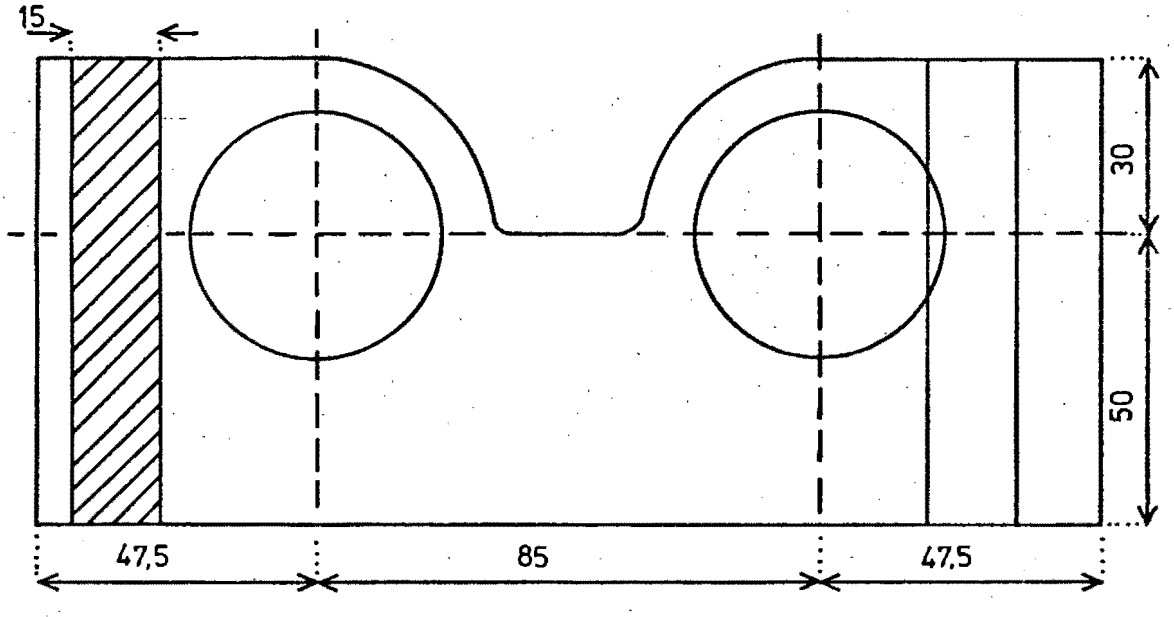

PART NO.4

FIGURE G2c

APPENDIX H

SEM IMAGE ANALYSIS OF COMMINUTED QUARTZITE PARTICLES FROM AUTOGENOUS MILLS

The values of the shape factors of each of the particles of the examined groups of particles, which are described in section 6.3.2 and summarized in table VIII, are listed in the tables H-I to H-VII.

TABLE H-I

Surface and outline area shape factors of particles taken from the run-of-mine feed of a fully autogenous test mill.

	ka	ko
	0,3784	0,0679
	0,4311	0,0649
	0,4461	0,0552
	0,3411	0,0566
	0,4011	0,0623
	0,4307	0,0609
	0,3881	0,0669
	0,3594	0,0539
	0,3994	0,0613
	0,4007	0,0604
ARITHMETIC MEAN VALUE	0,3976	0,0610

TABLE H-II

Surface and outline area shape factors of particles taken from the interior of a fully autogenous test mill.

	ka	ko
	0,4980	0,0719
	0,4497	0,0690
	0,4269	0,0525
	0,5698	0,0701
	0,3213	0,0538
	0,3401	0,0629
	0,3628	0,0673
	0,1722	0,0427
	0,4767	0,0676
	0,3662	0,0598
	0,4294	0,0647
	0,4760	0,0694
	0,4394	0,0687
	0,3711	0,0593
	0,4618	0,0631
	0,4077	0,0611
	0,4773	0,0701
	0,4336	0,0681
	0,4001	0,0607
	0,4337	0,0621
ARITHMETIC MEAN VALUE	0,4138	0,0630

TABLE H-III

Surface and outline area shape factors of particles taken from the output of a fully autogenous test mill.

	ka	ko
	0,5421	0,0970
	0,7403	0,0670
	0,4847	0,0735
	0,4371	0,0691
	0,5217	0,0883
	0,5001	0,0699
	0,4949	0,0711
	0,4227	0,0631
	0,3918	0,0611
	0,3711	0,0577
ARITHMETIC MEAN VALUE	0,4880	0,0717

TABLE H-IV

Surface and outline area shape factors of particles taken from the product of laboratory autogenous mill after an 120 minutes milling period.

	ka	ko
	0,2979	0,0476
	0,3507	0,0621
	0,3409	0,0519
	0,0935	0,0140
	0,4677	0,0669
	0,4733	0,0614
	0,3471	0,0521
	0,5611	0,0741
	0,4811	0,0781
	0,3711	0,0567
ARITHMETIC MEAN VALUE	0,3775	0,0567

TABLE H-V

Surface and outline area shape factors of particles taken from the product of laboratory autogenous mill after a 240 minutes total milling time.

	ka	ko
	0,4994	0,0637
	0,4001	0,0603
	0,3570	0,0584
	0,3632	0,0603
	0,4443	0,0689
	0,4316	0,0611
	0,4101	0,0607
	0,2701	0,0503
	0,4127	0,0633
	0,4015	0,0612
ARITHMETIC MEAN VALUE	0,3990	0,0608

TABLE H-VI

Surface and outline area shape factors of particles taken from the product of a laboratory autogenous mill after a 360 minutes total milling time.

	ka	ko
	0,4331	0,0617
	0,4589	0,0671
	0,5489	0,0719
	0,4387	0,0654
	0,3711	0,0593
	0,4214	0,0614
	0,4948	0,0693
	0,3991	0,0611
	0,4177	0,0641
	0,4913	0,0701
ARITHMETIC MEAN VALUE	0,4470	0,0648

TABLE H-VII

Surface and outline area shape factors of particles taken from the product of a laboratory autogenous mill in n-butyl alcohol environment after an 120 minutes milling period.

	ka	ko
	0,419	0,0627
	0,499	0,0694
	0,373	0,0601
	0,543	0,0737
	0,459	0,0666
	0,453	0,0651
	0,421	0,0600
	0,477	0,0701
	0,500	0,0709
	0,407	0,0613
ARITHMETIC MEAN VALUE	0,455	0,0659

APPENDIX I

PUBLISHED WORK

The fracture and thermal weakening of quartzite in relation to comminution

by A. KANELLOPOULOS* and A. BALL*

INTRODUCTION

Present methods of rock breakage are inefficient since approximately 10^8J (30 kW. hr) of energy are used to convert 1 tonne of rock into 100 μm particles whereas a measured value of surface energy of 2Jm^{-2} indicates that 4×10^4J should be sufficient[1]. The difference must be wasted as kinetic, thermal and acoustic energy in addition to the plastic deformation and wear of the cutting, crushing and milling machinery.

Since the excavation and comminution of rock for the purpose of mineral extraction is a process of tfacture it would seem reasonable or apply physical theories in order to investigate the optimum conditions. In this way it could be hoped that the present inefficient techniques could be improved or discarded in favour of better systems. Although two authors, Rumpf[2] and Schoenert[3] have given attention to this type of approach, it would seem an appropriate time to consider the particular case of quartzite since several papers have recently appeared in the literature which examine in detail the fracture and deformation of quartz[4, 5, 6].

The first section of this paper therefore examines the physics of fracture with reference to quartz. Thermal treatments are then considered as methods of introducing sharp cracks and the potentials of the technique are estimated from the results of some laboratory experiments.

ENERGY BALANCE DURING FRACTURE

Any description of the fracture process must obey the principle of conservation of energy. Griffith[7] balanced the input of strain energy with the production of new surface. It has been realised that energy may be dissipated in several other forms in addition to surface energy. The fragments produced will possess kinetic energy and cause acoustic vibrations. The conditions of stress at the crack tip may promote plastic strain by dislocation motion and the severe lattice distortion may cause heat dissipation. Certain materials may also radiate energy as a result of electron excitation at the crack tip. From the point of view of comminution these additional forms of energy represent an inefficiency. Ideally, all the energy produced by external forces should be converted into surface energy only.

At any instant during fracture under condition of constant stress, σ_f, thermodynamics requires that the total energy of the system remains constant. Thus

$$U-(El+S+D)=\text{const}$$

where U is the work done by external forces, El is the elastic energy produced, S is the surface energy produced and D is the energy dissipated in other forms. During crack growth

$$d(El-U)/dc+dS/dc+dD/dc=0$$

The expression $-\sigma_f^2C^2/E^*$ has been derived by Inglis[8] for the net energy potential of the specimen stressed in uniaxial tension i.e. $(El-U)$, and $S=4\gamma c$ where γ is the surface energy per unit area and $2c$ is the crack length. Thus

$$dD/dc=2\sigma_f^2c/E-4\gamma$$

Initially, before the crack grows, D will be zero at $c=c_o$ and propagation will only commence, according to the Griffith formulation, when the rate at which available potential energy increases in the specimen can equal the rate at which surface energy is required. It is important to note that although the rate of increase of potential energy increases linearly with the crack length, the surface energy is produced at a constant rate. Thus an increasing amount of energy becomes available for kinetic, plastic, thermal and other dissipative processes during fracture propagation. From this type of reasoning it would seem that no improvement in efficiency is possible since a given amount of elastic strain energy is required for the initial propagation of the crack. However, the situation is never ideal in terms of the Griffith energy criterion for the following reasons. Although the length of the nucleating notch or flaw may satisfy the formulation at the given applied stress, the tensile stress at the crack tip may be insufficient to break the atom bonds and effect propagation. The 'sharpness' of the crack tip determines the concentrated stress at the crack tip ($\simeq2\sigma(c_o/p)^{\frac{1}{2}}$ where σ is the applied stress and p is the crack tip radius) and, unless the radius approaches atomic dimensions, the external stress will be in excess of the stress indicated by the Griffith criterion. In general therefore an overstress is required for fracture unless special techniques are used to produce sharp crack nuclei. This overstress results in the rapid acceleration of the crack to high velocities and large dissipation of strain energy as kinetic energy. Thus the generation of a high denisty of *sharp* cracks in the rock by some treatment would reduce the general stress level required for comminution and so increase the efficiency of the grinding process.

Since brittle fracture propagates in response to the local tensile stress at the tip of a pre-existing notch or crack, the configuration of the externally applied stress will determine the magnitude of the applied stress required to produce the critical stress at the pre-existing notch or flaw. Pure uniaxial tension is a very efficient configuration while a uniaxial compressive is only 1/8

*Department of Metallurgy and Materials Science, University of Cape Town.

as effective according to the predictions of Griffith. Experimental work on single crystals of quartz suggests that the ratio is 1/20 while the strength in bending is only slightly greater than that for uniaxial tension. It is obviously important to choose a comminution process which is efficient in producing tensile stresses within the particles. Pure tension is impossible for particle breakage but bending forces could be achieved with careful design of the plattens of a crushing machine or the rolls of a mill.

Any comminution process which involves stressing by impact loading is likely to be inefficient in terms of energy utilisation. A stress applied by impact will, in general, be far in excess of that which is required to propagate fracture from an existing flaw. The excess energy will be dissipated as kinetic energy. This will result in mechanical wear and a temperature increase of the machinery. In a process such as milling, there may be secondary impacts but a large proportion of these will be against the containing walls. The occurrence of plastic deformation in the rock at the crack tip would also represent a proportion of wasted energy but, more important, is the blunting action which would result. If the applied stress generated a local shear stress that was in excess of the critical resolved shear stress for plastic flow of the particular material under the given testing conditions, then the crack would plastically blunt. The reduced tensile stress concentrating effect of the blunt crack then results in a higher fracture stress. Thus conditions favourable to plastic flow in the quartzite must be avoided in comminution processes. Fortunately this does not present any practical difficulty in the case of quartzite, since it has been shown[4] that dislocation motion is not appreciable below temperatures of about 600°C. The presence of water is known to influence the stress required for the fracture of silicate materials. Experimental evidence indicates that the water molecule is capable of hydrolysing the Si—O bond. The reaction will be activated by the concentrated stress at a notch in a stressed body. In this way the presence of water molecules will aid the sharpening process and lower the external stress required for fracture of comminution.

In view of these discussions the ideal comminution system would comprise a slow crushing process on finely serrated plattens or between grooved rolls. This could generate 3-point bending in the particles and ensure minimum dissipation as the kinetic and thermal energies. The breakage should be performed in wet conditions. This configuration would lead to compaction or 'bedding' of the particles and loss in crushing efficiency with time. The problem may be eliminated by vacuum withdrawal of the fine particles through numerous small holes in the lower platten and a vibratory or rotary motion of the upper platten. High frequency or ultrasonic vibrations could aid breakage in addition to dispersing the fines.

A CONSIDERATION OF THERMAL FISSURING

The importance of introducing high densities of sharp cracks or fissures into quartzite which would subsequently act as crack nuclei during crushing and comminution has been discussed in the previous section. This fissuring could be achieved by thermal techniques on account of

(i) the differential thermal expansion or contraction due to temperature gradients within particles of rock, which can be produced by thermal shock,
(ii) the inter-granular stresses which will be generated between the individual crystals of the quartzite due to anisotropy of thermal expansion,
(iii) the stresses produced by volume changes which accompany the $\alpha \rightarrow \beta$ phase transition at 573°C, and
(iv) the stresses produced by volume changes of mineral inclusions and gaseous evolutions.

Certainly factors (i) and (iii) cause rapid fracturing of single crystals of quartz. Rapid changes in temperature of as little as 150°C from ambient promotes multi-cracking of crystal plates. Heating through the phase transition temperatures at rates as low as 1°C per second causes fracture due to the sudden volume change of 0,86%. The stresses generated by the four mechanisms can be estimated as follows:

(i) the maximum triaxial tension which can be developed at the centre of a sphere of quartz which has a radius $b=1$ cm, an average thermal conductivity, $k=8{,}9\ \mathrm{W.m^{-1}K^{-1}}$, a specific heat $c=1{,}18\times10^{3}\mathrm{Jkg^{-1}{}^{0}C^{-1}}$, density $\rho=2{,}6\times10^{3}\mathrm{kgm^{-3}}$, a mean coefficient of linear thermal expansion $\alpha=10{,}6\times10^{-6}\mathrm{C^{-1}}$ and Young's Modulus $E=100\ \mathrm{GNm^{-2}}$, when it is subjected to a sudden increase in temperature $\triangle T$ is given approximately by

$$0{,}38\ \alpha\ E\ \triangle\ T$$

The maximum tensile stress is attained after a time

$$t=0{,}057\ b^{2}c\rho/k$$

Thus in the present case the stress will reach 200 $\mathrm{MNm^{-2}}$ in about 2 seconds when suddenly heated to 200°C and 360 $\mathrm{MNm^{-2}}$ in a similar time when suddenly heated to 600°C. The corresponding strains at the centre will be approximately 2×10^{-3} and $3{,}6\times10^{-3}$ respectively. Temperature gradients produced on rapid cooling will produce stresses of similar magnitudes.

(ii) The trigonal symmetry of α-quartz is manifested in the anisotropy of the thermal expansion coefficients. The expansion coefficient along the C-axis is $7{,}5\times10^{-6}\mathrm{K^{-1}}$ and normal to the C-axis the expansion coefficients have the value of $13{,}7\times10^{-6}\mathrm{K^{-1}}$. Thus, on heating or cooling a polycrystalline quartzite sample, stress will be generated due to the misfit of any one grain with respect to the 'average' surrounding matrix. An estimate of the misfit can be made in the following way. Consider the removal, at a given temperature, of a spherical anisotropic grain of unit diameter from the average matrix. Now, on change of temperature $\triangle T$, the hole will have increased (or decreased in the case of cooling)

its diameter by $10,6 \times 10^{-6} \triangle T$, and the grain will have changed its dimensions by $7,5 \times 10^{-6} \triangle T$ and $13,7 \times 10^{-6} \triangle T$ along the normal to the C-axis respectively. The resulting maximum strain which will have to be accommodated when the grain is inserted into the hole, will be about $\pm 2/3 \times 3,1 \times 10^{-6} \triangle T$. The factor of 2/3 is introduced because the system is now constrained. The strain on increasing the rock temperature from ambient to 200°C will be $\sim \pm 4 \times 10^{-4}$ and from ambient to 600°C it will be $1,2 \times 10^{-3}$. The corresponding stresses will be about 40 MNm^{-2} and 120 NMm^{-2}. From the previous discussion one would expect that the tensile stresses generated in the direction of the C-axis on heating and the tensile stresses generated normal to the C-axis on cooling would promote microcracking during thermal cycling treatments.

(iii) During the $\alpha \rightleftarrows \beta$ transformation in quartz at 573°C, there is a sudden change in density. The volume increases by 0,86% at the phase change and the axial ratio of the structure shows a discontinuous change. On heating a sample of quartz or quartzite through the transformation temperature internal stress will be produced on account of the volume change at the interface between untransformed regions and transformed regions. Extremely uniform heating would be required to avoid this cause of stress. If the anisotropy of linear dimensions is ignored then the introduction of a small volume of α-quartz in place of an equal mass of α-quartz would result in an 'unconstrained' strain of $1/3 \times 8,6 \times 10^{-3}$ and a constrained strain of $2/9 \times 8,6 \times 10^{-3}$ or about 2×10^{-3}.

(iv) The stresses generated during the decomposition of mineral inclusions such as pyrites are difficult to estimate but the volume changes and the release of gaseous products may well be sufficient to initiate flaws.

Our experimental observations confirm this conclusion.

It can be seen that the strains generated for the reasons considered can attain values in the region of 2 to 3×10^{-3}. The magnitude of the resulting tensile stress which may induce cracking is not easy to assess since the shape of the particles and grains will not be spherical as assumed in the above treatments. Stress concentration geometries may increase the stress to values above those calculated above viz. 40→300 MNm^{-2}. The criterion for fissuring will then be the relative magnitude of the stress created and the measured strength of unnotched crystals and transgranular strength of quartzite. The former is given as 83 to 110 MNm^{-2} while the latter will be considerably smaller. It can thus be concluded that considerable microfracturing will be produced and by applying a rapid temperature nc rease to about 600°C. Further cracking could be produced by a subsequent quench from this temperature.

EXPERIMENTAL WORK AND RESULTS

The following experimental techniques were used to estimate the weakening effect of thermal treatments and to monitor the microfissuring produced. Five types of rock have been investigated and these have been designated A fine grained quartzite containing little or no mineral particles, B fine grained quartzite containing mica particles, C fine grained quartzite containing pyrites and mica, D pebble quartzite containing pyrites and mica and E synthetic quartz crystals.

(1) Tensile Strength of Quartzite

A convenient way of measuring the tensile strength of rock is the Brazilian test. Samples, 25 mm dia.

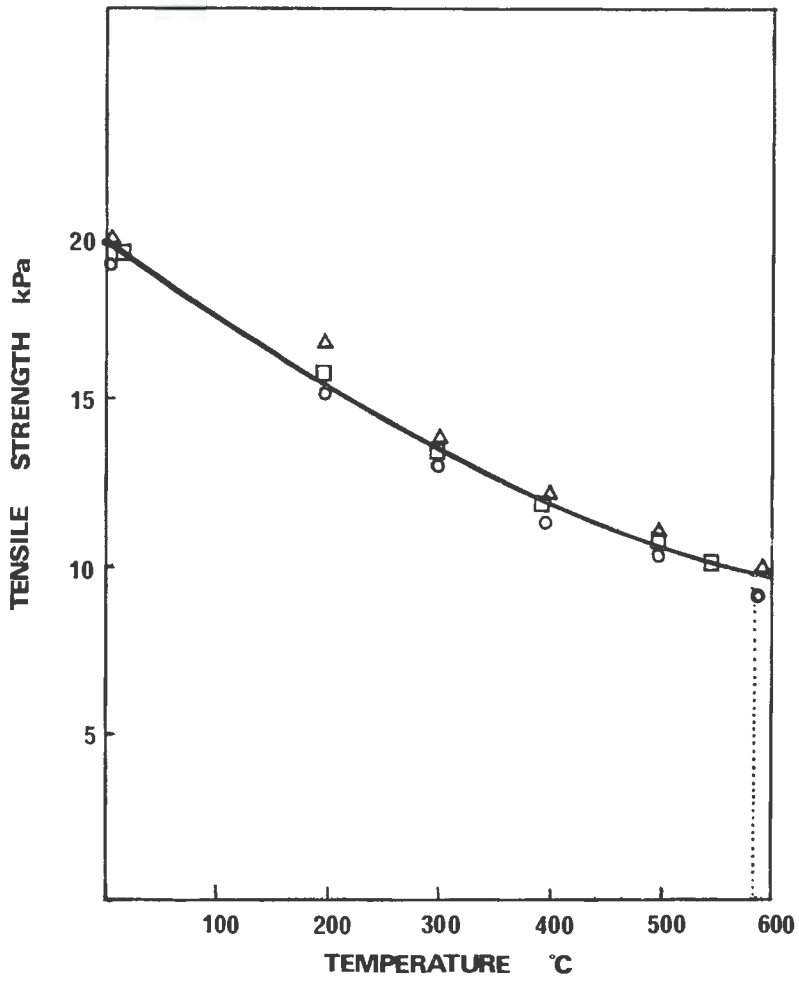

Fig. 1—Influence of the temperature of heat treatment on the tensile strength of quartzite (A, B, C)

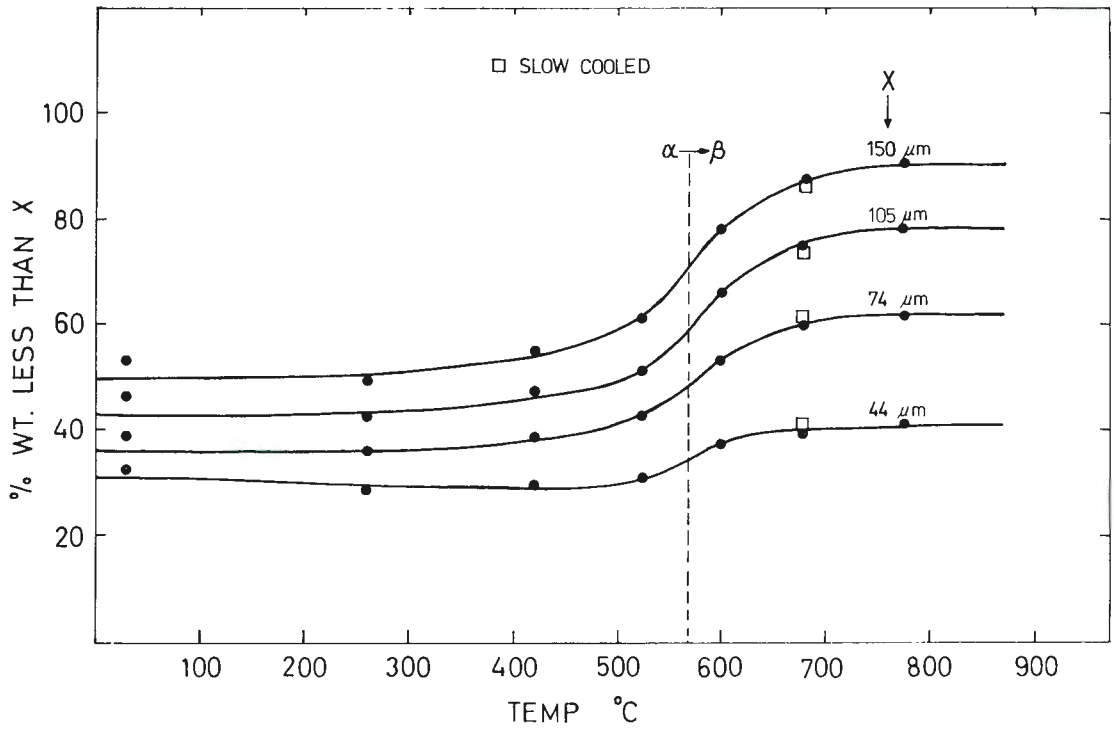

Fig. 2—Influence of the temperature of heat treatment on size distribution of ball milled quartzite (D)

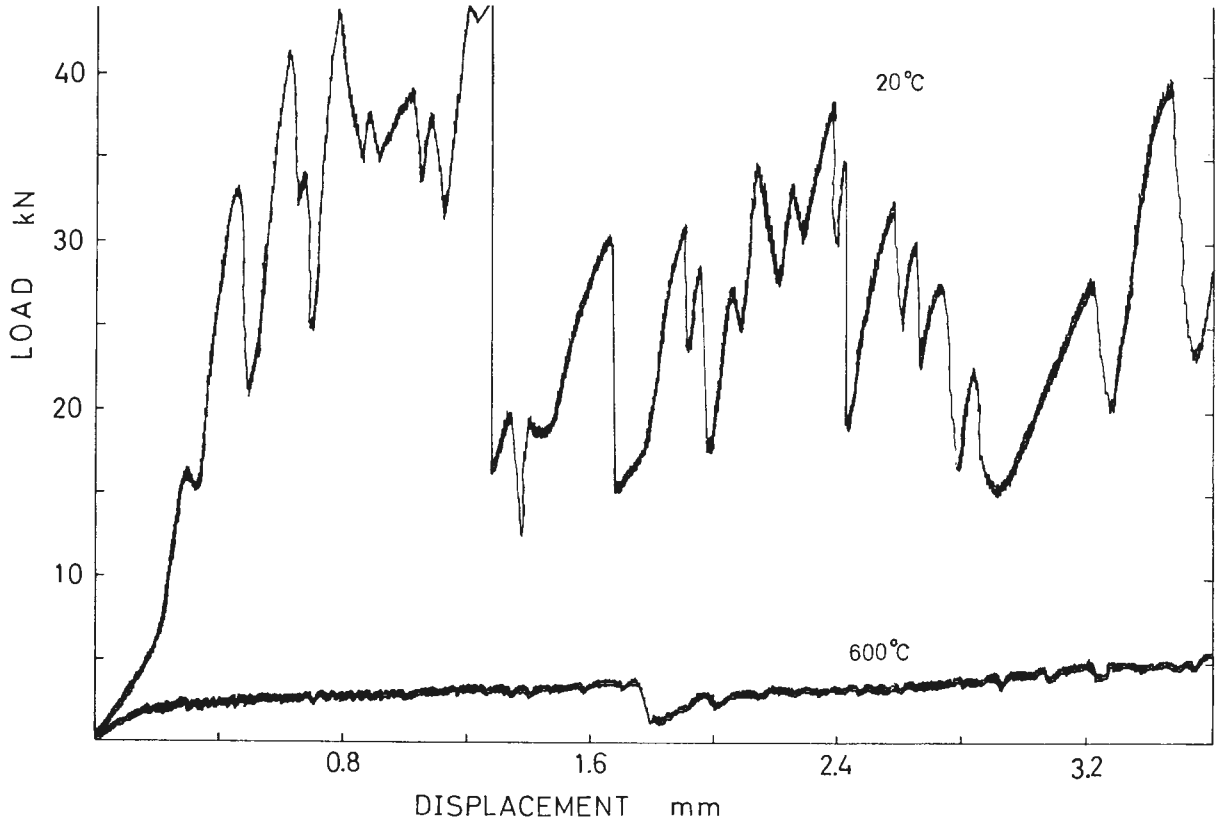

Fig. 3—Typical recorded traces of the variation of the load during the compression of quartzite specimens which had been heated and quenched from the temperatures indicated

and 50 mm in length, were compressed between plywood faced plattens, and the tensile strength was estimated by using the value of the maximum load P sustained by the specimen in the expression $2P/\pi DL$ where D is the diameter of the specimen and L is its length. The values obtained for the samples of rocks A, B and C after quenching from various temperatures are shown in Fig. 1. The strength falls continuously with quenching temperatures and a 50 per cent reduction of the original strength is achieved by a quench from 600 °C. The quenching in these experiments was performed by quickly removing the specimen from the furnace and immersing it in cold running water.

(2) Ball Milling and Crushing Experiments

Three experiments were performed to assess the influence of thermal treatment upon comminution properties of quartzite.

(i) Small pieces of rock (type D) (< 1 cm diameter) were loaded into a stainless steel cage which was then suspended in the hot zone of a vertical furnace. After 15 minutes the cage was allowed to fall into water at ambient temperature. The experiment was carried out for six elevated temperatures. In one experiment, the rock was slowly cooled from 680 °C. Each cage of treated rock was then ball milled for a constant time using a feed size of 2,38 to 4,76 mm. The resulting particle size distributions are plotted on four curves in Fig. 2 as the resulting percentage less than 44, 74, 105, 150 μm as a function of the temperature of heat treatment.

(ii) Pieces of rock (type D) of approximately 50 mm diameter were quickly introduced into a vertical furnace which had been set at given temperatures. After 15 minutes the rock was released into water at room temperature. The experiment was carried out for six different temperatures. In addition, a rock sample was slowly cooled from 700 °C. The samples were then put, together with a small amount of water, into a special cup and then crushed in a testing machine at a rate of 0,021 mm sec^{-1}. Typical load-displacement curves are shown in Fig. 3. The resulting particle size distributions are plotted in Fig. 4 as a function of heat treatment temperature.

(iii) Small 10 mm cubes of rock (type D) were heat treated in a similar manner to those in experiment (ii) and then crushed in compression. The size distribution of the product is shown in Fig. 5 as the percentage of the total weight which is retained in the screens of the sizes indicated.

The three experiments clearly show that heat treatment above 400 °C improves the comminution. However, large improvements are not realized until temperatures above the $\alpha \rightleftarrows \beta$ transition are used. Further experiments are now in progress in order to assess the importance of heating and cooling rates.

(3) Dilatometry

Dilatometry has been carried out on samples of synthetic quartz crystals and the various quartzite rocks (A, B, C and D). Specimens

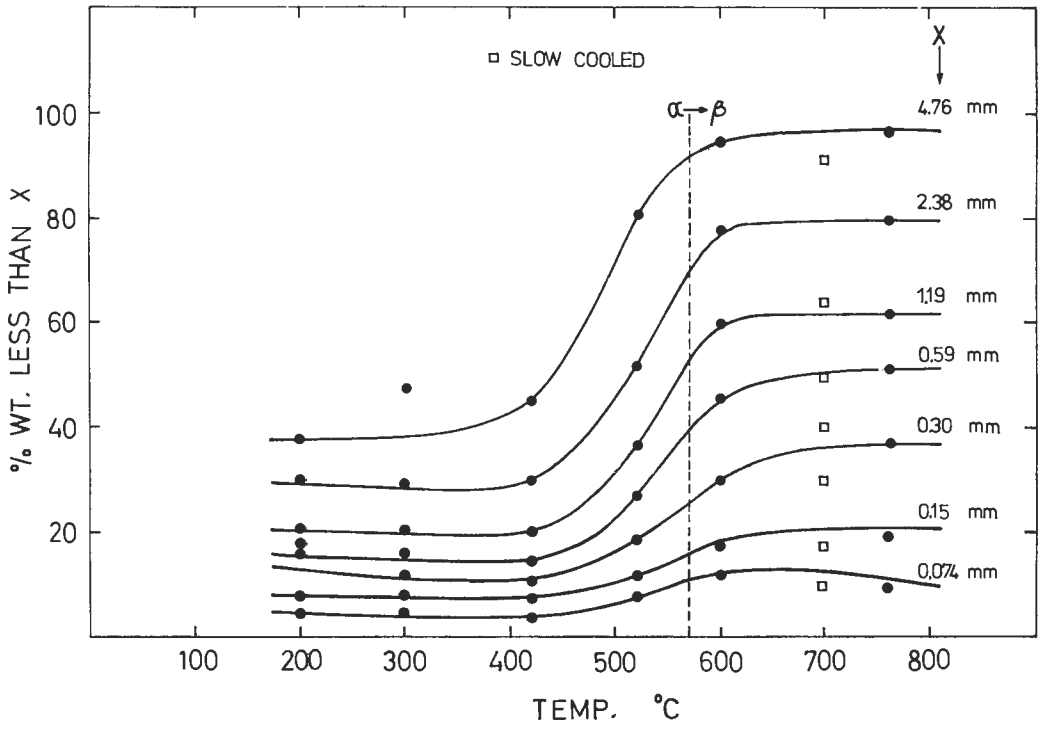

Fig. 4—Influence of the temperature of heat treatment on size distribution of crushed quartzite (D)

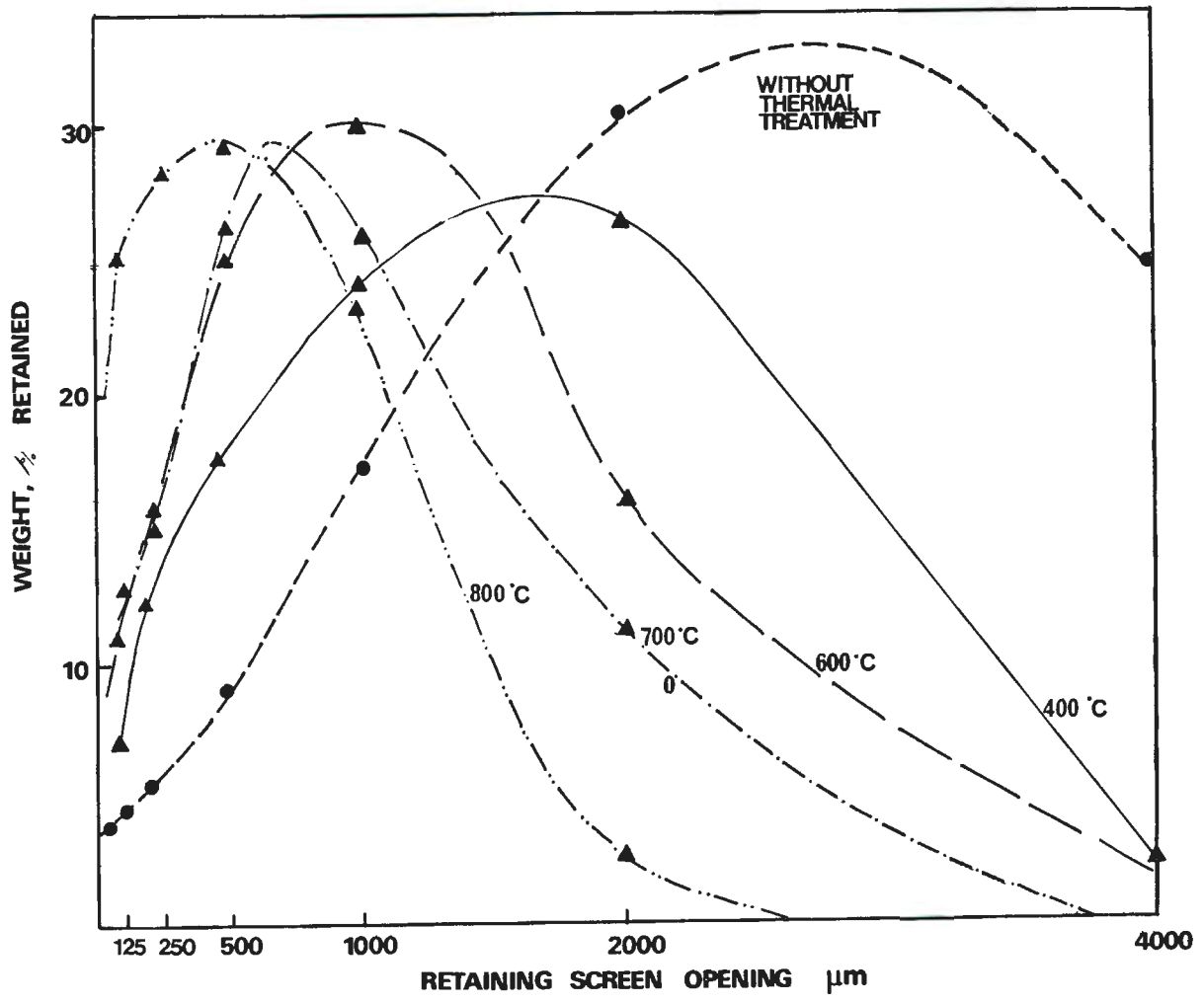

Fig. 5—Screen analysis of crushed quartzite (C, D) after heat treatment at various temperatures

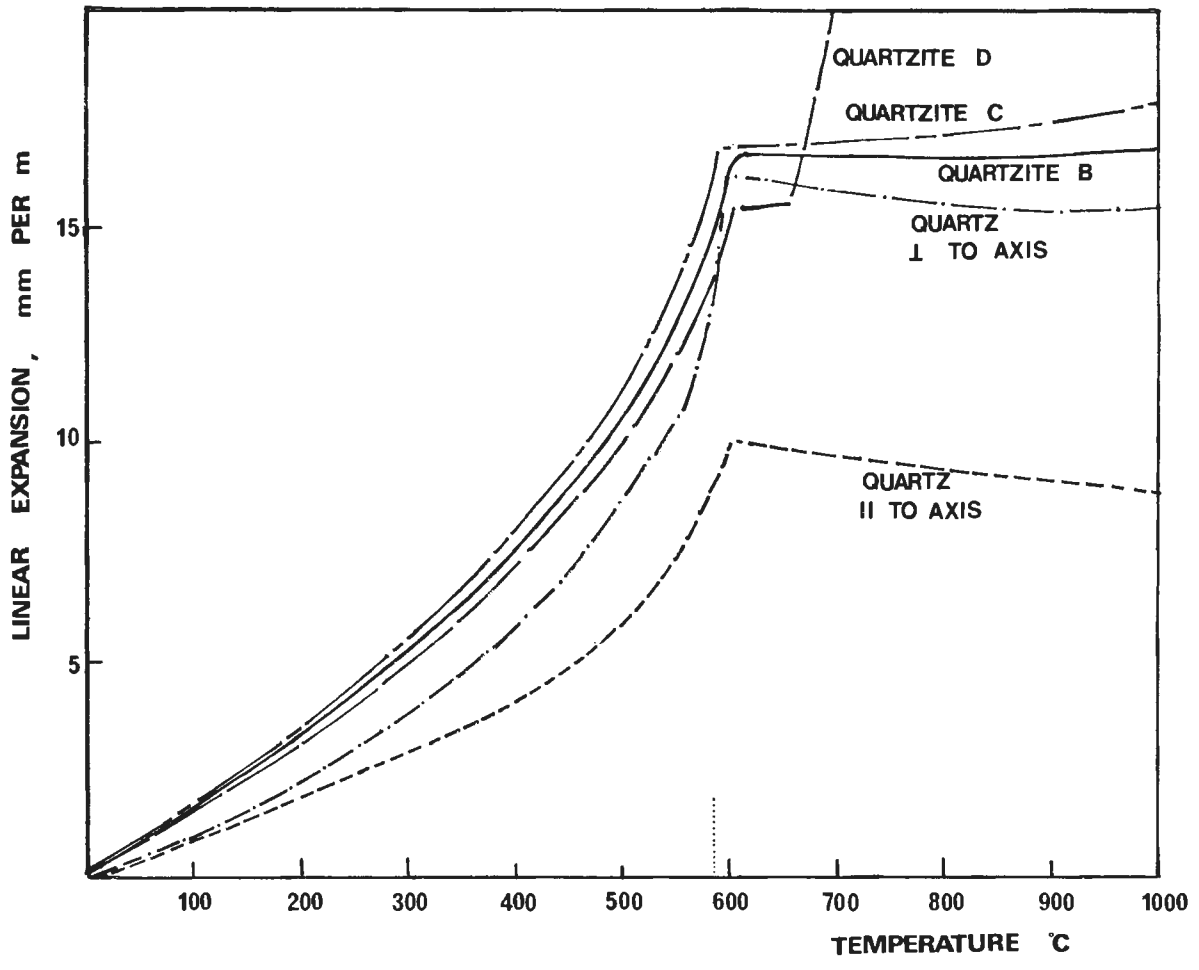

Fig. 6—Experimental data of the linear thermal expansion of quartzite (A, B, C, D) and quartz (after Kozu and Saiki[9])

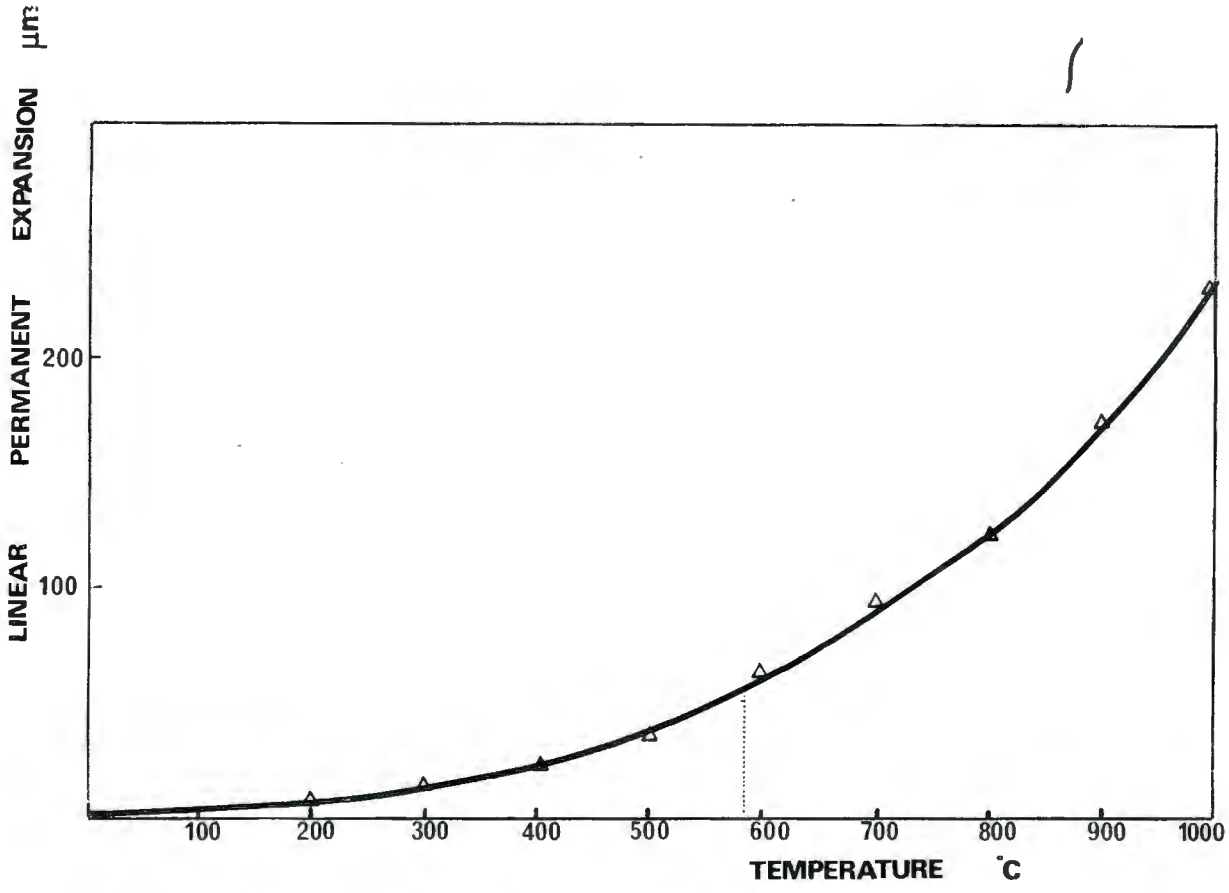

Fig. 7—Permanent dilatation of quartzite (B) after heating and cooling to the given temperature

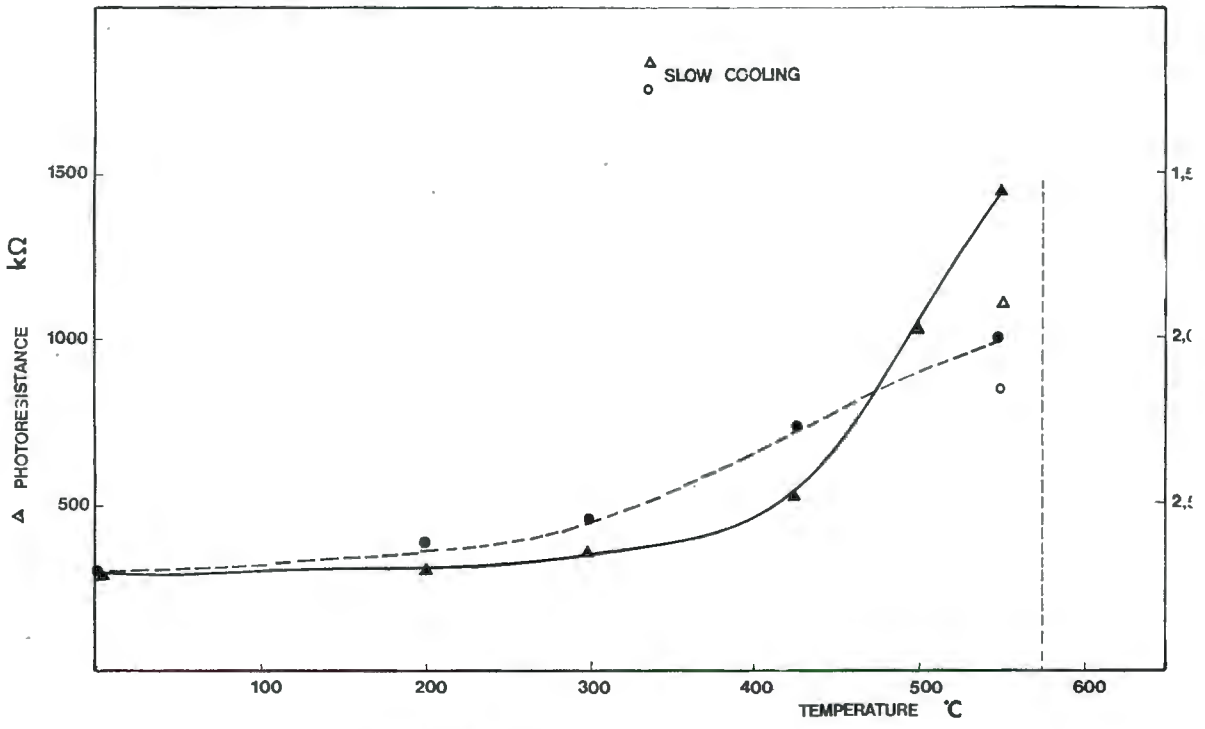

Fig. 8—Experimental data on fracture detection of quartzite C, after heating at various temperatures and quenching in water
(a) Photoresistance tests
(b) Ultrasonic tests

free of cracks and defects were carefully chosen and cut to the dimensions $50 \times 3 \times 3$ mm with parallel end faces. The results for heating to 1000 °C at a rate of 8 °C per min. are shown in Fig. 6. The curves are very similar and approximate to those previously published for quartz crystals[9]. It should be noticed that the specimens C and D which contain many mineral inclusions show large dilations at temperatures above 600 °C. This may be due to the volume change on decomposition of the pyrites. The specimen of rock D contained a massive particle of pyrites and a large dilation occurred at approximately 640 °C.

The permanent deformations after slow cooling from various temperatures are shown in Fig. 7. The curve shows a smooth exponential increase with temperature and no discontinuity at the $\alpha \rightleftarrows \beta$ transition temperature. The permanent deformations are presumably due to microfractures and elastic strains produced by mineral transformations.

(4) Fracture Detection

Sections 6 mm thick of the rocks A, B, C and D and quartz crystal were polished on both faces to a 6 μm finish. These were heated in a fluidised bath furnace to temperatures up to 600 °C. After 15 minutes the specimens were removed and quenched in running water. In addition, a specimen of rock C and a specimen of synthetic quartz were heated in the bath at 550 °C and then allowed to cool slowly in the bath. The specimens were then examined and photographed by reflection microscopy. The fracture density was an obvious function of the heat treatment and many of the fractures seen in the rock samples appeared to be associated with inclusion particles. The density of micro-fractures was then determined by two different techniques. (i) The intensity of light transmitted, at fixed positions, through the specimen from a standard source was measured by means of a photoresistance cell. The recorded intensity (resistance) will be a function of the number of internal fractures which disperse the light. The results are shown in Fig. 8 and it can be seen that a significant increase in defects occurs in specimens which had been heated to temperatures above about 425 °C. (ii) The attenuation of an ultrasonic signal was measured as a function of the temperature of the heat treatment. The specimens used in the above experiments were placed between a probe and a receiver and the signals were recorded on an oscilloscope. The attenuation will be related to the density of cracks within the specimens and the results are included in Fig. 8. The form of the experimental results is similar to that obtained by the optical method. It can be concluded that extensive microfissuring occurs during heat treatment and the number and extent of fractures increases at ~425 °C.

DISCUSSION

It has been shown that sharp initiating fissures are required for efficient rock breakage and the possibility of introducing these fissures by thermal treatments has been the subject of the preliminary experiments described here. More work is required to establish the importance of the various factors *viz;* heating and cooling rates and the optimum density of fissures required. It would appear that temperatures as low as 400 °C may be sufficient to produce a significant increase in the efficiency of subsequent comminution. From an energy consideration the problem of heating rock to these temperatures is costly. Quartzite has a specific heat capacity of about 10^3J.kg^{-1}°C^{-1} in this temperature range and thus the energy required to reach 400 °C is approximately 4×10^8J.tonne^{-1}. If the subsequent grinding requires say 5×10^7J.tonne^{-1} then the total consumption is of the same order as that of the methods presently used in the industry. It would thus appear that the proposed thermal techniques do not warrant any further consideration. However, the following factors should be taken into account. (i) It has not yet been established whether the total mass of rock sample has to be heated. If effective weakening results from the strains induced by superficial heating then the thermal power required will be much reduced. (ii) The mechanical strength of the heat treated rock should remove the necessity for multi-stage breakage operations. The rock could be transferred directly to the rotary mills. (iii) The fragility of the heat treated rock is such that the subsequent breakage operations can be performed without the excessive mechanical wear of mill liners and components. The resultant saving in downtime and replacement parts could be substantial. (iv) Although the heat treatments described may be of minimal advantage in terms of the energy required for the comminution of the gold bearing quartzites of the Witwatersrand, the technique may be very effective for other mineral bearing rocks where large volume changes result from low temperature phase changes.

ACKNOWLEDGEMENTS

The authors gratefully acknowledge the financial support given by the Chamber of Mines for research into the fracture behaviours of quartzites. We are also indebted to Mrs J. Rieder for her assistance in the preparation of this paper.

REFERENCES

1. Ball, A. and Payne, B. W. *J. Mat. Sci.* to be published.
2. Rumpf, H. R. *International Congress on Fracture, Munchen* 8, bis 13 April 1973.
3. Schoenert, I., Umhauez, H., Klemn, W. Fracture 1969, *Proceedings of the 29th Int. Conf. on Fracture.* Brighton. April 1969.
4. Baeta, R. D., and Ashbee, K. H. G. *Phil. Mag.* 22. 1970. 601.
5. Hartley, N. E. W. and Wilshaw, T. R. *J. Mat. Sci.*, 8 1970. 265.
6. Swain, M. V., Williams, J. S., Lawn, B. R. and Beek, J. J. H. *J. Mat. Sci.*, 8. 1973. 1153.
7. Griffith, A. A. *Phil. Trans. R. Soc.*, A.221. 1921. 163.
8. Inglis, C. E. *Trans. Roy. Inst. Naval Architects*, 55. 1913. 219.
9. Sosman, R. B. *The properties of silica* Chemical Catalog. Co. New York. 1927.

MICROSCOPICAL OBSERVATIONS ON FRICTION TRACKS PRODUCED BY SLIDING QUARTZITE SURFACES

A.C. Kanellopoulos and A. Ball

Department of Metallurgy and Materials Science, University of Cape Town

The study of the frictional behaviour of rocks will allow a better understanding of the processes occurring in comminution systems. Witwatersrand quartzite specimens, taken from cylindrical drill cores of known surface roughness, were used for sliding tests carried out under point contact, at various relative speeds, under various normal loads and in the presence of various liquid environments. The coefficients of static and sliding friction were found to change with the normal loads, the sliding speeds and the initial surface roughness in a different manner for each environment used. Changes in the frictional mechanisms involved were indicated by these results and a S.E.M. examination of the friction tracks produced on the specimens, has provided an understanding of these mechanisms.

For a medium grained quartzite (~ 1mm), the friction tracks formed in water were found to change with the sliding speed or the normal load in the following manner. No distinguishable surface damage on the sliding track was observed for tests performed under loads smaller than 15N for a constant sliding speed of $8{,}46 \times 10^{-5} ms^{-1}$ (fig. 1) or under a normal load of 20N for speeds lower than $4{,}23 \times 10^{-5} ms^{-1}$. These conditions do not promote grain removal or fracture and thus the surface asperities "climb" each other according to the roughness theory of friction[1,2]. For loads between 15 and 40N or sliding speeds between $4{,}23 \times 10^{-4}$ and $4{,}23 \times 10^{-5} ms^{-1}$ only the tips of the surface asperities fail by brittle cleavage fracture, as it is shown in fig. 2 and at high magnification in figs. 3 & 4, verifying the friction mechanism proposed by Byerlee[3]. For normal loads higher than 40N or sliding speeds higher than $4{,}23 \times 10^{-4} ms^{-1}$, the friction theory of adhesion and ploughing, proposed by Bowden and Tabor[4] for metals, is appropriate since the smooth extruded appearance of the phyllosilicates in the friction groove and the presence of the fine gouge-debris shown in figs. 5, 6 & 7, is evidence of plastic flow processes. Some quartz grains are simultaneously removed by intergranular failure of the surrounding phyllosilicates, as is shown by the flakes in the grain cavity of fig. 8.

Using different environments, such as normal alcohols, ethylene glycol, oleic acid, acetone or toluene, or different surface finishes of the rock specimens, the above mechanisms were found to occur in different regimes of normal load and sliding speed. This behaviour can be explained in terms of the changes induced in the solids by adsorption phenomena.

References

1. Wilks, E.M. & Wilks, J., 1959, Phil. Mag., 38, 158.
2. Rabinowicz, E., 1965, Friction and Wear of Materials, Wiley, N. York.
3. Byerlee, J.D., 1967, J. Appl. Phys., 38, 2928.
4. Bowden F.L. & Tabor, D., 1964, The Friction and Lubrication of Solids II, Claredon Press, Oxford.

The N.I.M. and the Chamber of Mines are acknowledged for their support.

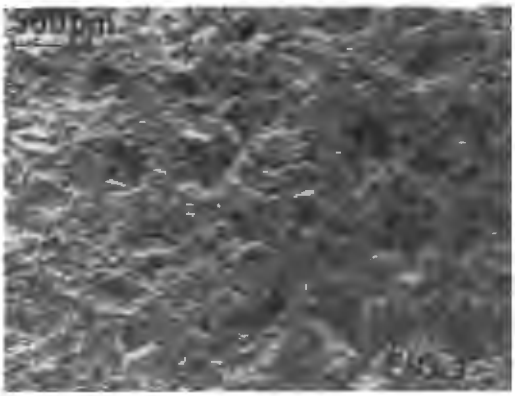

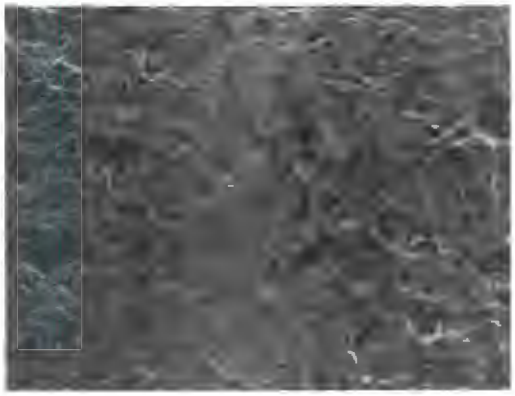

FIG. 3

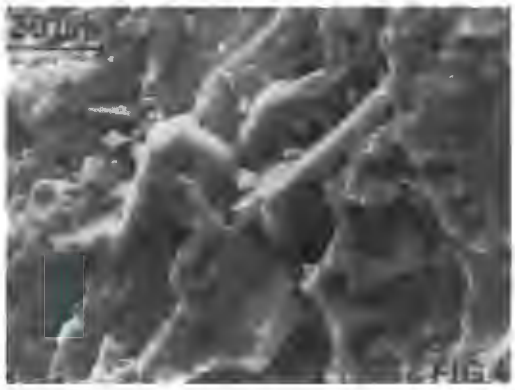

FIG. 4

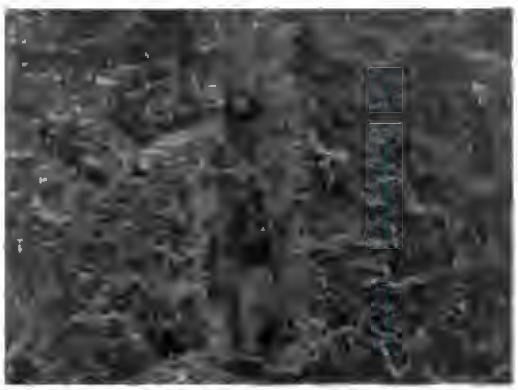

FIG. 6

FIG. 7

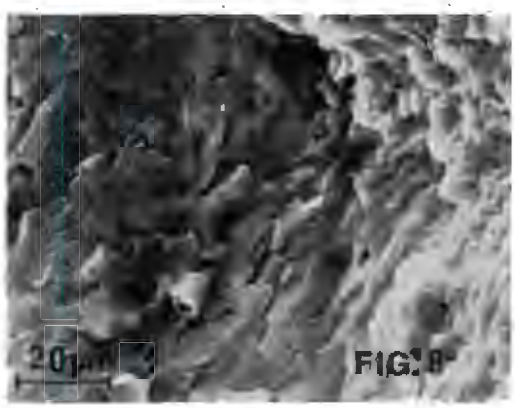

FIG. 8

S.E.M. CHARACTERISATION OF AUTOGENOUSLY COMMINUTED QUARTZITE

A.C. Kanellopoulos and A. Ball

Department of Metallurgy and Materials Science, University of Cape Town

The shape and the surface morphology of autogenously comminuted quartzite particles have been studied in order to assess the mechanisms. The particles were sampled[1] from the product of a laboratory autogenous mill of 160mm int. dia. and from various operation stages of a wet, fully autogenous "Aerofall" test mill of 1,52m int. dia. An evaluation of the shape characteristics of the particles was performed via the area A, the perimeter P and the maximum diameter D of the two dimensional S.E.M. image, using a planometer, a chart odometer and a micrometer respectively. Two shape factors were established, viz. the surface shape factor A/D^2 and the outline area shape factor A/P^2. An increase of the 'angular roundness' of the particles from the laboratory mill was found for longer times (>120mins.), while similar shape changes were observed for the test mill particles taken from the run-of-mine feed, mill interior and cyclone overflow respectively (figs. 1, 2 & 3). The shape characteristics of particles taken from the product of compression (fig. 4) and abrasion (fig. 5) tests were found to be similar to the ones of the milling particles. This indicates that abrasion and impact mechanisms are of importance in autogenous milling compared with attrition, since this process is known to produce round particles e.g. natural quartz sand rounded by aeolian attrition.

Although the quartzite particles were found to increase their 'angular roundness', their surface morphology contains cleavage facets and fracture patterns, irrespective of milling times. This indicates that comminuting events employing fracture are of importance in an autogenous mill. The presence of gouge-free and adhering particles of colloidal size, is probably associated with plastic flow phenomena of included mineral constituents, since an S.E.M. examination of surfaces (fig. 6) and detritus (fig. 5), taken from the wear of quartzite drill cores showed the occurrence of ploughing of hard particles into softer ones.

Microstructural defects, favouring transgranular fracture (fig. 7) were found to be present in comminuted particles. These defects may derive from the geological history of the rock. This is supported by the high density of similar defects in thermally treated particles[2] (fig. 8). From a mineral processing point of view, intergranular fracture is more desirable than the transgranular one since the minerals are concentrated at the grain boundaries. Further comminution represents energy wasted, and the presence of the very fine particles is associated with a decreased efficiency of the subsequent separation operation. The same applies for the plastic flow detritus produced by abrasion.

The N.I.M. and the Chamber of Mines are acknowledged for their support and the E.M. Unit at U.C.T. for experimental assistance.

References

1. Taggart, A.F., 1953, Handbook of Mineral Dressing, Wiley, N. York.
2. Kanellopoulos, A.C. & Ball, A., 1975, Jnl. S.A. Inst. Min.Met., 76, 45.

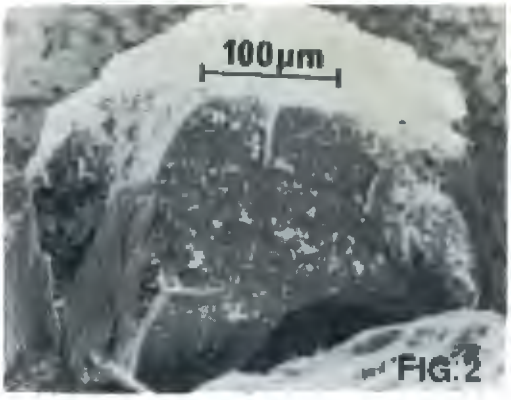

FIG. 2

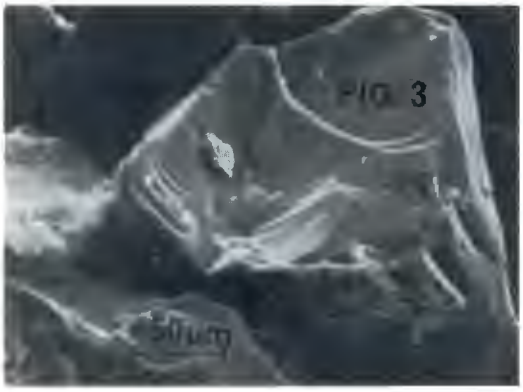

FIG. 4

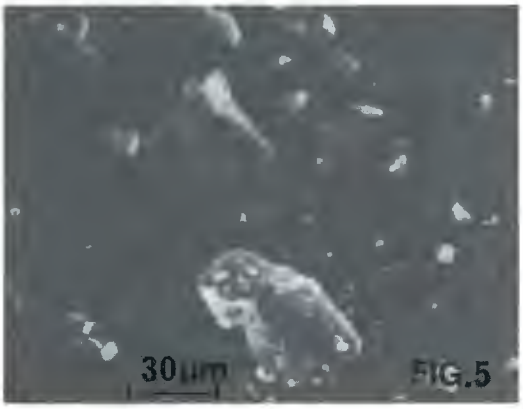

FIG. 5

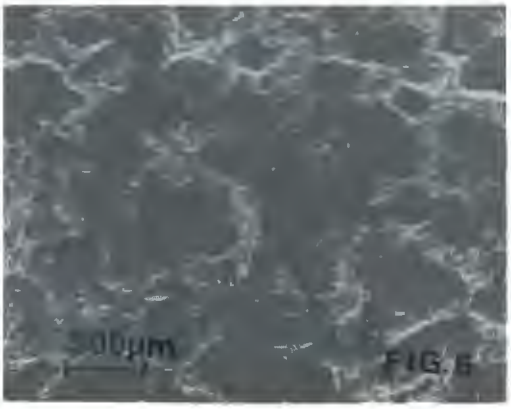

FIG. 6

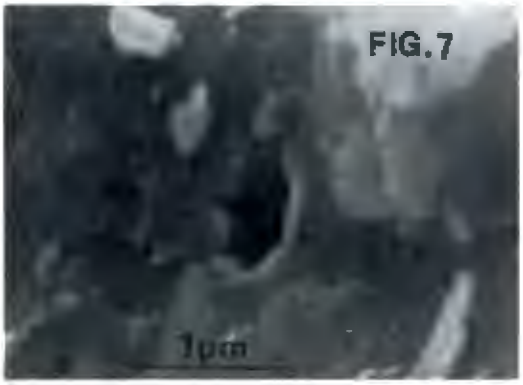

FIG. 7

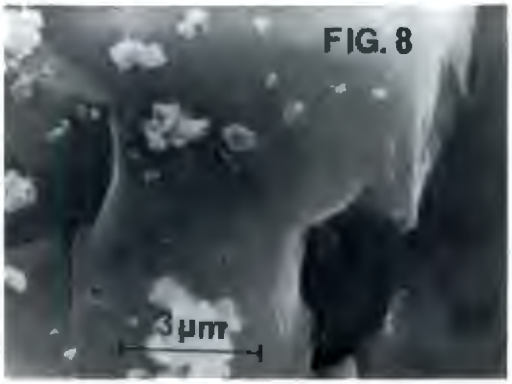

FIG. 8